PhD-FSTM-2020-10
The Faculty of Sciences, Technology and Medicine

DISSERTATION

Defence held on 27/03/2020 in Esch-sur-Alzette

to obtain the degree of

DOCTEUR DE L'UNIVERSITÉ DU LUXEMBOURG

EN SCIENCES DE L'INGÉNIEUR

by

Dolgion ERDENEBAT
Born on 28 March 1988 in Ulaanbaatar, (Mongolia)

CONDITION ASSESSMENT OF BRIDGE STRUCTURES BY DAMAGE LOCALISATION BASED ON THE DAD-METHOD AND CLOSE-RANGE UAV PHOTOGRAMMETRY

Dissertation defence committee

Prof. Dr.-Ing. Andreas Zilian, Chairman
Professor, University of Luxembourg, Faculty of Science, Technology and Medicine

Prof. Dr.-Ing. Norman Teferle, Vice-Chair
Professor, University of Luxembourg, Faculty of Science, Technology and Medicine

A-Prof. Dr.-Ing. Danièle Waldmann, Dissertation supervisor
Assistant-Professor, University of Luxembourg, Faculty of Science, Technology and Medicine

Prof. Dr.-Ing. Steffen Marx
Professor, Technische Universität Dresden, Institut für Massivbau

Prof. Dr.-Ing. Marc Gutermann
Professor, Hochschule Bremen, Institut für Experimentelle Statik

1 Danksagung

Die vorliegende Arbeit entstand während meiner Tätigkeit als Doktorand am Institut (Institute of Civil and Environmental Engineering INCEEN) an der Fakultät für Naturwissenschaften, Technologie und Kommunikation der Universität Luxemburg und im Rahmen des Forschungsprojekts „STATOSTRUC“ zur Zustandsbewertung von Brücken im Zeitraum vom 15.05.2015 bis 12.05.2020.

Mein besonderer Dank gilt Frau Prof. Waldmann als meine direkte wissenschaftliche Betreuerin. Ihre wertvollen Anregungen, die kooperative Unterstützung sowie das angenehme Arbeitsklima trugen maßgeblich zum Gelingen dieser Arbeit bei. Zudem danke ich Herrn Prof. Andreas Zilian von der Universität Luxemburg für die fachübergreifende, interdisziplinäre Begleitung der Arbeit. Herrn Prof. Norman Teferle möchte ich mich für die fachspezifische Unterstützung der Arbeit, die Bereitstellung der Fachliteraturen, sowie für die Empfehlungen bedanken.

Aufrichtig danken möchte ich den Professoren Steffen Marx von der Leibniz Universität Hannover und Marc Gutermann der Hochschule Bremen für das Interesse an der Forschungsarbeit und für die Mitwirkung in meinem Prüfungskomitee.

Darüber hinaus danke ich meinen Kollegen der technischen Abteilung Marc Seil, Gilbert Klein, Claude Colle, Cédric Bruyère, Logan Filipe Freitas Moreira, Ed Weyer, Ken Adam, Grace Ligbado, Vicente Reis Adonis, Ralph Reiter und Remi Radinovic für die engagierte Unterstützung der zahlreichen experimentellen Untersuchungen. Für die Ermöglichung des Drohnenflugs im Rahmen des Brückenversuchs danke ich Herrn Prof. Holger Voos, Herrn Prof. Miguel Angel Olivares und Herrn Dr. Jose Luis Sanchez Lopez.

Ein großer Dank gilt Herrn Fréderic De Oliveira und Herrn Gilberto Fernandes von Administration des Ponts et Chaussées Luxembourg für die außerordentliche Kooperationsbereitschaft und die Realisierung des großformatigen Brückenversuchs in Altrier.

Des Weiteren bedanke ich mich Herrn Harald Krause von Photo Mess Systeme AG für die Unterstützung zur professionellen Anwendung der Photogrammmetrie-Software Elcovision 10.

Außerordentlich danke ich Herrn Dr. Michael Weiler für die Herstellung des ersten Bezugs zu diesem Projekt. Meinen direkten Kollegen Gelen Gael Chewe Ngapeya, Vishojit Bahadur Thapa, Patrick Pereira Dias, Lorenc Bogoviku, Hooman Eslami und Laddu Bhagya Jayasinghe für die stetige Diskussionsbereitschaft und die kollegiale Zusammenarbeit. Herrn Dietmar Backes bedanke ich mich für die produktiven Gespräche und die Zusammenarbeit. Weiterhin danke ich den Studierenden Muamer Kajevic, Jorge Goncalves, Yann Fux, Laurent Oestreicher, Jonathan Sousa Coimbra, die im Rahmen ihrer Studien-, Bachelor- und Masterarbeiten das Projekt, insbesondere die Versuche tatkräftig unterstützt haben.

Nicht zuletzt bedanke ich mich bei meiner Familie, den Eltern und den Freunden. Mein größter Dank gilt meiner Frau und unseren gemeinsamen Kindern für den Rückhalt in den vergangenen Jahren.

Luxemburg, Januar 2020

Dolgion Erdenebat

“Men build too many walls and not enough bridges”

Joseph Fort Newton

2 Contents

3 Abstract

3.1 Lëtzebuergesch

Déi aktuell Dissertatioun präsentéiert eng sougenannte "Deformation Area Difference (DAD)" Method fir den Zoustand vun existente Brécke ze bewäerten, besonnesch fir d'Erkennung vu steifechkeetsreduzéierende Schied. D'Method baséiert op der enger Säit op konventionellen stateschen Last Deformatiounstester an anerersäits op enger héig präziser Miessung vun der struktureller Verformung. D'Laascht op der Bréckekonstruktioun gëtt als Deel vum Serviceabilitéitslimit Status generéiert fir eng net zerstéierend Inspektioun ze erméiglechen.

Am Laf vun Tester am Labo goufen déi innovativst Miestechnike benotzt, woubäi d'Fotogrammetrie villverspriechend Resultater geliwwert huet. Mat der Hëllef vun zousätzleche Studien iwwer d'Aflëss vu Kameraqualitéit a Kalibréierung konnten Grenzen vun der Mosspräzisioun vun der Fotogrammetrie ënnersicht ginn.

Béid, déi theoretesch Ermëttlungen an d' Labostester, hunn den erfollegräiche Gebrauch vun der DAD Method fir d'Identifikatioun vu lokalem Schued gewisen. Dofir gouf dat éischt in-situ Experiment op enger eenspanneger, virgedréckter Bréck zu Lëtzebuerg duerchgefouert. Déi gemossen Donnéeën goufen kombinéiert mat statisteschen Ermëttlungen baséierend op Finite Element Berechnungen a kënschtlech generéiertem Mossdauschen fir d'Applikatiounsgrenzen ze bestëmmen. Dës sinn definéiert duerch d'erreechbar Moossgenauegkeet, den identifizéierbaren Grad vum Schued, erfuerderlech Unzuel un Miesswidderhuelungen, Afloss vun der Positioun vum Schued, der optimaler Gréisst vun der struktureller Verformung, etc..

Déi praktesch Entwécklung vun der DAD Method ergänzt den aktuellen Stand vun der Technik an dréit zu enger zouverléisseger Bewäertung vun der Brécke Konditioun bäi.

3.2 English

The provided dissertation presents a so-called “Deformation Area Difference (DAD)” method for condition assessment of existing bridges, especially for the detection of stiffness-reducing damages. The method is based on the one hand on conventional static load deflection experiments and on the other hand on a high-precision measurement of the structural deflection. The experimental load on the bridge should be generated within the serviceability limit state in order to enable a non-destructive inspection.

In the course of the laboratory tests, the most innovative measuring techniques were applied, whereby the photogrammetry has delivered promising results. With the help of additional studies on the influences of camera quality and calibration, the measuring precision of photogrammetry could be brought to its limits.

Both the theoretical investigations and the laboratory tests showed the successful use of the DAD method for the identification of local damages. Therefore, the first in-situ experiment was carried out on a single-span, prestressed bridge in Luxembourg. The knowledge gained from this was combined with statistical investigations based on finite element calculations and artificially generated measurement noise effect in order to determine the application limits, such as the achievable measurement precision, identifiable degree of damage, required number of measurement repetitions, influence of the damage position, optimal size of the structural deformation, etc.

The development of the DAD method ready for application usefully supplements the state of the art and contributes to the reliable assessment of the bridge condition.

3.3 Deutsch

Mit der vorliegenden Dissertation wird eine sogenannte „Deformation Area Difference (DAD)“ Methode zur Zustandsbewertung von Bestandsbrücken, insbesondere zur Detektion von

steifigkeitsreduzierenden Schäden, vorgestellt. Das Verfahren basiert einerseits auf herkömmlichen statischen Lastverformungsversuchen und andererseits auf einer hochpräzisen Vermessung der Bauwerksverformung. Die Belastung des Brückenbauwerks wird im Rahmen des Grenzzustands der Gebrauchstauglichkeit erzeugt, um eine zerstörungsfreie Inspektion zu ermöglichen.

Im Zuge der Laborversuche wurden die innovativsten Messtechniken angewandt, wobei die Photogrammmetrie vielversprechende Resultate geliefert hat. Mithilfe von zusätzlichen Untersuchungen über die Einflüsse der Kameraqualität und der Kalibrierung konnte die Messpräzision der Photogrammmetrie an ihre Grenze gebracht werden.

Sowohl die theoretischen Untersuchungen als auch die Laborversuche zeigten den erfolgreichen Einsatz der DAD Methode zur Identifikation von lokalen Schäden. Deshalb konnte das erste in-situ Experiment an einer einfeldrigen vorgespannten Plattenbrücke in Luxemburg realisiert werden. Die daraus gewonnenen Erkenntnisse wurden mit statistischen Untersuchungen basierend auf Finite Elemente Berechnungen und künstlich erzeugten Messrauschen kombiniert, um die Anwendungsgrenzen, sowie die erreichbare Messgenauigkeit, den identifizierbaren Grad der Schädigung, die erforderliche Anzahl der Messwiederholung, den Einfluss der Schadensposition, die optimale Größe der Bauwerksverformung etc., zu definieren.

Die praxisreife Entwicklung der DAD Methode ergänzt den Stand der Technik sinnvoll und trägt zu der zuverlässigen Bewertung des Brückenzustands bei.

3.4 Français

La dissertation présente une méthode dite «Deformation Area Difference (DAD) Method» pour évaluer l'état des ponts existants, en particulier pour la détection des endommageements réduisants la rigidité. D'une part, la méthode est basée sur des tests conventionnels de déformation statique et d'autre part sur des mesures de haute précision de la déformation structurelle. La charge sur la structure du pont est générée dans le cadre de l'état limite de service pour permettre une inspection non destructive.

Au cours des tests en laboratoire, les techniques de mesure les plus innovantes ont été appliquées et plus spécifiquement la photogrammétrie a donné des résultats prometteurs. La précision des mesures par la photogrammétrie a été optimisée par des études supplémentaires de l’influence de la qualité de l’étalonnage.

Les investigations théoriques et les tests de laboratoire ont montré que la méthode DAD avait été utilisée avec succès pour l'identification des endommagements locaux. Par conséquent, une première expérience a été réalisée in situ sur un pont précontraint à travée unique au Luxembourg. Les connaissances acquises ont été combinées à des investigations statistiques basées à la fois sur des calculs d'éléments finis et sur le bruit de mesure généré artificiellement, afin de déterminer les limites d'application telles que la précision de mesure réalisable, le degré identifiable des endommagements, le nombre requis de répétitions de mesure, l'influence de la position des endommagements, la taille optimale de la déformation structurelle, etc.

Le développement pratique de la méthode DAD aide à compléter l'état de l'art et à contribuer efficacement à l’évaluation fiable de l'état des ponts.

3.5 Монгол

Энэхүү диссертацид одоо байгаа гүүрүүдийн нөхцөл байдлыг үнэлэх, ялангуяа гүүрний даацыг бууруулж буй эвдрэлийг тогтоох зорилгоор " Deformation Area Difference (DAD)" гэх шинэ технологийн аргыг санал болгож байна. Энэхүү технологи нь нэг талаас гүүрэнд ердийн статик ачаалал өгөх туршилтан дээр буюу нөгөө талаас ачааллаас шалтгаалан буй нугаралтыг өндөр нарийвчлалтай хэмжихэд суурилдаг. Ачааллын хэмжээ нь хэрэглээний даацаар хязгаарлагдсан тул туршилтын явцад нэмэлт эвдрэл өгөхгүй болно.

Лабораторийн туршилтын явцад хэмжилтийн хамгийн шинэлэг багажуудыг ашигласан бөгөөд үүний дунд фотограмметри нь илүү их хүлээц өгөхөөр үр дүн үзүүлсэн. Камерын чанар ба тохируулгын нөлөөллийн талаархи нэмэлт судалгааны тусламжтайгаар фотограмметрийн хэмжилтийн нарийвчлалыг асар ихээр нэмэгдүүлэх болсон.

Шинээр гаргаж ирсэн DAD технологийн арга нь онолын судалгаа болон лабораторийн туршилтууд дээр суурилан тухайн эвдрэлүүдийн байршлыг амжилттай тогтоож чадаж байгаа нь батлагдсан. Тиймээс бодит гүүрэн дээрх анхны туршилтаа Люксембург улсад амжилттай хийв. Үүнээс олж авсан ололтууд нь тухайн технологийн аргыг цааш нь хөгжүүлэхэд үнэтэй хувь нэмэр оруулсан. Гүүрний туршилт, тооцооллын аргаар гаргаж авсан хиймэл хэмжилтийн байгажны нөлөө болон статистикийн тооцоогоор дамжуулан, тогтоож болох эвдрэлийн хэмжээ, шаардлагатай хэмжилтийн давтамжийн тоо, эвдрэлийн байршлаас шалтгаалах нөлөө, хэмжилтийн нарийвчлалын нөлөө, туршилтанд шаардлагатай гүүрний хэлбэлзэл гэх мэт технологийн хягаарлалтуудыг тогтоосон.

DAD гэх энэхүү технологийн арга нь практикт хүртлээ боловсорч чадвал одоо хэрэглэгдэж байгаа арга барилд нэмэр болох төдийгүй гүүрний эвдрэлийг олж тогтоох буюу найдвартай үнэлэлт өгөхөд үнэтэй хувь нэмэр оруулах юм.

4 General

4.1 Motivation

Millions of bridge structures exist worldwide and serve as the core of our infrastructure. For example, there are about 850,000 road bridges in China [1], about 700,000 in Japan [2], about 610,000 in USA [3], and about 39,000 in Germany [4]. However, each bridge structure has to be inspected regularly within a certain period of time depending on the national standards [5]. In this context, the significance and the huge effort of the regular inspection become apparent.

The inspection of bridge structures, according to the state-of-the-art, essentially carried out visually from a very close distance. In the case of suspected damage inside the structure, additional procedures are used. Nevertheless, there is a residual risk that damages in the interior of the load-bearing structure remain undetected.

Unfortunately, the collapse of existing bridge structures repeatedly occurs despite regular inspections. J. Scheer's book from 2010 already includes the vast number of 536 cases about bridge collapses, whereby bridge crashes still happen again and again. Currently cases are for example twice in October 2019 in Su'ao, Taiwan and Wuxi, China, in November 2019 in Mirepoix-sur-Tam, France and Savona, Italy etc.

It is of great interest for the public to rely on secure, reliable and economic infrastructure. On the one hand the steady rising average age and on the other hand, the ever-increasing number of heavy transporters bring the capacities of existing bridge structures to their limits. However,

technological developments open up new possibilities to consider such problem statements from a different perspective and to develop innovative approaches.

Within this research project, a method is developed for early detection of structural damages in the combination of conventional static loading tests and most modern measurement techniques. First of all, the method is tested on several laboratory experiments for the detection of structural damages using high-precision deflection measurements. The high-precision deflection measurement is regarded as the most important factor for the method, which has progressed from displacement sensors to levelling, total station, laser scanner and finally to the application of close-range photogrammetry applied on a large-scale drone. The final study was carried out on a real bridge structure in Luxembourg, which enabled the definition of the application limits for the developing method.

4.2 Aims

The objective of this work is the development of a method for localisation of damages in existing bridge structures based on static load deflection experiments. The so-called “Deformation Area Difference” (DAD) method presupposes on the one hand a high-precision deflection measurement along the bridge and on the other hand a reference system, which can be the initial deflection measurement after the construction or a theoretical model of the structure. Since the method relatively detects the damage over the bridge length, an absolute accuracy of the deflection measurement or the reference system is not necessary. The non-destructive static load test requires compliance with the maximum deformation within the serviceability limit state. In contrast, the detectable degree of the structural damage depends on the precision of the deflection measurement. Therefore, different investigations for the application of the DAD method are targeted:

- differentiation between damage and planned stiffness change
- influence of environmental conditions such as temperature
- structural influence such as asphalt layer, type of the structure
- suitable measurement techniques
- reachable precision for the deflection measurement

- separation of possible damage from the measuring error
- required size of the experimental bridge deflection in relation to the serviceability limit state

Furthermore, it is of high importance to verify the theoretically proven DAD method on experimental tests within the laboratory and real condition. In order to define the identifiable damage degree and the required measurement precision, the following tasks should be clarified:

- Detectable damage degree depending on the measurement precision
- Influence of the damage position
- Required number of the measurement repetition

4.3 Structure of the thesis

This dissertation is a cumulative thesis and consists of four peer-reviewed publications (listed in section 4.4.1), which are submitted respectively published in top-ranking journals within the category Q1 according to the Journal Citation Ranking and Quartile Scores [6]. The structure of the thesis starts with an introduction, followed by the four papers and concludes with a summary and outlook. Between each paper, a brief conclusion of the previous paper and a brief introduction to the next paper is presented. Further six peer-reviewed conference papers (section 4.4.2) will be shortly introduced within the introduction of the thesis.

Chapter 5 Introduction: The introduction gives an overview of the study and represents the correlations of the papers. It also contains detailed information and supplementary data such as the development of the methodology, the description of the laboratory experiments, the preparation of the calibration wall and bridge test, the background and the aim of the study etc.

Chapter 6 Introduction to the publication I: gives a short introduction to the first paper.

Chapter 7 Publication I: The Deformation Area Difference (DAD) method for condition assessment of reinforced structures: chapter 7 represents the content of the first paper without any changes to the published version. The paper includes the description of the theoretical background for the DAD method, case studies based on finite element models and an

application of the method on a laboratory experiment with reinforced beam structure. The publication I is already published in the Journal Engineering Structures.

Chapter 8 Transition to the publication II: makes a short summary of the first paper and introduces the second paper.

Chapter 9 Publication II: Curvature based DAD-method for damage localisation under consideration of measurement noise minimisation: The second paper includes the development progress of the DAD method, namely the consideration of the measurement noise effect and density of the measuring point distances. The publication II is already published in the Journal Engineering Structures.

Chapter 10 Transition to the manuscript III: makes a short summary of the second paper and introduces the third manuscript.

Chapter 11 Manuscript III: The influence of camera calibration and quality for high-precision structural deflection measurements by close-range photogrammetry: The close-range photogrammetry delivered promising results according to the findings regarding the measurement techniques. The paper contains a study about the measurement precision of close-range photogrammetry, in particular about the influence of camera calibration and quality. The manuscript III is already submitted to the Journal Measurement, however it is still not published.

Chapter 12 Transition to the manuscript IV: makes a short summary of the third manuscript and introduces the fourth manuscript.

Chapter 13 Manuscript IV: Application of the DAD method for damage localisation on an existing bridge structure using close-range UAV photogrammetry: The fourth paper contains in the first half the results from the real bridge experiment. The second half represents the investigation about the applicability of the DAD method within the conditions such as measurement precision, damage location, bridge deflection, measurement repetition etc. The manuscript IV is already submitted to the Journal Engineering Structures, however it is still not published.

Chapter 14 Conclusion and outlook: the conclusion contains the summary of the whole study and papers. It also gives recommendations about the outlook and future work.

4.4 List of papers

4.4.1 Journal papers (Q1)

1. **D. Erdenebat**, D. Waldmann, F. Scherbaum and F. N. Teferle, "Deformation Area Difference (DAD) method for condition assessment of reinforced structures", *Engineering Structures*, vol. 155, pp. 315-329, 2018
2. **D. Erdenebat**, D. Waldmann and F. N. Teferle, „Curvature based DAD-method for damage localization under consideration of measurement noise minimization", *Engineering Structures*, vol. 181, pp. 293-309, 2019
3. **D. Erdenebat**, D. Waldmann and F. N. Teferle, „ The influence of camera calibration and quality for high-precision structural deflection measurements by close-range photogrammetry", *Measurement*, submitted
4. **D. Erdenebat** and D. Waldmann, „Application of the DAD method for damage localisation on an existing bridge structure using close-range UAV photogrammetry ", *Engineering Structures*, submitted

4.4.2 Peer-reviewed conference papers

5. **D. Erdenebat**, F. Scherbaum, D. Waldmann, "Investigation of temperature-dependent stiffness variation of a layer of asphalt and their possible effect on the deformation behaviour of concrete structures", *EVACES'15, 6th International Conference on Experimental Vibration Analysis for Civil Engineering Structures*, Duebendorf, 2015
6. **D. Erdenebat**, D. Waldmann and F. N. Teferle, „Numerical investigation of bridges with the aim of condition assessment in applying the Deformation Area Difference method (DAD-method) and selecting appropriate measurement techniques", *IALCCE'16, 5th International Symposium on Life-Cycle Civil Engineering*, Delft, 2016
7. **D. Erdenebat** and D. Waldmann, "Condition assessment and damage localisation for bridges by use of the Deformation Area Difference Method (DAD-Method)", *International fib Symposium on Conceptual Design of Structures*, Cape Town, 2016

8. **D. Erdenebat**, D. Waldmann and F. N. Teferle, „Laboratory experiment for damage assessment using the DAD-method", *SMAR'17, 4th Conference on Smart Monitoring, Assessment and Rehabilitation of Civil Structures*, Zurich, 2017
9. **D. Erdenebat**, D. Waldmann and F. N. Teferle, „Static load deflection experiment on a beam for damage detection using the Deformation Area Difference Method", *IALCCE'18, 6th International Symposium on Life-Cycle Civil Engineering*, Ghent, 2018
10. D. Waldmann and **D. Erdenebat**, „ Potential of the Deformation Area Difference (DAD)-Method for Condition Assessment of Bridge Structures", *SMAR'19, 5th Conference on Smart Monitoring Assessment and Rehabilitation of Civil Structures*, Potsdam, 2019

4.4.3 Authors contributions

Paper No. 1 according to 4.4.1:

D. Erdenebat, Conceptualization, Methodology, Validation, Formal analysis, Investigation, Resources, Data curation, Writing original draft, Visualization, **D. Waldmann,** Conceptualization, Methodology, Validation, Resources, Writing review & editing, Supervision, Project administration, Funding acquisition, **F. Scherbaum,** Conceptualization, Methodology, Formal analysis, **F.N. Teferle,** Writing – review & editing.

Paper No. 2 according to 4.4.1:

D. Erdenebat, Conceptualization, Methodology, Validation, Formal analysis, Investigation, Resources, Data curation, Writing original draft, Visualization, **D. Waldmann,** Conceptualization, Methodology, Validation, Resources, Writing review & editing, Supervision, Project administration, Funding acquisition, **F.N. Teferle,** Writing – review & editing.

Paper No. 3 according to 4.4.1:

D. Erdenebat, Conceptualization, Methodology, Software, Validation, Formal analysis, Investigation, Resources, Data curation, Writing original draft, Visualization, **D. Waldmann,**

Resources, Writing review & editing, Supervision, Project administration, Funding acquisition, **F.N. Teferle,** Writing – review & editing, Supervision,

Paper No. 4 according to 4.4.1:

D. Erdenebat, Conceptualization, Methodology, Validation, Formal analysis, Investigation, Resources, Data curation, Writing original draft, Visualization, **D. Waldmann,** Conceptualization, Methodology, Validation, Resources, Writing review & editing, Supervision, Project administration, Funding acquisition.

Paper No. 5 according to 4.4.2:

D. Erdenebat, Validation, Investigation, Writing original draft, Visualization, **F. Scherbaum,** Conceptualization, Methodology, Validation, Formal analysis, Investigation, Resources, Data curation, Visualization, **D. Waldmann,** Conceptualization, Methodology, Validation, Resources, Writing review & editing, Supervision, Project administration, Funding acquisition.

Paper No. 6 according to 4.4.2:

D. Erdenebat, Conceptualization, Methodology, Validation, Formal analysis, Investigation, Resources, Data curation, Writing original draft, Visualization, **D. Waldmann,** Conceptualization, Methodology, Validation, Resources, Writing review & editing, Supervision, Project administration, Funding acquisition, **F.N. Teferle,** Writing – review & editing.

Paper No. 7 according to 4.4.2:

D. Erdenebat, Conceptualization, Methodology, Validation, Formal analysis, Investigation, Resources, Data curation, Writing original draft, Visualization, **D. Waldmann,** Conceptualization, Methodology, Validation, Resources, Writing review & editing, Supervision, Project administration, Funding acquisition, **F.N. Teferle,** Writing – review & editing.

Paper No. 8 according to 4.4.2:

D. Erdenebat, Conceptualization, Methodology, Validation, Formal analysis, Investigation, Resources, Data curation, Writing original draft, Visualization, **D. Waldmann,** Conceptualization, Methodology, Validation, Resources, Writing review & editing, Supervision, Project administration, Funding acquisition, **F.N. Teferle,** Writing – review & editing.

Paper No. 9 according to 4.4.2:

D. Erdenebat, Conceptualization, Methodology, Validation, Formal analysis, Investigation, Resources, Data curation, Writing original draft, Visualization, **D. Waldmann,** Conceptualization, Methodology, Validation, Resources, Writing review & editing, Supervision, Project administration, Funding acquisition, **F.N. Teferle,** Writing – review & editing.

Paper No. 10 according to 4.4.2:

D. Waldmann, Conceptualization, Methodology, Validation, Investigation, Resources, Writing review & editing, Supervision, Project administration, Funding acquisition, **D. Erdenebat,** Conceptualization, Methodology, Validation, Formal analysis, Investigation, Resources, Data curation, Writing original draft, Visualization.

5 Introduction

The planning of a building structure is based on a specific use. Both the intensity of the use as a design load and the values of the material properties on the resistance side are considered by means of statistical parameters. Old bridge structures were designed for much lower volume of traffic than the current traffic load, but with a great simplification of the static systems and the calculations. This compensation leads to a certain degree of load-bearing capacity reserve, which is visible due to very old constructions with still guaranteeing structural safety. However, this compensation does not always work since bridge collapses occur again and again due to overloading, material fatigue, natural disasters or also due to errors in planning and execution. Novel bridge structures are designed very precisely e.g. by modern and complex software programs, which makes the calculation more reliable but also eliminates the structural reserves due to the high level of utilisation. After the Second World War, the prestressed concrete structure as innovative construction methodology accelerated the construction of bridge structures. Although the successes in bridge engineering and ever increasing-spans were reported in the early days, bridge failures and damages are reported in recent decades [7]. Nowadays, engineers continuously produce technical innovations in relation to extravagant load-bearing structures such as bridges with increasing spans, lighter design and taller skyscrapers and towers [8]. The limited knowledge and experience of such innovative designs could lead to unknown phenomena and dangers. Essentially, the increase of total traffic on bridge structures is not decisive, but the proportion of heavy transporters. As an example, a 10 tonnes truck has 5000 times more impact on the load-bearing structure than a single ton passenger car [9]. In order to ensure the bridge safety and reliability at a higher level, there are country-specific standards and regulations such as NBIS for USA [10], DIN1076 for Germany

[11] etc. The close period of the bridge inspection in relation to the high number of existing structures makes the enormous effort and cost requirements recognisable. The reliability of the condition assessment essentially depends on the experience of the bridge inspector and the applied inspection techniques. In case of expected potential damages within the visual inspection, further procedures and techniques will be carried out. These can be e.g.: visual surface inspection, acoustical techniques such as impact-echo method, ultrasonic, infrared or thermal imaging inspection, coring resp. chipping, ground-penetration radar (GRP), half-cell potential test, endoscopy, electrical resistance measurement, testing of the water content in concrete using the calcium carbide method [12], measurement of carbonation depth, determination of chloride content, rebound hammer, chain dragging and hammer sounding, measurement of adhesive pull strength. The frequently identifying damages are: steel cracking/fatigue, pack rust, concrete cracking, concrete efflorescence, settlement, scour, superstructure traffic impact, steel section loss, steel out-of-plate (compression members), deck traffic impact (load capacity), substructure traffic impact, culvert barrel distortion etc. [13]. However, it is difficult to identify the condition of the structural components during the visual inspection as many of damages are inside the load-bearing structureand not visible. Therefore, many research projects are carried out based on dynamic and static structural analysis in order to be able to detect damages which reduces the stiffness of structures and often not visible.

The research project on condition assessment of bridge structures is in progress for many years at the University of Luxembourg and carried out within several PhD dissertations. Waltering [14] studied about damage assessment using structural dynamic behaviour based on several experimental beams and two different bridge structures in Luxembourg. Within the findings of the research project, he could determine the influence of structural damages based on eigenfrequencies, modeshapes and non-linear dynamic properties. However, he concluded that the modal properties strongly depend on the environmental conditions, which requires a permanent monitoring of a bridge structure and additionally static tests to obtain a full description of the structural behaviour.

The aim of the study of Bungard [15] was to identify changes in dynamic and static parameters due to structural changes, especially for the in-situ conditions. Within his study about bending modeshape curvature, he identified discontinuities at the position of reduced stiffness in the

numeric simulations and proposed an equation to determine the Modeshape Area Differences (MSAD) (equation (1)).

$$MSAD\ in\ \text{part i} = \left[\frac{\Delta Ai_1^2}{\Delta A_1^2} + \frac{\Delta Ai_2^2}{\Delta A_2^2} + \cdots + \frac{\Delta Ai_n^2}{\Delta A_n^2}\right] = \sum_{m=mode\ 1}^{mode\ n}\left[\frac{\Delta Ai_m^2}{\Delta A_m^2}\right] \quad (1)$$

The author shows using the results of laboratory experiments that both the static and dynamic behaviour of reinforced and prestressed concrete slabs reacts depending on the stiffness changes such as cracks, whereby more significant for the static behaviour. Furthermore, he presents the influence of environmental condition on a bridge structure using long-term monitoring about for one year. It is visible that the eigenfrequencies strongly depend on the temperature condition and the scatter of the observed damping values are relatively high. The author assumes that the main reason for the changes in eigenfrequencies comes from the temperature sensitivity of the asphalt layer. The work concludes that the detection of damages, which slightly affect the stiffness, cannot or are very difficult to detect using dynamic damage identification methods.

Mahowald [16] summarised the results and findings, which were gained within the previous projects. He focused on the evaluation of the modal parameters, on the environmental impacts and furthermore on the measurement errors. He denoted the eigenfrequencies and the flexibility matrices as most trustful damage indicators. However, the critical point should be the repeatability issues regarding the results. He tested the reproducibility of the measurement results on laboratory experiments with reinforced and prestressed concrete beams as well as on an in-situ bridge structure. The long-term monitoring of the bridge structure showed that the changes of temperatures influence the modal parameters, which do not necessarily indicate structural damages. He stated the conditional possibility of dynamic structural analysis for monitoring of bridges, but the necessity of the visual structural inspections are clearly pointed out.

Frank Scherbaum [17] focused on his work on the influence of the temperature-dependent stiffness of the asphalt layer for bridge structures. This investigation is particularly necessary for in-situ bridge experiments with dynamic or static excitations. Within the study, a reinforced concrete slab with and without asphalt layer were tested in a climatic chamber for different level of temperature and humidity. Furthermore, a long-term monitoring of bridge structure and

a test on a bridge with and without asphalt layer including successive damaging process were carried out. The results of the investigations showed that the influence of the asphalt layer can be in the double-digit percentage range depending on the temperature and the whole structural stiffness. Scherbaum provided in his work the first version of the "Deformation Area Difference (DAD)" method with the label "Flächendifferenzmethode (FDM)" based on static deflection measurements. The provided method considers the area between the reference and measured curves from deflection (equations (2) and (4)), inclination (equation (3)) and curvature (equation (4)).

$$FDM_{i,Bending} = \frac{\Delta A_{i,Bending}^2}{\sum_1^n \Delta A_{i,Bending}^2} \tag{2}$$

$$FDM_{i,Inclination} = \frac{\Delta A_{i,Inclination}^2}{\sum_1^n \Delta A_{i,Inclination}^2} \tag{3}$$

$$FDM_{i,Curvature} = \frac{\Delta A_{i,Curvature}^2}{\sum_1^n \Delta A_{i,Curvature}^2} \tag{4}$$

The inclination is determined due to the first derivation of the deflection values and the curvature due to the second derivation. The areas between the curves can be calculated using the values at each deflection measurement point. The FDM values are between each squared area normalised by the sum of the total squared area. However, the method was applied only on theoretical examples and not discussed based on real experiments.

The proposed dissertation is the continuation of the research project "Condition assessment of bridge structures" and particularly based on the static load deflection experiments for the localisation of structural stiffness influencing damage. The provided "Deformation Area Difference (DAD)" method is described in sections 7.2, 9.2 and 13.2. The DAD method requires, on the one hand, a reference system, which should consider all local stiffness influencing elements of the structure and on the other hand a high-precision deflection measurement, which is essential for the detection of smaller damage. The behaviour of the structural deflection generally depends on various factors such as normal force, bending moment, shear, creep, shrinkage, temperature, movement of support structure etc. (equation

(5)). However, the global effects such as temperature, creep, shrinkage and even the support movement have no material influence on the detection of local damages (see section 7.6.2 and 7.6.3).

$$\bar{1} * f = \int \left\{ \bar{N} \left[(1+\varphi) * \frac{N}{EA} + \alpha_T * Z + \varepsilon_S \right] + \bar{M} * \left[(1+\varphi) * \frac{M}{EI} + \frac{\alpha_T * \Delta T}{d} \right] + \bar{V} * K_Q * \frac{V}{GA} \right\} dx + \sum \bar{N}_c * \frac{N_c}{c_F} + \sum \bar{M}_c * \frac{M_c}{c_m} - \sum \bar{C}_i * \Delta S_i - \sum \bar{M}_i * \Delta\varphi_i \quad (5)$$

$\int \bar{N} * \frac{N}{EA} dx$	Normal force
$\int \varphi * \bar{N} * \frac{N}{EA} dx$	Creep due to normal force
$\int \bar{N} * \alpha_T * T \, dx$	Temperature expansion
$\int \bar{N} * \varepsilon_S \, dx$	Shrinkage
$\int \bar{M} * \frac{M}{EI} dx$	Bending moment
$\int \varphi * \bar{M} * \frac{M}{EI} dx$	Creep due to bending moment
$\int \bar{M} * \frac{\alpha_T * \Delta T}{d} dx$	Variable temperature distribution
$\int K_Q * \bar{V} * \frac{V}{GA} dx$	Shear force
$\sum \bar{N}_c * \frac{N_c}{c_F}$	Strain spring
$\sum \bar{C}_i * \Delta S_i$	Settlement of supports
$\sum \bar{M}_i * \Delta\varphi_i$	Twist of supports

In case of local damage, the location of the maximum deflection moves in the direction of the damage, but the indication of the damage is not detectable using only the deflection curve. However, the detection of stiffness influencing damage can be identified using the curvature of the structure (Figure 5.1), which corresponds to the second derivation of the deflection line (equation (25)). The main adjustment of the DAD method compared to the FDM method [17]

is done using the mathematical description (equation (27)). Namely, the determination of the area under the curve of curvature requires the calculation of the integral of curvature. The integration of the curvature curve leads to the inclination angle, which corresponds to the first derivation of the deflection value (equation (24)).

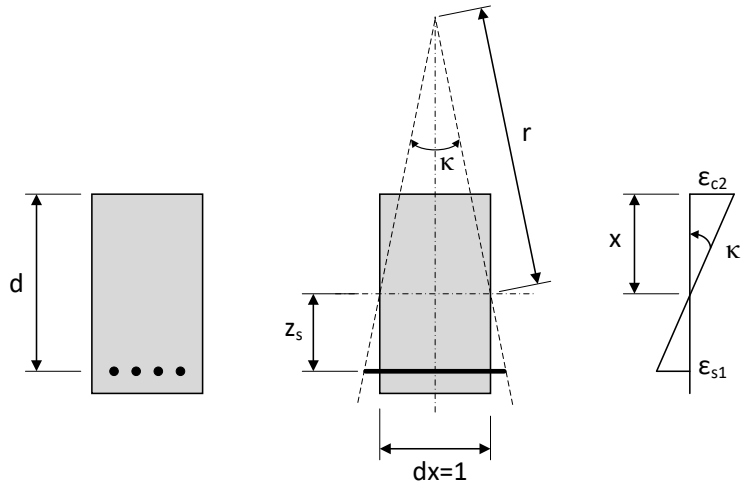

Figure 5.1. Relation between curvature and strain [18]

The application of the DAD method using the inclination angle values improves the sensitivity of the damage detection and spares the approximation step according to equation (26) with the prerequisite of small experimental deflections. The final version of the DAD method is provided in section 7.2.

As shown with equation (5), the deflection of the beam includes a part of shear deflection. The simplified modelling of the reference system commonly neglects the effect from the shear force deflection. The percentage amount of the deflection due to shear force is considered in the following. A discussion has been carried out on a static system comparable to the first laboratory beam (Figure 7.9) with the span of 3.60 m.

$$w(x) = w_{Bending}(x) + w_{shear}(x) \tag{6}$$

According to the equation (26), the second derivation of the bending line corresponds to the bending moment and stiffness relation, which is the curvature. Then, the double integration of

the curvature corresponds to the deflection line due to bending moment according to the equation (7)

$$w_{Bending}(x) = -\int \left[\int \frac{M}{EI} dx\right] dx + C_1 x + C_2 \tag{7}$$

$$w_{Shear}(x) = \int \frac{Q}{GA_s} dx + C_S \tag{8}$$

The constant of the integration for the shear is calculated for $w(x = 0) = 0$, which results in $C_S = 0$. The loading of the experimental beam took place at midspan with $x = \frac{l}{2}$ of the beam (see section 7.3). Therefore, the shear force amounts for the one span beam with a single load F at mid-span to $Q = \frac{F}{2}$. The result of the integral corresponds to $w_{Shear} = \frac{Q}{GA_S} * x$. Thus, equation (9) consists of the deflection part from bending under a point load and from the shear force.

$$w = \frac{Fl^3}{48EI} + \frac{Fl}{4GA_S} = \frac{Fl^3}{48EI} * \left(1 + \frac{12EI}{GA_S l^2}\right) \tag{9}$$

The deflection part from the shear force is the $\frac{12EI}{GA_S l^2}$ (equation (9)).The inscription of the beam cross-section of 25/20cm, Young's Modulus of E=3500 kN/m² and Shear Modulus of 1458 kN/cm², to the deflection part of shear force leads to $\frac{12*3500*25*20^3}{12*1458*25*20*360^2} = 0.0074$ [-]. In other words, the deflection part from the shear force amounts to only 0.741 % for the condition of the laboratory experiment. The DAD method should enable a non-destructive application within the serviceability limit state of a structure, which requires small experimental deflections anyway. The deflection due to shear force is therefore very low and can be neglected.

As already mentioned, the curvature of the structure depends on the stiffness (equation (25)). In case of the exact measurement of the curvature, the amount of the stiffness reduction can be calculated. The principal illustration of the DAD method using the Figure 7.1 is created for a local damage of 60 %. The elastic modulus is reduced from 35000N/mm² to 14000 N/mm². The individual values of the finite element model are given in the following:

- Cross section b/h=7.50/0.80 m (see Figure 7.2)
- Point load F=1200 kN
- Bending moment at x=7.00 m M=4200 kN/m
- Elastic modulus, undamaged E_t=35000 N/mm²
- Elastic modulus, damaged E_d=14000 N/mm²
- Damage position 6.0≤x≤8.0 m
- Degree of damage 60%
- Moment of inertia $I_t=I_d$=0.2287 m⁴
- Stiffness, undamaged EI_t=8005 MNm²
- Stiffness, damaged EI_d=3202 MNm²

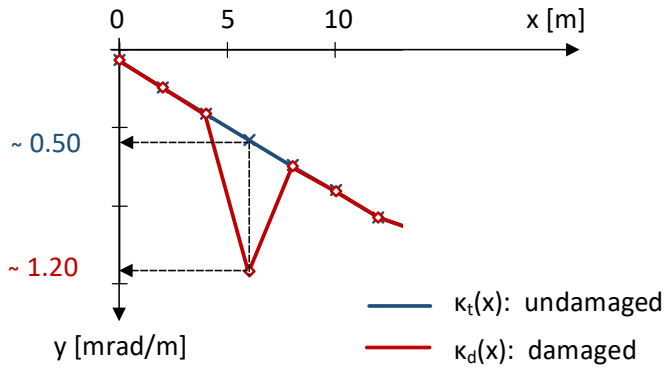

Figure 5.2. Section of the curvature curve (Figure 7.1)

The curvature values for the undamaged and damaged systems are determined due to the double derivation of the deflection curve. At the position of the damage, the curvature values amount to:

- Curvature, undamaged κ_t=0.50 mrad/m=0.00050 m^{-1}
- Curvature, damaged κ_d=1.20 mrad/m=0.00120 m^{-1}

The relationship of bending moment and curvature value allows the determination of the stiffness (equation (26)). Theoretical calculations deliver values of deflection and inclination angle, from which the curvature value can be calculated.

$$EI_t(x = 7.0m) = \frac{4.200}{0.00050} = 8400\ MNm^2$$

$$EI_d(x = 7.0m) = \frac{4.200}{0.00120} = 3500\ MNm^2$$

The determined degree of damage equals to:

$$1 - \frac{EI_d}{EI_t} = 1 - \frac{3500}{8400} = 0.583 = 58.3\%$$

The degree of damage can also be calculated from the relation between the curvature values at the position of damage:

$$1 - \frac{\kappa_t}{\kappa_d} = 1 - \frac{0.50}{1.20} = 0.583 = 58.3\%$$

The determined degree of damage nearly corresponds to the given stiffness reduction in the finite element calculation of about 60%. However, real measurements of bridge structures deliver noise affected deflection curves. The measurement noise effect increases due to the multiple derivation procedure. Therefore, the exact determination of the damage degree is not possible based on noise affected deflection values. However, the DAD method enables the localisation of the stiffness reducing damage using the curvature values.

The description of the equation (5) shows that the deformation behaviour of a structure depends on various factors. However, the deformations due to temperature, creep, shrinkage, shear force, support displacement, etc. have a global impact on the structural deflection. It is therefore possible to detect the damage by comparing the real measurement with the reference system. The DAD method is not influenced by the global deformation changes and detects damages based on a relative comparison of the measurement with the reference system.

As described in the section 7.2.1 the curvature corresponds to the second derivation of the deflection curve respectively to the relationship between bending moment and structural stiffness. The prerequisite of the deformation calculation and the assumption are based on the Bernoulli's hypothesis. This presupposes that the cross-section of the structure remains flat in the deformed state [19]. The assumption that the second derivative corresponds to the deformation of the curvature (equation (26)) applies to small deformations related to the structural span. However, the DAD values have the advantage that they are determined directly

from the inclination angle values due to the considering of the area differences. This saves the approximation step as described in section 7.2.2. Furthermore, the prerequisite for the small deformation is fulfilled anyway, since the DAD method is a non-destructive method. Within the scope of the in-situ bridge experiments, the structural deflection due to the static loading does not exceed the serviceability limit state.

Within the study, several laboratory experiments with reinforced concrete beams and a steel beam have been carried out (Figure 5.3). The post-treatment of the concrete was carried out in accordance with the standards DIN EN 13670/DIN 1045-3 [20] as well as the test of the Young's Modulus, the compression strength and the tensile splitting strength. The experimental results are presented in sections 7.3, 9.4 and 11.6. The loading of the beam was carried out using a path-controlled hydraulic press.

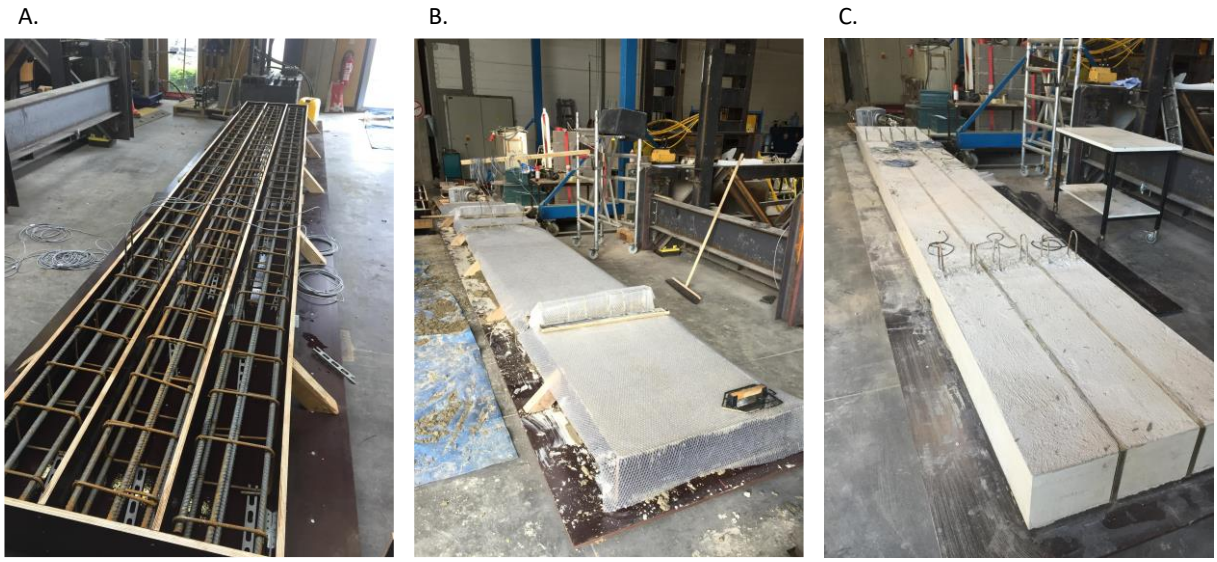

Figure 5.3. Creation of the experimental reinforced beams

The experimental reinforced concrete beams have been gradually loaded. The load steps started at the lower stage without cracks, then with cracks and finally with yielding of the reinforcements. Part A in Figure 5.4 shows the load deflection curves for the theoretical calculation of the experimental test as well as for the measured values in function of different load levels. The theoretical calculation is done using several methods such as linear calculation based on elastic theory, iterative calculation using the unit load and bending moment curvature relation, simplified calculation using rectangle compression stress distribution as well as based

on two software RSTAB and Sofistik with non-linear material behaviour. The iterative calculation using the unit load considers the stiffness of the structure due to the bending moment and curvature relation. The curvature curve changes at the crack moment and yielding of the reinforcement, which could be defined based on the condition of equilibrium according to the used concrete and reinforcement properties. The change of the stiffness and deflection are determined iteratively between the mentioned ranges. The simplified calculation was carried out using the rectangle distribution of the concrete in the compression zone compression. The inner tensile and compression forces were calculated with the help of inner lever arm z, by what the tension of the reinforcement results. The tension of the reinforcement is related to the curvature, which enables the determination of the structure stiffness. The software RSTAB bases on the beam theory, while the Sofistik bases on the finite element method. Both software are able to consider non-linear material properties. The calculations from the different methods delivered quite similar results, however the measured deflection is higher (Figure 5.4).

It is visible that the first reduction of the stiffness occurs at a load level of about 5.0 kN due to cracking of the concrete in the tensile zone and the second at about 50 kN due to yielding of the reinforcement. The failure of the beam occurred at about 58 kN, whereby theoretically at about 54 kN due to the compression failure of the concrete. The measured deflection of the beam was higher than the theoretical values, probably due to the creeping effect, stepwise loading process respectively due to loading for each step and then unloading etc.

The part B of Figure 5.4 shows the effective stiffness in relation to the different load levels. The reduction of the stiffness due to the cracking of concrete amounts to about 50 % and the yielding of the reinforcement leads to a stiffness reduction of about 80 %. The serviceability limit state is not exceed before reaching the load step of 30 kN, which was limited due to the maximum deflection of span length l divided by 250, namely l/250. The detection of the cracked areas respectively the area with the reduced stiffness could be identified using the DAD method and presented in section 7.5.2.

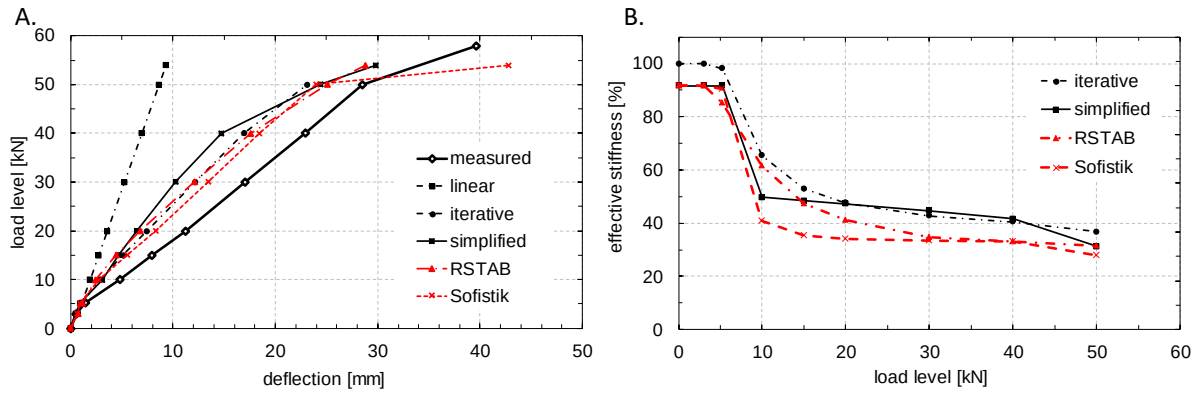

Figure 5.4. A. Load deflection behaviour B. Reduction of the effective stiffness of the experimental beam

The applied most modern techniques for the deflection measurements were levelling Leica DNA03, total station Leica TS30, laser scanner Leica P20, displacement sensors HBM and close-range photogrammetry using the software Elcovision 10. Each of the measurement techniques has its advantages as well as disadvantages and can therefore not be excluded from the start for further applications. The levelling is a reliable and easy to handle technique. The levelling delivers only values about vertical height differences, which exactly fulfil the requirement of deflection measurement. It is recommended for any load-deflection experiment on bridge structures. However, the effort considerably increases for longer bridges. The measurement is usually carried out with the help of additional staff. The total station enables automatic measurement when adhesive reflectors are used. However, the measurement accuracy reduces accordingly. The highest accuracy can be achieved by manual angle measurement from two different positions. However, the measurement effort significantly increases for the high number of measuring points along the investigated bridge. The advantage of the total station is the three-dimensional measurement results. Therefore, the total station is recommended for the measurement of reference targets when the photogrammetry is applied. The laser scanner is able to record high-density point clouds within a short time. However, the measurement accuracy depends on the surface conditions (roughness, colour etc.) and is expected to be lower than the levelling, total station, displacement sensors and photogrammetry. The displacement sensors measure uniaxial displacements with a very high frequency. The accuracy of the displacement sensors depends on the sensor length and requires a stable scaffold system. It is well suited for monitoring of structural behaviour, dynamic analysis over a period.

However, the installation of high-density measuring points along a bridge structure using displacement sensor would lead to a disproportionate effort. In comparison, the photogrammetry is simply manageable and able to deliver highly accurate deflection measurement depending on the applied software, camera and calibration. Within the first and second laboratory experiments, a full-frame camera Nikon D800 was used. The calibration of the camera has been done using a wall with a size of about 7.0x3.0 m and with 40 targets.

The second reinforced beam experiment is presented in section 9.4. The approach of the second test is comparable with the first test, so with gradually loading, stiffness reductions due to cracking, yielding of the reinforcement and due to failure of the concrete in the compression zone. The point distance of this test amounted to 10 cm while it was 25 cm for the first test. The highly dense measuring point distance allowed the additional investigation on the measuring point distance and its impact on the application of DAD method (section 9.3.3). Furthermore, the second paper (section 9) includes the development of the DAD method, which considers the smoothing of the deflection curve affected by noise due to the real measurements (see section 9.3). In order to enable the smoothing, a reference curve without noise is required. As a reference curve, the polynomial regression of a certain degree is generated using the measured deflection (section 9.3.2). The experimental beam theoretically deflects due to a point load as a polynomial function of third-degree (equation (51)) and due to the dead load as a polynomial function of fourth-degree (equation (50)), however before cracking of the concrete and within the linear elastic range. For deflection curves including reduced sections, a higher degree of polynomial regression is needed. An analysis of the required degree of polynomial regression is carried out in detail in section 11.6.

Both experiments on the reinforced concrete beam delivered successful results concerning the detection of damages. As already mentioned, the cracks in the concrete beam, yielding of the reinforcement and failure of the concrete in the compression zone have been denoted as damage. The reduction of the stiffness amounted to 50 %-80 %. The cracks were moreover distributed over the length of the experimental beam. Therefore, the implementation of the experiments was a major challenge with regard to the detection of local damages, especially for a small degree of damage. Thus, the third laboratory experiment was carried out using a steel beam with local damages at three different positions and with different degrees of damages (see section 9.4.5). The steel beam was locally damaged according to various damage scenarios,

namely from 5.2 % to 71.5 % of the bending stiffness. The achieved measurement precision of photogrammetry ranged from 0.06 mm to 0.11 mm using the calibrated full-frame camera Nikon D800 with a fixed lens of 50 mm. The local damages starting from 23.8 % were able to be detected based on the DAD method, whereby the experimental deflection did not exceed the serviceability limit state. However, the analysis about the measurement noise effect (Figure 9.30) showed that the hydraulic press influenced negatively the precision of the deflection measurement. For this reason, the following questions arose:

- Is the capacity of the photogrammetry fully used?
- To what extent a static load deflection experiment can increase the sensitivity of the DAD method?

The promising results from photogrammetry led to further investigations about the photogrammetry. The principle of the close-range photogrammetry is to reconstruct objects from two-dimensional images. In general, the two-dimensional images of the objects include hidden parts, loss of information, lack of contrast or limiting size. The determination of the three-dimensional pixel coordinate is only possible when several images of the measuring object are taken from different positions and when reference lengths or dimensions are known in the considered system. It is the so-called bundle block adjustment in the photogrammetry, which furthermore considers the viewing parameters such as camera pose, radial distortion of the lens, and location of the principal point. Furthermore, it is necessary to describe the optical process of capturing in regard to light sources, properties of the surface, the medium through which the light travels, sensor and camera technology etc., when the reconstruction of an object is carried out from photographs [21]. Figure 5.5 shows the typical accuracies of different measurement methods depending on the object size.

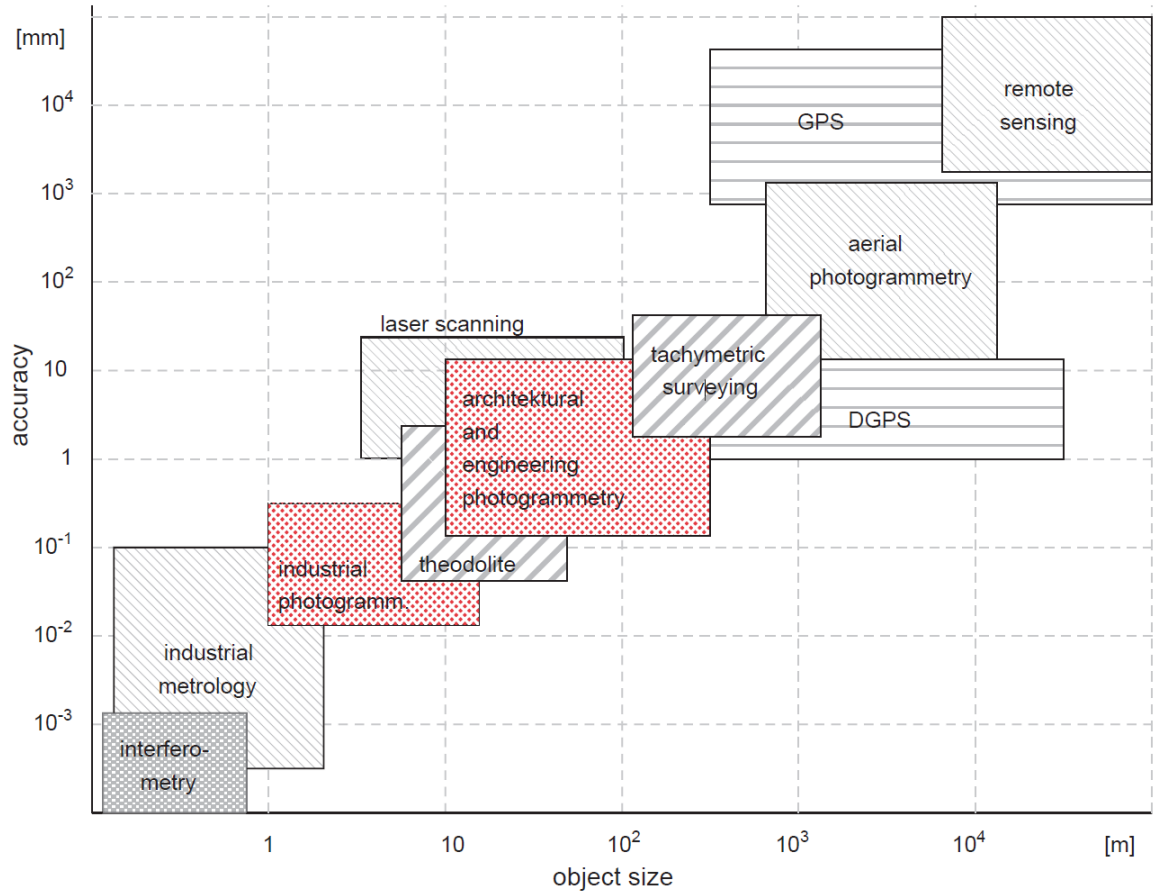

Figure 5.5. Relationship between typical object size and accuracy for different measurement methods [21]

The accuracy for the photogrammetry (Figure 5.5) approximately ranges from 0.10 mm to 10 mm in relation to the object size between 10 m and several hundred meters. The photogrammetry can be divided into multiple categories:

- Satellite photogrammetry h> circa 200 km
- Aerial photogrammetry h> circa 300 m
- Terrestrial photogrammetry from a fixed terrestrial location
- Close-range photogrammetry h< circa 300 m
- Macro photogrammetry > 1(microscope imaging)

The presenting study focuses on the close-range photogrammetry for engineering application, particularly for deflection measurement of bridge structures. The process of the close-range photogrammetry takes place based on the steps data input, calculation and output. The input

data are the measured image coordinates, control points and parameters, which are determined due to the camera calibration. The calculation process based on the bundle block adjustment. The output data are the interior and exterior orientations, three-dimensional object points, statistics and error analysis. In photogrammetry, the calibration of the applied camera is of great importance when high measurement accuracy is expected. The camera calibration aims to determine the geometric camera model, which is described by the interior orientation parameters. In principle, a camera is a spatial system with planar imaging area such as the film or the electronic sensor. In the practical application of photogrammetry, each lens of the camera generates distortion (Figure 5.6). Mathematically, the perspective centre is the point where all straight lines from all image rays pass. However, in optical projection a compound of external and internal perspective centre is to define. This is the intersection point of the optical axis with the entrance pupil EP and the exit pupil E'P. The position and the size of EP and E'P depend on the chosen aperture.

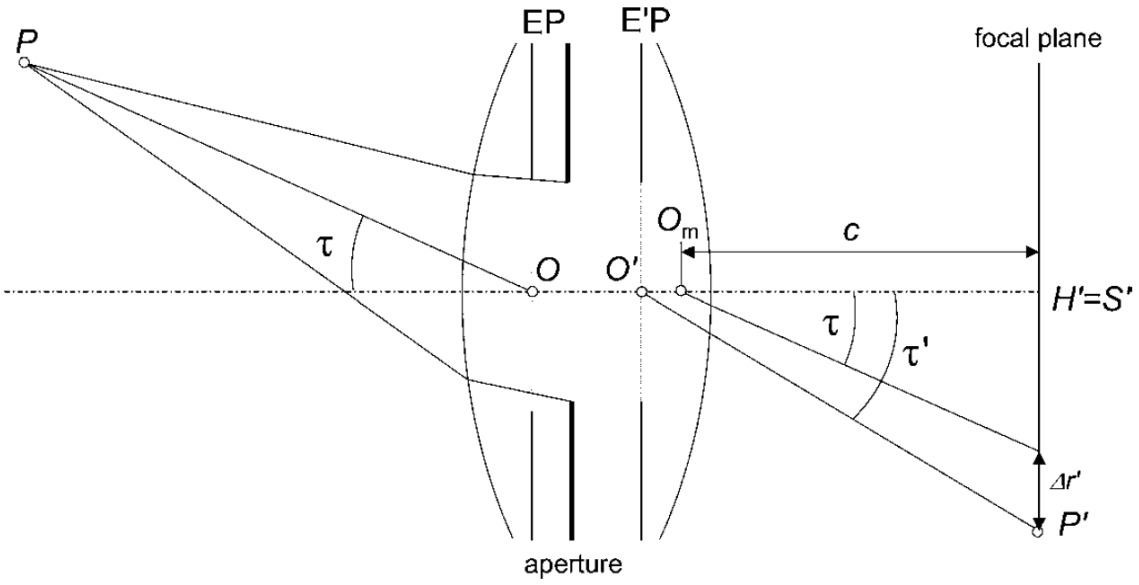

Figure 5.6. Perspective centre and principal distance (after Kraus [22])

Depending on the camera lens, there are the perspective centre O', the principal distance c and the location of the principal point H' (Figure 5.6 and Figure 5.7). Due to the principle of the central point, there are deviations of the capturing point P in the camera sensor as radial and

tangential distortion. The perspective centre for the standard cameras is approximately equal to the image centre H'≈M', which is studied and shown in Figure 11.10 using the applied cameras within the study.

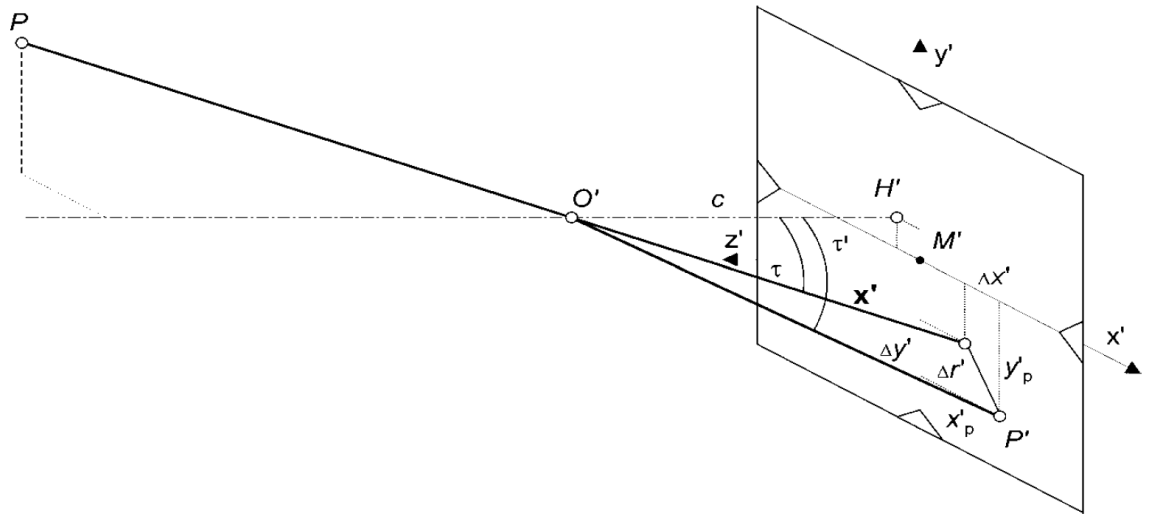

Figure 5.7. Interior orientation of a camera [21]

The focal length of the lens is approximately equal to the normal distance from the image plane to the perspective centre c≈f', when focused at infinity (Figure 5.8). The capacity of the light gathering for a lens is defined due to the relationship between the iris diameter d' of the entrance pupil EP and the focal length f.

$$relative\ aperture = \frac{d'}{f} \tag{10}$$

The ratio of the diameter of the EP to the focal length corresponds to the field of view α'.

$$\tan \alpha' = \frac{d'}{2f} \tag{11}$$

d' Iris diameter of the entrance pupil

f Focal length

α' Field of view

The 2Ω in Figure 5.8 is the format angle respectively the field angle. This is given by the maximum usable image angle related to the diagonal of the image format s' and the principal distance c. The study about the principal distance to the focal length is carried out within the research project and presented by Figure 11.12.

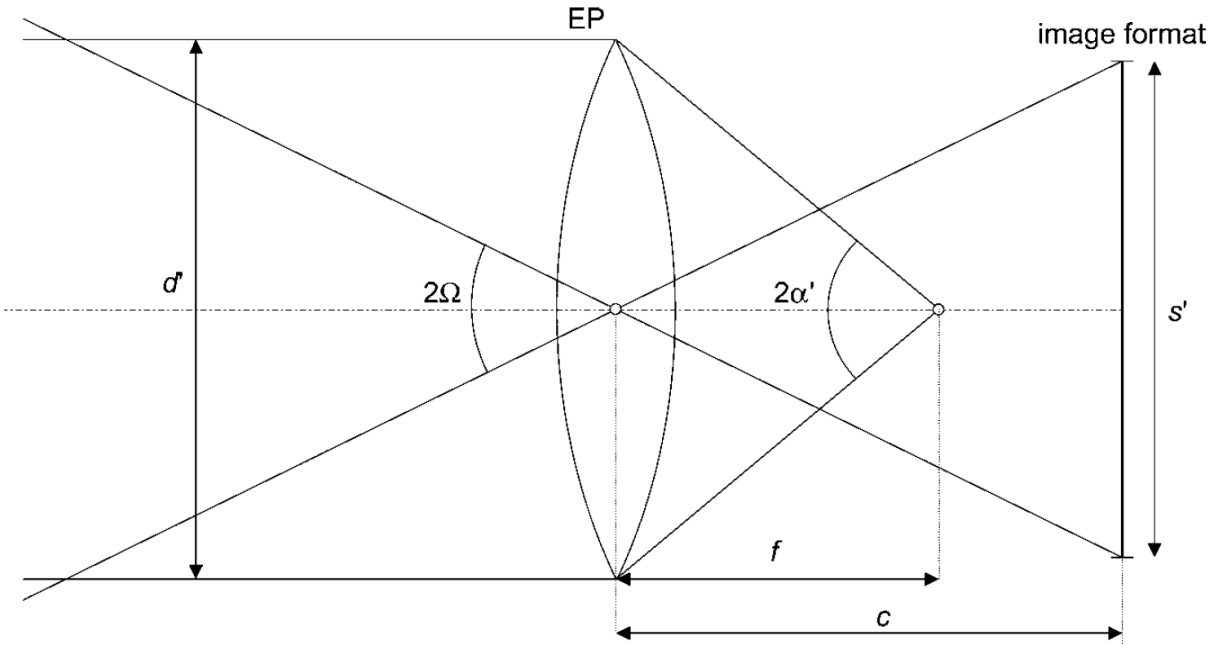

Figure 5.8. Field of view and format angle [21]

The effect of radial-symmetric distortion Δr' is the parameter describing the deviations from the central perspective (equation (12)). The results of the study regarding the investigation of radial distortion of applied cameras are presented in Figure 11.11. The analysis of the interior orientation parameters from the experiments are presented in Figure 11.13 and in Figure 11.15.

$$\Delta r' = r' - c * \tan\tau \tag{12}$$

Δr' Value of radial-symmetric distortion

r Image radius, distance from the principal point

τ Angle of incidence

In comparison, the exterior orientation consists of six parameters. The parameters describe the spatial position and the orientation of the camera coordinate system related to the object

coordinate system, as shown in Figure 5.9. The vector $\mathbf{X}_0$ defines the spatial position of the image coordinate system orientated to the perspective centre O' (equation (13)). **R** is the orthogonal rotation matrix with three independent rotations ω, φ, κ, which defines the angles in the space (equation (14)). The elements of the rotation matrix r_{ij} can also be described as algebraic variables (equation (15)).

$$\boldsymbol{X}_0 = \begin{bmatrix} X_0 \\ Y_o \\ Z_o \end{bmatrix} \tag{13}$$

$$\boldsymbol{R} = \boldsymbol{R}_\omega \boldsymbol{R}_\varphi \boldsymbol{R}_\kappa \tag{14}$$

$$\boldsymbol{R} = \begin{bmatrix} r_{11} & r_{12} & r_{13} \\ r_{21} & r_{22} & r_{23} \\ r_{31} & r_{32} & r_{33} \end{bmatrix} \tag{15}$$

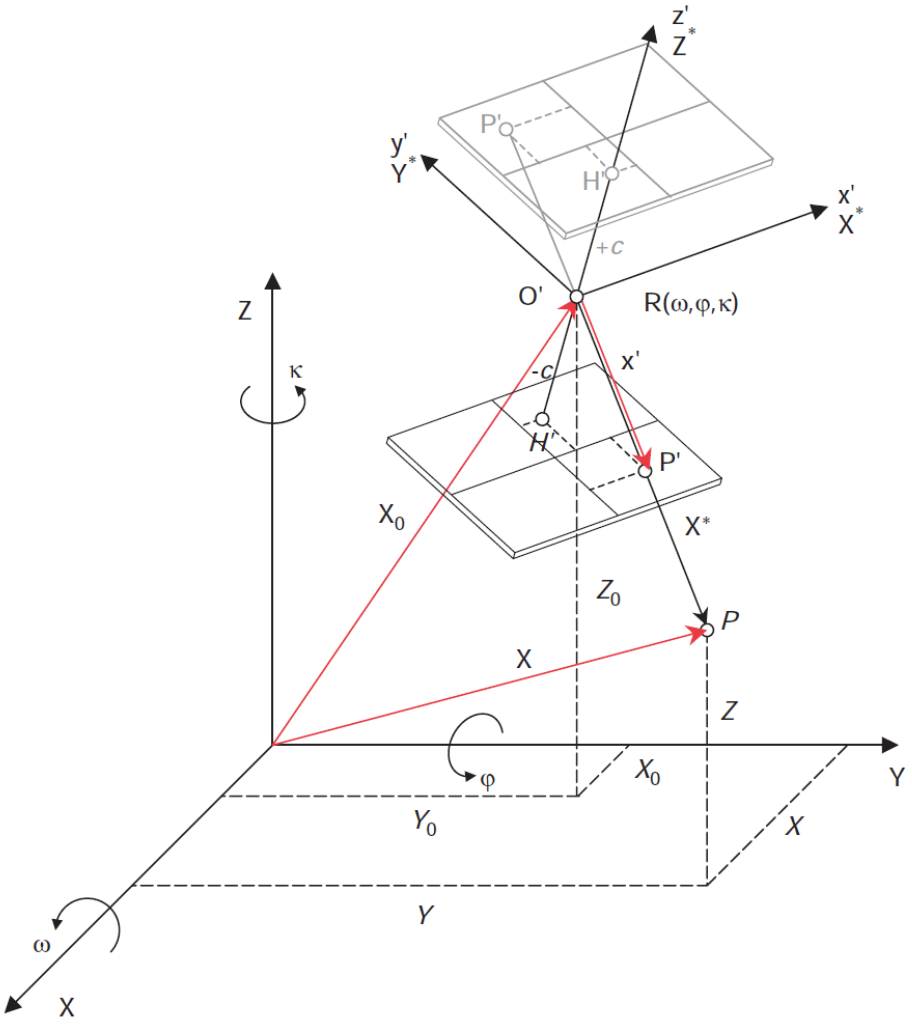

Figure 5.9. Exterior orientation and projective imaging [21]

The exterior orientation parameters of the study are presented in Figure 11.14 and in Figure 11.16.

Figure 5.10 shows the background for the focussing of the camera. In practice, the projected point is sharply observed when the circle of confusion is less than ø20 µm for photographic systems and 1 pixel for digital imaging sensors. As shown in Figure 5.10, not only the point P is sharply observed but also all points between P_1 and P_2.

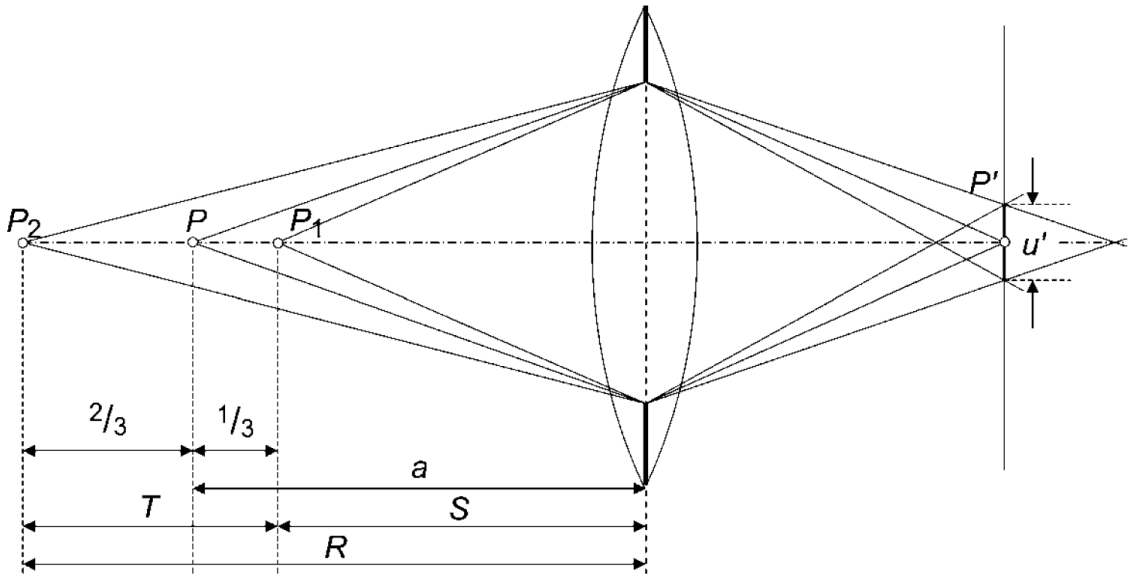

Figure 5.10. Focusing and depth of field [21]

The sharply focused range (between P_1 and P_2) can be determined as follows:

$$R = \frac{a}{1 + K} \tag{16}$$

$$S = \frac{a}{1 - K} \tag{17}$$

$$K = \frac{k(a - f)u'}{f^2} \tag{18}$$

k f-number

f focal length

a focused object distance

The defocusing circle u' is determined according to equation (19).

$$u' = \frac{S - R}{S + R} * \frac{f^2}{k(a - f)} \tag{19}$$

Finally, the depth of field can be determined as follows:

$$T = S - R = \frac{2u'k(1+\beta')}{\beta'^2 - \left(\frac{u'k}{f}\right)^2} \tag{20}$$

β’ imaging scale

The equation (20) makes it visible that the depth of field depends on the focal length, imaging distance, f-number and imaging scale when the circle of confusion diameter is given. Figure 5.11 graphically shows the depth of field as a function of the image scale number. The image scale number is the ratio between the object distance h and the principal distance c. In other words, the higher the distance to the object, the higher is the depth of field respectively the lower the focal length or principal distance the higher is the depth of field.

$$m = \frac{h}{c} \tag{21}$$

The depth of field increases when the object distance increases, however when the aperture is reduced.

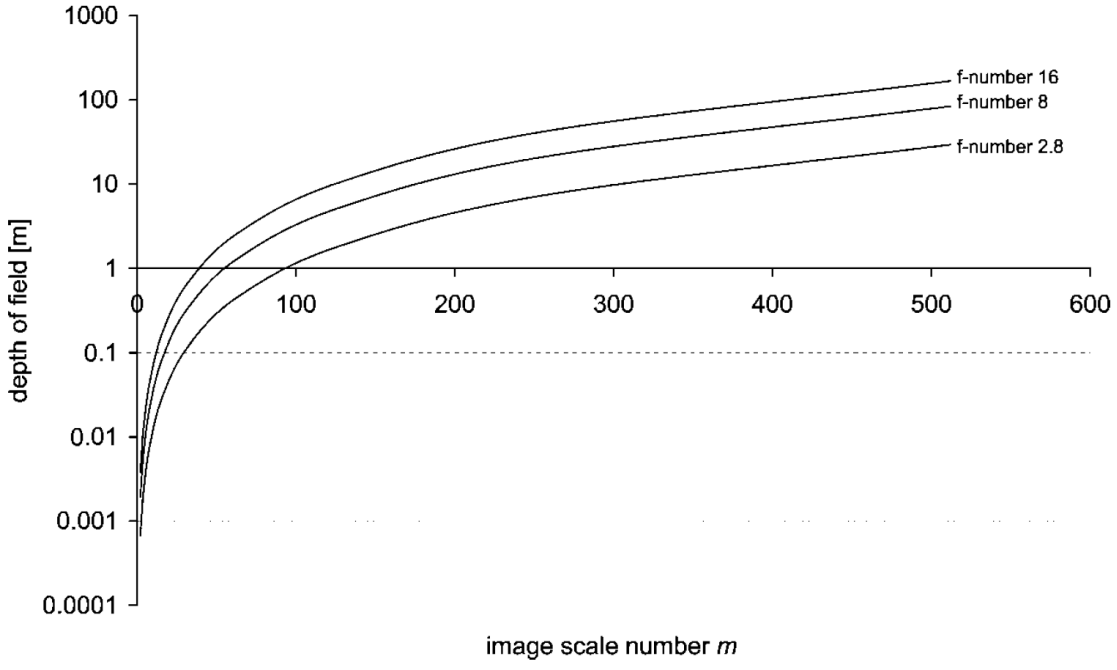

Figure 5.11. Depth of field as function of image scale number [21]

The optimal distance for focussing the applied cameras are determined within the study and shown in section 11.4.2.

The measurement of the structural deflection by close-range photogrammetry faces additional challenges as follows:

- Deflection measurement along a long structure
- Few possible positions for reference targets (e.g. at support structures)
- High requirement on the measurement precision
- Temperature difference between calibration and measurement
- High requirement on low shutter speed for application of a drone
- High range for the depth of the field for oblique captures
- Differently exposed measuring object depending on the environment
- Requirement on the durability for the measuring targets for periodical measurements
- Accessibility of the capture positions

The experiment on a bridge structure within the presenting work shows the achieved measurement precision, influence from drone flight, etc (section 13.4.1). A literature review on the structural deflection measurements and comparable projects are presented in section 11.1.

Within the study, the investigation of the close-range photogrammetry is focused on the impacts on the measurement precision, particularly concerning the increase of calibration wall size and the quality of the camera. The initial photogrammetry measurements have been carried out as mentioned above using the full-frame camera Nikon D800 with 36.8 MP and calibrated using a calibration wall with the size of about 7.00x3.00 m (see section 11.3 and 11.4). In order to improve even more the precision of close-range photogrammetry, the quality of the camera, the size of the calibration wall as well as the number of the targets for calibration have been increased.

Figure 5.12. Installation of the calibration wall in Halle d'Essais in Belval

A new calibration wall (Figure 5.12) is generated in the experimental hall in Belval with targets that can be arranged in a flexible way. The calibration wall is equipped with 163 targets on a plastic frame of 150x150 mm (Figure 5.13). The number and position of the targets can be adjusted at any time. Furthermore, there is also the option of hanging several cubes in order to generate 3D effects and thus, increase the calibration quality in the wall plane, respectively the three-dimensionality.

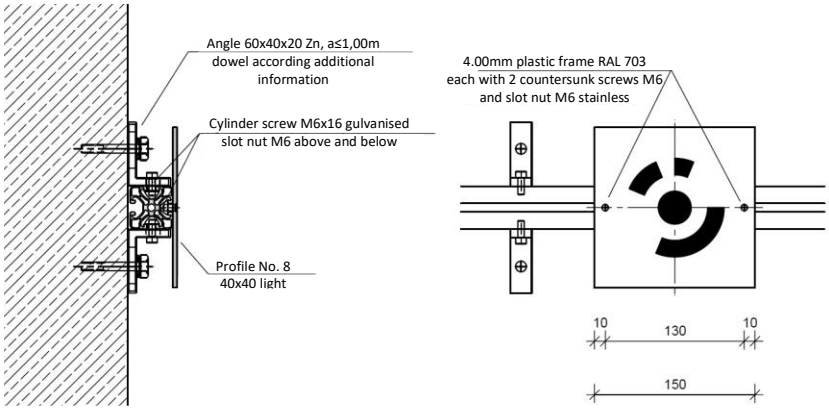

Figure 5.13. Target size and installation

In contrast to the improvement of the calibration wall, the quality of the camera has been increased to a medium format camera Fujifilm GFX50S with 51.4 MP. In order to investigate the impacts of the calibration and camera quality, additional experimental parts have been carried out. First, several series of calibrations were conducted using both cameras and both calibration walls (Figure 11.7). Second, an experiment for the measurement of structural

deflection was carried out using the last reinforced concrete beam as shown in Figure 5.3. The measurement of beam deflection was carried out for both cameras without calibration and with calibrations (Figure 11.8). The bridge structures were usually built to cross obstacles such as a river, roads, valley etc. This is the reason why the measuring of the bridge deflection along the longitudinal axis often faces challenges. Therefore, the capturing of the images for photogrammetry from a drone is proposed. However, it has to be examined firstly whether a drone can carry a large-format camera such as GFX50S and secondly whether the vibration of the flight leads to blurred images. The influence of the camera and calibration quality was done based on an additional experiment with several series of calibrations using both cameras Nikon D800 and GFX50S as well as both calibration walls with the 40 and 163 targets. A study about the influence of camera and calibration quality for measurement of structural deflection was carried out within the fourth load-deflection experiment in the laboratory (section 11.6).

Many theoretical examples with variation of the damage degree (section 7.6.1), different static systems (7.6.2), temperature effect (section 7.6.3), changing stiffness (7.6.4), laboratory examples (section 7.5.2, section 9.4.4, section 9.4.5 and section 11.6) have shown the successful application of the DAD method for localisation of stiffness reducing damages. However, the theoretical calculations and laboratory experiments represent the optimal test conditions. Theoretical calculations deliver exact values, which are not influenced by measurement precision. The setup of the laboratory experiment is optimised and has a small dimension compared to a real bridge structure. Therefore, the implementation of an in-situ bridge experiment is very important. The first real bridge experiment could be organised in cooperation with the *Administration des Ponts et Chaussées Luxembourg*. In total, there are suggested four different bridge structures in Ralingen, in Cruchten, in Altrier and Moestroff were suggested.

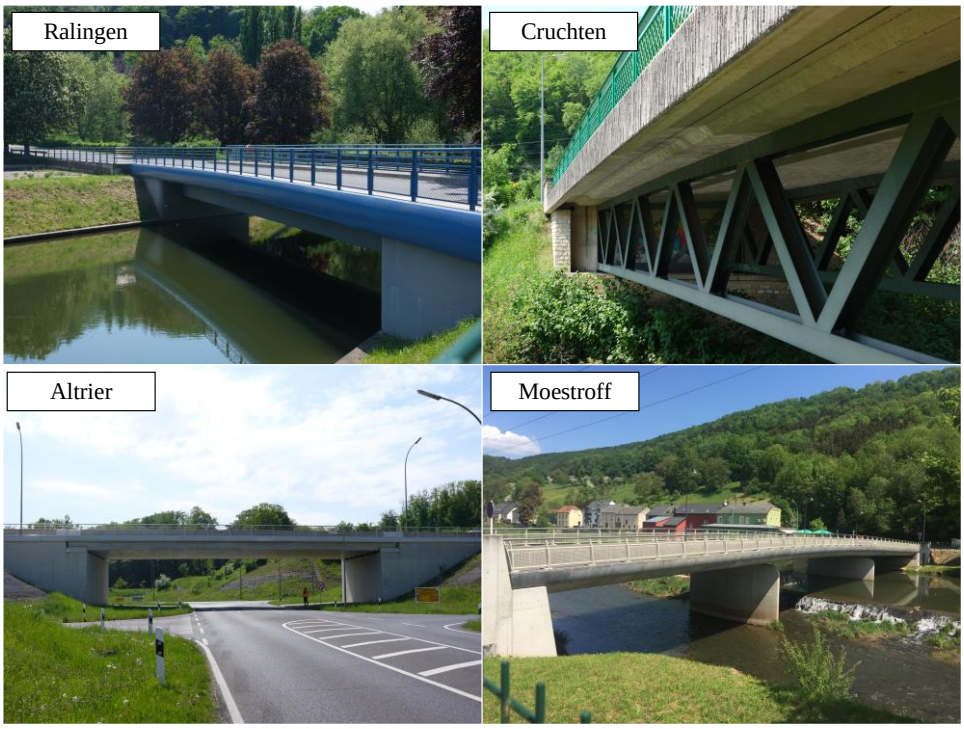

Figure 5.14. Bridges in Luxembourg to choose for the first in-situ experiment

Within the first real bridge experiment, it was attempted to find the most optimal condition in order to achieve meaningful results. The general and most important requirements are as follows:

- the deformability of the load-bearing structure
- access to the bridge in order to install several reference measurement techniques
- free space surrounding the bridge for the drone flight
- existing documents about the bridge design for the realistic reference system and to define the experimental load
- cardinal direction of the bridge because of the shadowing effect for the photogrammetry
- possibility to close the traffic

Concerning the deformability of the load-bearing structure, the bridges in Altrier and Moestroff were the most appropriate. The access to the bridges in Rosport, Cruchten and Moestroff were comparable respectively similar because of crossing over rivers. The best accessible was the bridge in Altrier because of the low height and crossing over a road. Also, regarding the existing documents, free space for the drone flight and closing the traffic, the bridge in Altrier

emphasized in comparison to the others. The setup and results of the bridge experiment are presented in detail in sections 13.3 and 13.4.

The successful application of the real bridge experiment and the findings enabled the further development of the DAD method. The bridge experiment showed the feasibility of a static load-deflection experiment within the serviceability limits state, the sufficient structural deflection for the application of the DAD method, the applicability of the measurement techniques, the achievable measurement precision and the smooth operation of a drone.

The further investigation based on the statistical analysis was carried out using the finite element model of the experimental bridge and artificial noise effect (section 13.5). The artificial noise effect is similar to the real measurement noise and normally distributed. The standard deviation of the noise can individually vary, which artificially generates a large number of experimental results. The following investigations have been carried out based on the statistical analysis in order to identify the limitation of the DAD method:

- Identifiable degree of damage (section 13.5.2)
- Required precision of the measurement technique (section 13.5.3)
- Influence of the damage position (section 13.6)
- Required amount of the structural deflection (section 13.5.3)
- Recommended number of the measurement repetition (section 13.7)

The analysis was carried out for the standard deviation of 0.01 mm to 0.09 mm, deflection size of l/600 to l/2500 and damage degree of 10 % to 90 %. The result of each combination was calculated for 30 different random noise effect. The last section of the fourth paper gives a recommendation for practitioners of the DAD method.

Figure 5.15 shows the relation between structural stiffness and the cross-section dimension such as height h, width b, elastic modulus E, degree of reinforcement ρ and the condition I and II for reinforced structures. The height of the cross-section has an influence of third degree, while the elastic modulus and the cross-section width are linearly related. The curve h is generated by the variation of the cross-section height, which is directly linked to the stiffness by $I=b*h^3/12$. The cross-section width b and the elastic modulus are in linear correlation. The diagram in Figure 5.15 is generated based on the material properties and the cross-section relation of the

reinforced concrete experimental beams. The first cracking reduces the stiffness by about 5-15 % depending on the degree of reinforcement. At this stage, the concrete is still partly supporting in the tension zone. In the condition II, after cracking of the concrete in the tensile zone, the reduced stiffness amounts to 40-60 %. In the condition II, the compression stress distribution in the concrete changes from linear to non-linear respectively from triangular stress distribution to a parabolic distribution as well as up to a complete plasticization of the concrete in the compression zone. The yielding of the reinforcement or failure of the concrete in the compression zone happens depending on the quality of the concrete and the degree of the reinforcement, which reduces the bending stiffness by around 80-90 %.

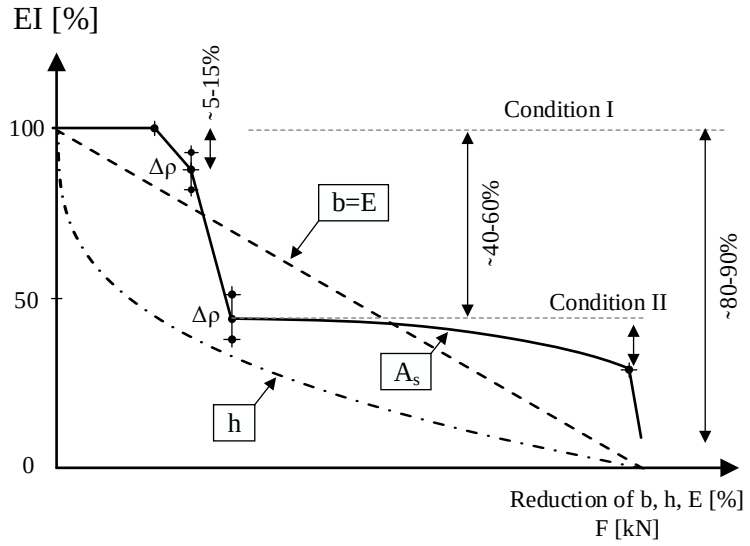

Figure 5.15. Stiffness reduction related to cross-section height, width, elastic modulus cracking, yielding of reinforcement, degree of reinforcement

As shown in Figure 5.15 the cracking of the concrete in the tensile zone leads to a significant amount of stiffness reduction. However, the reduction of the stiffness after the cracking of concrete is related to the degree of reinforcement. The lower the degree of reinforcement, the higher is the reduction of stiffness. Figure 5.16 illustrates this relationship. It is also visible that the increase of tensile reinforcement does no longer increase the stiffness of the structure beginning from a certain degree of reinforcement. According to method of μ_{Eds}, the uneconomical range starts at the μ value of 0.290 [23].

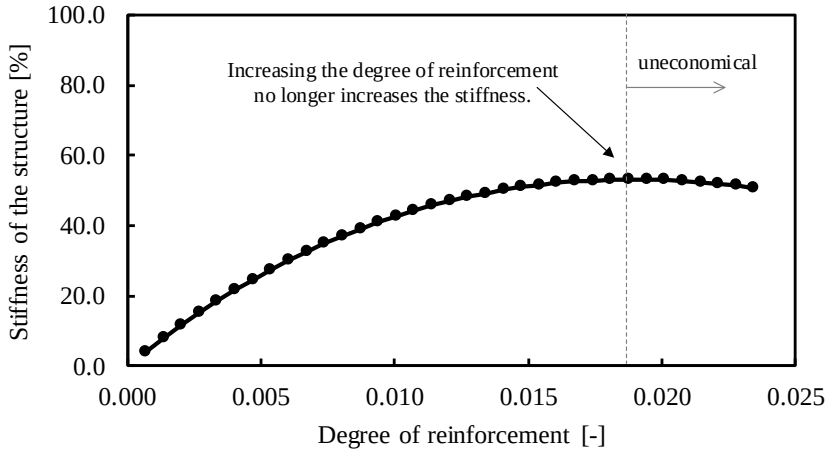

Figure 5.16. Stiffness reduction due to cracking related to the degree of reinforcement

As already mentioned, the provided dissertation mainly consists of four journal papers. However, there are additionally six peer-reviewed conference papers which have been published and which are not included in the content of this thesis (see section 4.4.2).

In comparison to the provided DAD method, there are different research projects with a similar aim of detection of damage in bridge structures. In principle, the methods can be mainly divided into methods based on dynamic excitation analysis and methods based on static loading tests. The dynamic structural responses react to damage in the structure, but the localisation of the damage faces major challenges. In general, the damage identification methods based on the dynamic analysis focus on the parameters such as natural frequencies, mode shapes, modal flexibility and damping ratio. Furthermore, the dynamic analysis is influenced by the factors e.g. the stiffness change of the asphalt layer in function of temperature variation. In comparison, structural responses from static analysis allow not only the identification of the stiffness changes but also the localisation of damages. Several research projects focus on the influence line with moving load in order to detect structural changes such as damage. There are currently no research methods which based on the structural deflection measurement along the structural length in order to identify potential damage.

The condition and damage assessment in bridge structures are categorised into four levels according to [24].

- Level 1: Identifying the presence of damage

- Level 2: Detecting the presence of damage and its location
- Level 3: Quantifying the severity of damage and its location
- Level 4: Quantifying the reserve capacity of the structure

Within the following comparison, different damage detection methods according to the level 2 with comparable prerequisites such as static loading, deflection measurements etc. are presented. The most recent research methods are presented in the following. The literature review and the review of existing methods with the aim of damage detection are presented in the introduction of the four main papers in the sections 7.1, 9.1, 11.1 and in section 13.1.

Yang et al. [25] investigated structural damages based on moving load and deflection measurements at local positions. However, the method is presented on theoretical examples with FEM calculations. The example consists of a one span beam with 35 elements and artificial damage at two positions with a damage degree between 10 % and 40 %. The research work shows the possibility of damage detection using curvature values, which are determined as shown in equation (22). The curvature values c_v^i are determined based on the deflection vectors d and the length of the structural element Δx. The authors showed the sensitivity of the damage detection depending on noise effects. While the detection of damages starting from 10 % were possible based on the exacted values of FEM calculations, the detectability decreased to 20%-30 % for a noise effect of 1 %. The authors did not mention the amount of the measurement noise effect with a unit scale and the suitable measurement technique.

$$c_v^i = \frac{d^{i+1} - 2d^i + d^{i-1}}{(\Delta x)^2} \tag{22}$$

Jang et al. [26] presents the DVL method for detection of structural damages based on static strain measurements. The method is presented on numerical simulations and an experimental test. The experiment was carried out on a three-dimensional truss structure with a moving load. The strain resolution of the applied system NI-DAQ amounts 1 micro-strain. The experiment was conducted on an undamaged structure and on a damaged structure with 40 % stiffness reduction. The detection of the stiffness reduction was hardly influenced by noise and the reliable detection of the damage was uncertain. The authors mentioned that the improvement

of the strain resolution from 1 micro-strain to 0.001 micro-strain would significantly improve the results.

The accuracy of the measurement techniques is often the challenge for various methods for localisation of structural damage. This is shown in the study of Lee and Eun [27] with the aim of damage detection using static measurement data. The method is presented on two numerical examples with local damages, different loading positions and noise contaminated displacements. First of all, the response of the structure at the intact state should be saved for the subsequent analysis as reference. The theoretical examples show that the detection of damage respectively the absolute value of stress difference (ASD) is able to be detected after a 20 % loss of the section's stiffness depending on the different noise level. The dependency of the measuring point, measurement accuracy, degree of damage for real structures are questioned.

Huseynov et al. [28] presents a bridge damage detection method using rotation measurements and experimental validation. Authors showed the results of a simply supported experimental beam with 5.4 m span, rotation measurements of uniaxial accelerometers and multiple damage scenarios. The experimental beam was equipped with four accelerometers and two axle detection systems at the both supports. The structure was loaded with a moving four-axle vehicle with the speed of 1.05 m/s. As result of the experiment, the differences between the average rotation from damaged system and the undamaged systems are shown. The sensitivity of the damage detection is strongly depending on the location of the sensors. The optimum location for the rotation measurement is the support for simply supported bridges. Authors mentioned that the rotation can be accurately measured by accelerometer. The method requires a measurement of the rotation from the undamaged state.

The most recent methods for detection of damages based on static analysis are presented. The former and existing methods are reviewed within the introduction of the main papers and presented in the sections 7.1, 9.1, 11.1 and in 13.1.

6 Introduction to the publication I

The first publication essentially consists of the introduction, description of the DAD method, description of the laboratory experiment and the applied measurement techniques, discussion of the results and additional case studies based on theoretical finite element models. The introduction gives an overview about the techniques and methods for inspection of bridge structures, the results from comparable research studies and shows the importance of an innovative method for detection of damages as a contribution to the state-of-the-art.

Within the description of the DAD method, the relationship between deflection behaviour and the stiffness of the structure becomes clear. It also shows the reason why the DAD values consider the area difference and use the first derivation of the deflection values.

The laboratory experiment consists of a reinforced concrete beam, which is gradually loaded. The cracked area in the structure increases due to the rising amount of the experimental load. The cracked area has a reduced stiffness, which was able to be identified based on the deflection measurement and the DAD method. The case studies based on the theoretical finite element models show the independence of the DAD method from global influences such as temperature, asphalt layer etc. The investigation of different static systems or beam structure with changing stiffness along the longitudinal axis has also been presented.

7 Publication I: The Deformation Area Difference (DAD) method for condition assessment of reinforced structures

Abstract

The investigation and condition assessment of bridges have a very high priority in the construction industry today. Particularly, due to the fact that many bridge structures are getting old and partly reach the end of their useful life, the control and condition assessment of bridge structures have become very important and essential. The present research work introduces an efficient new method for condition assessment called the Deformation Area Difference (DAD) Method. This new method represents an attractive alternative to visual inspection and long-term monitoring. In this paper, the new method with its theoretical background is presented and explained by means of a laboratory experiment and some additional theoretical calculation examples. The experimental investigations have been realised on a reinforced concrete beam, which has been gradually loaded until failure. For each load step, the stiffness reduction and the apparent cracking have been monitored. High-precision measurements such as close-range photogrammetry, digital levelling and displacement sensors have been used for the determination of the deflection curve. The DAD method has been applied to identify the area of the crack pattern of the laboratory experiment. Furthermore, the method is discussed with regard to the load level and the precision of the deformation measurements. On the basis of the laboratory experiment, the applicability of the DAD method for damage detection could be

proven. Furthermore, the sensitivity of the method with regard to the damage degree, the static system, the damage position and the impact of temperature variation were analysed.

Keywords <Deformation Area Difference Method; condition assessment; bridge construction; localisation of damage; inclination; curvature; deflection line>

7.1 Introduction

Owners of civil engineering structures have to ensure the load bearing capacity, safety and durability of structures under consideration of the economic efficiency. This requires regular and competent inspections of these structures, such as bridges, which are key elements of a long-term economic conservation strategy. In future years, the biggest challenge years will be to develop procedures, which allow an easy and cost-effective condition assessment of bridge structures. Many of the existing bridge structures worldwide were built using reinforced and prestressed concrete design concepts. The origins of most of the damages of reinforced or prestressed concrete structures, which lead to a stiffness reduction, occur inside of the structures. Currently the control and the condition assessment tasks are carried out by visual inspection [29] [11], leading to a detailed damage analysis if required. Today bridge structures are subjected to increasing traffic volumes while vehicles are also becoming heavier. Furthermore, with increasing age the bridges are also exposed to chemical attacks caused by, e.g., water or oil penetration [30]. Techniques such as radar detection [31], infrared thermography [32], ultra-sonic measurement [33], half-cell method [34], impact-echo method [35], chain dragging and hammer sounding [36] are suited for large-scale non-destructive investigations. The functionality of these methods is commonly similar, whereby each inspection technique is specialised for detection of certain damage types and has its own characteristics and limitations. Most of them are used for condition assessment of bridge decks, but the applicability is limited, e.g., to a certain range of temperature, to a certain depth where damage can still be localised, to a certain moisture content or due to challenging data interpretation, etc. [37]. In contrast, methods like the calcium-carbide method, endoscopy [38], rebounding hammer (Schmidt hammer) [39] or laboratory investigations are deployed to further locate and characterise an identified damage after a visual inspection of the bridge structure. Using the given inspection methods stiffness reducing damages cannot reliably be detected.

A global or local stiffness reduction such as, e.g., concrete cracking, failure of tendon or reinforcement and a deficit of tendon coupler can influence the load bearing capacity of a structure, which can be analysed by a load-deflection experiment. Several research projects are focused on the identification of stiffness reducing damages by means of dynamic and static analysis of bridge structures [40] [41] [42]. It has been proven [43] that the dynamic and static experimental data include decisive information about the stiffness reduction and the respective damages. Boumechra [44] presented in his work a new approach for damage identification for bridge structures using numerical calculations. Particularly, he took into consideration the static load deflection behaviour of two models with generated damage. The analysing factor was the deflection value at one position, but with variable position for an applied static force. Using his algorithm, he ascertained an approximate correspondence of damage detection. However, his method for damage detection requires the analysis of the initially undamaged beam, which poses a problem for existing bridge structures. A definitive and exact conclusion of the condition of a structure cannot be provided using the results of one single load deflection analysis when no reference measurements for a known reference condition are given. Stöhr et al. [45] investigated in their work the influence line of a laboratory beam and a real bridge with local damages. Thereby, an inclinometer was installed at the support, measuring the change of the inclination angle with load increase. A discontinuity in the curve of the influence line could be identified due to damage of the structure. However, by considering only the measured influence line the localisation of damage turned out to be difficult because of its unsteady curve and some noise in the measurement. The measured influence line could be used for the identification of structural damage, but the measurements were affected by noise. In their further research, it is planned to use measured static influence lines for finite element model updates in order to allow a reference-free condition assessment. Li [46] investigates the issue of damage identification of structures using optical measurements. In the extended literature review, the dynamic damage identification methods and static response data-based damage identification methods are compared. In comparison to dynamic-based identification methods, the literature of static methods is limited. Static load deflection methods often require continuous displacement measurements along the beam, which is unrealistic depending on the size of structure, on the local conditions or on the measurement techniques. Therefore, some

research develop methods such as spline interpolation or moving load analysis to generate a complete set of displacement data [47] [48].

He, et al., [49] present a damage detection method for beam structures which are loaded by a quasi-static moving load. This deflection method is based on displacement measurements where the relationship between damage parameters and displacement influence lines is investigated. The theoretical background of the method which is based on Euler-Bernoulli [50], is presented numerically and experimentally. First the localisation of the damage is achieved by using the displacement influence line (DIL). Then the damage index is quantified. The changes in the DIL point to damages whereas the damage localisation index is calculated. The damage quantification requires a certain number of displacement sensors, which should measure close to damage. The results from the calculation and from the experiment show peaks in the area of damages. However, the author mentions difficulties for damage detection due to measurement noise effects. Further corresponding damage detection methods using moving loads are presented in [51] [52] [53]. Sun, et al., [54] develop a method based on curvature to detect damages in structures such as bridges. The damage respectively the discontinuity of the curvature curve is identified by using static load deflection measurement with variable load positions. The measurement takes place using a displacement sensor at mid-span of the beam. Furthermore, they investigate the influence of measurement noise and trie to reduce noise effects. The localisation of discontinuities was possible depending on the ratio of noise and damage.

Another approach for condition assessment of bridges is given by dynamic excitation of the structures and analysis of their response. These methods need reference measurements and thus, require long-term structural health monitoring over a longer time period [55]. Therefore, a large volume of observation data has to be processed and reliably evaluated. The installation of a bridge monitoring system is often linked to the issue of establishing and guaranteeing a fixed reference point for the measurement techniques. Moreover, the dynamic data analysis requires broad experience and practice to differentiate all external influences such as environmental impacts, various traffic loads, the stiffness influencing asphalt layer [56] and temperature effects [57]. By using dynamic analysis, the global excitation of a structure is provoked, which includes all global effects of structure such as the influence of the support conditions, the

stiffness change due to temperature variation of asphalt etc. In order to identify all influencing factors, several in-situ bridge tests have been carried out. Sung et al. [58] tried to determine the initial static and dynamic behaviours using a series of experiments on a newly constructed bridge to determine its initial condition. Using the finite element model updating the evaluation of bridge safety thresholds could be defined. Tracking and monitoring of the bridge will continue into the future to make appropriate decisions in case of threshold exceedance. The further optimisation of dynamic analysis could show potentials for condition assessment of bridges, but the related efforts and time consumption should be taken into account.

Lee [59] used the ambient vibration data for the damage diagnostic of steel girder bridges. The potentially damaged member of the bridge is screened with the mode shape curvature, which is calculated from the second derivatives of the identified mode shapes. The localisation of damage was realised, but there were some false damage alarms at several locations in the screening process. With an increasing number of influencing factors on the data set, the probability of errors and ambiguous results increases.

So, it has been proven by several studies that the dynamic and static experimental data included decisive information about the stiffness reduction and respective damages. However, the fundamental problem of the condition assessment of bridges and damage detection remains the unknown initial condition of existing bridge structures as well as their sensitivity to global effects such as changes of temperature/humidity and changes of support conditions. The existing inspection techniques are specialised for certain damage types and have limited usability as well as reliability. Furthermore, the noise in the measurements of static or dynamic tests complicates a meaningful and clear condition assessment of existing bridges.

In order to solve these problems, a method, which does not depend on global effects, was developed within this research work to analyse and evaluate the remaining load-bearing capacity and reliability of existing structures. The proposed Deformation Area Difference (DAD) method requires data from a reference system this could be as well measurements from the initial condition of the structure as a numerical non-linear finite element model of the structure. The method is able to indicate all kind of stiffness reduction due to local damage of a bridge structure, independent of the degree of damage. The method is based on a simple load-

deflection experiment using a specific data processing. The DAD-method is the first method which is able to detect all kind of damage by comparing a reference state to a modified damage state, being able to identify large damaged areas as well as small local damage. Furthermore, this is the first time that the deflection line over the whole length of a structure is measured and investigated as the current methods are too sensitive to noise effects. This is different for the DAD-method when combined to innovative measurement technologies where point clouds with minimum standard deviation are generated. Using the data of the load-deflection experiment, the inclination angle and the curvature were determined, whereby the discontinuity of the structure along the longitudinal axis can be detected and localised in case of local damage-induced discontinuities. However, the inclination angle and the curvature are calculated from the first, respectively second derivation of the deflection line, which behave unsteady without a precise measurement. Therefore, to validate the method on real structural elements, laboratory experiments on a gradually loaded reinforced concrete beam have been realised and several measurement techniques were applied and compared. The damaged area of the concrete experimental beam was detected by applying the DAD-method. The applied measurement techniques were close-range photogrammetry, digital levelling, displacement sensors and strain gauges. The manuscript starts with the theoretical description of the DAD-method. Subsequently, the laboratory experiment will be presented in consideration of boundary conditions such as application of the measurement techniques, possible errors and the characteristic of the load deflection behaviour. Furthermore, the variability of each static system and the insensitivity of the DAD-method to thermal effects will be presented using numerical finite element calculations.

7.2 The Deformation Area Difference-method

7.2.1 Relation between deflection line, inclination angle, curvature and stiffness

The deflection of a structure is generally calculated according to equation (23) and consists of deflections due to bending moments, shear forces, axial forces and temperature

expansion/retraction. Therefore, it is obvious that the deflection of a structure depends on e.g. the loading, the temperature conditions, the material properties, respectively the stiffness of the structure. The control of the loading and the measurement of the deflection and temperature conditions allow to calculate the real stiffness of the structure. Considering bridge structures, the deflection due to shear is generally small compared to the deflection due to bending. Furthermore, the temperature conditions have a global influence on the deformation behaviour of bridge structures and will not impact the deflection line locally.

$$w(x) = \int_0^l \frac{M}{EI}\bar{M}dx + \int_0^l \frac{V}{GA_V}\bar{V}dx + \int_0^l \frac{N}{EA}\bar{N}dx + \int_0^l \frac{T_u - T_o}{h}\alpha_T\bar{M}dx + \int_0^l T_S\alpha_T\bar{N}dx \tag{23}$$

w Deflection

M Bending moment

V Shear force

N Axial force

EI Bending stiffness

GA_V Shear stiffness

EA Axial stiffness

T_u Temperature at lower edge

T_o Temperature at upper edge

α_T Coefficient of thermal expansion

T_S Temperature along the longitudinal axis

The first derivation of the deflection line (equation (24)) enables the calculation of the inclination angle:

$$w'(x) = \frac{\delta w(x)}{\delta(x)} = \varphi(x) \tag{24}$$

φ inclination angle

The value of the inclination continually changes along the longitudinal axis of the structure if there is no change in stiffness. The second derivation of the deflection line allows computing the curvature, which depends on the stiffness and the bending moment of the considered static system (equation (25)). The term in the denominator $\sqrt{[1 + w'(x)^2]^3}$ amounts to almost 1 for small deflection values. So, for the given application, a real bridge loaded at serviceability limit state, the prerequisite to make this simplification is fulfilled. On the other side, the curvature can also be calculated from the relation of the strain states of reinforcement and concrete (equation (26)).

$$k(x) = \frac{-w"(x)}{\sqrt{[1 + w'(x)^2]^3}} = \frac{M(x)}{EI(x)} \tag{25}$$

$$k(x) \approx -w"(x) = \frac{1}{r} = \frac{-\varepsilon_{c2}}{x} = \frac{\varepsilon_{s1} - \varepsilon_{c2}}{d} = \frac{\varepsilon_{s1}}{d - x} = \frac{M(x)}{EI(x)} \tag{26}$$

κ Curvature

εc2 Compressive strain of concrete

εs1 Tensile strain of steel reinforcement

h Height of the cross-section

r Curvature radius

x Height of the concrete compression zone

d Static height

7.2.2 The principles of the DAD-method

The deflection curve of a structure, which has been measured during a static loading test, depends on the stiffness of the structure. Unfortunately, this curve is also influenced by global effects such as the boundary conditions at support or the temperature conditions. Especially the condition of non-structural layers such as the asphalt layer could lead to a huge impact: with changing thermal conditions, the stiffness of the asphalt layer changes considerably and thus, influences the global deflection behaviour of the structure. In case of an assessment of the structure by comparison to reference measurements of the initially intact structures no clear analysis can be done. To avoid this problem of global effects, the analysis of the structure must be done locally by identifying discontinuities. Therefore, the DAD-method has been developed. It provides the capability to detect and localise a stiffness reducing damage without the need of an exact reference measurement of the structure in undamaged condition. However, a theoretical model of the structure is needed as reference system. The theoretical background of the DAD-method will be explained in the following by using an example: a finite element calculation of a 30 m long bridge using the software SOFiSTiK (Figure 7.1 and Figure 7.2). The structure is modelled as a single span bridge and loaded at the middle of the span. The chosen loading of 1200 kN corresponds to two trucks each weighting 600 kN. In this case a linear calculation is performed with concrete type C40/50. The FE-mesh corresponds to an equivalent density of the measurement points of the deflection line (Figure 7.3). The curves of the deflection, the inclination angle and the curvature at an undamaged state (blue line) and at a damaged state (red line) are represented in Figure 7.1. When applying the method on real structures, the curves of the damaged state would correspond to experimentally measured values. Here, the damage is simulated by a reduction of the bending stiffness of the section at a quarter of the beam length by about 60 % what is realised within the model by a reduction of the Young's Modulus of 60%. The large stiffness reduction is chosen in order to clearly present the method. However, an example with very small damage will be presented in chapter 7.6.1. As a result of the locally reduced bending stiffness, a higher deflection and a re-localisation of the maximum deflection towards the location of damage can be identified. However, the maximum deflection is not located at the exact position of the damage. In order to detect a local discontinuity, the measured curves of the deflection line, the inclination angle and the curvature

are compared to the expected theoretical curves. The damaged system shows a kink point in the inclination angle curve, respectively a considerable peak in the curvature curve (Figure 7.1). However, a precise interpretation and an accurate reproduction of these curves requires a high number of measurement points. Furthermore, the detection is influenced by the degree of damage. The curves of the deflection, the inclination angle and the curvature do not allow to detect small damages associated with a small reduction of the bending stiffness. In this case, the curves for the damaged and undamaged state are approximately superposed (section 7.6.1).

For the application of the DAD-method and the calculation of the DAD-values, the area between the undamaged and damaged curves is considered (blue area in Figure 7.1). The undamaged curves of a reference system can be taken from an initial measurement or from a numerical model. In principle, the total area between the undamaged and damaged curves are divided in a number of the finite mesh units accordingly to the measurement grid (ΔAi in Figure 7.1). The DAD-value is the square of each area $\Delta Ai2$ divided by the square of the total area $\Sigma\Delta As2$ (equation (27)). The squaring of the values allows to increase the damage detection sensitivity and the detection of still smallest discontinuities. The reduction of global effects such as global stiffness variations or thermal influences is enabled through the normalization of each area $\Delta Ai2$ by dividing it by the sum of total area differences $\Sigma\Delta As2$.

The basic precondition of the method is a load-deflection experiment on a real structure with high precision measurements of the deflection line. This is particularly important if the curve of the curvature will be used to detect and localise a damage as it is calculated from the second derivative of the deflection line. Therefore, a poor recording of the measurements leads to increased noise in the curve of the curvature.

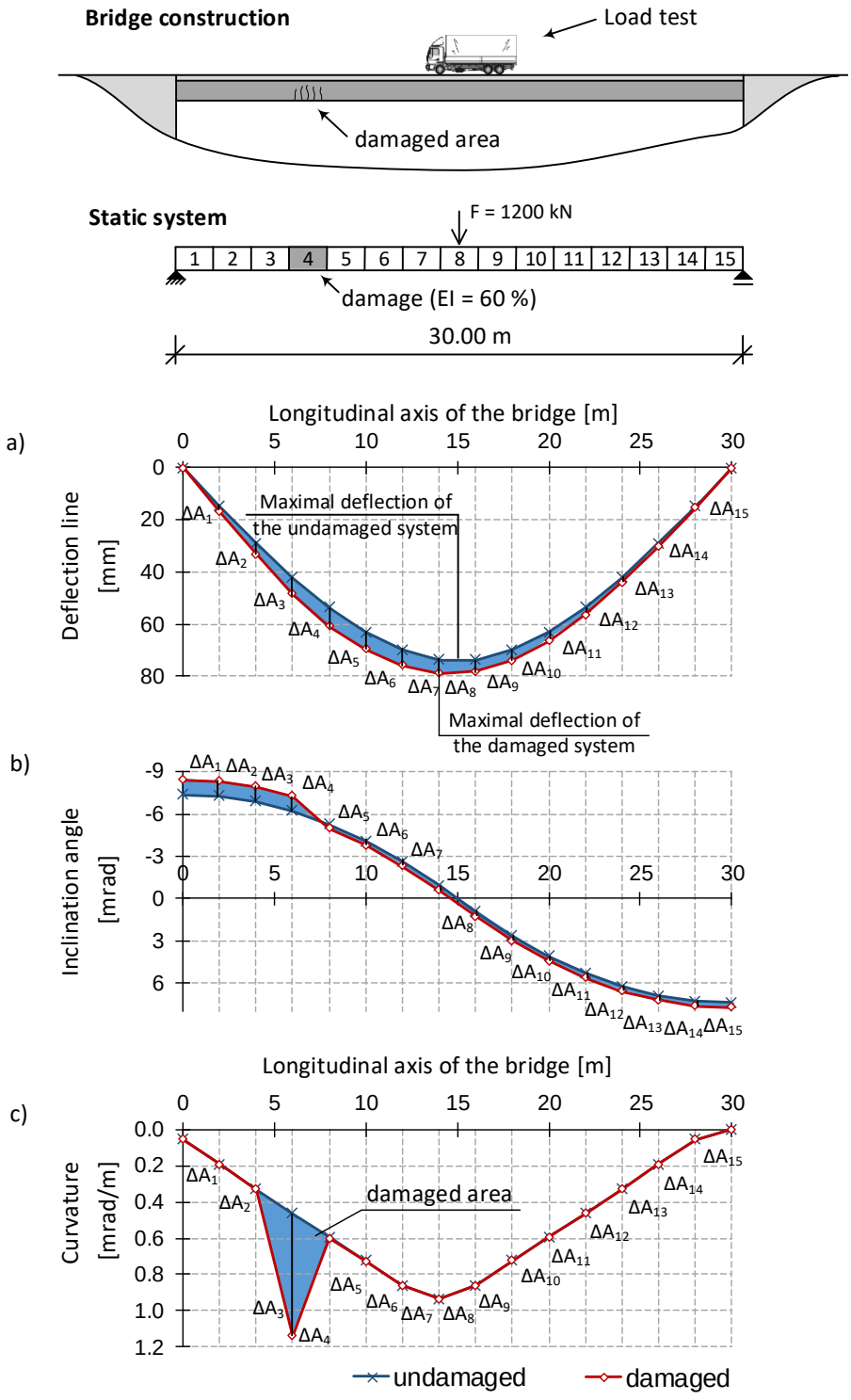

Figure 7.1. Principle of DAD-Method: a) deflection line, b) angle of inclination and c) curvature over the length of the single-span bridge [60]

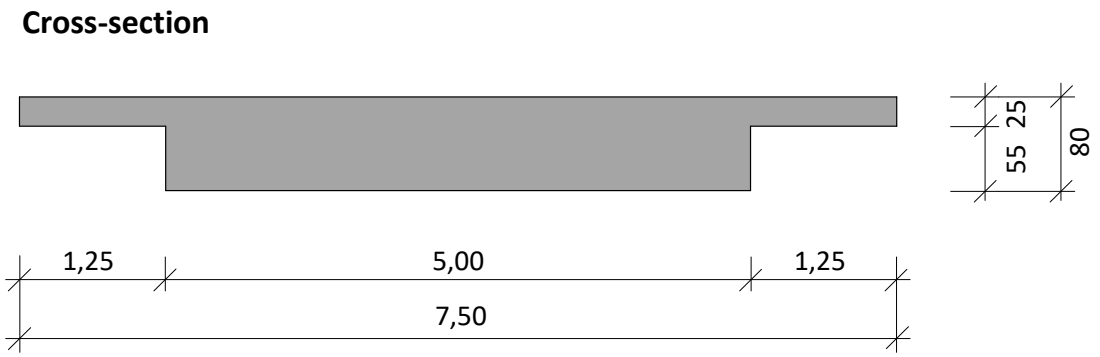

Figure 7.2. Cross-section of the bridge example

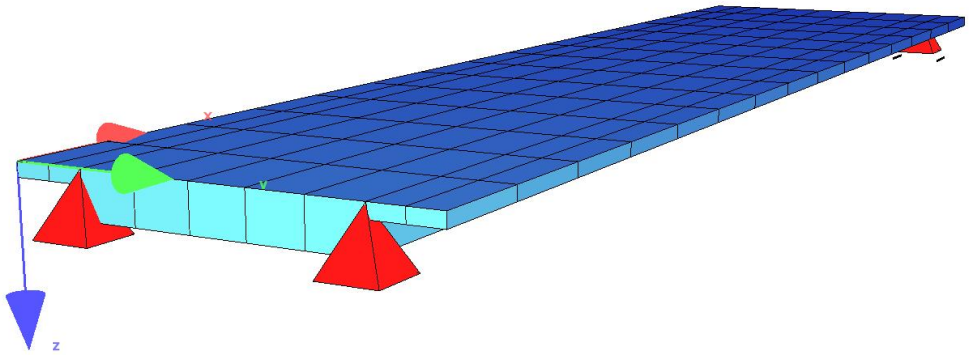

Figure 7.3. FE-model of the bridge example

Possible stiffness irregularities of the undamaged structure are part of a measured reference system and must also be considered in case of modelling the reference system so that the localisation of discontinuities can only be attributed to damage. A case study which takes into account a planned stiffness change is carried out in section 7.6.4.

In equation (27) the general formula of the DAD-values is given. The DAD-values are the squared values of the area difference between the curves of deflection line, inclination angle and curvature generated with the analysed structure state and the respective curves generated with the undamaged reference system. The explicit description of the equation for deflection, inclination and curvature are given in equation (31), (32) and (33). All individual steps for the calculation of the different area values are explained in detail in the following.

$$DAD_i(x) = \frac{\left[\int_{i-1}^{i} f_{d,i}(x)dx - \int_{i-1}^{i} f_{t,i}(x)dx\right]^2}{\sum_{i=1}^{n}\left[\int_{i-1}^{i} f_{d,i}(x)dx - \int_{i-1}^{i} f_{t,i}(x)dx\right]^2} = \frac{\Delta A_i^2}{\sum_{i=1}^{n}\Delta A_i^2} \quad (27)$$

DAD Deformation Area Difference value

f_d Function (deflection, inclination or curvature) of the damaged curve

f_t Function (deflection, inclination or curvature) of the theoretical, undamaged curve

ΔA_i^2 Area difference from section i

$\sum_1^n \Delta A_i^2$ Total area difference over the whole structure length

To calculate the curves of the inclination angle and the curvature, the coordinates of the calculated and measured deflection line are required. The derivation of the deflection line can be calculated by using the equations (24) and (26) (Figure 7.4).

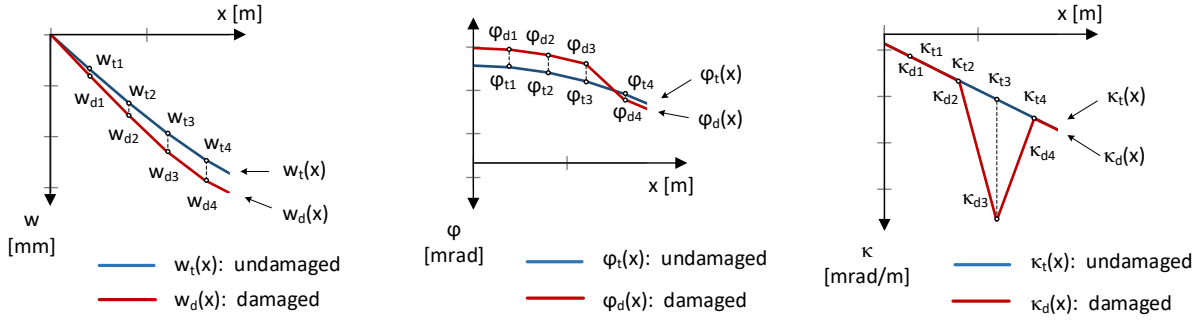

Figure 7.4. Individual values from the deflection line, the inclination angle and the curvature

As already mentioned, the DAD-values will be determined by the area differences between the damaged and the undamaged curves. The area difference of the deflection lines can be directly calculated by using the measured values (Figure 7.4 and equation (28)). The area difference within the inclination angle diagram is the integral of the function the inclination function φ(x) (equation (29)) respectively the area difference within curvature diagram is the integral of the curvature function κ(x) (equation (30)). According to the relation between the deflection line and the inclination angle as well as according to the relation between the inclination angle and the curvature (equations (24) and (26)), the respective subtraction of the integral functions are

carried out. Therefore, considering the inclination angle, the area difference between the two curves is calculated by the subtraction of the integral functions between damaged and undamaged curves (equation (29)). Based on the relation between the deflection line and the inclination angle (equation (24)), it becomes evident that the area difference of the two curves of the inclination angle can be calculated directly from the deflection values (equation (29)). The same applies to the area difference of curvature curves. The derivation of the inclination angle corresponds to the curvature according to equation (26). Therefore, it can also be calculated directly from the inclination angle values (equation (30)). Thus, the double derivation of the deflection line is not needed anymore for the determination of the DAD-values from curvature, which reduces the noise related to multiple derivations.

$$\sum_{i=1}^{n} \Delta A_{w,i}^2 = \sum_{i=1}^{n} \left[\int_{i-1}^{i} w_{d,i}(x)dx - \int_{i-1}^{i} w_{t,i}(x)dx \right]^2 = \sum_{i=1}^{n} \left[\frac{(x_i - x_{i-1})(w_d(x_i) - w_t(x_i) - w_t(x_{i-1}) + w_d(x_{i-1}))}{2} \right]^2 \quad (28)$$

$$\sum_{i=1}^{n} \Delta A_{\varphi,i}^2 = \sum_{i=1}^{n} \left[\int_{i-1}^{i} \varphi_{d,i}(x)dx - \int_{i-1}^{i} \varphi_t(x)dx \right]^2 = \sum_{i=1}^{n} [w_d(x_i) - w_d(x_{i-1}) - w_t(x_i) + w_t(x_{i-1})]^2 \quad (29)$$

$$\sum_{i=1}^{n} \Delta A_{\kappa,i}^2 = \sum_{i=1}^{n} \left[\int_{i-1}^{i} k_{d,i}(x)dx - \int_{i-1}^{i} k_t(x)dx \right]^2 = \sum_{i=1}^{n} [\varphi_d(x_i) - \varphi_d(x_{i-1}) - \varphi_t(x_i) + \varphi_t(x_{i-1})]^2 \quad (30)$$

Then the DAD-values can be determined as described in equation (27) by using the equations (28) to (30) for the determination of the DAD-value of the deflection line (equation (31)), for

the determination of the DAD-value of the inclination angle (equation (32)) and for the determination of the DAD-value of the curvature (equation (33))

$$DAD_{w,i}(x) = \frac{\Delta A_{w,i}^2}{\sum_{i=1}^{n} \Delta A_{w,i}^2} = \frac{[w_d(x_i) - w_t(x_i) - w_t(x_{i-1}) + w_d(x_{i-1})]^2}{\sum_{i=1}^{n} [w_d(x_i) - w_t(x_i) - w_t(x_{i-1}) + w_d(x_{i-1})]^2} \quad (31)$$

$$DAD_{\varphi,i}(x) = \frac{\Delta A_{\varphi,i}^2}{\sum_{i=1}^{n} \Delta A_{\varphi,i}^2} = \frac{[w_d(x_i) - w_d(x_{i-1}) - w_t(x_i) + w_t(x_{i-1})]^2}{\sum_{i=1}^{n} [w_d(x_i) - w_d(x_{i-1}) - w_t(x_i) + w_t(x_{i-1})]^2} \quad (32)$$

$$DAD_{\kappa,i}(x) = \frac{\Delta A_{\kappa,i}^2}{\sum_{i=1}^{n} \Delta A_{\kappa,i}^2} = \frac{[\varphi_d(x_i) - \varphi_d(x_{i-1}) - \varphi_t(x_i) + \varphi_t(x_{i-1})]^2}{\sum_{i=1}^{n} [\varphi_d(x_i) - \varphi_d(x_{i-1}) - \varphi_t(x_i) + \varphi_t(x_{i-1})]^2} \quad (33)$$

$DAD_{w,i}$ Area difference value from section i resulting from the deflection line

$\Delta A_{w,i}^2$ Area difference of the segment i between the studied deflection lines

$\sum_1^n \Delta A_{w,i}^2$ Total area difference enclosed by the studied deflection lines over the whole structural length

$DAD_{\varphi,i}$ Area difference value from section i resulting from inclination angle

$\Delta A_{\varphi,i}^2$ Area difference of the segment i between the observed inclinations

$\sum_1^n \Delta A_{\varphi,i}^2$ Total area difference enclosed by the studied inclinations over the whole structural length

$DAD_{\kappa,i}$ Area difference value from section i resulting from curvature

$\Delta A_{\kappa,i}^2$ Area difference of the segment i between the studied curvatures

$\sum_1^n \Delta A_{\kappa,i}^2$ Total area difference enclosed by the studied curvatures over the whole structural length

In the following, Figure 7.5 shows the calculated DAD-values for the structure given in Figure 7.1. Concerning the DAD-values from the deflection curves, the curve has the tendency to move towards the damaged area (Figure 7.5 a.). However, the most interesting information about the local damage can be taken out of the last two diagrams namely the DAD-values from inclination

angle (Figure 7.5 b.) and curvature (Figure 7.5 c.). Particularly, the DAD-value from curvature highlights the exact position of the damage. Thus, the DAD-method allows a reliable recognition of the damages in these cases.

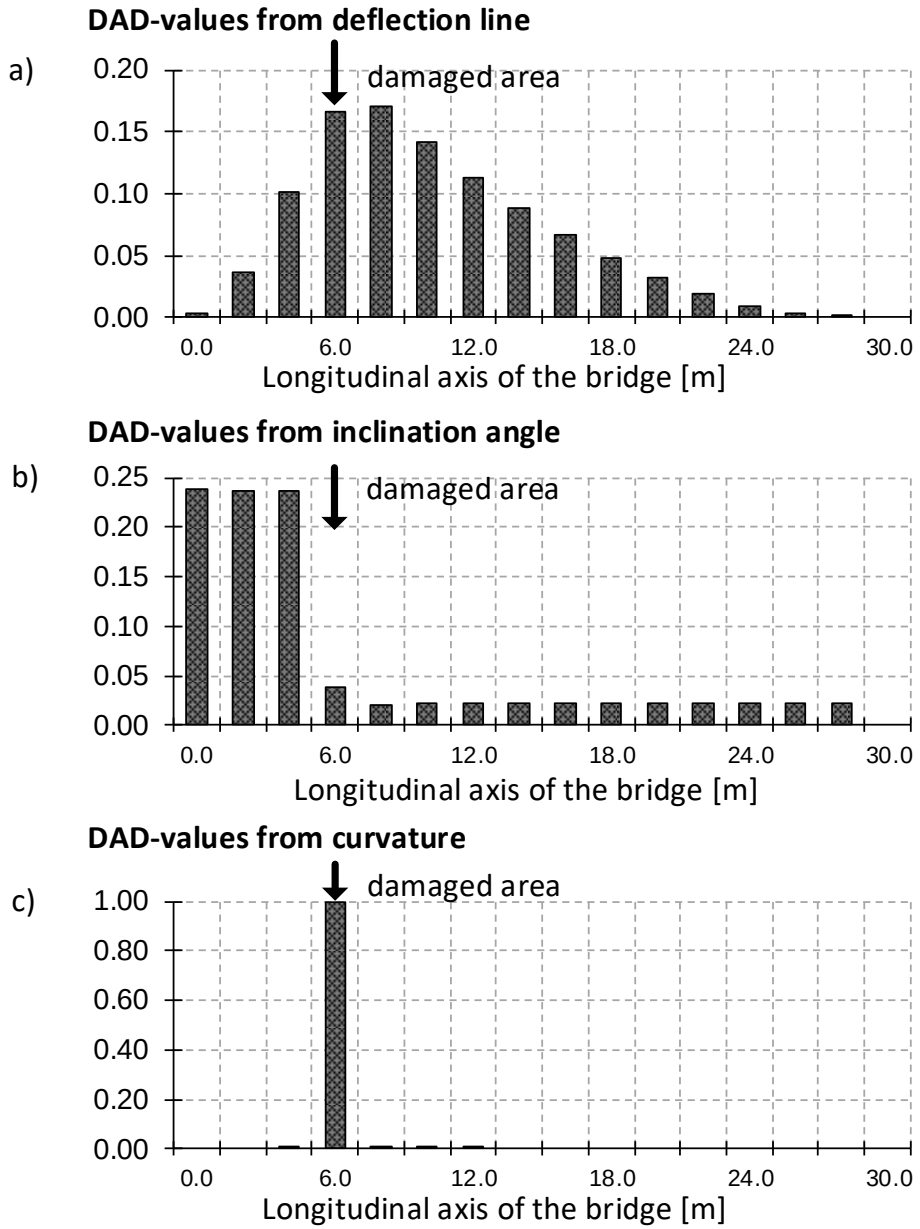

Figure 7.5. DAD-values computed from the deflection line, the inclination angle and the curvature exemplified on a single-span bridge [60]

7.3 Description of the laboratory experiment

The applicability of the DAD-Method for condition assessment on a real structure was studied on an experimental beam in the laboratory. The beam consisted of reinforced concrete with a span length of 3,60 m (Figure 7.6). The materials used were concrete class C40/50 and reinforcement of type B500B (Figure 7.7). The loading of the beam was applied in the middle of the span length and was gradually increased. In total 9 load steps were performed, each one was carried out twice (Table 1). The duration of each loading amounts about two hours with path controlled loading. This duration was set to allow the measurement of the deflection and to control the creep effects of the reinforced beam. The plasticity of the beam was controlled by means of repetition of the load steps. The loading started at state I without cracking at 3,0 kN and is increased gradually with growth of the crack pattern (Table 1). The loading of the beam finished with the failure of concrete in the compression zone at 58,0 kN. The detection of cracks was carried out by visual inspection for each load step. The main objective of the experiment is to identify the area with reduced stiffness (crack pattern) using the DAD-values, which will be compared to the visually detected cracks. However, as already explained, the application of the DAD-method requires precise identification and localisation of damage using deflection measurements of high accuracy. Therefore, in the following several modern measurement techniques were applied and investigated regarding their accuracy and usability.

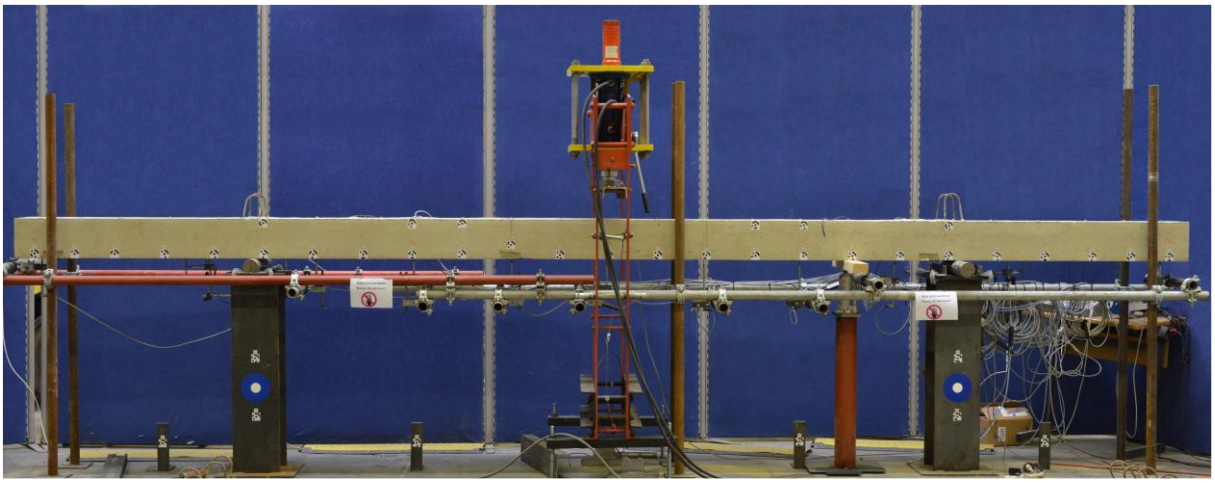

Figure 7.6. Laboratory experiment with the reinforced concrete beam [60]

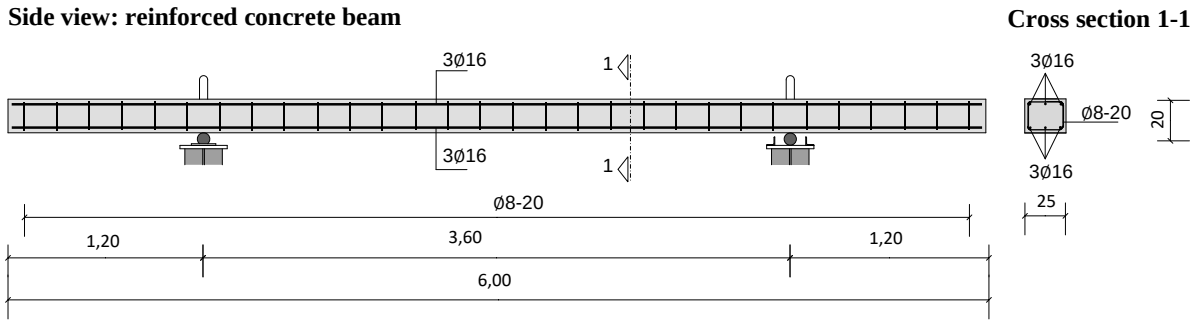

Figure 7.7. Reinforcement of the laboratory beam [60]

7.3.1 Load-deflection behaviour of the laboratory beam

The measured load-deflection behaviour of the laboratory beam is investigated and compared to a FE-analysis (Figure 7.8). The finite element model of the laboratory beam consists of a non-linear calculation also in consideration of non-linear material behaviour. The mesh size of the line-type model amounts 10 cm in longitudinal axis. With increasing loading, the reinforced concrete beam suffers different stiffness reductions due to the formation of cracks. The first load step of 3,0 kN was chosen to remain in an un-cracked state and did not generate any cracking. The second load step of 5,23 kN corresponded to the theoretical load of the expected first crack. The load steps from 10,0 kN to 40,0 kN generated a range of successive crack formation (Table 1 and Figure 7.8). In Table 1 and Figure 7.8, the load–deflection behaviour at state I represents the linear, undamaged condition of the beam without crack whereas the load–deflection behaviour at state II reflects the non-linear, cracked condition of the beam without contribution of concrete in tension between the cracks. Each load increase lead to the development of additional cracks, whereby the area with reduced stiffness in longitudinal direction of the beam increased. The successive cracking at state II considerably reduced the stiffness of the reinforced concrete beam. Generally, depending on the reinforcement content, the material properties and the dimensions of the cross section, the reduction of stiffness ranges between 30 % and 80 % [61] [62]. For the experimental beam, the cracking of the concrete in the tensile zone reduced the stiffness by about 50 %. This stiffness reduction has been calculated with equation (26) by using the curvature values from the double derivation of the deflection line and the corresponding bending moment Due to a further increase of the load, a

growth of the cracked area was observed while no further stiffness reduction could be noticed. At load step of 50,0 kN, the yielding of the tensile reinforcement was reached due to which the deflection significantly increased (Figure 7.8). The failure of the beam is defined here as failure of the concrete in the compression zone (Figure 7.22). After the concrete failure, the remaining stiffness amounted to about 20 % at mid-span.

Table 1. Load steps, crack pattern and measured deflection

Load step Nr.	Load [kN]	Description of beam condition	Measured deflection [mm]
1	3,00	state I	0,50
2	5,23	first crack	1,00
3	10,0	successive crack formation	4,50
4	15,0	successive crack formation	7,90
5	20,0	successive crack formation	10,6
6	30,0	successive crack formation	17,0
7	40,0	successive crack formation	22,6
8	50,0	yielding of the reinforcement	28,7
9	58,0	concrete failure in the compression zone	40,0

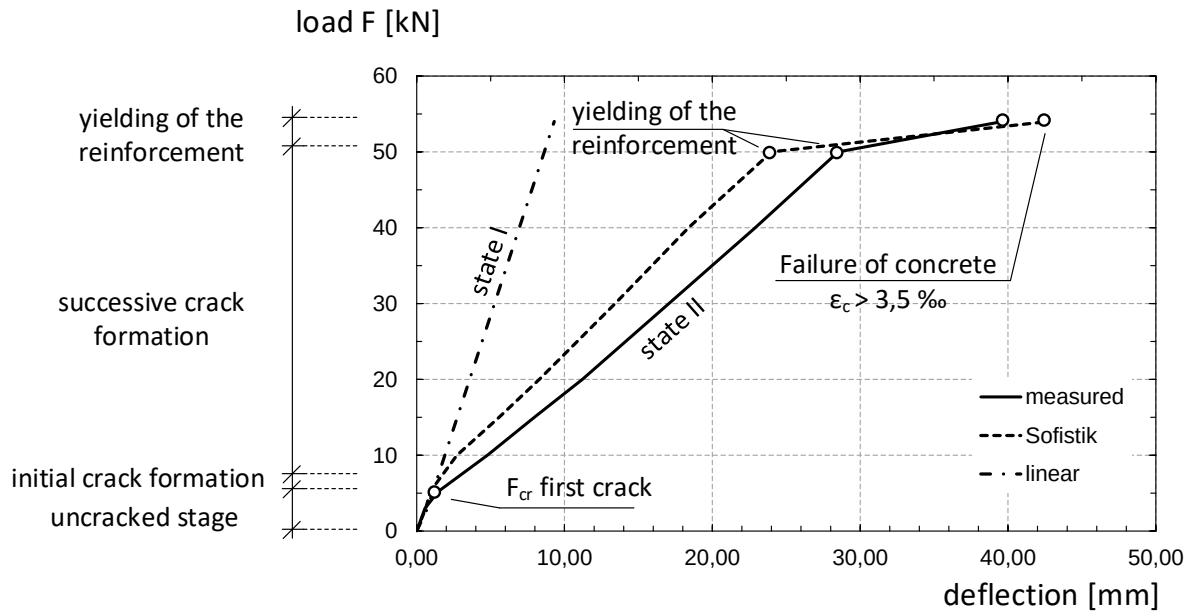

Figure 7.8. Load-deflection behaviour of the laboratory beam [60]

7.4 Applied measurement techniques

The most decisive part to identify damaged areas of a structure using the DAD-method is the high-precision measurement of the deflection curve. Therefore, different measuring techniques have been compared in the following. The applied measurement techniques were a) displacement sensors from HBM (Höttinger Baldwin Messtechnik) with a measuring length of 50 mm and 20 mm, b) levelling using a high-precision digital level Leica DNA03 with bar-coded measurement staffs and c) close-range photogrammetry using a calibrated full-frame digital SLR camera Nikon D800. The advantages of photogrammetry have already been discussed with respect to bridge inspection/monitoring. Within several research projects, photogrammetric methods were applied for deflection measurement or bridge monitoring under dynamic excitation [63] [64] [65]. Depending on the focus of the work, the considerable potential of photogrammetry for bridge monitoring has been shown. High-accuracy deflection measurement in range of 0,10 mm for laboratory condition [63] or depending on the type of cameras, temporal resolution from 1 Hz to 20 Hz can be achieved [65]. The displacement sensors needed an additional support structure, which was independent of the experimental beam (Figure 7.6 and Figure 7.9). The levelling took place on the top of the beam using prepared

benchmarks and nearby reference benchmarks in the laboratory. While the levelling observations were analysed using standard office software, the captured imagery was analysed using Elcovision 10, a specialized photogrammetry suite. The application of special bar-coded targets, which were fitted to the side of the beam (Figure 7.9), allowed the photogrammetry software to automatically find the targets in all images employed during the bundle adjustment. This produced very high precisions for the coordinates of the targets. Figure 7.10 shows the point cloud from photogrammetry and the positions of the image captures as produced in Elcovision. It is noted here that prior to taking the imagery at the beam the camera was calibrated using the in-house camera calibration facility.

Following points about measurements can be summarized:

a) The displacement sensors have a very high accuracy and can measure with high frequency which allows an interpretation of the performance of the structure over time. However, their in-situ applicability on real structures is limited due to the need of a high number of sensors. Furthermore, all sensors must be able to measure the displacement relative to a rigid level. This is not always possible, especially in the case of long bridges as the accessibility from the bottom side is not necessarily given.
b) Digital levelling is highly precise and easily performed but it requires additional man power and exactly defined benchmarks. The time required to perform the measurements increases depending on the number of measured points, which could lead to inaccuracies as the deflection curve usually changes due to temperature variations or due to creeping effects under loading. There is also a higher risk of measurement errors as for the displacement sensors as the accuracy could be influenced by human handling.
c) The highly precise photogrammetric measurement requires preinstalled targets (Figure 7.22) and shows high potential for the application to real bridge structures due to its high flexibility and accuracy. Furthermore, the flexibility of this method could be increased further with the help of modern imaging technology and from platforms such as unmanned aerial vehicles, ie. drones.

Before the load-deflection experiment was carried out, a small additional test was performed in order to compare the accuracy of the applied measurement techniques under laboratory

conditions. In this experiment the beam was lifted on one side and set back to the original position. The comparison of the measurement techniques showed very high agreement and was generally at the sub-millimetre level. It was therefore decided that the application of the DAD-method would be based on the photogrammetric data. The localisation of the damage depends particularly on the density of measuring points. Furthermore, photogrammetry shows high potential for the application to the monitoring of real bridge structures.

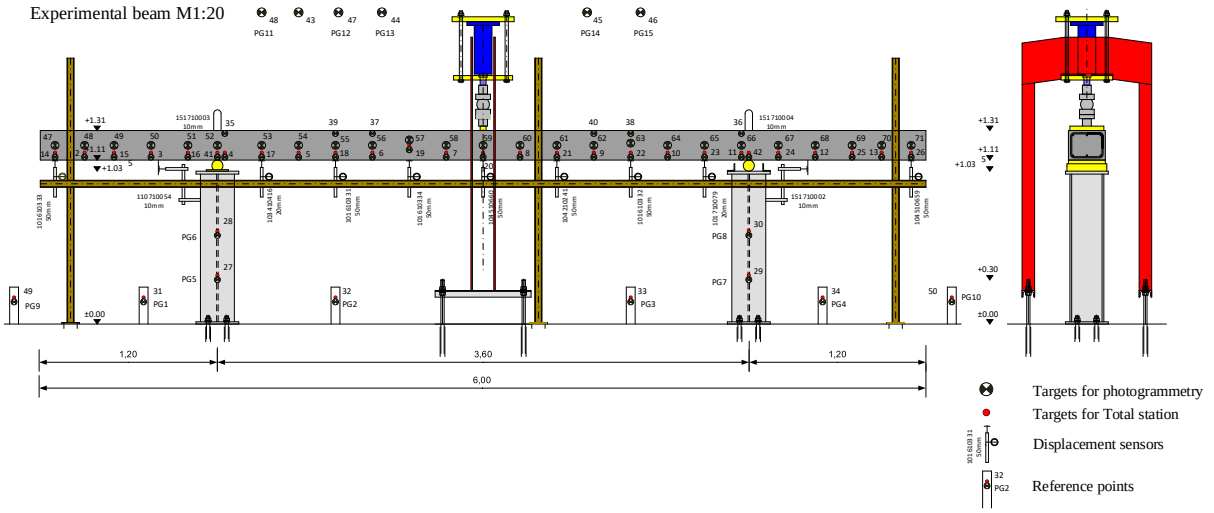

Figure 7.9. Experimental beam with the targets for measurement techniques [30]

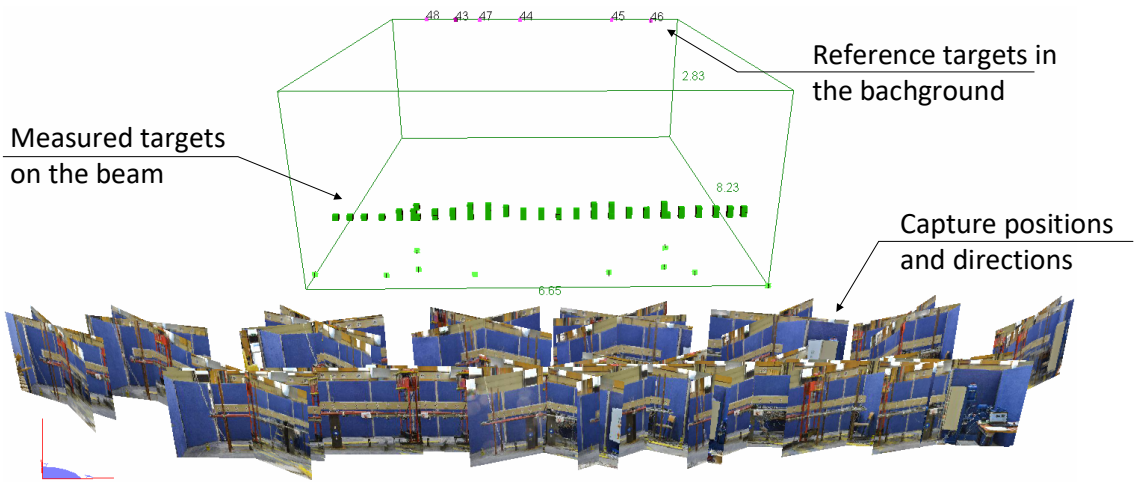

Figure 7.10. Photogrammetry point cloud and capture positions

7.5 Condition assessment of the beam using the DAD-Method

7.5.1 Detectable damage and influencing factors

The monitoring of the beam has been done in the area where cracks were expected: between the two supports on a span length of 3,60 m. As already stated all following discussions are based on the results obtained by close-range photogrammetry. The limit of the detectable damages is influenced by several factors. The data generated by each measurement technique during the experiments presented specific standard deviations. The standard deviation for the photogrammetric results amounted to about 0,17 mm under laboratory condition. Then, the loading of the beam with the hydraulic press was carried out path controlled. However, to hold the path for each load step small movements of the hydraulic press were to be expected due to force regulation. Therefore, the standard deviation for the path control amounted to about 0,07 mm. Furthermore, the survey of the crack pattern was done visually. Also, the density of the measuring grid had a high influence on the localisation of the cracked area. The impact of all these effects were studied on the load steps of 5,23 kN, which corresponds to 9 % of the ultimate load, and 20 kN, which corresponds to 34 % of the ultimate load. The measured deflection of the beam amounted to about 1,00 mm at mid-span for the load step of 5,23 kN (Table 1). Therefore, at this low loading the aforementioned effects have a high impact on the results and the deflection measurements could be influenced by about 24 %. The deflection for the load step of 20 kN was 10,6 mm and here the relative influence remained much smaller with 3% (Figure 7.11). Consequently, the influencing factors are proportionally higher for small deflections (section 7.4). On the basis of these results the question arises how can the minimum load level, which is needed to generate accurate results, be determined. The recommendation is to remain within the serviceability limit state. For the laboratory beam with a span of 3,60 m, the maximum permitted deflection would be calculated from l/250 according to EC 2, which leads to a deflection of 14 mm. The limitation of the maximum deflection for bridge structures under serviceability limit state is strictly regulated. The value generally varies from l/400 to l/1000 [66] [67] of the span length. However, the large span of bridge structures would allow measurable deflection in the range of centimetres under the serviceability limit state. This proves that the method would still be applicable for this large scale of real structures. Figure

7.12 and Figure 7.13 show the inclination angle and curvature for these two load steps, which are calculated from the first respectively second derivation of the deflection line.

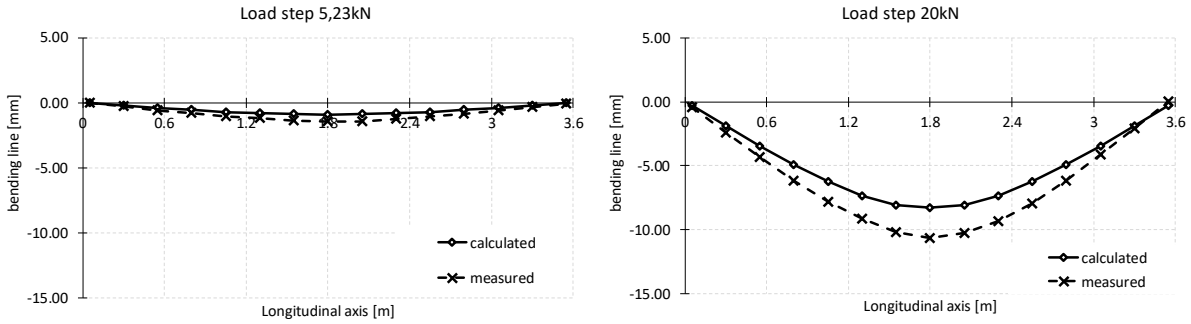

Figure 7.11. Deflection values for a) load step 5,23 kN and b) load step 20 kN

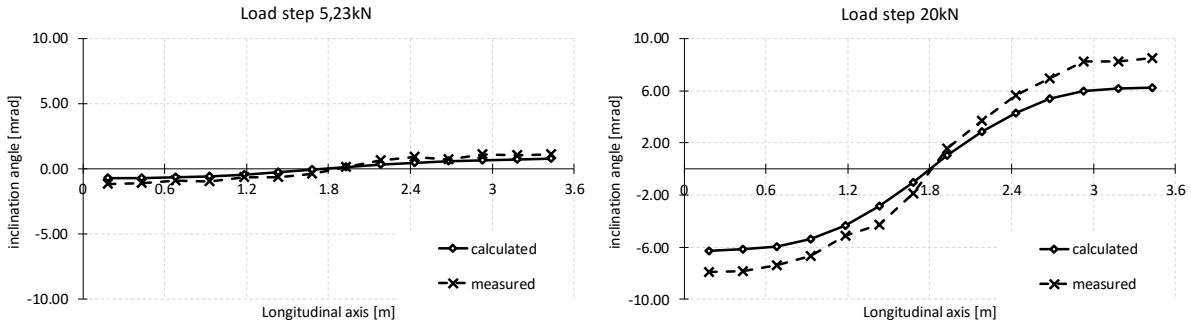

Figure 7.12. Inclination angle for a) load step 5,23 kN and b) load step 20 kN

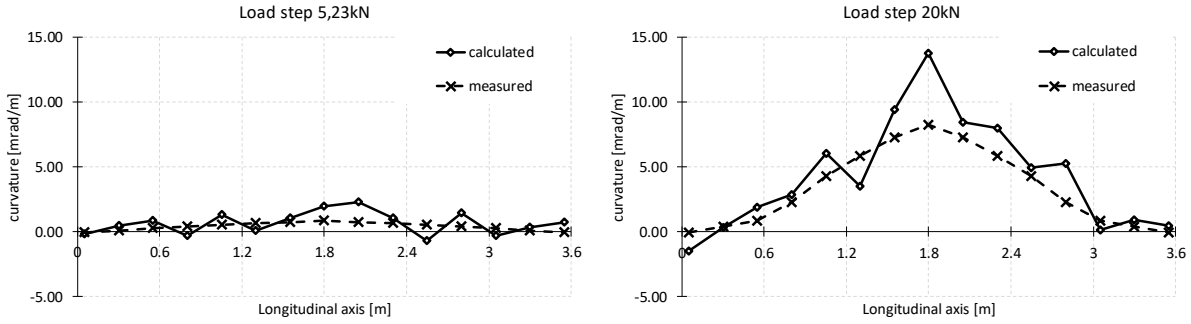

Figure 7.13. Curvature for a) load step 5,23 kN and b) load step 20 kN

7.5.2 DAD-values for the experimental beam

In the following, the results of the condition assessment of the beam in function of the different load steps will be discussed by using the DAD-Method. The DAD-values from the curvature were calculated using equation (33) and the results were presented in Figure 7.14 to Figure 7.21. Beneath each of these figures, the outcome of the DAD-Method from the analysis of the curvatures is compared to the depicted crack pattern of the experiment. As already mentioned, for small deflections (Figure 7.14), the influence of measurement precision (section 7.5.1) was proportionally high. The DAD-values for the load steps 5,23 kN (9% of ultimate load) and 10 kN (17% of ultimate load) showed no clear localisation of the cracked area. This was due to the fact that the measured deflections of 1,00 mm and 4,50 mm (Table 1) were too small and were highly influenced with up to 24 % already only by the standard deviations of the measurement technique and of the hydraulic (Figure 7.14 and Figure 7.15). However, the localisation of the crack pattern area was successful for the load steps from 15 kN to 50 kN using the DAD-values (from Figure 7.16 to Figure 7.20). The serviceability limit state was first exceeded at 30 kN with a deflection of 17,0 mm. Thus, the applicability of the DAD-method as non-destructive method for damage localisation and condition assessment has been proven. The localisation of the failure of the beam could also clearly be identified by using the DAD-values (Figure 7.21). As a result, it can also be deduced that the accuracy of the applied measurement technique was sufficient for the damage detection of the analysed beam.

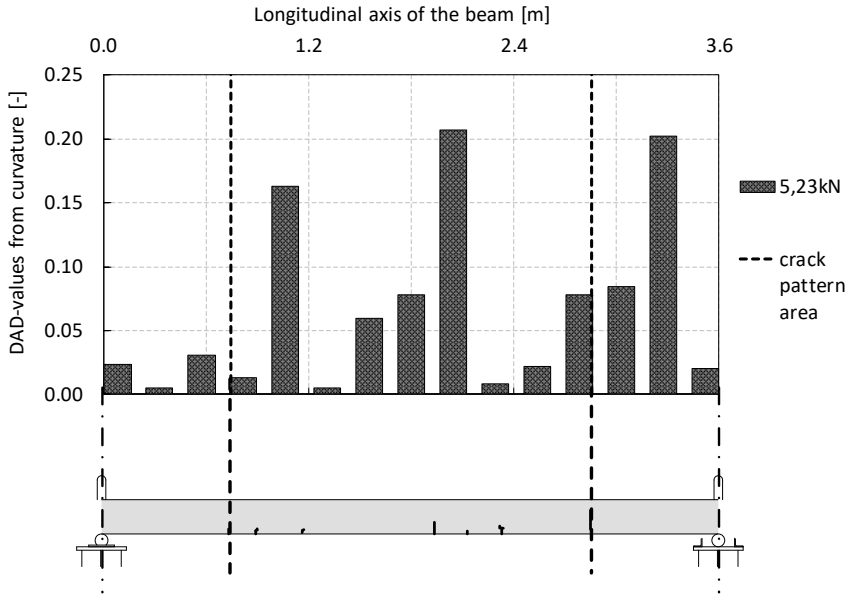

Figure 7.14. DAD-values from curvature and detected crack pattern for the load step of 5,23 kN (9% of ultimate load)

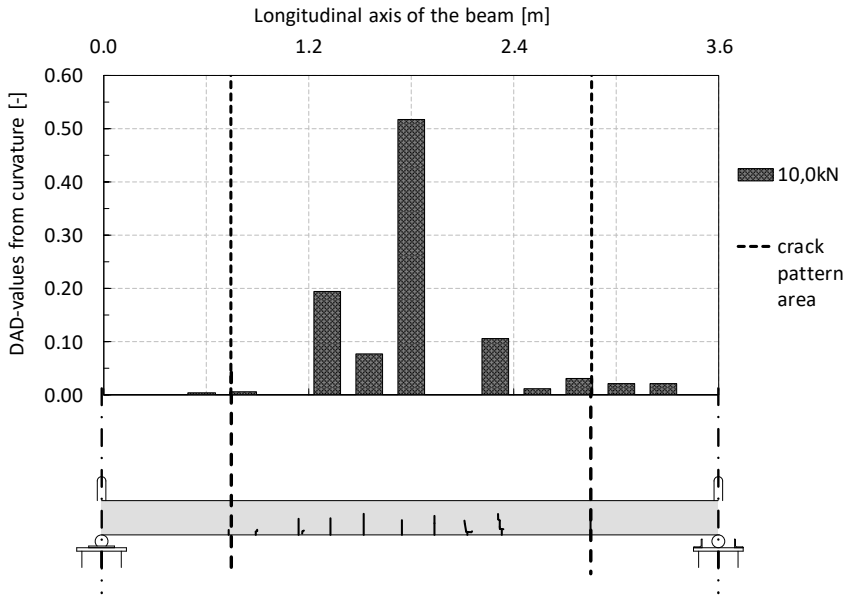

Figure 7.15. DAD-values and detected crack pattern for the load step of 10,0 kN (17 % of ultimate load)

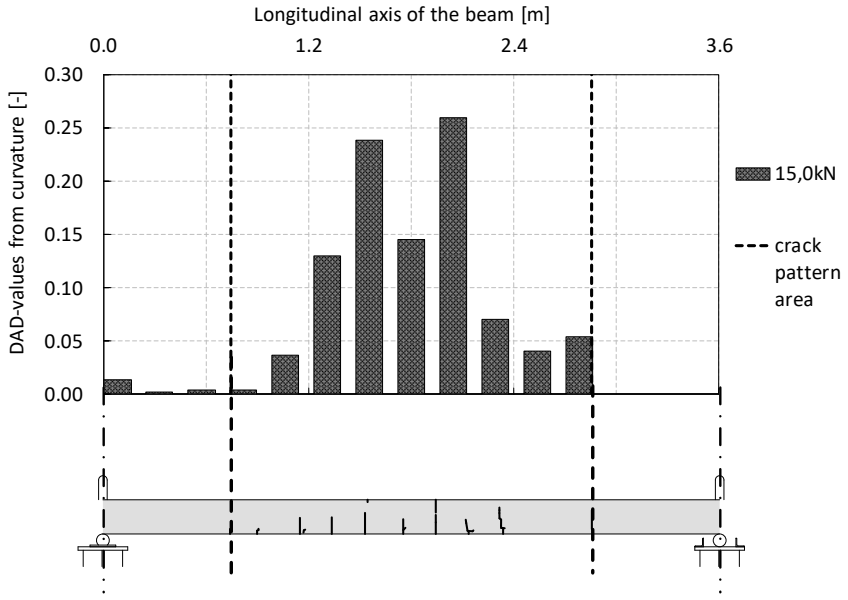

Figure 7.16. DAD-values from curvature and detected crack pattern for the load step of 15,0 kN (26 % of ultimate load)

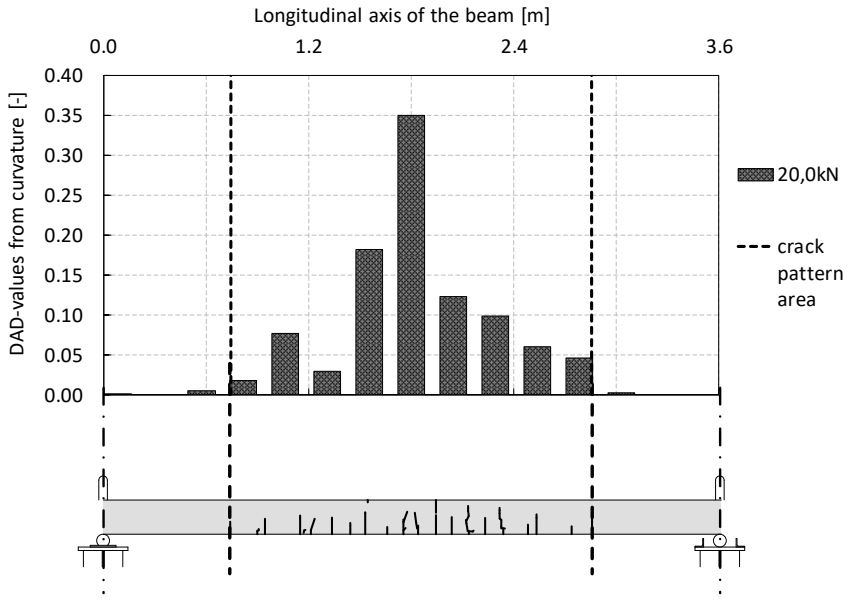

Figure 7.17. DAD-values from curvature and detected crack pattern for the load step of 20,0 kN (34 % of ultimate load)

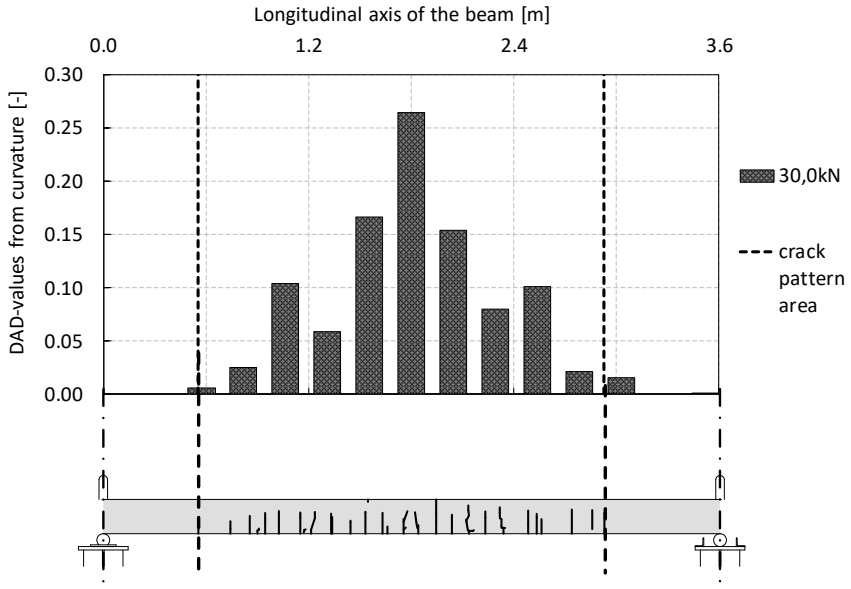

Figure 7.18. DAD-values from curvature and detected crack pattern for the load step of 30,0 kN (52 % of ultimate load)

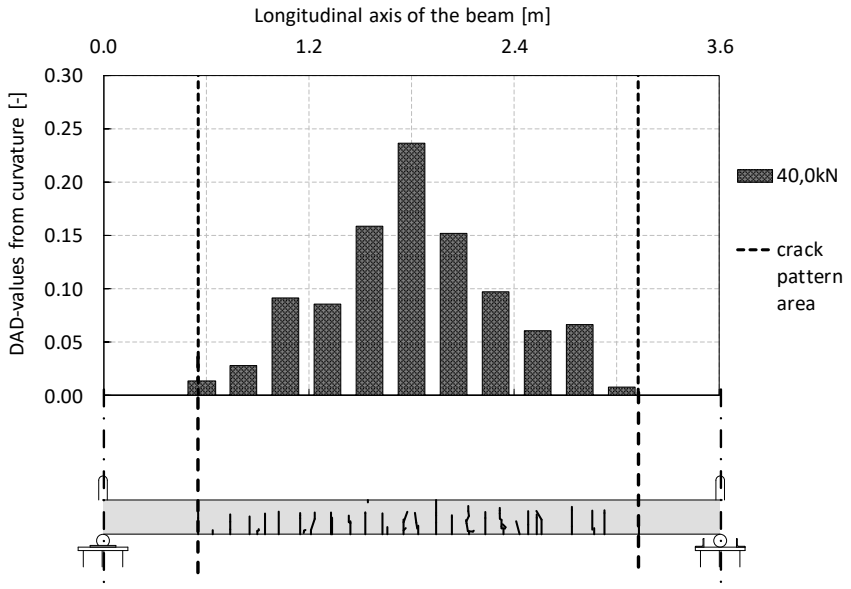

Figure 7.19. DAD-values from curvature and detected crack pattern for the load step of 40,0 kN (69 % of ultimate load)

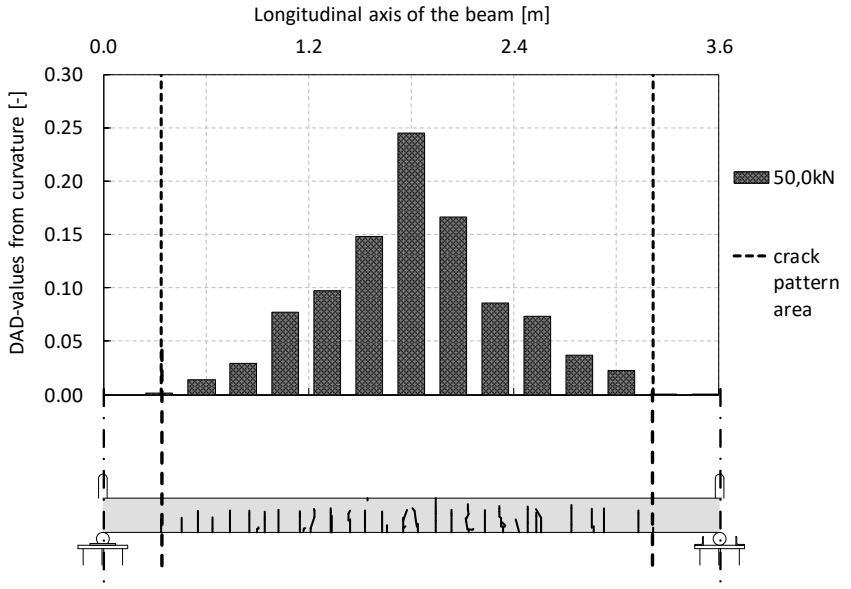

Figure 7.20. DAD-values from curvature and detected crack pattern for the load step of 50,0 kN (86 % of ultimate load)

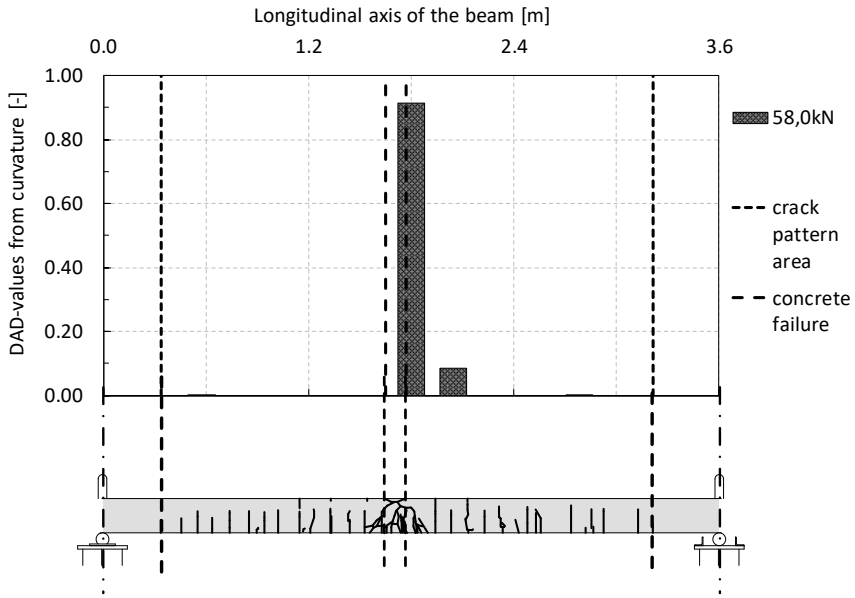

Figure 7.21. DAD-values from curvature and detected crack pattern for the load step of 58,0 kN (ultimate load)

As already mentioned, the failure of the reinforced beam occurred at 58 kN due to a failure of the concrete in the compression zone (Figure 7.22).

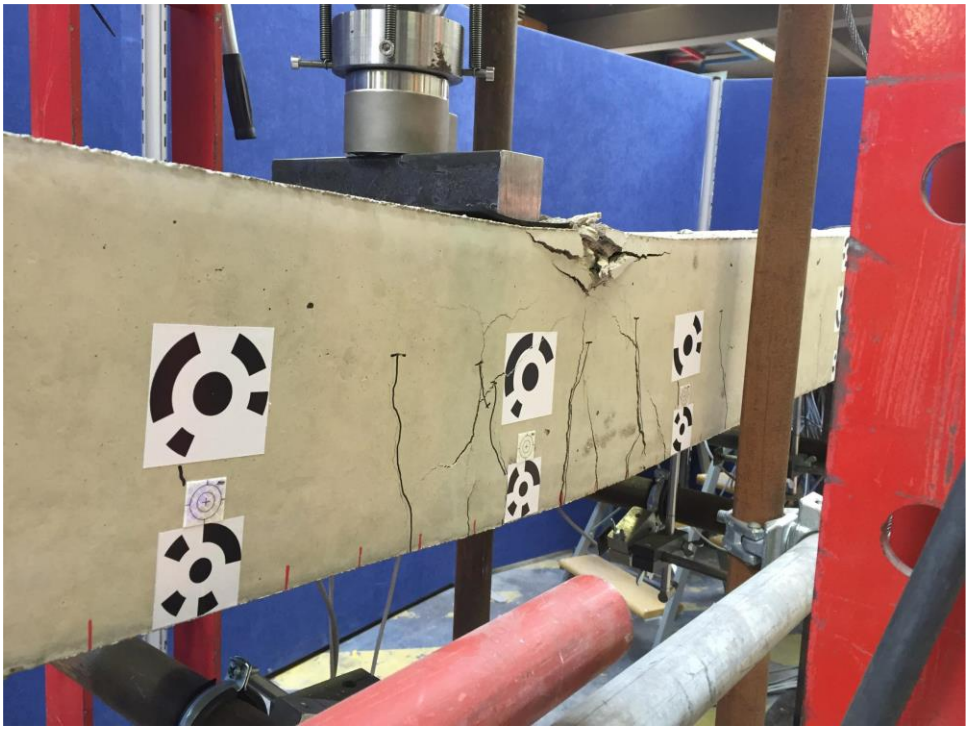

Figure 7.22. Deflection failure of the beam

Figure 7.23 shows the summary of the DAD-value diagrams for the load steps 15 kN, 20 kN and 30 kN. These are the load steps in the area of the serviceability limit state.

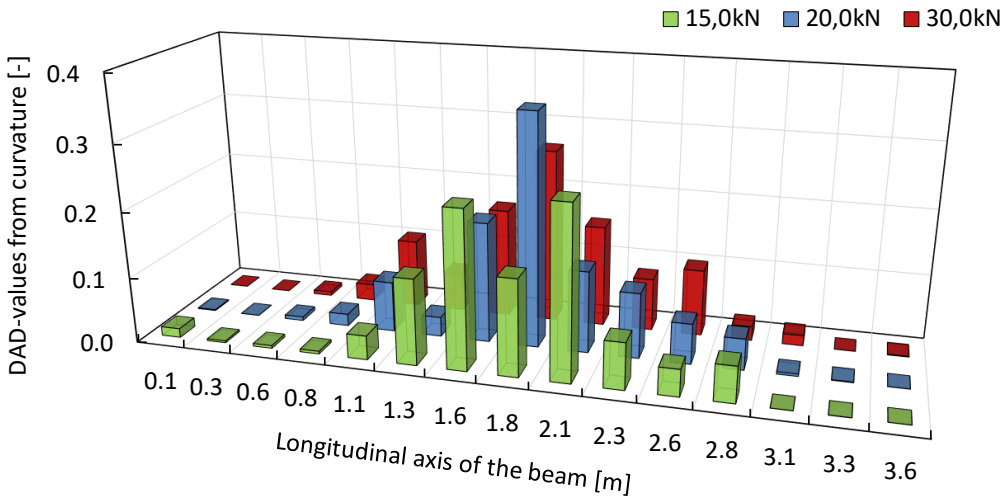

Figure 7.23. DAD-values from load steps 15 kN, 20 kN and 30 kN

7.6 Investigation based on theoretical calculations

As in the previous section, the applicability of the DAD-Method has been proven by the verification of an experimental test. In this section, some theoretical analysis will be carried out to further demonstrate the effectiveness of this method. Therefore, several different static systems will be investigated where the damage position, damage degree and load cases will be varied. For these cases, only the curvature DAD-values will be discussed.

7.6.1 Variation of the degree of damage

So far the analysed systems mostly showed relatively large damages with respectively large stiffness reduction. For the simulation of the example in the introduction e.g. a stiffness reduction of 60 % has been chosen, whereas the stiffness reduction of the laboratory experiment due to cracking was about 50 % for the crack pattern area, which increased to about 80% after yielding of the reinforcement. In the following, the bridge example is shown, but with a very small damage of 1 % stiffness reduction at a quarter of the span (Figure 7.24).

In Figure 7.24, the first three curves show the resulting deflection, inclination and curvature lines which have been calculated by a FE-calculation for the undamaged as well as for the damaged beam. When comparing the undamaged curve to the damaged one, no visible changes in all these curves can be identified. The reduction of the bending stiffness by only 1 % does not lead to any detectable change of the deflection line as well as of the curves of the inclination angle or the curvature.

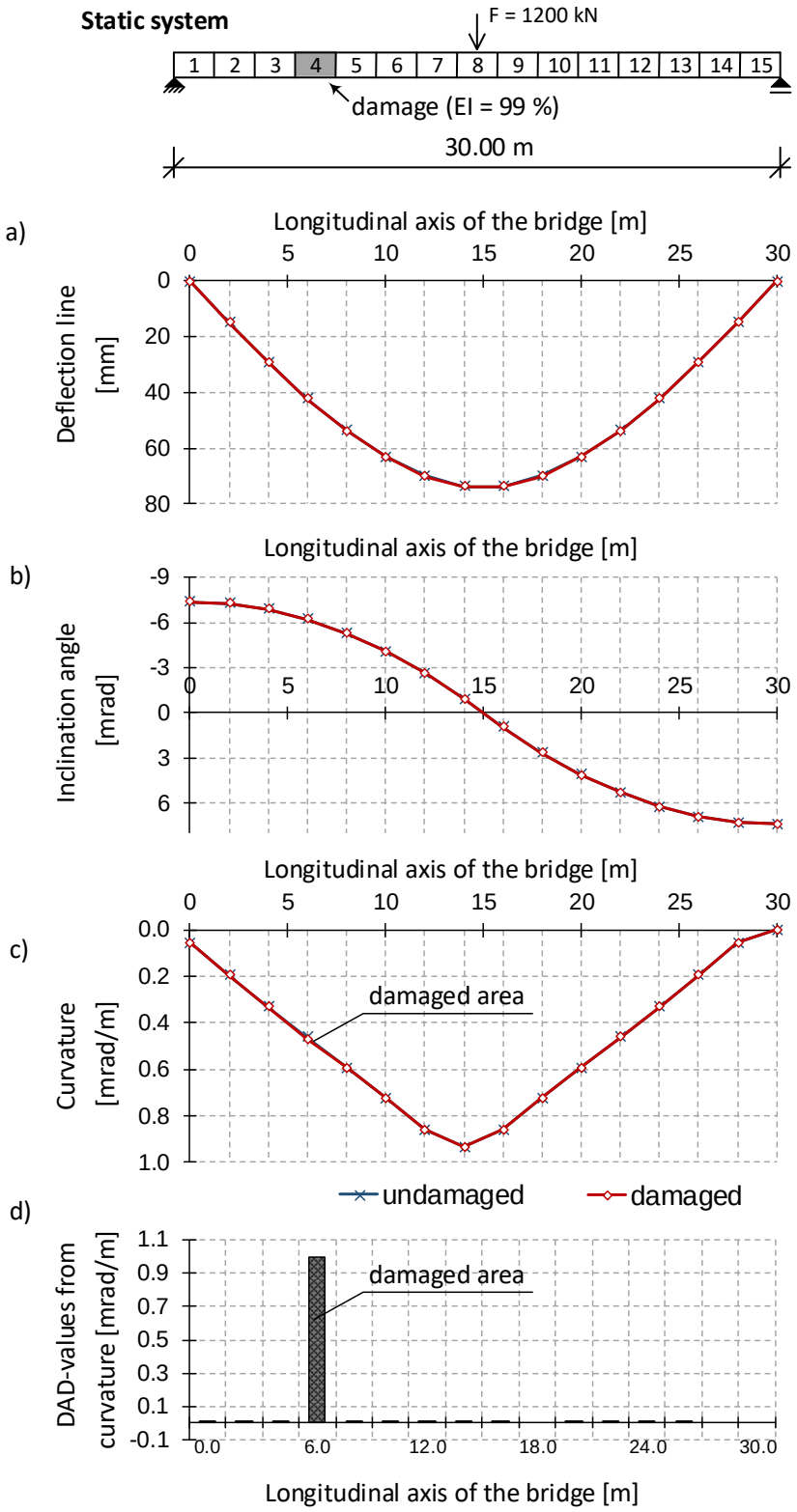

Figure 7.24. Example of a beam with 1% stiffness reduction

Only the application of the DAD-Method permits a clear identification of the stiffness loss due to damage (Figure 7.24). Thus, in this case, the DAD-Method is still valid as long as the performed measurements are precise enough.

7.6.2 Application of the DAD-method on different static systems and for different damage positions

The demonstration in the previous section has shown that the DAD-Method is applicable for single-span girders independent of the degree of damage as far as the measurement precision is sufficient enough. However, within the laboratory experiment it has been shown that the damage detection was successful in the range of the serviceability limit state. In the following, the damage assessment will be realised on two other static systems: a single-span girder with cantilever (Figure 7.25) and a two-span girder (Figure 7.26). In the first example, the damage is generated at the position of the left support by a 50 % reduction of the bending stiffness. In the second example, the damage is located at the middle of the first span. The position of the load is insignificant for the localisation of damage using the DAD-values. In the diagram of the DAD-values, shown in Figure 7.25 and Figure 7.26, the localisation of damage corresponds to the generated damage in the FE model.

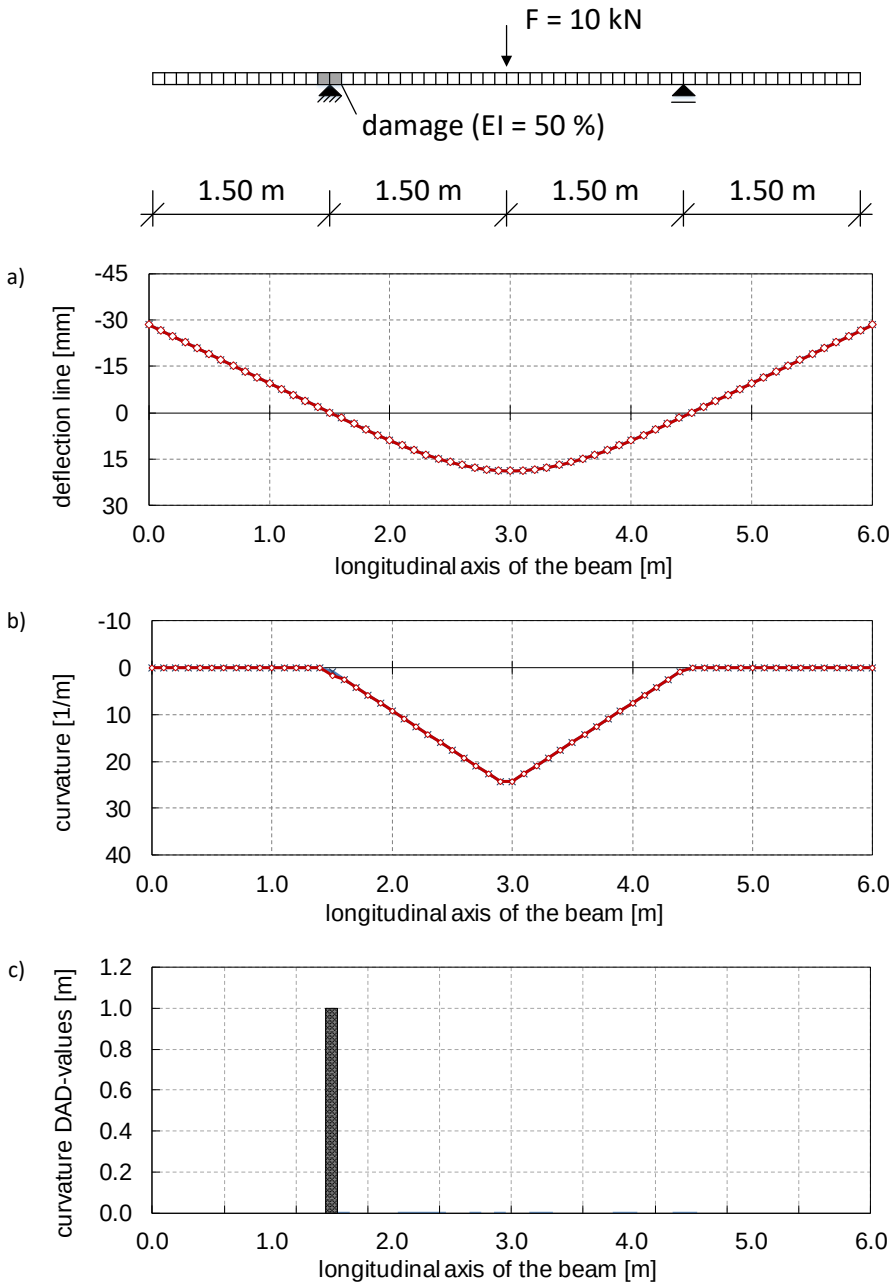

Figure 7.25. Single-span beam with cantilever damaged at the first support

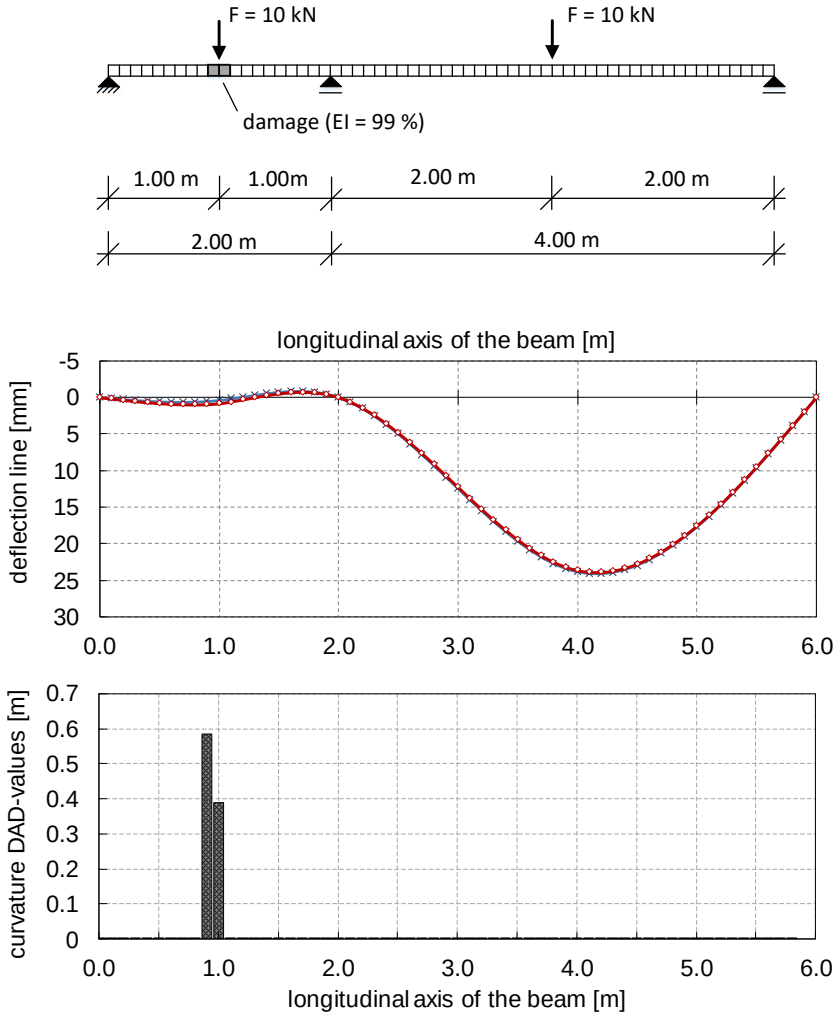

Figure 7.26. Two-span beam with a local damage at the middle of the first span

7.6.3 Effect of temperature changes on the DAD-Method

It is known that temperature changes affect the deformation behaviour of structural elements which makes it difficult to interpret the results of commonly used assessment techniques: if a data set generated during a first condition assessment test is compared to a data set of a second test after several months, the temperature conditions have changed between the tests and thus, even if the condition of the structure has not changed, the interpretation of the stiffness of the structural elements out of the measured data will not be the same for both measurements. This is particularly true for bridge structures which are still in use and covered on their top-layer by

an asphalt layer. The rigidity of asphalt increases with a decrease in temperature and vice versa. Therefore, for commonly used assessment techniques, this effect should be known before any assessment of the structure can be performed by comparing the deflection line, the inclination angle or the curvature. This is difficult as the bonding behaviour between the asphalt and the load bearing structure must be known. However, as the bonding behaviour also depends on the temperature, it is nearly impossible to take into account this effect in all its dimensions.

In the following, this problem will be analysed using FE-calculation with the DAD-Method applied to a single span girder, damaged at mid-span. The damage is simulated by a 1% decrease of the bending stiffness at mid-span. Two data sets have been generated by the FE model. The first data set was calculated for a given temperature without any damage and the second one was calculated by introducing a local damage at mid-span and by further loading the section over its whole length by a temperature gradient of $\Delta T = 30$ °C. This temperature gradient could be the result of a heating of the top side of the structure by the sun. As the top side of a structural element is heated more than the bottom side, an upward directed deformation occurs and counteracts against the downwards directed deformation due to loading or due to damage. The calculated curvature DAD- values are depicted in Figure 7.27. It shows a discontinuity in the range of the damage and also indicates the effect of the temperature gradient over the whole length of the structure. In this way it clearly identifies the damage as well as the temperature change. This identification of damage is related to the fact that the DAD-Method analyses local effects which are normalized over the whole length of the structure and it is, therefore, insensible to the global effects due a temperature variation for the detection and localisation of damage.

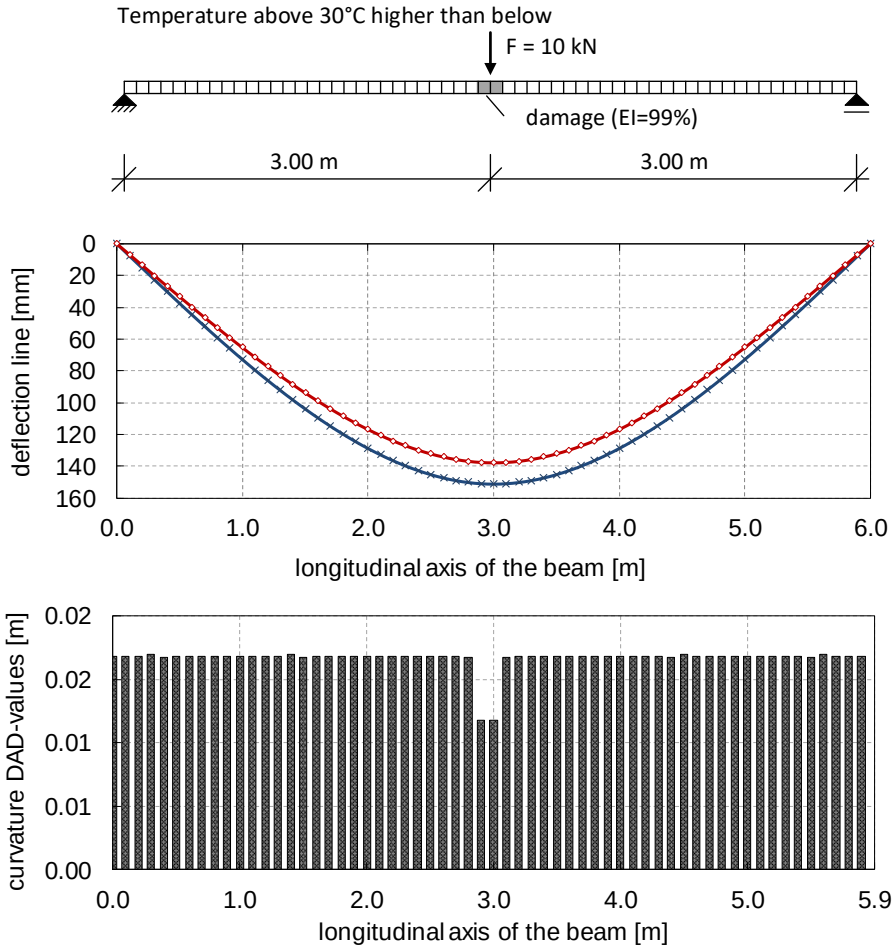

Figure 7.27. Example of a girder with temperature influence and local damage

7.6.4 Case study with planned stiffness change

The previous examples as well as the experimental beam are based on simple linear elements. However, real structures or main girders of real bridges often have planned discontinuities such as surfaces curvatures, , cross members, variable heights etc. The following example shows the application of the DAD-method on a structure with variable stiffness along the beam. The example consists of a 25 m long girder (Figure 7.28) of a bridge structure where the cross-section is shown in Figure 7.29. The girder has a haunch next to the supports areas (between the axis B and C and between the axis F and G) as well as local transverse stiffening elements in the axis C, D, E and F (Figure 7.28). The girder is loaded at mid-plan. The stiffness of the girder is reduced to 60% at 16,40 m from the left support. For the application of the DAD-

method, a finite element model is created with a local stiffness reduction of 60 % at this section by reducing the Young's Modulus again by this amount (Figure 7.30).

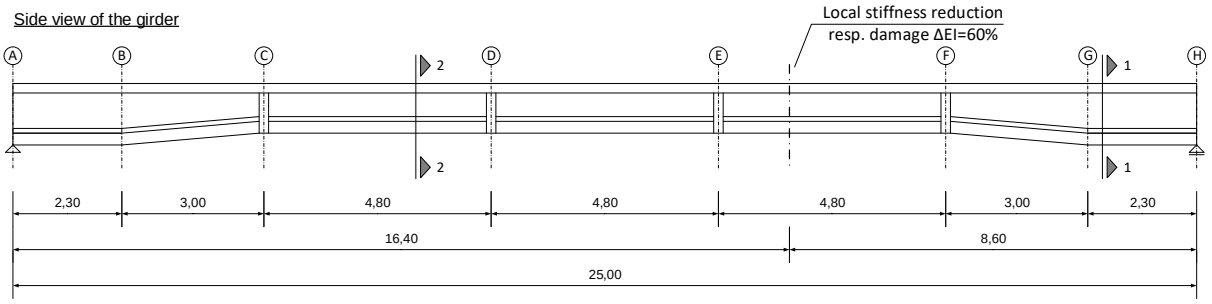

Figure 7.28. Example of a girder with stiffness discontinuities at undamaged state

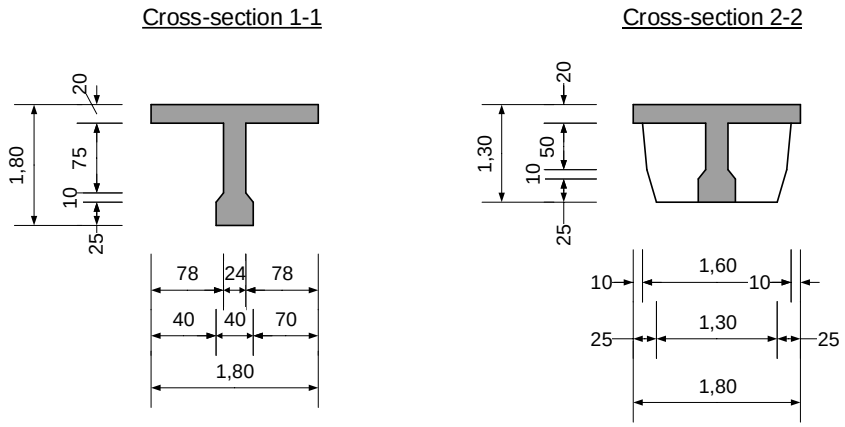

Figure 7.29. Cross-sections of the girder

Two models have been generated: a first model without damage serving as reference system and a second damaged model. In Figure 7.31, the black lines indicate the results for the reference system without damage and the red lines the results for the system with local damage. The black dashed lines indicate the damage position. Considering the deflection curves respectively the inclination angles (Figure 7.31 a) and b) the discontinuity due to damage is not clearly visible. Indeed, the curvature curve (Figure 7.31 c)) shows discontinuities at the section of the structural discontinuities as well as on the section of the damage. So with the simple deflection, inclination and curvature curves the discontinuity due to local damage could not be distinguished from the structural discontinuities. However, when considering the DAD-values in (Figure 7.32), only the discontinuity due to damage becomes apparent as this constitutes the

only difference between the reference system and the damaged system. The DAD-values from curvature (part c in Figure 7.32) definitely localise the damage even if the structure has planned stiffness discontinuities, as these are already present in the reference system.

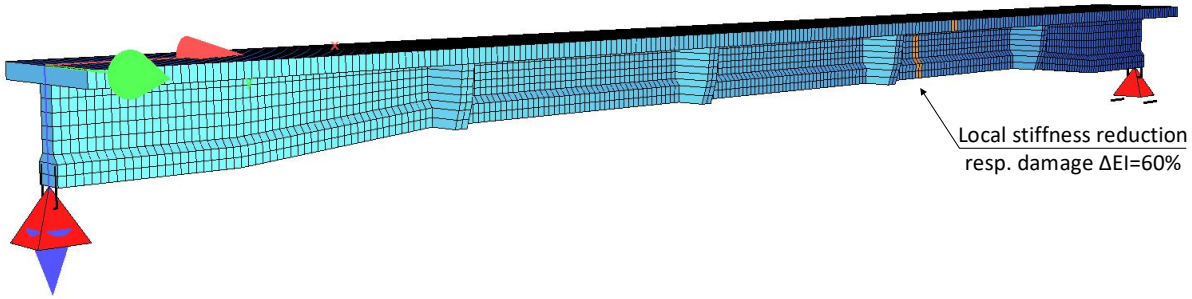

Figure 7.30. Non-linear Finite element model of the girder

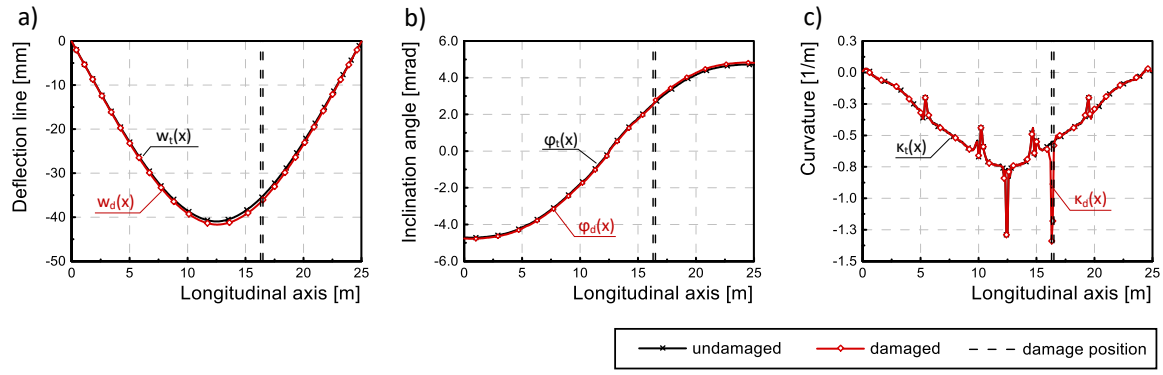

Figure 7.31. Deflection line, inclination angle and curvature for the bridge girder

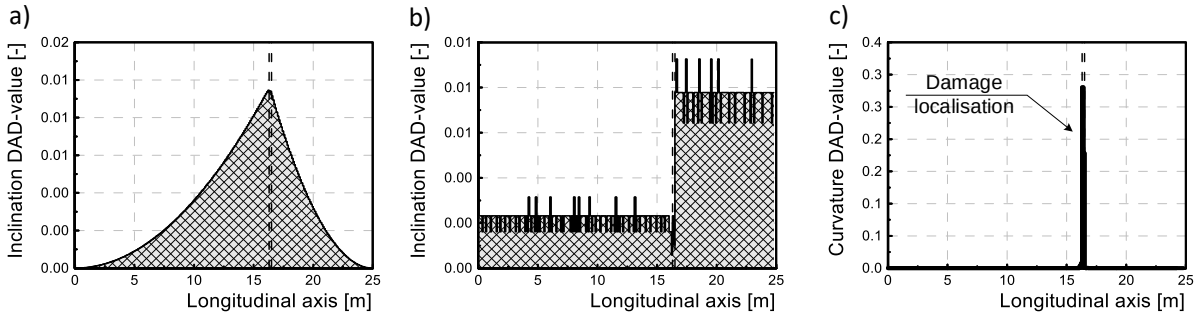

Figure 7.32. DAD values from deflection line, inclination angle and curvature for the bridge girder

7.7 Summary

The reliable identification of damages to bridge structures is important as a precise damage evaluation allows an early and efficient bridge preservation. Until now, visual inspections or laborious long-term monitoring systems were the principal methods used for damage detections. The current state-of-the-art allows the detection of damages only at the surface or close to the surface of the structures.

In this article, a method is presented which allows the identification and localisation of stiffness reducing damages based on a single measurement of the deflection line during a load test. The deflection line along the total structure length is recorded using modern geodetic techniques to analyse the condition of the structures. The new DAD-Method is presented and discussed based on theoretical calculations and on a laboratory experiment. It was found that the DAD-values from the simple deflection line show changes of the system, but are not suitable and able to localise the damage. For this the evaluation of the DAD-values from the analysis of the inclination angle and the curvature were shown to be more suitable. Within the laboratory experiment, a single span reinforced concrete beam was prepared. The beam was gradually loaded at mid-span and several stiffness reductions occurred due to a progressive cracking. The main objective of the experiment was to enable the identification and the localisation of the cracked area using the deflection values. The curvature DAD-values, which were calculated by double derivation of the deflection line, allowed a reliable localisation of the crack pattern. The identification of the cracked area was even possible at the load steps under the serviceability limit state, thus the DAD-Method could be applied as non-destructive inspection method for condition assessment of bridge structures. Also for the shown examples with a single local damage, the DAD-values indicate discontinuities at the damaged areas. So, within this paper it could demonstrated that this method is able to identified large spread damage zones as well as very local damage for different damage levels. In case of structures with planned stiffness changes along the longitudinal axis, the curve of the curvature includes several discontinuities, which has to be distinguished from local damages. A theoretical example shows an analysis of such a damaged system with the DAD-method. Again, the localisation of the damage was clearly possible despite the unsteady curvature curve. However, the essential prerequisite of the method application is the highly precise measurement of the deflection line along the bridge

structure. Therefore, several modern measurement techniques such as close-range photogrammetry, levelling and displacement sensors were applied and compared within the laboratory experiment. From this photogrammetry showed high potential for the application of the DAD-Method with its standard deviation amounting to 0,17 mm while the measured deflection amounted to 9,3 mm for the load step of 20 kN under serviceability limit state. Thus, the influence due to the accuracy of the measurement technique is relatively small with 2 %.

The investigation of different static systems has shown that the method is applicable and constitutes a real supplement to commonly used condition assessment methods. Theoretical examples have shown that the method is even able to provide clear results in the case of small damages (1 % stiffness reduction). The insensitivity of the method in case of a temperature gradient in the structure has also be demonstrated by the means of a theoretical calculation. For the further research, the DAD-method will be extended to the analysis of slab and shell structures as these are common structural bridge element. Thus, it has been shown that the DAD-Method is nearly independent of the damage degree, no exact reference system in initial condition is needed and that it is nearly insensitive to global influences such as temperature effects. In a next step the application of the DAD-Method will be proven on real bridge structures.

8 Transition to the publication II

8.1 Conclusion of the first paper

Within the paper, the application of the DAD method on several theoretical case studies and a laboratory experiment was shown. The case studies have proven that the DAD method is able to detect damages independent on the global effects and planned stiffness influencing members. The reduction of stiffness due to cracking in the experimental reinforced concrete beam amounts about 50 %, which could be clearly detected using the DAD values. The standard deviation for the photogrammetry measurement amounted about 0.17 mm including the vibration from the path-controlled hydraulic press. A theoretical example showed that a damage degree of 1 % could be detected based on the DAD method for exact precise measurement values. Therefore, further investigations for different experimental systems and measurement noise effects were needed.

8.2 Introduction to the second paper

The second publication starts with the introduction and additional literature review compared to the first publication. The main novelty of the second paper is the consideration of the measurement noise effect for the application of the DAD method. Since the measurement precision of each target is known, the noise affected deflection curve could be smoothed within the standard deviation. The advantage of this procedure is to identify the structural discontinuity exclusively. In addition, the damage localisation accuracy depends on the density of the measurement point distances, namely the closer the measuring points the more exact the

localisation of damage. However, the closer the measuring points the smaller the height differences respectively changes of inclination angles between two points, which leads to a higher influence of the measurement noise effect. Therefore, a study about the measuring points distance is done and presented within the paper. Furthermore, the paper includes results of two laboratory experiments with a reinforced concrete beam, which is gradually loaded and with a steel beam, which is gradually damaged at three different positions. The evaluation of the experimental data includes the consideration of the measurement noise effect and the measurement point distances.

9 Publication II: Curvature based DAD-method for damage localisation under consideration of measurement noise minimisation

Abstract:

Several research projects on condition assessment of bridges have proven that structural responses from dynamic excitation or static loading are influenced by local damages and thus, could be used for the detection and localisation of damages. Particularly, the curvature of structures is directly depending on their stiffness. In order to localise the discontinuities in curvature lines resulting from damage, this paper uses the so-called Deformation Area Difference Method (DAD), which is based on static load deflection tests on bridge structures. The DAD-method for damage localisation is presented within the paper using a theoretical example, which is then verified by two laboratory experiments. The first experiment consists of a reinforced concrete beam, which is loaded stepwise until failure of the concrete in the compression zone. Due to the load increase, the tensile zone of the beam starts cracking, leading to a stiffness reduction. The application of the DAD-method allows identifying the cracked area from the measurement of the deflection line. However, a challenge and a prerequisite for the applicability of the DAD-method is the highly accurate measurement of the deflection line. Therefore, one of the most modern measurement techniques such as digital photogrammetry is applied. Nonetheless, the accuracy of each measurement technique is limited. The second laboratory experiment consists of a steel beam, which is locally damaged at three positions. The

degree of the damage is stepwise increased in order to identify at which degree of damage the applied DAD-method is still able to identify and localise damage.

In this work, the focus lies on the minimisation of the effect of noise resulting from the limited measurement precision. Possible solutions were examined and proposed based on methods such as data smoothing using polynomial regression, consideration of standard deviation and measurement point variation. The reduction of the noise effect leads to an increase in the sensitivity of the damage localisation. The DAD-method has proven its potential for practical application through the successful localisation of cracking in the concrete beam.

9.1 Introduction

Over the past few decades, against the background of the rapid development of international transport, the maintenance, repair and preservation of infrastructure is becoming increasingly important. Structures such as bridges are core elements of a healthy infrastructure and ensure besides the crossing over the barriers, the secure traffic flow in the main hub of roads. In 1970, the proportion of road freight transport amounted to about 52,1 % in the 15 EEC countries which reached 79,3 % in 2002 [68]. According to the report on transport from the European Commission, the portion of freight transport will reach expectedly about 80 % by 2050 [69]. The bridge structures and roads are claimed differently depending on the weight and transition of individual vehicles whereas not vehicles are relevant but the number and weight of the passing axles. In order to estimate the influence of the different axle transitions on the structure's condition, AASHTO-Road-Tests [70] has determined an equivalence factor to convert lighter or heavier axle loads to a standard 10 tons axle load. The reference value of the axle load amounts to 10 tons. This assumes that damage increases with the fourth power of the static axle loads. A 12 tons-truck with a front axle load of 5 tons and a rear axle load of 7 tons causes approximately 1/3 of the damage compared to a single passage of a standard 10 tons axle load (equation (34)). So, the comparison of a car with an axle load of 1 ton and a truck with an axle load of 10 tons clearly shows the impact of trucks on road or bridge structures. Namely, a car with axle load of 1 ton causes 1/5000 times less damage than a truck with an axle load of 10 tons (equation (35)) [9].

$$\left(\frac{5t}{10t}\right)^4 + \left(\frac{7t}{10t}\right)^4 = 0{,}30 \cong \frac{1}{3} \tag{34}$$

$$\left(\frac{1t}{10t}\right)^4 + \left(\frac{1t}{10t}\right)^4 = 0{,}002 = \frac{1}{5000} \tag{35}$$

Statistics show the number of bridges for several countries:, the USA counts over 600 000 interstate, state and city bridges and Germany counts about 35 000 road bridges and about 30 000 railway bridges [8]. About 11 % of the bridges in the USA and about 12% of the bridges in Germany [71] have been identified as structurally deficient [72]. The increasing average age of the existing bridges shows a growing tendency for deficient structures. Each country has its own rules about the local onsite inspection sequence of existing bridges, which always requires considerable effort, skilled and trained staff and appropriate technique. These facts explain the urgent need for appropriate methods for reliable condition assessment of bridges.

Many studies have examined the damage levels of bridges and impacts, which are influencing the load bearing capacity of bridges [73] [74] and confirm that damage leads to a change in the structural response of the structures by static loading tests as well as dynamic excitation tests [75]. This expertise is nowadays used by many research projects for developing long term monitoring concepts for structures. The long-term monitoring systems are used to control all changes in the structural response, which become apparent during the measurement period. The verification of possible changes in the structural response are detected by comparing the new data with initial measurement results as well as by comparing them with the results of a numerical model of the structure [76]. However, long term monitoring of structures comprises several problems. At first, structural health monitoring only allows to measure the structural response over its lifetime, but it cannot serve as independent method for condition assessment of bridge structures. The measured data is also difficult to be integrated into the bridge model. The newly installed measurement techniques for long-term monitoring are threatened by aging effects, because the ageing processes of those measurement techniques are usually faster than the aging of the structure itself. Some investigations [77] show that the effort of early failure warning systems by using real-time monitoring. However, such early warning systems cannot

predict sudden failures such as, e.g., failures due to shear which always occur suddenly and brittle compared to a ductile failure due to bending [78] [42]. Compared to methods based on mode shapes and traditional frequency analysis, methods based on static loading tests show several advantages. Lantsoght et al. [79] summarised the state-of-the-art on load testing of concrete bridges. Particularly, the diagnostic load testing, proof load testing, testing of other types of structures and current codes and guidelines were discussed. The authors argue that there is still a need for the development of a unified recommendation for proof load, loading protocol and stop criteria.

Static load deflection experiments with defined position of load or with moving load along the longitudinal axis of the structure provide clearer statement about damage assessment. Stöhr et al. [80] presents a method based on static measurements using a inclinometer applied to beam systems. The inclinometer is positioned at the support of the beam, which is stressed under a moving load. The aim of the study was to compare the initial measurement of the influence line with the one after the local stiffness reduction to enable the localisation of damage. Despite the noise of the inclination measurement, the influence lines from both damage scenarios show good tendency in agreement to the calculated FE-Model. The author showed also the possibility of positioning the inclinometer near mid-span. In the second half of the paper, an experiment on a real pedestrian bridge was presented. The 23,56 m long bridge was loaded with a truck with a total weight of about 6,0 tons. The total weight of the truck was equal to the applied uniform design live load, wherefore the test could be considered to be non-destructive. Due to this loading a stiffness reduction of 15% was achieved. Further comparable research projects using inclinometers and influence lines were presented in [81] and [82].

Sun et al. [54] developed a method based on the evaluation of curvature to detect damages in structures such as bridges. The main objective of their study was to minimize the noise effect of the measurement technique under consideration of the standard deviation. This paper showed results from a laboratory experiment with a steel beam and results from a finite element bridge model. The experimental beam was loaded at different positions along the beam. The measurement of the movement took place at mid-point using a laser displacement meter. The local damage, respectively, stiffness reduction of 60 % was created at the one-third-way of the span. The length of curvature interval was investigated for several cases. Consequently, the

minimum ratio of noise/damage effect could be calculated. Therefore, it is advised to minimize the noise level under consideration of the noise/damage ratio. For both cases, the laboratory experiment and the finite element calculation, the damage localisation was better traceable for a damage severity of over 50 %.

He et al. [49] presented a damage detection method for beam structures using quasi-static moving load induced displacement responses. They investigated the correspondence between damage parameters and displacement influence lines. The theoretical background of the method is based on the features of the Euler-Bernoulli method [83]. The effectiveness of the proposed method was proven by using numerical and experimental examples. The change in the displacement influence line (DIL) indicated the damage, from which the damage localisation index could be deduced. The application of the method was subdivided as follows: first, the localization of the damage using the DIL, then the damage level quantification can take place. For the damage level quantification, a certain number of displacement sensors was needed, which should be positioned in the area of localized damage. The measured and calculated DIL showed peaks in the region of damage. However, the effect of noise resulting from the measurement affected the accuracy of damage localisation. Further corresponding damage detection methods using moving loads were presented in [84] [52] [85] [53].

Technological developments have left their mark on measurement techniques. Modern measurement techniques such as digital photogrammetry opened new ways for the development of innovative methods for inspection of structures [86] [87] [88]. Close-range photogrammetry has already been used for the determination of the three-dimensional geometry of bridges since 1970 [89]. A literature review for the last 20 years is presented in [90]. Jiang et al. [91] used close-range photogrammetry for deflection measurement of a laboratory bridge test and of a field bridge test. The applied cameras for their study was a Kodak Pro SLR/n camera with a 36x24 mm, 13,85 million pixel CMOS sensor and a Kodak DCS660 camera with a 27x18 mm, 6 million pixel CCD sensor. The reached accuracy of the photogrammetric results for laboratory condition ranged from about -0,41 mm to +0,89 mm and for the field study from about +0,10 mm to +1,33 mm. Nishiyama, et al., [92] applied photogrammetric methods for crack monitoring. They used reflective targets around the crack in order to measure the change of the crack. The reached precision amounted to less than 0,10 mm using digital image captures

from a distance of 10,0 m and less than 0,20 mm from a distance of 25 m. Comparable studies for the measurement with photogrammetric methods for laboratory or field tests were presented in [93] [94].

The first part of the DAD-method was presented in [95] und included the theoretical background, several case studies with stiffness and temperature variations, as well as results from a laboratory experiment. In this work, the further development of the DAD-method is presented which considers the measurement precision, respectively, the standard deviation of the applied measurement technique. So, the measured deflection line could be smoothed in the range of the standard deviation in order to increase the precision of damage detection using the DAD-method. Since the smoothing of the curves requires a reference curve, a polynomial regression of multiple degrees was determined from the measured data. Riveiro et al. [93] described a similar process in their work, but they used the second degree of polynomial regression as the underclearance of bridges had been measured. Within the development of the DAD-method, in addition to the smoothing, several investigations have been carried out: various distances between the measurement points, automated evaluation process, correlation of several standard deviations due to measurement or hydraulic effects etc., have been analysed. The application has been verified by an additional laboratory experiment (Figure 9.1), whereby the reduction of the noise effects becomes apparent due to the further development of the method.

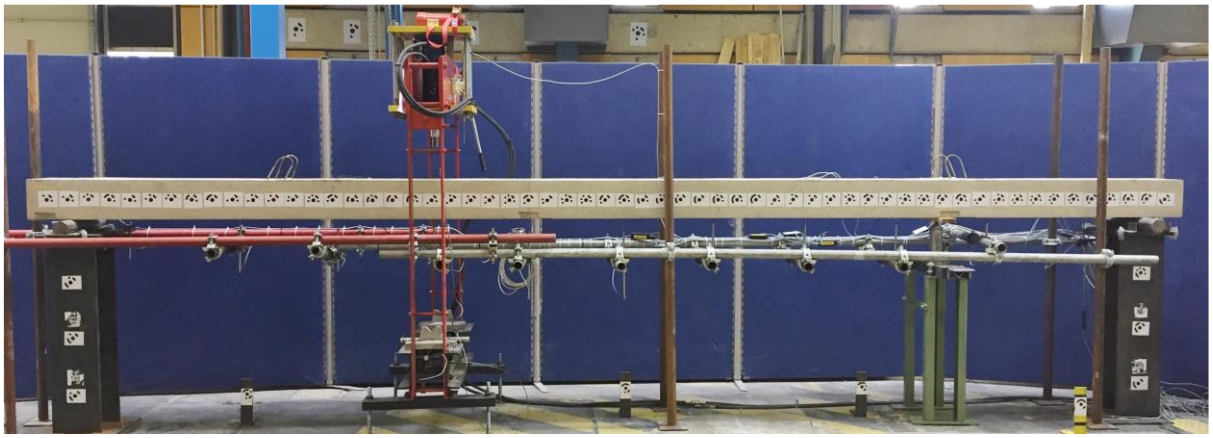

Figure 9.1. Experimental reinforced concrete beam with eccentrical loading

Further laboratory experiments, theoretical applications of the DAD-method, and further comparisons of several modern measurement techniques were presented in [96] [30] [97].

9.2 The Deformation Area Difference Method (DAD-method)

The basis of the DAD-method is the bending line, respectively, the deflection line resulting from a theoretical model of a structure and from an in-situ load deflection measurement. In case of local structural damage, the continuous stiffness curve along the longitudinal axis will present a disruption. The stiffness of a structure is in relation to the bending moment and the curvature. The curvature corresponds, in case of small deflections, to the second derivation of the deflection line. The small deflection is ensured by the non-destructive load deflection test within the serviceability limit state. The first derivation of the deflection line corresponds to the inclination angle, whereby the second derivation of the deflection line corresponds, as already mentioned, to the curvature of the structure. In turn, the curvature is equal to the relation between the bending moment and stiffness of the structure [30] [98]. Consequently, each stiffness change leads to discontinuities in the course of the curvature line. However, the change in stiffness can originate from possible damages, but also from the shape of the construction due to, e.g., coves, cross members or due to different widths over the length of the bridge. Therefore, the separation of both kinds of discontinuities is essential and a reference system including the scheduled stiffness change is required. A finite element model under consideration of the planned stiffness change along the longitudinal axis of the structure can be used as a reference system for the application of the DAD-method. Alternatively, an initial deflection measurement of a bridge structure can serve as a reference system after its manufacture. Subsequently, the discontinuity respectively the local damage of the structure will be localised using the algorithmic of the DAD-method.

The DAD-method considers particularly the area between the measured curves and the reference, respectively, theoretical curves of the deflection lines, inclination angles and curvatures from the load deflection experiment. In the following, the principle of the DAD-method will be introduced by using the results of the laboratory experiment (Figure 9.1). The aim of the test is to localise the cracked area using the DAD-method based on a load deflection experiment. Figure 9.2 shows exemplary the crack pattern in the beam for load step 20 kN. The

cracks were detected during the experiment and illustrated in Figure 9.2. The cracking in the reinforced concrete beam led to a stiffness reduction of approx. 60%.

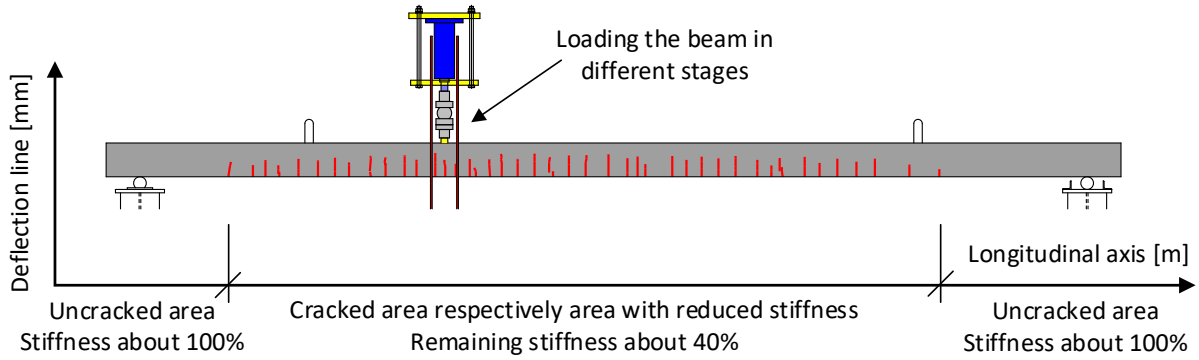

Figure 9.2 Crack pattern of the experimental beam for load step 20 kN

The theoretical background will be presented using Figure 9.2 and Figure 9.3. The part a. of Figure 9.3 illustrates the deflection lines wt(x) from the theoretical calculation serving as reference, wd(x) the deflection line with damage and wr(x) the deflection line from the polynomial regression. In a real application on a bridge the damaged deflection line wd(x) would be actually the measured deflection. To explain the method, the deflection line from the nonlinear calculation of the experimental beam was used in order to take into account the stiffness reduction caused by cracking. The polynomial regression is required to smooth the deflection line. A more detailed description and application of the polynomial regression can be found in section 9.3.2. Part b. of the Figure 9.3 shows the inclination angle from the reference system φt(x), from the damaged system φd(x) as well as from the polynomial regression φr(x). Part c. shows the curvature for all three variants. The comparison of the stiffnesses between the linear calculation EIt(x) and non-linear calculation EId(x) is illustrated in part d. of Figure 9.3. The DAD-method particularly investigates the area between the reference curves and the measured curves, which is shown as blue area in Figure 9.3. The considered area between the curves is then subdivided into several sections. The length of the sections corresponds to the distances between the deflection measurement points. The denser these points, the more accurate the localisation of the damage will be. Also, the mesh density of the finite element model of the structure must be at least as large as the distances of the measurement points.

Subsequently, the individual areas are squared and normalized by the sum of the individual squares of the areas according to equation (27).

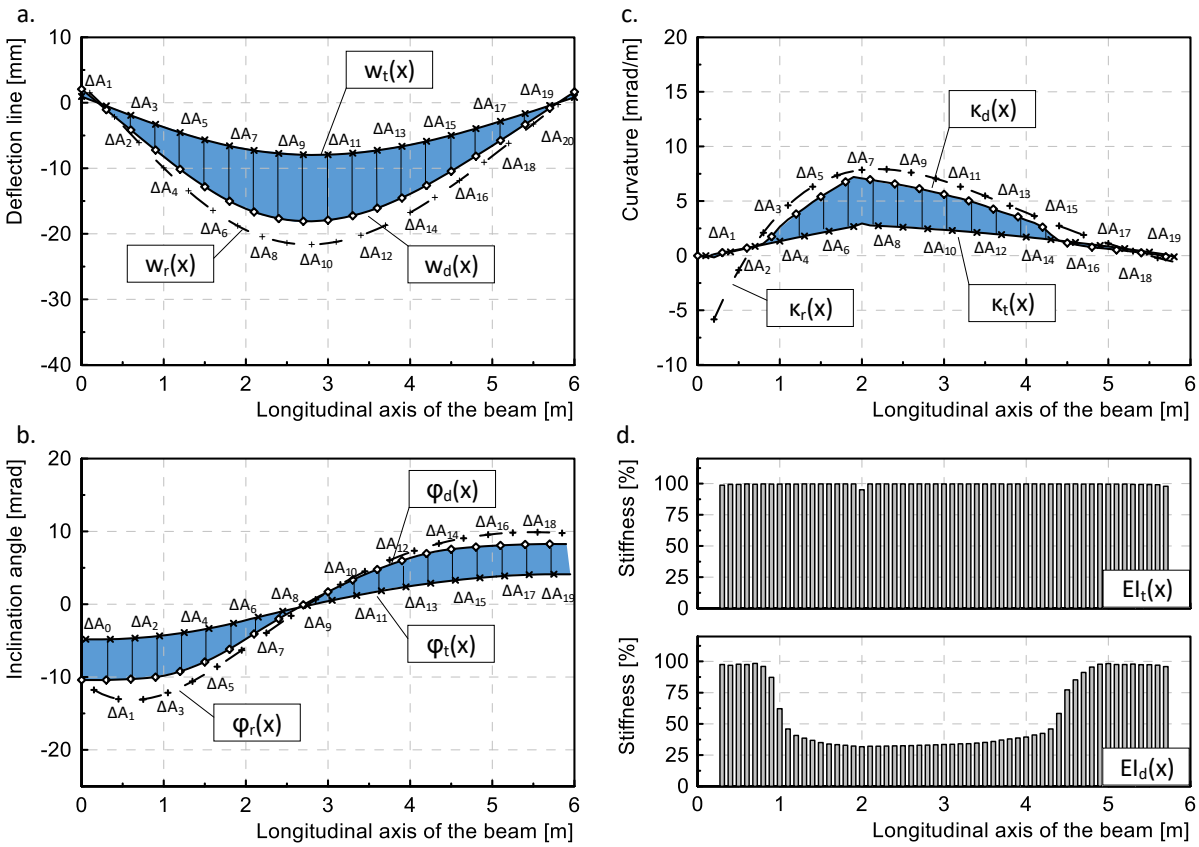

Figure 9.3. Principle of the DAD-method illustrated by the laboratory experiment

$w_t(x)$:Function of the theoretical deflection line

$w_d(x)$: Function of the measured resp. damaged deflection line

$w_r(x)$: Function of the polynomial regression of deflection

$\varphi_t(x)$: Theoretical inclination angle resulting from the first derivation of the theoretical deflection

$\varphi_d(x)$:Damaged inclination angle resulting from the first derivation of the damaged deflection

$\varphi_r(x)$: Function of the polynomial regression for inclination angle

$\kappa_t(x)$: Theoretical curvature resulting from the second derivation of the theoretical deflection

$\kappa_d(x)$: Damaged curvature resulting from the second derivation of the damaged deflection

$\kappa_r(x)$: Function of the polynomial regression for the curvature

The DAD-values are determined as already mentioned by the ratio between the squared area section and the sum of the squared area sections. The general formulation of the DAD-method is described in equation (27). The area differences between the theoretical and the measured results correspond to the difference between the integral functions of the theoretical and the measured characteristic equations regarding the deflection line, inclination angle and the curvature (equation (27)).

$$DAD_i(x) = \frac{\left[\int_{i-1}^{i} f_{d,i}(x)dx - \int_{i-1}^{i} f_{t,i}(x)dx\right]^2}{\sum_{i=1}^{n}\left[\int_{i-1}^{i} f_{d,i}(x)dx - \int_{i-1}^{i} f_{t,i}(x)dx\right]^2} = \frac{\Delta A_i^2}{\sum_{i=1}^{n}\Delta A_i^2} \tag{36}$$

$f_t(x)$: Theoretical function of the deflection line, the inclination angle or the curvature

$f_d(x)$: Measured resp. damaged function of the deflection line, the inclination angle or the curvature

Consequently, it is possible to complete the common equation for the DAD-values (equation (27)) with each area difference value for deflection line (equation (31)), for inclination angle (equation (32)) and for curvature (equation (33)).

$$DAD_{w,i}(x) = \frac{\Delta A_{w,i}^2}{\sum_{i=1}^{n}\Delta A_{w,i}^2} = \frac{[w_d(x_i) - w_t(x_i) - w_t(x_{i-1}) + w_d(x_{i-1})]^2}{\sum_{i=1}^{n}[w_d(x_i) - w_t(x_i) - w_t(x_{i-1}) + w_d(x_{i-1})]^2} \tag{37}$$

$$DAD_{\varphi,i}(x) = \frac{\Delta A_{\varphi,i}^2}{\sum_{i=1}^{n}\Delta A_{\varphi,i}^2} = \frac{[w_d(x_i) - w_d(x_{i-1}) - w_t(x_i) + w_t(x_{i-1})]^2}{\sum_{i=1}^{n}[w_d(x_i) - w_d(x_{i-1}) - w_t(x_i) + w_t(x_{i-1})]^2} \tag{38}$$

$$DAD_{\kappa,i}(x) = \frac{\Delta A_{\kappa,i}^2}{\sum_{i=1}^{n}\Delta A_{\kappa,i}^2} = \frac{[\varphi_d(x_i) - \varphi_d(x_{i-1}) - \varphi_t(x_i) + \varphi_t(x_{i-1})]^2}{\sum_{i=1}^{n}[\varphi_d(x_i) - \varphi_d(x_{i-1}) - \varphi_t(x_i) + \varphi_t(x_{i-1})]^2} \tag{39}$$

Detailed descriptions, a derivation of the formula as well as several case studies are published in [95]. The application of the DAD-method based on a laboratory experiment, a consideration of measurement noise minimisation and the results will be presented in the following chapters.

9.3 Procedure of the DAD-method

The application of the DAD-method is summarized in the flowchart in Figure 9.10. As already discussed, the the DAD-method is based on the measurement of the deflection line which is compared to a theoretical model of the investigated structure. The method is able to localise damages independent on the global influences such as temperature or non-structural layers such as the asphalt layer. However, the limitation of the damage detection depends on the precision of the applied measurement technique. Important prerequisites regarding the measurement techniques consist in a high density of measurement points to enable the creation of a continuous deflection line, high precision of the measurements and suitable applicability for in-situ bridge tests. The identification of discontinuities of the structure using the DAD-method is based on probability calculations considering the standard deviation of the applied measurement technique. According to the DAD-method, the deflection line is derived several times, in order to calculate the inclination angle and the curvature. Thus, the effect of noise resulting from the measurement precision increases obviously. The main advancement of the method compared to [95] is that the noise from the measurement is considered in the evaluation process. Although, the measurement with photogrammetric methods allows very high precision, but this is not absolute and has a certain standard deviation such as any other measurement technique. Therefore, the measured deflection line has a certain noise in the range of the standard deviation. Damage that causes discontinuities in the range of standard deviation cannot be clearly assessed. Therefore, in the next step, the measured deflection will be smoothed in the range of the standard deviation of the measurement technique so that only the discontinuities beyond the standard deviation become relevant.

The smoothing of the measured deflection requires a reference curve. Therefore, a polynomial regression of the measured deflection values was chosen as reference curve. A similar procedure was applied in the work of Sun, et al. [54]. Nonetheless, the degree of the polynomial regression should be chosen individually from one case to another, as it depends essentially on the type of the static system, the way of the loading and the shape of the deflection line. Riveiro et al. [93] used linear data fitting in their work because they measured the underclearance of bridge structures which usually has a straight course (a. Figure 9.4). The laboratory experiment within this paper is stressed due to self-weight as well as due to a single load. The deflection

curve resulting by a uniformly distributed load has the form of a fourth degree parabola whereas the deflection curve resulting from the single load has the form of a third degree parabola. Figure 9.4 illustrates schematically the various possibilities for data fitting.

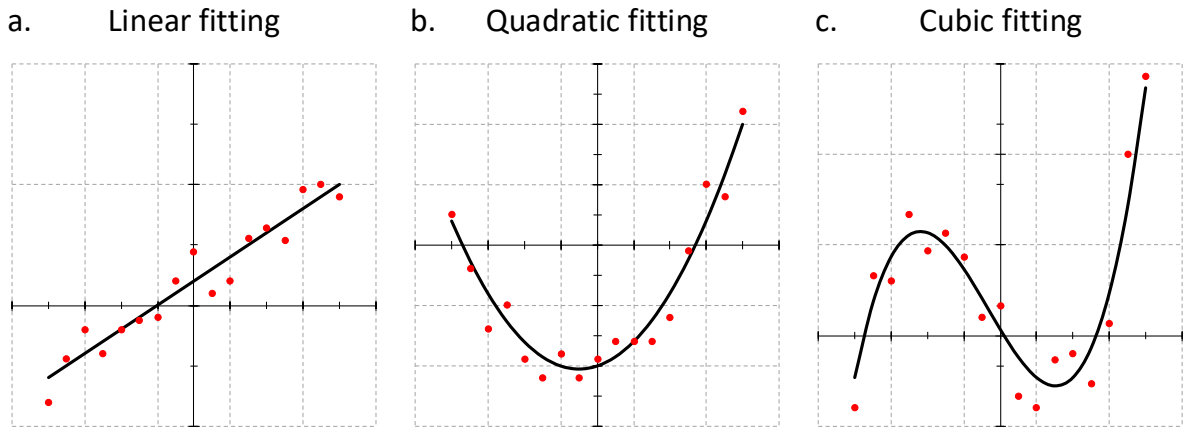

Figure 9.4. Fitting of measured data a. linear fitting b. quadratic fitting c. cubic fitting

In the process of data evaluation, the decision on the degree of the polynomial regression is taken on the basis of the measured deflection line. The deviating values from the continuous course of the deflection line are shifted towards the direction of the polynomial regression within the range of the standard deviation of the measurement technique. Subsequently, the inclination angle and curvature will be calculated from the smoothed deflection values. In the next step, an additional consideration of measurement point variation will be taken into account. The individual steps of the procedure will be explained in more detail in the following subsections.

9.3.1 Standard deviation

The precision of the measurement of the deflection over the total length of a structure is limited by the scatter of the measurement technique. Each measurement technique has a limited precision; however most modern measurement techniques allow high accuracy and small standard deviations. The measurement of the deflection over the total length of the bridge structure comprises many data points, which form a point cloud. Each measured data point has an individual standard deviation. The deflection line of the experiment is measured by close-

range photogrammetry. The photogrammetry is applied using a full-frame camera Nikon D800 and the point cloud is managed using a processing software of Elcovision 10. In order to allow high precision measurements, several settings and prerequisites must be taken into account. The camera is equipped with a 50 mm fixed focal length lens. An important prerequisite for precise measurement with photogrammetry is the calibration of the applied camera. For the calibration of the camera, the University of Luxembourg is equipped with a wall with a dimension of 13 x 7m and with 163 photogrammetry targets (Figure 9.5). The adjusted shutter speed amounts to 1/30 sec, ISO2000 and the F-stop amounts to f/10 and remains the same both for the calibrations and for the measurement of the specimen's deflection. The captures are taken using a remote camera shutter and from a tripod to avoid blurring.

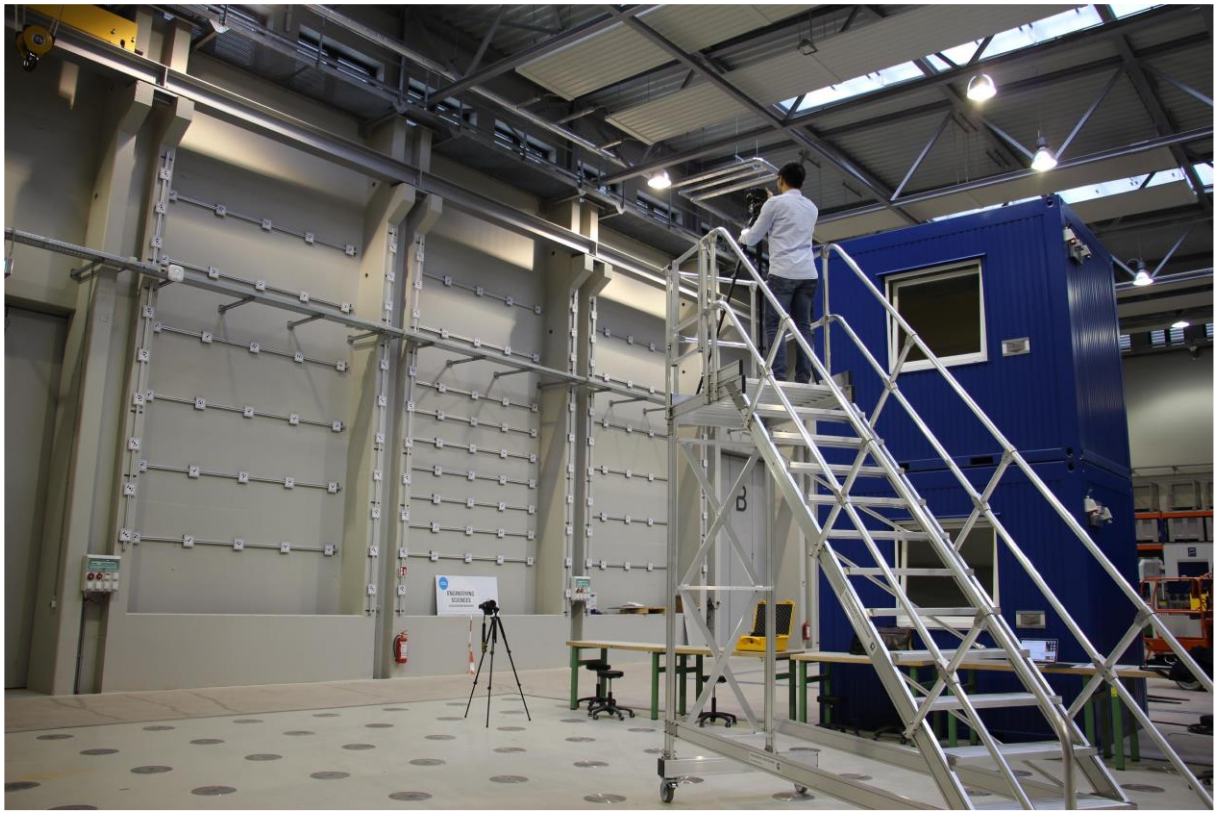

Figure 9.5. Process of camera calibration using a large scale calibration wall with the dimension of about 13,0x7,0 m and 163 targets

The application of close-range photogrammetry allows high precision measurement of the deflection line, whereby the standard deviation of the technique is taken into account to reduce the noise effects and to smooth the measured deflection curve. Figure 9.6 shows the standard

deviations of each measurement point exemplary for the load steps 5 kN, 15 kN and 40 kN. The reached precision of photogrammetry varies in the range of 0,06 mm to 0,11 mm (Figure 9.6).

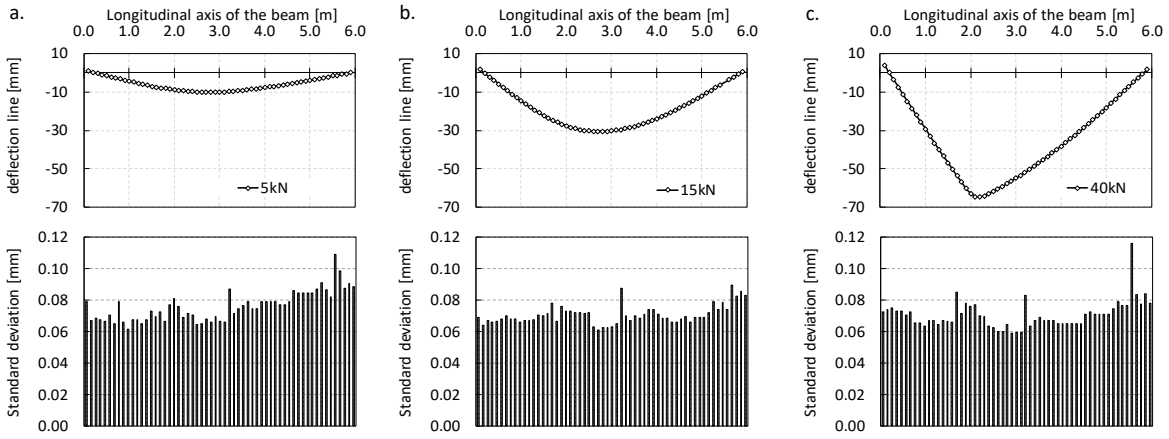

Figure 9.6. Standard deviations resulting from close-range photogrammetry exemplary for the load steps 5 kN, 15 kN and 40 kN

9.3.2 Polynomial regression and smoothing of the deflection line

The calculation of the curvature leads to an increase of the noise effect due to double derivation of the measured deflection. Within the DAD-method, the discontinuity of the structural behaviour from a load deflection experiment is investigated. The DAD method has already demonstrated that even a very small stiffness change of 1% is identifiable when applying the method on deformation values from FE calculations [95]. So, the identification of damage will not be limited by the DAD-method itself, but only by the applied measurement technique. The accuracy of the measurement results by using photogrammetry is defined by the standard deviation with a probability of 66,7 %. The experiment shows that the very accurate measurement of the photogrammetry achieves a minimum standard deviation of about 0,08 mm (Figure 9.6), which could be improved depending on the camera and calibration quality. Discontinuities within the standard deviation cannot be separated from the measurement accuracy. However, it is possible to smooth the measured deflection data to identify discontinuities outside the standard deviation range. The identified discontinuities outside of

the standard deviation point to stiffness changes respectively to damages. Damage producing discontinuities in the range of the standard deviation will not become apparent, but repeated measurements can minimize the probability of random peaks and will improve reliably the damage detection. The DAD-method is able to localize damage depending on the accuracy of the applied measurement technique: only damage, which affects the deflection measurements of a structure stronger as the variations inherent to the measurement accuracy, will become apparent. To illustrate this point, further investigations on the relationship between the measurement accuracy and the degree of damage is presented using the results of a second laboratory experiment in section 9.4.5. In order to smooth the measured data, a reference curve is required. Figure 9.7 shows the principle of the smoothing process. In Figure 9.7, there are 7 measuring points in total (green triangular markers) for the deflection of a beam with 6 m span length. Each point has an individual standard deviation. The red dashed line shows the course of the deflection line from the FE calculation. A polynomial regression is generated from the measurement data and serves as reference curve for smoothing. The polynomial regression is shown in Figure 9.7 with a blue dot-dash line. As already mentioned, the degree of the polynomial regression has to be chosen under consideration of the static system, type of loading and the form of the deflection line (equation (40)). The decision about the degree of polynomial regression has to be taken individually from case to case. A first verification of the regression degree can be done by comparing the second derivation of the measured deflection line with the polynomial regression line. The regression degree is augmented until these two lines show visually good agreement. However, the correspondence of the polynomial regression can also be expressed in numbers by using the correlation coefficient according to Pearson (equation (42)). The higher the degree, the closer the correlation to the measured curve of deflection line.

Due to the precision of the measurements, the standard deviation resp. the noise is very small. Thus, the agreement in numbers according to Pearson is almost 100%. For the experimental beam a polynomial regression of the sixth degree is applied. The degree of the polynomial regression is chosen according to the agreement with the measured values. With this choice, the correlation coefficient amounts to 0,99 for all load levels. By smoothing the measured raw data, the measurement points are shifted within the range of the standard deviation in direction of the reference curve (equation (43)). Here, the reason why the polynomial regression is chosen as reference to smooth the measured value becomes clearer. If the deflection curve from the

FE-calculation (red dashed line) would be used as reference curve to smooth the measured values, which are affected by noise (green triangular targets in Figure 9.7), all measured values would be shifted together in the direction of the curve from FE due to smoothing process. In fact the measured values will be shifted only globally in direction of the reference and the effect of noise would remain the same. In contrast, when the reference curve is determined due to polynomial regression as an optimal continuous curve, the curve from the measured values is moved in the direction of the continuous reference curve. In other words, all measuring points are shifted individually in the direction of the continuous reference curve. The limit is, as already mentioned, the level of the standard deviation of the photogrammetry. In Figure 9.7, the red rhombic markers represent the deflection points after the smoothing. Thus, the deflection line (solid black line) is created with less noise effect. By means of this smoothing process, the damage respectively the discontinuity can be identified separately from the measurable accuracies. Thus, any discontinuities that might be caused by the standard deviation of the measurement technique are excluded. Consequently, one has also to mention that all damage, which affects the structure in the range of the measurement accuracy, will remain undetected.

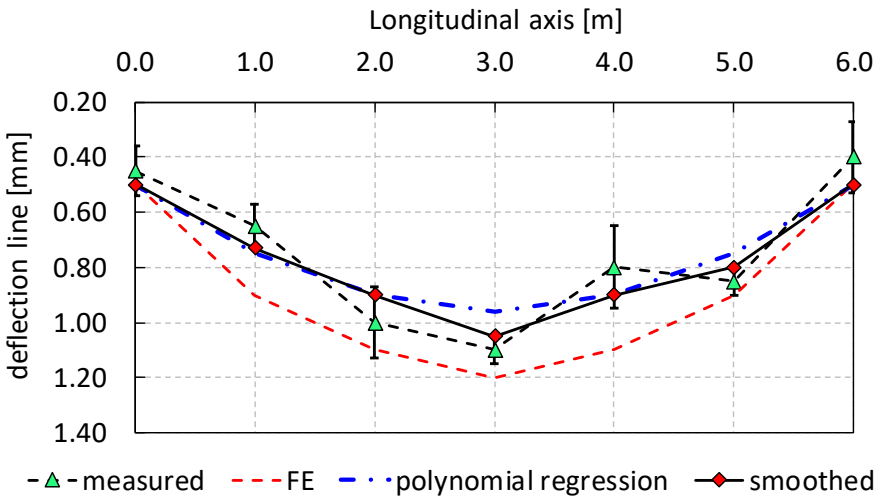

Figure 9.7. Individual standard deviations for each measurement point

$$\begin{bmatrix} y_1 \\ y_2 \\ y_3 \\ \vdots \\ y_n \end{bmatrix} = \begin{bmatrix} 1 & x_1 & x_1^2 & \cdots & x_1^m \\ 1 & x_2 & x_2^2 & \cdots & x_2^m \\ 1 & x_3 & x_3^2 & \cdots & x_3^m \\ \vdots & \vdots & \vdots & & \vdots \\ 1 & x_n & x_n^2 & \cdots & x_n^m \end{bmatrix} \begin{bmatrix} a_0 \\ a_1 \\ a_2 \\ \vdots \\ a_m \end{bmatrix} + \begin{bmatrix} \varepsilon_1 \\ \varepsilon_2 \\ \varepsilon_3 \\ \vdots \\ \varepsilon_n \end{bmatrix} \tag{40}$$

$$w_r(x) = \sum_{i=1}^{n} a_i x^i \tag{41}$$

$$r = \frac{\sum(x - \bar{x})(y - \bar{y})}{\sqrt{\sum(x - \bar{x})^2 \sum(y - \bar{y})^2}} \tag{42}$$

$$\begin{cases} w_d(x) = w_m(x) - 0{,}50 \cdot s(x) \geq w_r(x), & if \quad w_m(x) \geq w_r(x) \\ w_d(x) = w_m(x) + 0{,}50 \cdot s(x) \leq w_r(x), & if \quad w_m(x) < w_r(x) \end{cases} \tag{43}$$

y_i: Representation of the polynomial regression in the form of a matrix

$w_r(x)$: Function of the polynomial regression of deflection

r: Correlation coefficient according to Pearson

$w_m(x)$: Function of the raw measured deflection line

$w_d(x)$: Function of the measured resp. damaged deflection line after smoothing

s(x): Standard deviation resulting from the measurement technique

9.3.3 Consideration of measurement point variations

The density of the measurement points is of essential importance. In principle, the denser these points the more accurate will be the localisation of the damage. Nonetheless, the closer the points to each other, the smaller are the height differences between the points (Figure 9.9). Figure 9.9 also shows the standard deviations for the points. If the inclination angle will be determined from one point to the next point, the height differences between the points would be comparatively small (part a. Figure 9.9) compared to the size of the standard deviation. Therefore, the results would be influenced more by the standard deviation. In comparison, in part b. of Figure 9.9 a variation is given where only every third point is considered. There it can be seen that the standard deviation of the measurements was less influence on the results. The optimum ratio of the point distances depends on the standard deviation respectively on the size of the measurement noise, the size of the deflection and on the degree of damage. Sun et al.

[54] represented the optimal relation between the noise, damage and curvature calculation interval, which has initially a decreasing tendency and then an increasing one. The optimal value is defined at the lowest point of the relationship (Figure 9.8).

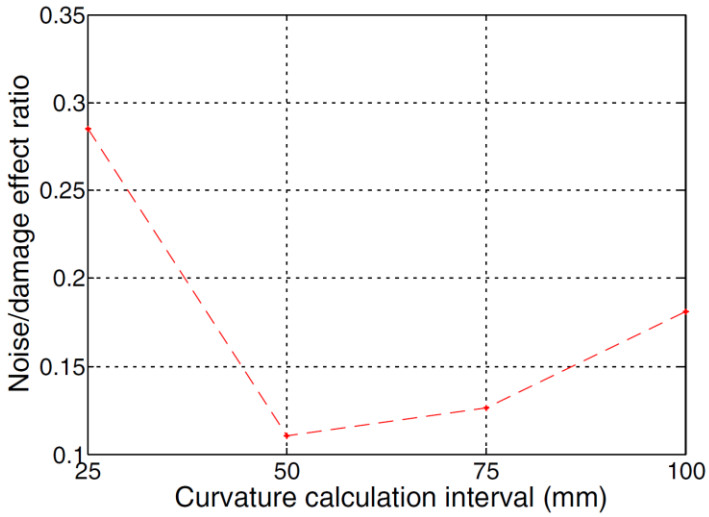

Figure 9.8. Curvature calculation interval according to Sun et al. [54]

So, the precision of the damage localisation is depended on the measurement point distances. The application of this consideration becomes clearer using the results from the laboratory experiment in section 9.4.3.

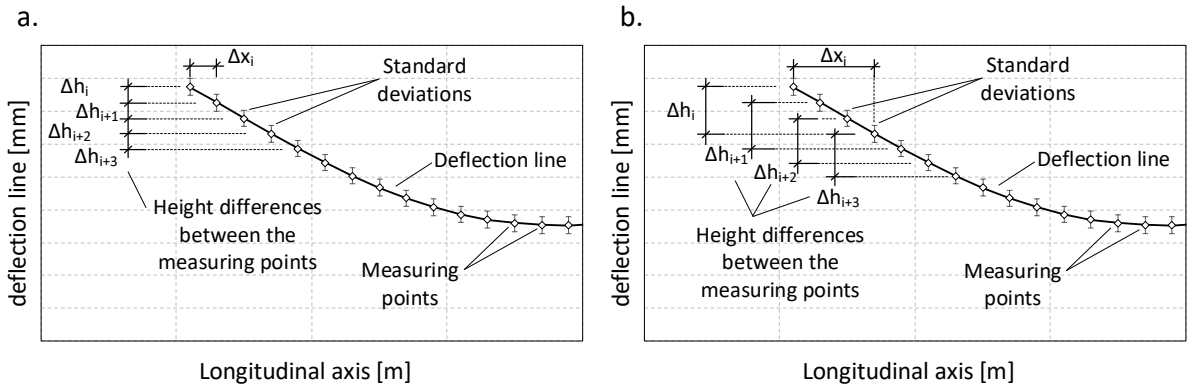

Figure 9.9. Measurement point variations a. point to the next point; b. point to the next third point

9.3.4 Summary of the evaluation procedure based on flowchart

In the following, the summary of the complete evaluation procedure will be presented using the flowchart in Figure 9.10. The initial aim of the DAD-method is the detection and localisation of damage in bridge structures. The basics for the application of the method are on the one hand the theoretical model of the bridge structure considering all planned stiffness changes or the initial deflection measurement after the construction, and on the other hand the measurement of the deflection line. The prerequisite is in particular a high-precision measurement of the deflection line along the longitudinal axis of the bridge structure. Since the theoretical results from the finite element model are not affected by measurement noise, the inclination angle and the curvature of the reference curve can be directly determined. However, the measured deflection line includes an effect of noise due to measurement precision. As already mentioned, the smoothing of the measurement noise requires a reference curve, which is given by polynomial regression (part A. in Figure 9.10). The degree of the polynomial regression should be calculated individually depending on the loading, deflection line and measurement noise. The smoothing of the raw data is presented in part B. of Figure 9.10 and limited within the range of the standard deviation from photogrammetry. Several variations of the limit value analysis become necessary and will be calculated according to the equation (43). After the smoothing the deflection line, the inclination angle and the curvature are determined according to equations (24) and (25) (part C. Figure 9.10).

$$\varphi(x) = w'(x) = \frac{\delta w(x)}{\delta(x)} \tag{44}$$

$$k(x) \approx \varphi'(x) = w''(x) = \frac{\delta^2 w(x)}{\delta^2(x)} \tag{45}$$

$\kappa(x)$: Curvature

$w(x)$: Bending resp. deflection

$\varphi(x)$: Inclination angle

In the next step, as already explained in detail, the measurement point variation will be investigated. The aim of the measuring point variation is to find the optimum of measurement point distances from one measurement point to the next one. Finally, the algorithm of the DAD-method will be applied (equations (31), (32), (33) and part D. of Figure 9.10), whereby the peaks in the course of DAD-values indicate possible stiffness changes or damages.

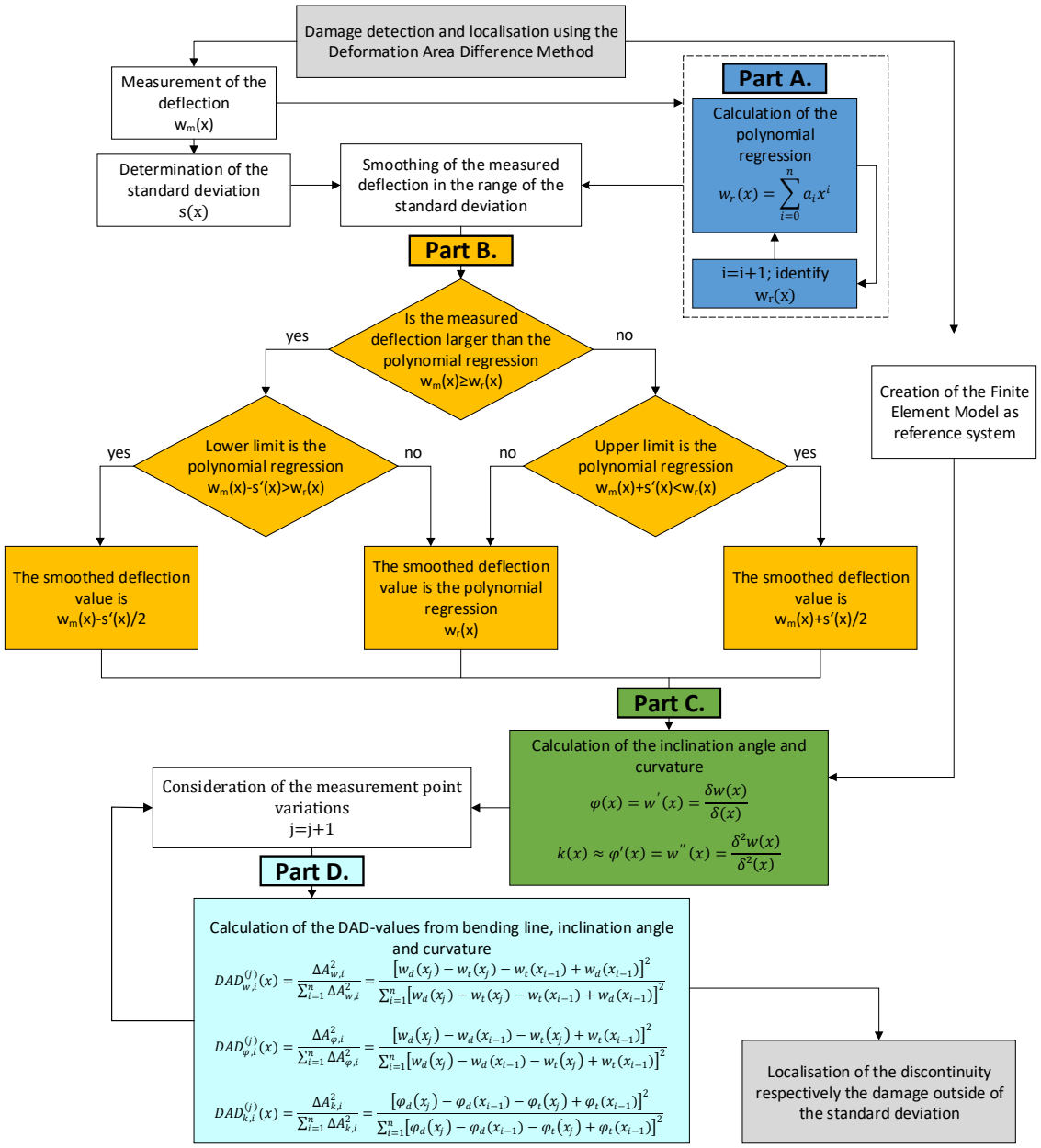

Figure 9.10. Flowchart of the damage detection using the DAD-method

9.4 Laboratory experiment

The application of the DAD-method for localization of damage, respectively, stiffness reduction is tested on an experimental beam (Figure 9.11). The laboratory test consists of a reinforced concrete (Figure 9.12) beam with a total length of 6,00 m and with a span of 5,60 m. The loading of the beam takes place eccentrically at 1,80 m from the left support. The loading is path-controlled and the load steps are 5 kN, 10 kN, 20 kN, 30 kN and 40 kN. At the first load step, the beam starts to receive cracks in the area of the load application. However, the first two load steps do not lead to excess of the deflection in the serviceability limit state. With the increasing load, the cracked area spreads along the longitudinal axis of the beam. The stiffness reduction resulting from cracking amounts about 60 % for the experimental beam. In case of suitable localisation of the cracked area within the load steps 5 kN and 10 kN, the method could be suitable for its application within the serviceability limit state as non-destructive damage detection method. At the load step of 40 kN, the expected collapse of the beam occurred due to the concrete failure in the compression zone. The detection of each crack is accurately carried out with a crack magnifier. For each load step, the deflection line is measured using photogrammetry and displacement sensors. Along the beam, several coded photogrammetry targets were positioned at intervals of 10 cm. Reference targets were installed at the bottom, on both supports and in the background of the experimental beam (Figure 9.11). The main objective of the experiment is to identify the discontinuities resulting from the different stiffness reduction scenarios and to compare them with the detected crack pattern.

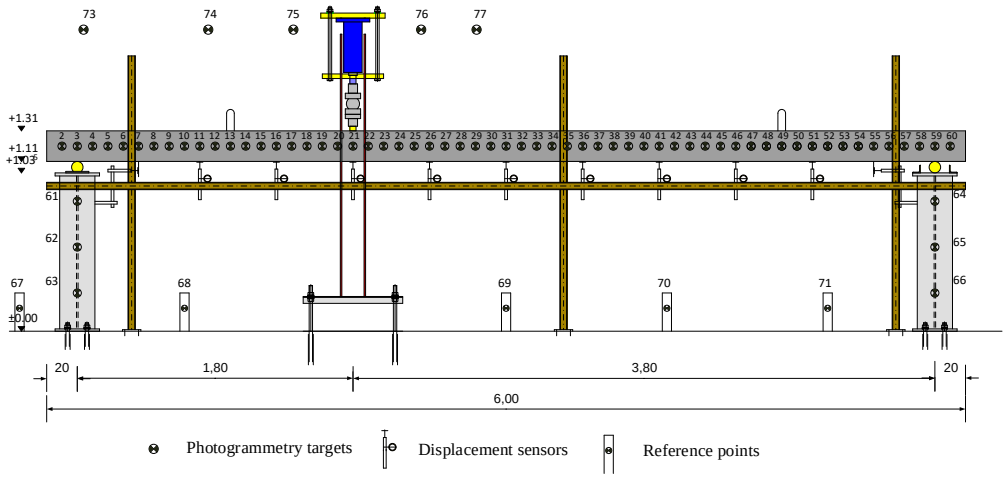

Figure 9.11. Setup of the laboratory experiment with a reinforced concrete beam [97]

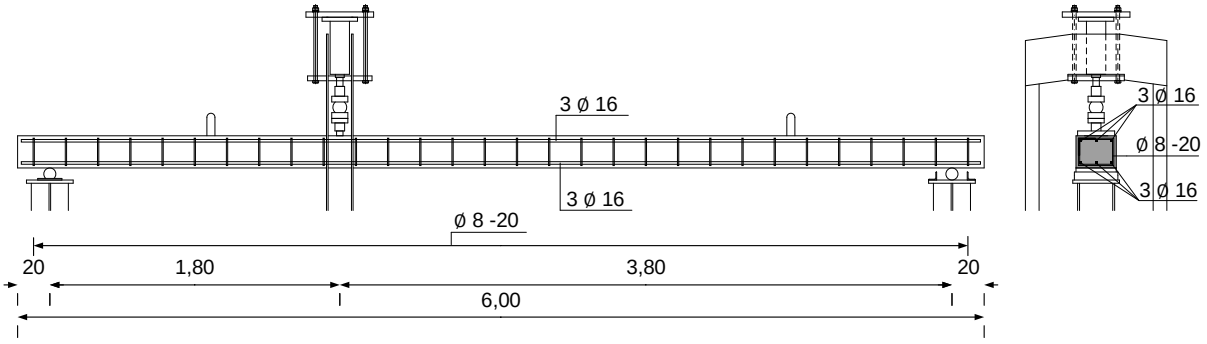

Figure 9.12. Side view (left side) and cross sectional view of the loading situation and the laboratory beam (with reinforcement)

9.4.1 Theoretical calculation compared to the measurement

Before the experimental test is carried out, the load deflection behaviour of the reinforced beam is investigated using linear and non-linear calculation with the finite element software SOFiSTiK The statically determined single-span beam is simulated using the quad-elements with the side length of 10 cm. In order to create a model close to reality, the partial safety factors are set to 1.0 and the beam is stressed by a line load over the beam width. The non-linear calculation considers the stiffness reduction due to cracking, due to yielding of the reinforcement and concrete compression failure. Figure 9.13, Figure 9.14 and Figure 9.15 show the deflection lines, inclination angles and curvatures for the load steps 10 kN, 20 kN and 40 kN. In Figure 9.13, Figure 9.14, it can be observed that the measured deflection is slightly larger than the deflection from the nonlinear calculation. Within the laboratory test, the reinforced concrete beam is loaded by path-controlled hydraulic. The stepwise loading of the beam took place by repeated loading and unloading, while the deflection due to creep effects increased continuously. For each load step took 2 hours were needed to complete the measurement. Therefore, the difference between the measured and the calculated deflection can be explained by the additional creep deflections due to the stepwise loading and unloading process. Figure 9.15 includes also the deformation values after concrete failure in the compression zone. Here, the deflection resulting from the nonlinear calculation is higher than from the measurement. This can be explained by the fact that the measurement of the deflection took place after unloading the beam where the elastic part of the deformation had already

receded. As already mentioned, the inclination angle is calculated due to the first derivation of the deflection curve and the curvature due to the double derivation of the deflection line. The increased noise effect due to the multiple derivations is clearly recognizable in the following figures.

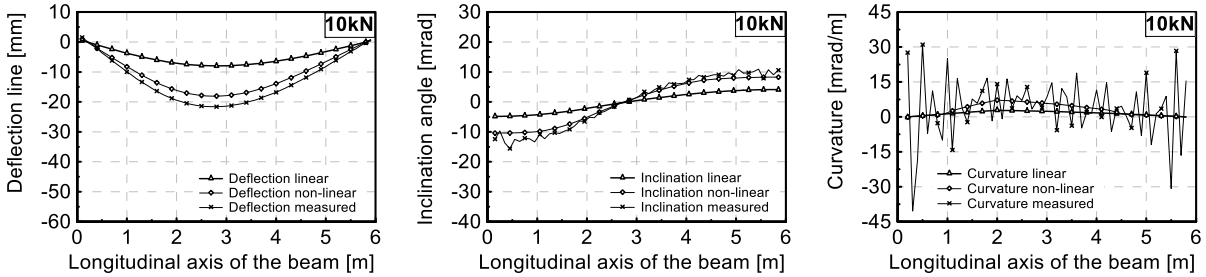

Figure 9.13. Measured and calculated deflection lines, inclination angle and curvature for the load step 10 kN

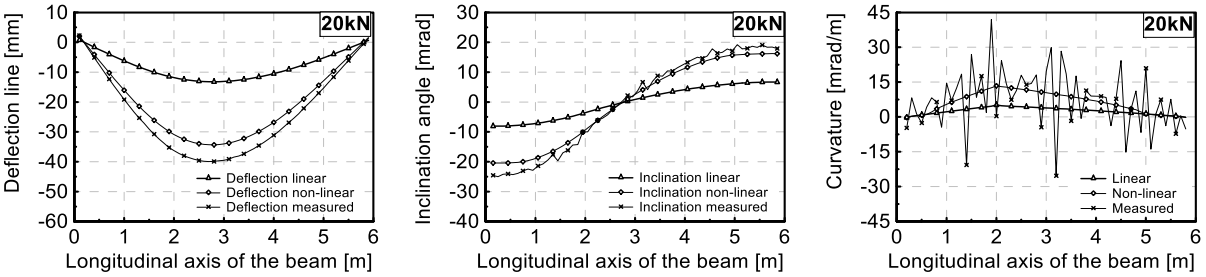

Figure 9.14. Measured and calculated deflection lines, inclination angle and curvature for the load step 20 kN

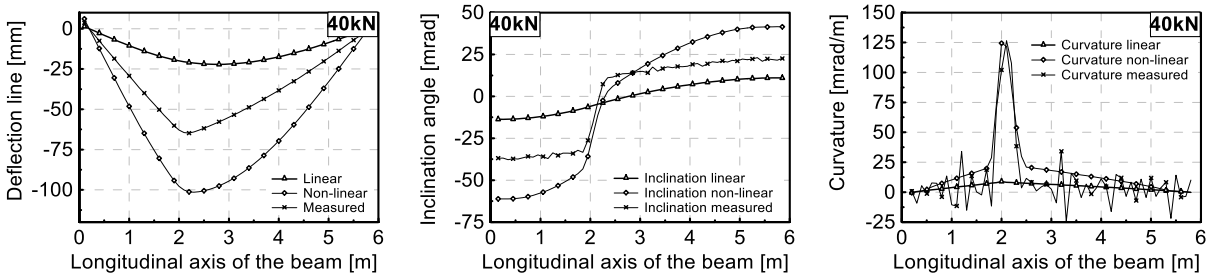

Figure 9.15. Measured and calculated deflection lines, inclination angle and curvature for the load step 40 kN

9.4.2 Consideration of the measurement accuracy and smoothing the curves

The standard deviation from the photogrammetric measurement ranges from 0,06 mm to 0,10 mm. The values of the standard deviation are used for the smoothing of the deflection curve according to the description of the DAD-method. As already discussed, in order to enable the smoothing of the deflection curve a reference curve is needed. Therefore, a polynomial regression is chosen as a reference system. The degree of the polynomial regression amounts to six for the experimental beam (for more information see section 9.3.2). Figure 9.16 and Figure 9.17 show the curvature curves calculated from the second derivation of the measured deflection line for each load step as well as the polynomial regression sixth degree and the smoothed curvature course. It is important to choose the appropriate degree of the polynomial regression. Otherwise, the smoothing of the curve can have only a global effect without reducing noise the effects (see section 9.3.2). The second derivation of the polynomial regression is the curvature of the polynomial regression, which is presented as red line in Figure 9.16 and in Figure 9.17. The tendency of the curvature line resulting from the polynomial regression shows some deviations at the beginning and at the end of the longitudinal axis of the beam. This is particularly visible in part c. of Figure 9.16 and in Figure 9.17. Here, the polynomial regression is not at the average of the curvature noise. The consequences thereof become clear in the experimental result related to the following chapter.

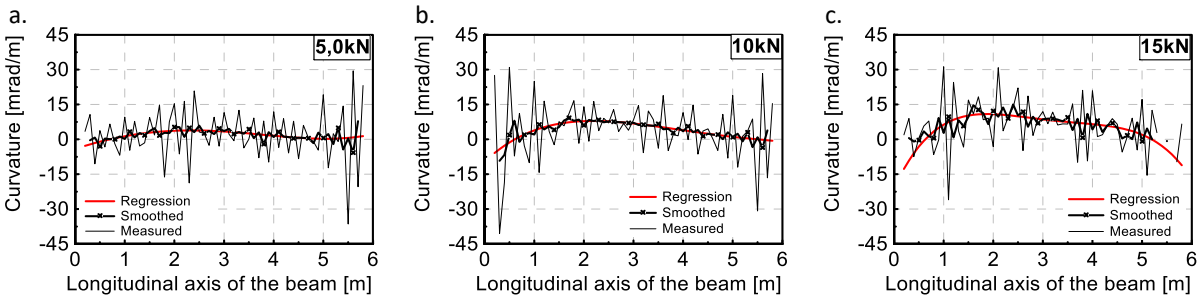

Figure 9.16. Course of the curvature “red” from polynomial regression, “black with marker x” after smoothing and “black” from the raw measurement, A. load step 5 kN, B. 10 kN, C. 15 kN

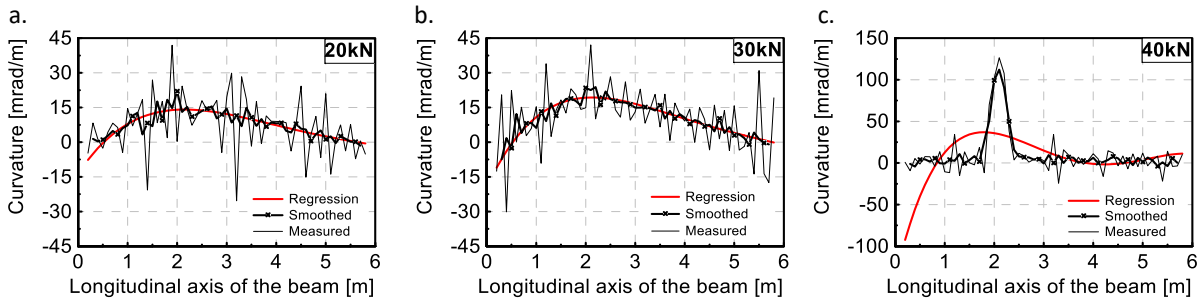

Figure 9.17. Course of the curvature "red" from polynomial regression, "black with marker x" after smoothing and "black" from the raw measurement, a. load step 20 kN, b. 30 kN, c. 40 kN

9.4.3 Consideration of measurement point variations

An important aspect of the data evaluation is the considered section length. Indeed, the distance between the measurement points respectively the density of the point cloud will directly influence the damage localisation accuracy. However, the considered section length must be chosen such that the noise effects of the measurement technique have limited influence only. For the laboratory experiment, the density of the measurement point amounted to 10 cm. Due to small deflections at the lower load steps, the resulting deflections remain small. Consequently, the height differences between one point to the next point is with a distance of 10 cm very small so that the standard deviation generates too much noise. Figure 9.18 shows the influence of the measurement point distance Δxi variation depending on the noise s(x) and height difference Δhi relation. In order to represent the ratio in percent, the influence of the standard deviation ($s(x)/\Delta hi$) for the case $\Delta xi=10$ cm is set to 100 % (Figure 9.18). The standard deviation from the measurement technique behaves relatively constant as shown in Figure 9.6. Figure 9.18 clearly showed that the influence of the standard deviation for smaller height differences (see also Figure 9.9) is considerably bigger and decreases exponentially as a function of the measurement point distances Δxi. Figure 9.19 shows the DAD-values for four investigated variations of possible section lengths (10 cm, 20 cm, 30 cm and 40 cm.). By choosing different section lengths, the results differ substantially. The DAD-values for 10 cm distances strongly differs from DAD-values for 20 cm, 30 cm and 40 cm, because the result is strongly affected by the noise effect. For the measurement point distances of 30 cm and 40 cm,

no significant changes become apparent. As in Figure 9.18 shown, by considering the measurement point variation of 30 cm, the influence is reduced by up to 23,7 %. The reduction of the influence from 30 cm to 40 cm amounts about 23,7-15,5= 8,2 %. Therefore, for the further analysis and evaluation of the experiment the section length of 30 cm (every third measurement point) has been chosen as the on the other hand a close-range measurement grid increases the accuracy of damage localisation. Accordingly, the damage localisation accuracy is limited to 30 cm. A detailed description of the backgrounds and procedures has already been provided in section 9.3.3.

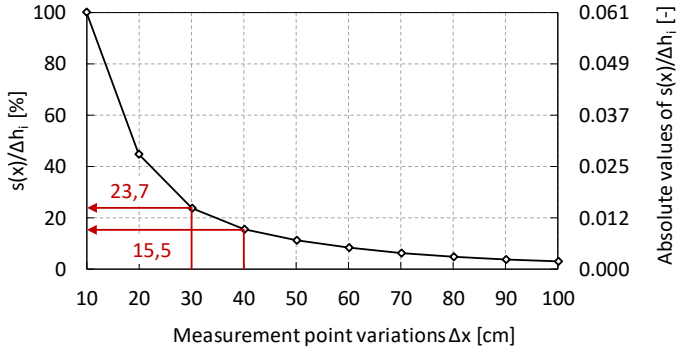

Figure 9.18. Influence of the measurement point variation depending on the standard deviation

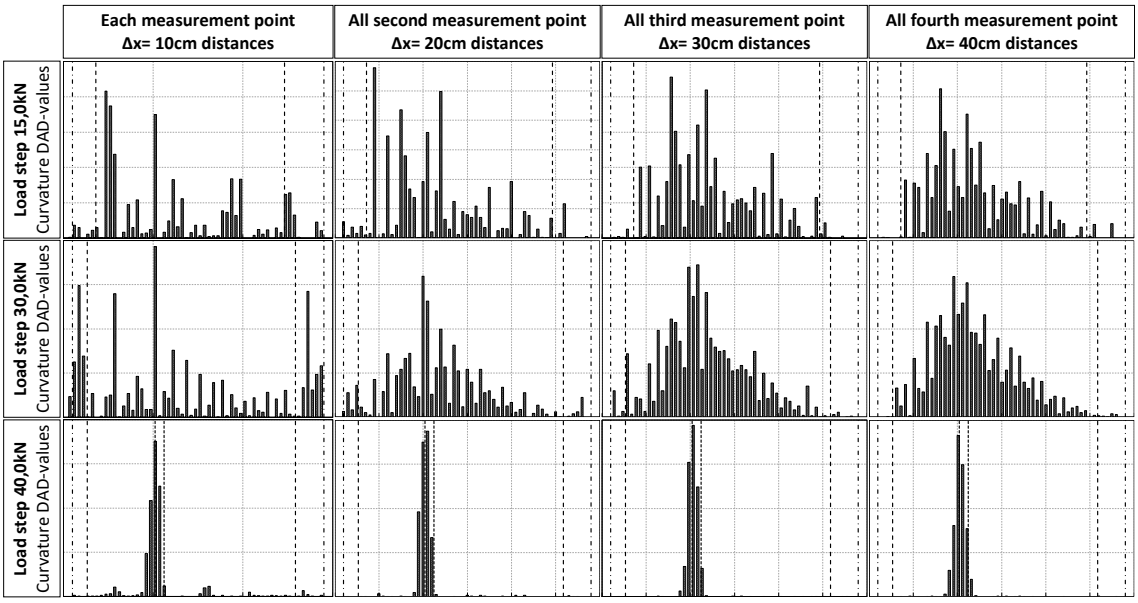

Figure 9.19. Different variation of investigated section length exemplary for the load steps 15 kN, 30 kN and 40 kN

9.4.4 Localisation of damage using DAD-method

As described in the experimental setup, each crack position and height is documented for each load step (part a. from Figure 9.20 to Figure 9.25). In this chapter, the localisation of the damage respectively local stiffness reduction due to cracking and concrete failure will be investigated. Thus, the DAD-values from curvature were calculated according to equation (33), which should highlight damage at discontinuities. Figure 9.20 to Figure 9.25 summarise the main results from the laboratory experiment. In part a. the documented cracks with their position and heights of the laboratory test are presented. Part b. shows the DAD-values for localisation of damage. The dash dotted lines in Part b. indicate the position of the supports and the dashed lines the beginning and ending of the cracked area. At load step 5,0 kN (Part a. Figure 9.20), some cracks with low density have been detected. The DAD-values show for the same load step (Part b. Figure 9.20) discontinuities in the same area with corresponding density. With load step 10 kN, the density increases as well as the cracked area (Figure 9.20 to Figure 9.24). The DAD-values from curvature show good accordance to the cracked area, which enables the localisation of the damage respectively area with the reduced stiffness. Figure 9.25 also clearly shows the localisation of the concrete failure at about 2,0 m by the horizontal axis.

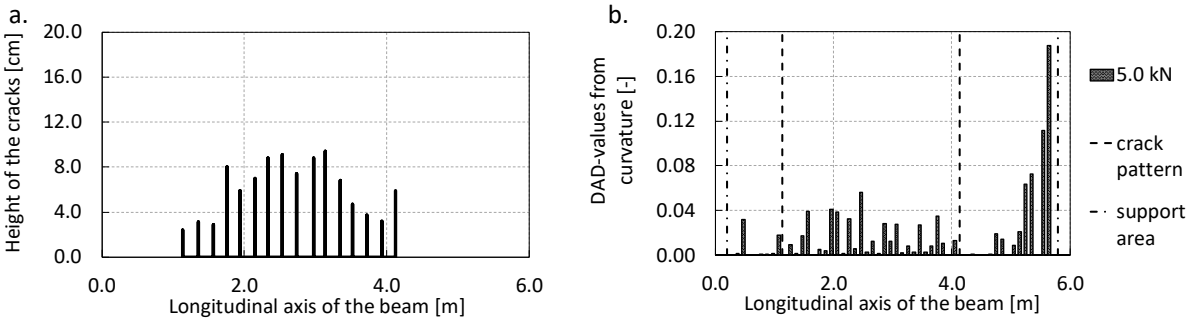

Figure 9.20. a. Detected cracks in the experimental reinforced beam, b. DAD-values from curvature for load step 5,0 kN

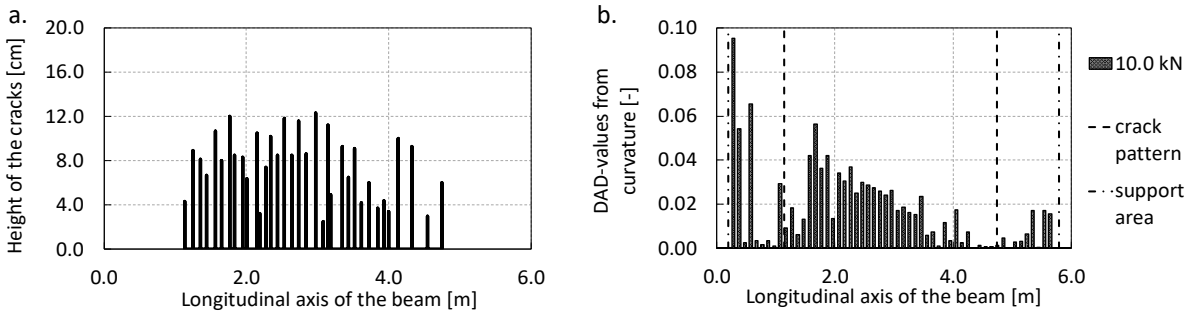

Figure 9.21. a. Detected cracks in the experimental reinforced beam, b. DAD-values from curvature for load step 10 kN

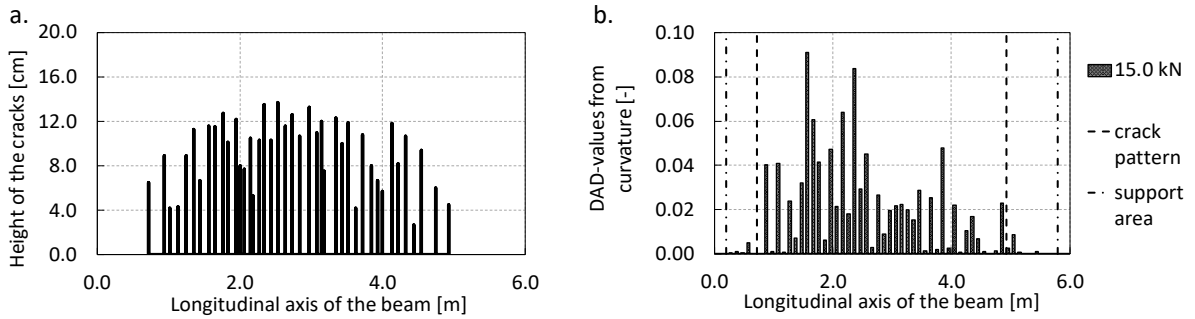

Figure 9.22. a. Detected cracks in the experimental reinforced beam, b. DAD-values from curvature for load step 15 kN

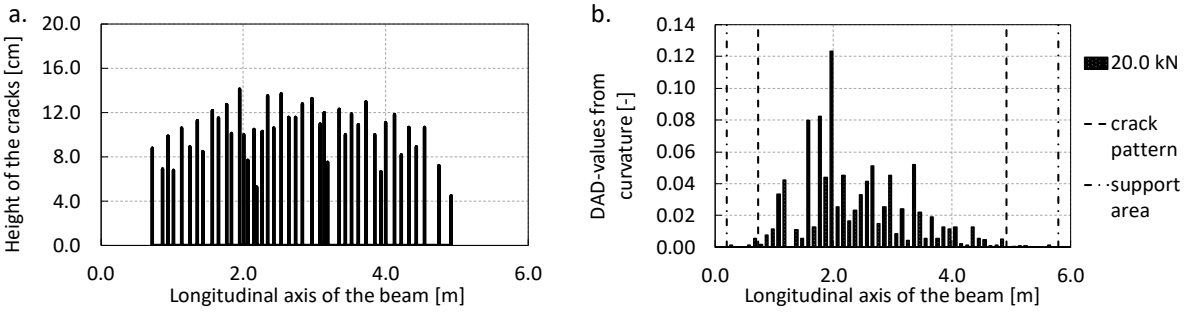

Figure 9.23. a. Detected cracks in the experimental reinforced beam, b. DAD-values from curvature for load step 20 kN

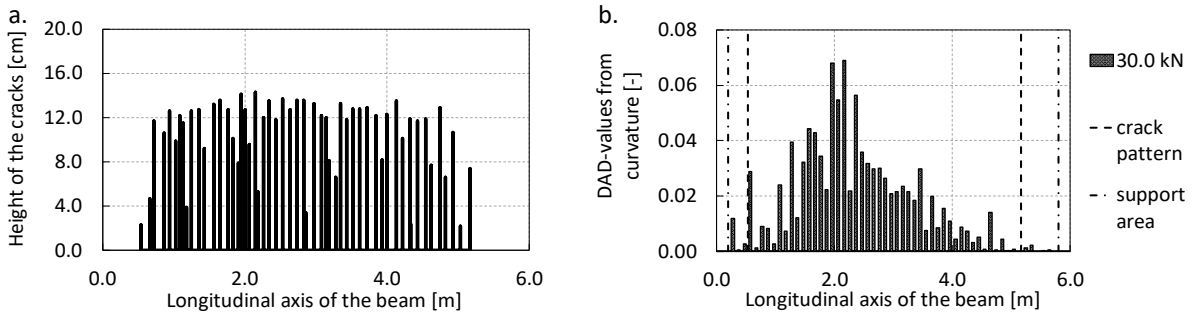

Figure 9.24. a. Detected cracks in the experimental reinforced beam, b. DAD-values from curvature for load step 30 kN

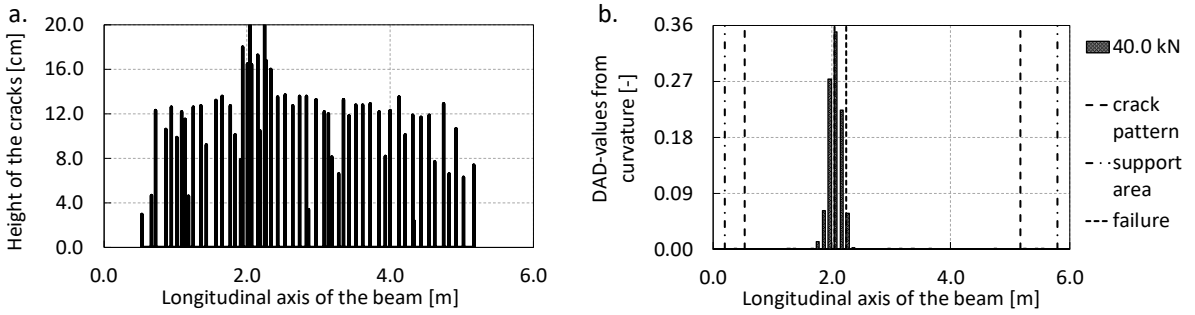

Figure 9.25. a. Detected cracks in the experimental reinforced beam, b. DAD-values from curvature for load step 40 kN

9.4.5 Case study: a steel beam experiment with local damages

The concept of damage detection for the case of crack formation in a concrete structure was shown in the previous chapters. Here, the loading of the beam was performed stepwise, whereby the width of the cracking area increased correspondingly. As measurement noise affects the accuracy of the method, more quantitative discussion on noise level and detectable damage severity is needed. Therefore, a laboratory test of a steel beam is presented and discussed (Figure 9.26) in the following. In contrast to the reinforced concrete beam, the cross-section of the steel beam is stepwise damaged at three defined positions. The advantage of the steel beam is the fact that no additional cracking is to be expected outside the damage positions. The path-controlled load using a hydraulic press is carried out so that the maximum deflection does not exceed the serviceability limit state (22 mm). The span of the beam amounts to 5,60 m and the

loading is applied at 2,00 m from the left end of the beam (Figure 9.26). In total, three different damage positions are planned: damage position 1 at 3,60 m, damage position 2 at 4,80 m and damage position 3 at 1,20 m from the left side of the beam. The measurement of the deflection is also carried out using photogrammetry with reference points positioned at the steel supports and on the floor.

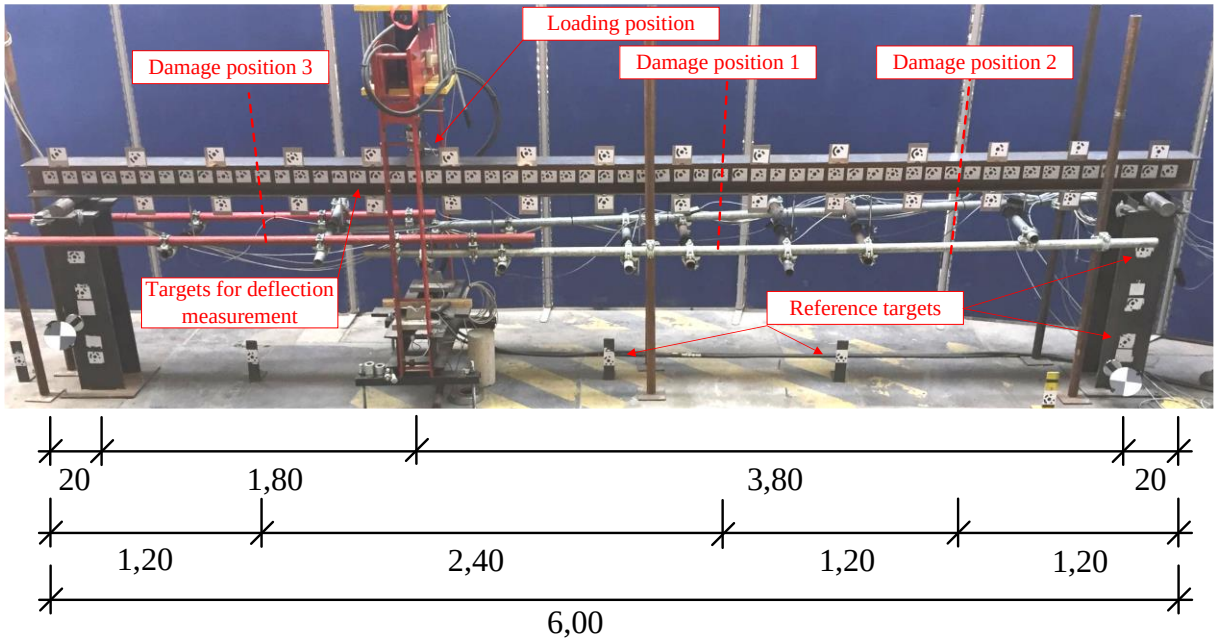

Figure 9.26. Laboratory experiment with a steel beam and local damages

The damaging of the cross-section is applied by slitting the bottom flange of the HEA180 steel profile (Figure 9.27). The paper includes the results of the experiment for four damage scenarios. Further results of the experiment with raw data without smoothing and the theoretical calculations can be found in [99]. Table 2 shows the degree of the damage which has been made manually at the three different positions by including the slit length within the flange and the deflection of the beam for the experimental load of 30 kN within the serviceability limit state. The slitting of the bottom flange is carried out gradually, symmetrically on both sides for each damage level (Figure 9.27). For damage case 1/2, the degree of the stiffness reduction amounts to 5,2 % and for damage case 1/4 and the degree of stiffness reduction was set to 23.8% at damage position 1 whereas the other two positions remain undamaged. Then for damage case 2/4, the degree of the damage at position 1 amounts to 49,0 % and to 23,8 % at position 2

whereas damage position 3 remains still undamaged. The last step 1/6 is subjected to a stiffness reduction of 71,5 % at position 1 and 49,0 % at the position 2 and 3. The slitting of the bottom flange is shown in Figure 9.27.

Table 2. Damage levels and degree, deflection under 30 kN load.

Damage case	Damage degree [%]			Slit length within the flange [mm]	Deflection [mm]
	at position 1	at position 2	at position 3		
1/2	5,2	-	-	20	17,79
1/4	23,8	-	-	80	17,82
2/4	49,0	23,8	-	140 | 80	17,91
1/6	71,5	49,0	49,0	180 | 140 | 140	19,70

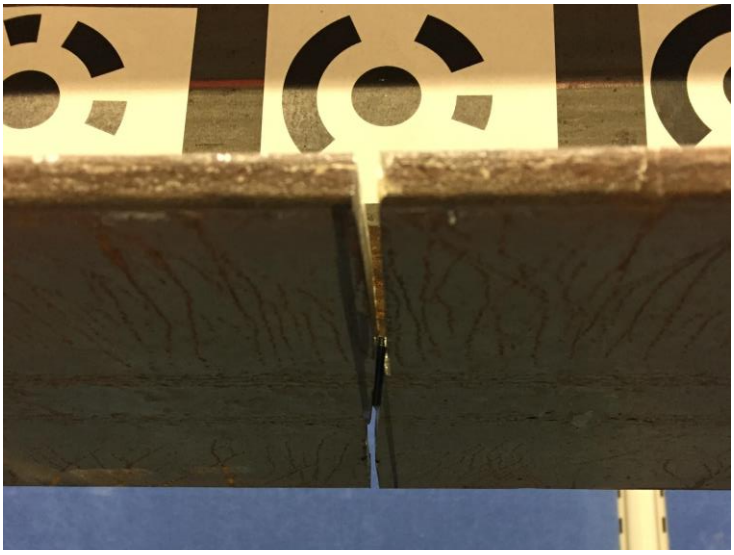

Figure 9.27. Damaging of the cross-section by slitting the bottom flange

The evaluation process of the test is similar as already presented in section 9.4. The smoothing of the measured deflection line has been carried out within the standard deviation of the photogrammetry measurement. As measurement point variation, each third measurement point with 30 cm distances has been chosen (similar to section 9.4.3).

Figure 9.28 shows the results of damage detection using the DAD-values from curvature for the four damage scenarios. Figure 9.28a. shows the DAD-values at a damage degree of 5,2 % at position 1. Due to the noise effects resulting on the one hand from the measurement accuracy and on the other hand, from the path-controlled hydraulic press, a damage localisation was not possible for such a small stiffness reduction. There is only a range of DAD-values between 0,10 and 2,00 visible. In case of no existing damages, the DAD-values show peaks especially in the area with higher noise level. Thus, the range between 0,10 and 0,60 indicates bigger noise effect. At the damage degree of 23,8 %, first discontinuities at the damage position become visible (Figure 9.28b.), but there are still some peaks resulting from the noise effects outside of the range of the photogrammetry standard deviation. The peak at the left end is caused by the measurement noise (Figure 9.28b.), which was already indicated in Figure 9.28a. The clearly identification of the damage degree of 23,8 % was not possible. However, the exact transition of the detectable degree of damage depending on the achieved measurement accuracy for this experiment lies in the range between 23,8 % and 49,0 %. In case of a stiffness reduction by about 49 % (Figure 9.28c.), the localisation of the damage was successfully achieved. The same diagram includes also the damage scenario at damage position 2 at damage degree of 23,8%. In case of two different damages, the larger one of the two could be clearly identified. The scaling of the vertical axis allows also the determination of damage level. Figure 9.28d. shows the clear identification of the damage at position 1, even for the case where the loading and the damage position do not coincide. Figure 9.29 shows the same diagram to the Figure 9.28c and d, but the vertical axis is zoomed in order to detect the next discontinuity after the largest one. However, the small DAD-values were highly affected by noise and could not be clearly detected. The next chapter examines the noise and achieved accuracy of the experiment to discuss the optimisation potential of the method.

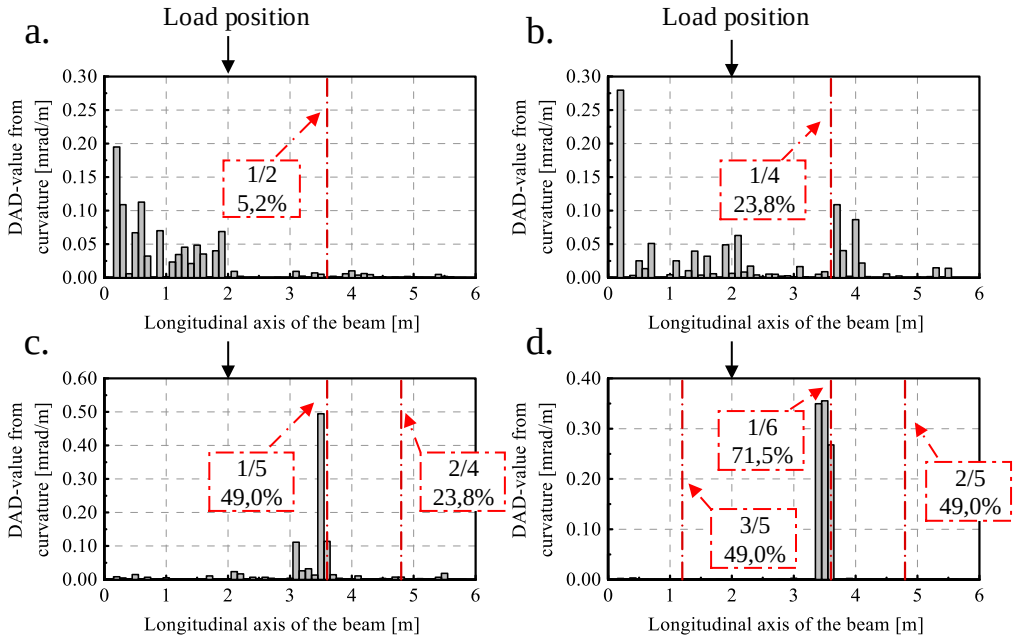

Figure 9.28. DAD-values from curvature a. damage position 1, damage level 2, damage degree 5,2 %; b. damage position 1, damage level 4, damage degree 23,8 %; c. damage position 2, damage level 4, damage degree 23,8 %, d. damage position 1

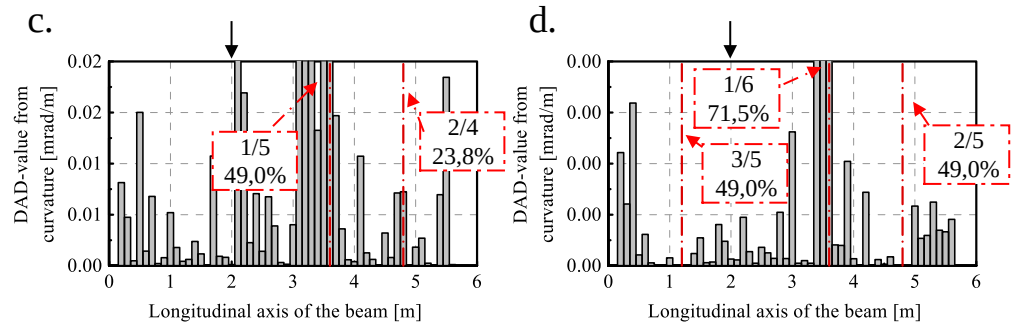

Figure 9.29. Zoom of the vertical axis of Figure 9.28c and d.

9.4.6 Analysis of the achieved accuracy and the noise effect

The DAD-method is used to localise damage in structures based on the measured deflection line. However, the accuracy of the deflection measurement is always affected by the applied technique. In this chapter, the noise level in the experiment will be discussed. Within the paper, two load deflection experiments with different damage scenarios and detection have already

been presented. As already mentioned, the loading of both beam specimens are carried out by using a path-controlled hydraulic press. The hydraulic press is technically in very good condition and able to carry out the load very stably for several hours (Figure 9.30) . Nevertheless, the accuracy of the measurement results is influenced on one hand by the measurement technique and on the other hand by the vibration of the hydraulic. Figure 9.30 shows a diagram for the loading process of the reinforced beam test. The vertical axis shows the deflection in millimetre and the horizontal axis the time in seconds. The measurement of the vertical deformation is done by using displacement sensors, which are positioned against the bottom surface of the concrete beam (Figure 9.11). The diagram shows the deflection of the beam for the applied load steps 5,0 kN, 10 kN, 15 kN, 20 kN and 30 kN measured at 2,00 m from the left end of the beam, so at the position of the loading. In the following, the vibration of the beam under the load and without load is discussed to show the impact of the vibrations of the hydraulic press. The zoomed part A. in Figure 9.30 shows the noise resulting from the hydraulic and from the displacement sensor, whereby the zoomed parts B and C present the noise only resulting from the displacement sensor. The difference between B.1 and B.2 is only the scale of the vertical axis. The parts A and B.1 as well as the parts B.2 and C are in the same scale. By analysing this data, a standard deviation of about 0,30 mm is found for part A and of about 0,01 mm for parts B and C. This means that although the deflection line was measured very precisely by photogrammetry (approx. 0,08 mm) and displacement sensors (0,01 mm), the total accuracy of the test was in the range of 0,30 mm. Nevertheless, the DAD-method has shown that damages in the range between 23,8 % and 49,0 % or more can be localised based on the laboratory experiments. An experiment with static load (without hydraulic press) would significantly increase the sensitivity of the damage detection. This proves the high potential of the method.

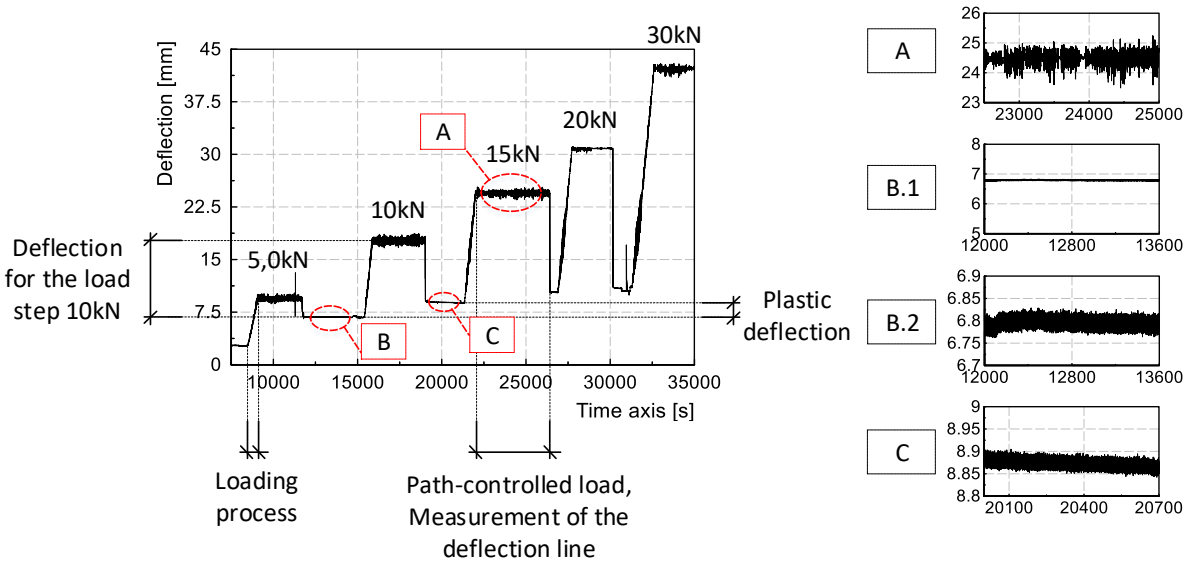

Figure 9.30. The noise effect for the reinforced concrete beam experiment

9.4.7 Summary

Within the paper, the so-called Deformation Area Difference Method based on static load deflection experiments for identification and localisation of local damages is presented. The application of the DAD-method requires a very precisely measured deflection line of the structure obtained by a static load test as well as a theoretical model of the structure as reference. The method considers the area between the deflection lines, the inclination angles and the curvatures from both, the theoretical model as well as from the real measurement. The calculation of the inclination angle and curvature requires a multiple derivations of the deflection line. However, due to these the effect of measurement noise is increased. The DAD-method considers the area between the curves, thus the function of the inclination angle and the curvature are again integrated, which leads again to a reduction of the noise effects. Naturally each measurement technique has a limited precision, even the photogrammetry.

The paper includes the description of the results from two laboratory experiments with a reinforced concrete beam and with a steel beam. The reinforced concrete beam is stepwise loaded until failure. The stepwise increase of the load leads to distinct crack patterns in the tensile zone, whereby the stiffness of the beam is reduced in this area. The aim of the study is

to identify and localise the cracked area only by the information of the measured deflection line which has been measured by close-range photogrammetry. In contrast, the steel beam is loaded by 30 kN so that the serviceability limit state is not exceeded. The cross-section of the steel beam was gradually damaged at several positions. The aim of the study was to determine which degree of damage can be identified by the applied measurement technique and achieved accuracy. For this, a full-frame camera Nikon D800 is applied which is calibrated using a calibration wall with several targets. The targets of the calibration wall are measured by total station Leica TS30.

The key findings can be summarised as follows:

a) The high precise measurement of the deflection line by using the technique of photogrammetry is enabled due to reference points (control points) and photogrammetric barcode targets. The calibration of the camera makes a significant contribution to the accuracy. Each measurement point is captured several times and delivers the coordinates of each point.
b) Afterwards, a standard deviation for each measurement points is calculated. The reached accuracy respectively the standard deviation within the laboratory experiment amounts to about 0,07 mm.
c) With the information of the standard deviation of photogrammetry, the measured deflection line is smoothed in order to reduce the noise effect and to identify with high probability discontinuities of the structure. The detected discontinuities out of the standard deviation for the photogrammetry are considered as a change in the stiffness or damage in the structure.
d) Further investigations such as measurement point variability or polynomial regression as reference for the smoothing of the curve are included. The influence resulting from the measurement noise and the height difference between the measurement points is investigated in order to identify an optimum relation.
e) An investigation of all accuracy influencing factors for the experiment is considered. Beside the measurement accuracy of photogrammetry, the loading process of the experimental beam using the path-controlled hydraulic had an influence for the total

accuracy of the test. Despite the total standard deviation, it was possible to identify the damage.

f) In case of several local damages in a structure, first only the biggest damage can be identified . Although, the detection of the next smaller damage can be done based on theoretical results, the presented experimental results could not show this. This will need further investigations.

The investigation of the steel beam has shown that the sensitivity of the method depends on the damage intensity and the achievable accuracy of the measurement technique. In the presented test, the achieved accuracy of the photogrammetry with the standard deviation of 0,06 to 0,11 mm was able to detect local stiffness reductions of about in the range between 23,8 % and 49,0 % or more. In general, the accuracy of photogrammetry could still be improved and reach standard deviation values of only 0,01 to 0,03 mm with the help of camera enhancement systems and an optimization of the calibration process. The total accuracy of the test could be significantly improved due to stable respectively static load. Therefore, there is still room to improve the sensitivity of damage detection using the DAD-method. During the first laboratory experiment, each crack in the concrete is documented and integrated to graphs. The comparison of the crack pattern with the course of the DAD-values shows good correlation. Even within the serviceability limit state of the beam with small deflections the DAD-method allowed the localisation of the cracked area. The second laboratory experiment with a steel beam proved that the method is also able to detect local damages. The steel beam was only slightly deformed so that the maximum deflection did not exceed the serviceability limit state. However, within the experiment, the noise resulting from the hydraulic press was technically not controllable and increased noise effects. For this reason the authors suggest that the loading for the next experiment should take place using a static load, which should improve the sensitivity of the method allowing the localisation of smaller damage.

The DAD-method shows considerable potential for the future for damage assessment from the combination of intelligent algorithms and innovative measurement techniques.

10 Transition to the manuscript III

10.1 Conclusion of the second paper

The second paper has shown the further development of the DAD method considering the measurement noise effect and the analysis of the measurement point distances. The detection of the cracked area in the experimental reinforced concrete beam was successful. The reached precision of the photogrammetry amounted about 0.07 mm, which was considered in the process of smoothing. The most suitable measurement point distance was 30 cm relating to the experiment. A case study with steel beam showed that the detection of damage degree is possible in the range between 23.8 % and 49 % or more. In case of several existing damages, only the highest damage degree could be identified within the achieved measurement precision.

10.2 Introduction to the third paper

The findings from the studies, which were presented in the previous journal papers (see section 4.4.1) or in the conference papers (see section 4.4.2), pointed to the high potential of the close-range photogrammetry application for the DAD method. The applied full-frame camera Nikon D800 was calibrated within the first laboratory experiment (chapter 7) on a calibration wall with the dimension of about 3.00x7.00 m and with 40 targets. The achieved precision amounted about 0.17 mm. Within the second laboratory experiment (chapter 9), the camera Nikon D800 was calibrated on a big size wall with the dimension of about 6.00x14.00 m and with 163 targets. The achieved precision amounted about 0.07 mm.

The promising results from the close-range photogrammetry measurement lead to further investigations about the precision influencing factors which is included in the manuscript III. In particular, the investigation is carried out based on calibration walls with 40 targets and with 163 targets and on cameras Nikon D800 with 36.8 MPixels and Fujifilm GFX50S with 51.4 MPixels. The study is carried out on a various number of calibration series and a further laboratory experiment for the measurement of the structural deflection. The analysis of the measurement precision is discussed based on noise effects which is filtered out from the deflection curve using polynomial regression.

11 Manuscript III: The influence of camera calibration and quality for high-precision structural deflection measurements by close-range photogrammetry

Abstract

For condition assessment of bridge structures, high-precision measurement techniques for the monitoring of structural deflection responses are in great demand. The proposed study is carried out to identify the reachable precision of close-range photogrammetry for structural deflection measurement as well as to identify the influence of calibration and camera quality. The applied cameras are the Nikon D800 and the Fujifilm GFX50S. Furthermore, two different calibration walls with the dimension of 7.0x3.0 m and 14x6.0 m are used. The influence of the calibration was tested on several calibration series using both cameras. Furthermore, the deflection measurement with close-range photogrammetry is carried out for a reinforced concrete beam. The precision analysis is done based on the noise effect, which could be filtered from the deflection curve using polynomial regression. As a conclusion the influence of the calibration, of the camera quality and of the calibration wall quality is discussed using experimental results.

11.1 Introduction

The ongoing development of digital photogrammetry has seen significant progress in recent years. This is driven by advances in both software and hardware, resulting in a wider and wider update of this measurement method. It is used for recording of traditional buildings [100] [101], for industrial applications [102], for monitoring soil structures [103] [104] [105], for archaeological studies [106], for topography [107] [108], for forensic investigations [109] [110] [111] [112], for applications with high-precision requirements [91] [90] [95] and much more [113] [114] [115] [116]. The applied algorithms for individual areas become more innovative, as well as the technological development of the imaging sensors [117]. However, for the optimal combination of algorithms and technology with the highest accuracies, a precise calibration of the camera is essential.

The proposed article reports on influencing factors for high-precision measurement with classical photogrammetric methods. Essentially, the variation of the camera quality and its calibration are investigated. Various sources confirm the suitability of different camera types as digital single-lens reflex (DSLR), compact cameras, mirrorless, metric cameras etc., for photogrammetric applications [118]. Basically, different types of camera calibration methods such as laboratory calibration [119], plumb-line calibration [120], on-the-job calibration [121], self-calibration [122], system calibration and test-field calibration exist [123]. The laboratory calibration is usually used for metric cameras, which is carried out by the manufacturer [124]. The plumb-line method uses a test-field with several straight lines, whereby the whole images are captured with distortions [125]. This distorted captures of the straight lines in the test field helps to determine the calibration parameters of the camera [126]. A portable frame consisting of several scale bars distributed in space represents the basis of the on-the-job calibration. This method is useful if self-calibration is not possible [127]. The self-calibration is an extension to the on-the-job calibration [128] [129]. Faugeras et al., [130] describe the method of self-calibration based on theory and experiments. The self-calibration requires a similar imaging process of the object as the test-field calibration process [131] [132] [133] [134]. The advantage of self-calibration is that the calibration is performed at the same point in time as the images of the object are captured. This also implies, for example, the same air pressure and temperature conditions. Even if a large number of images is required, the self-calibration method provides

the highest of accuracies in object reconstruction [125] [135] [136]. However, the prerequisite for a successful self-calibration is that the measuring-field is structured like a test-field calibration wall and the points to be measured are optimally within the control points. Within the system calibration, all components relevant for the photogrammetry are calibrated, i.e. interior IOP and exterior orientation parameters EOP. The complete system usually consists of several cameras, which are immobile and firmly positioned. Finally, it is the test-field calibration, which will be examined in more detail within this study. The basis for the test-field calibration is a suitable targeted field with known point coordinates. During the calibration process, the images are then taken from different positions with sufficient ray intersection geometry [124]. Well-defined and orientated object points for test-field calibration will allow high-accuracy measurements with photogrammetry [118].

Moe et al, [137], perform a test with circular retroreflective targets and a few coded targets using the software Australis, namely with two different calibration setups. The first one is a cage with a dimension of about 4.3 m including a series of targets and the second one is a small box with the dimension of about 60 cm. The software Australis determines the bundle adjustment based on a free network method and calculates the centre of the coded targets. Within the study, the author compares the calibration parameters for both calibration setups namely one with the cage and one with the box. The results of the study for both setups deliver values close to each other. The author's expectation is that the results of the box could approach the results of the cage providing additional targets on the box. Peipe and Tecklenburg [127], investigated in their study the influence of different commercial software for the photogrammetric calibration process. The applied software were DPA-Pro [138], CAP K^2 [139], Australis [140], PHIDIAS, and Phoxy. All software delivered very similar results concerning the parameters principal distance c, the position of the principal point x_0, y_0 except Australis. The reason for the slight deviation from Australis is that it uses a Gaussian lens distortion model for the parametrisation instead of a radial-symmetric distortion, which is used by the others. Honkavaara et al., [141] developed a geometric calibration method, which were empirically tested using several series and three UltraCamD digital large format photogrammetric cameras. The authors reported an achieved accuracy of a typical range of 2-3 µm. Napolitano et al., [142] investigated in their study the accuracy of photogrammetry for heritage structures with its precision influencing factors. In particular, they focused on the

statistical analysis of the repeatability. The author judges the quality of the software by the repeatability of the results. Therefore, they used 10 models, which were generated from the same 100 images. The repeatability of the results is presented using the software Agisoft Photoscan [143]. The repeatability of the results is shown by measuring several lengths several times. The standard deviation amounts 0.112 m by measuring a length of 14.9 m and 0.012 m for a length of 1.08 m, which was indicated as low repeatability. A statistic calculation determines the number of measurements required to minimize systematic errors based on two experiments. The results of the experiments showed that the effect of a bias started to stabilize from a number of series of four. Smith et al., [144] investigates the effect of the temperature and the removing of the lens for single-lens-reflex digital camera calibration parameters. A Nikon D100 camera with a 28 mm focal length objective is applied under the temperature range of about 0-25°C. The parameters such as radial lens distortion, the position of the focal point are particularly considered. For each investigation (removing lens and temperature change), three series have been carried out. It could be demonstrated that the radial lens distortion remains relatively stable due to the removing of the lens and due to remounting again. The influence of low temperatures seems to be higher for the location of the focal point. The authors provide a factor of 0.01 mm per 10°C as a reference value for the focal length. Pullivelli [145] studied in his work an easy-to-establish calibration test field and applied several off-the-shelf digital cameras. The calibrations are done based on the bundle adjustment with self-calibration using straight lines [146] [147] and applied among others on generating of three-dimensional CAD models of a building. The computed and measured distances have been compared to each other and amount approximately to 1-4 mm.

This paper investigates the precision influencing factors for close-range photogrammetry measurement. Principally, the context of the paper is comparable with the study of Pullivelli, as mentioned above, however the main goal is to apply the close-range photogrammetry especially for structural deflection measurement with highest-precision and to investigate the influence factors from test-field calibration quality and differences between high-resolution cameras. The applied cameras are a full-frame camera Nikon D800 with 36.8 megapixel and a medium format camera Fujifilm GFX50S with 51.4 megapixel. The first test-field is a calibration wall with the dimension of approx. 7.0x3.0 m and with 40 targets. The second test-field is a large-scale calibration wall with the dimension of 14.0x6.0 m and with 163 targets.

The coded targets are measured by the total station Leica TS 30 from two different positions. The evaluation of the data was implemented by using the photogrammetry software Elcovision 10 [148].

The first part of the study examines the influence of the camera calibration for high-precision close-range photogrammetry. In particular, what is the influence of a calibration and what is the repeatability of the results. The successful application of the high-precision close-range photogrammetry, in turn, could open up new practical applications such as a bridge inspection method [149]. Therefore, the results of the calibration run will be discussed in the second part using a load-deflection laboratory experiment with a reinforced concrete beam to measure the deflection line as precisely as possible. The deflection measurement is carried out using both cameras for three calibration runs, namely one without calibration, one with small and one with large wall calibration. The objectives respectively the contribution of the study can be summarized as follows:

- High precision measurement of structural deflection by close-range photogrammetry
- Application of two high quality consumer cameras
- Comparison of measurements with and without camera calibration
- Influence from two different test-field calibration walls
- The interdisciplinary application of the close-range photogrammetry for application of the Deformation Area Difference method for detection of damages in bridge structures.

Further experiments with photogrammetric measurement are presented in [96] [97] [30] [99] [150] [151] [152]. The evaluation of the measured deflection line will be individually carried out for each calibration runs and for each camera.

11.2 Background of the study

The measurement techniques are commonly used for engineering applications. Each measurement technique is selected depending on the requirement. Within a research project at the University of Luxembourg, a so-called Deformation Area Difference (DAD) method is developed in order to localise damages in bridge structures (equation (46)). The main requirement of the method is on the one hand the high precision deflection measurement and

on the other hand the high density of the measuring points along the bridge structure. Therefore, the authors tested various measurement techniques such as total station, laser scanner, displacement sensors, close-range photogrammetry and levelling [30]. The collected experiences from several laboratory tests and from a real bridge experiment showed high potential of close-range photogrammetry for the application of the DAD method. The close-range photogrammetry was able to measure the structural deflection using coded targets with very high-precision along the experimental beams respectively the bridge.

The deflection of the bridge structure resulting from a load test includes information about the load bearing capacity and structural stiffness. Therefore, the stiffness influencing local damages change the curve of the deflection and generates a local discontinuity. The local discontinuity can be particularly detected using the inclination angle of the structure, which is the first derivation of the deflection (equation (47)). The DAD method considers the area difference between the measurement and the reference system section by section, which is squared and normalized in order to highlight the damage position (equation (46)). Further explanation and case studies regarding the background of the DAD method are published in [95] [96]. The aim of this study is to investigate the precision influencing factors for the close-range photogrammetry for measurement of structural deflection.

$$DAD_{\kappa,i}(x) = \frac{\Delta A_{\kappa,i}^2}{\sum_{i=1}^{n} \Delta A_{\kappa,i}^2} = \frac{[\varphi_d(x_i) - \varphi_d(x_{i-1}) - \varphi_t(x_i) + \varphi_t(x_{i-1})]^2}{\sum_{i=1}^{n} [\varphi_d(x_i) - \varphi_d(x_{i-1}) - \varphi_t(x_i) + \varphi_t(x_{i-1})]^2} \quad (46)$$

$$w'(x) = \frac{\delta w(x)}{\delta(x)} = \varphi(x) \quad (47)$$

w(x) Deflection function of the bridge structure

φ(x) Inclination angle function of the bridge structure

$\varphi_t(x)$ Theoretical inclination angle from the reference system

$\varphi_d(x)$ Inclination angle from first derivation of the measured deflection

ΔA_κ Area difference between the reference and measured system

$DAD_k(x)$ Deformation Area Difference (DAD) value from curvature

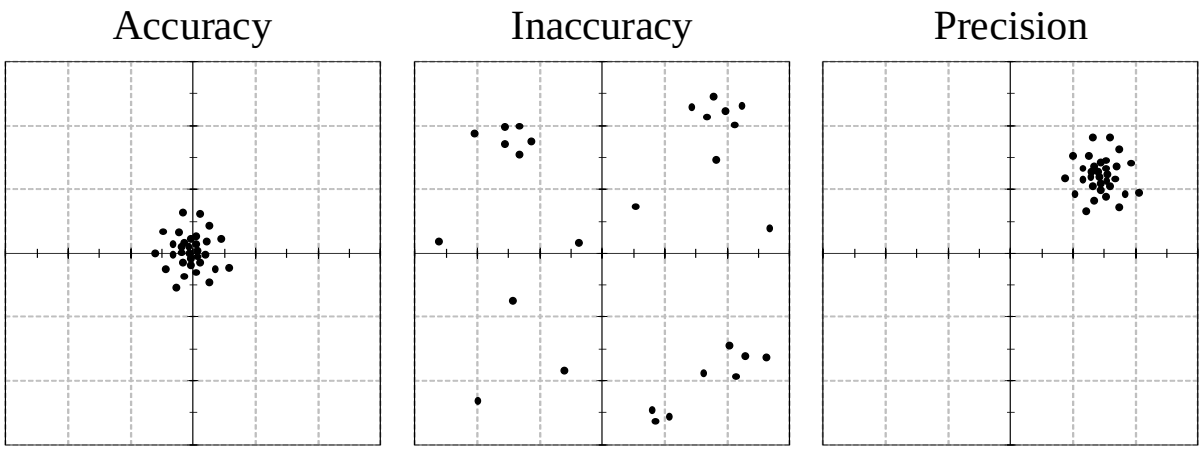

Figure 11.1. Definition of precision, inaccuracy and precision

Figure 11.1 shows the definition of the accuracy, inaccuracy and precision, which has a high importance for the provided case study. The presented DAD method is applied to identify local discontinuities based on relative structural deflection measurement. In order to define the accuracy of the measurement, a reference value or measurement is required. However, precision of the close-range photogrammetry is investigated based on the relative noise analysis in the section 7, especially according to the Figure 11.24 and to the Figure 11.25.

11.3 Used cameras

As already mentioned, within this study two different modern cameras, a Nikon D800 and a Fujifilm GFX50S are used. Table 3 shows a comparison of the technical data for both cameras. The full-frame camera D800 has 36.8 megapixels for a sensor size of 35.9x24.0 mm, while the medium format camera GFX50S has 51.4 megapixels for 43.8x32.9 mm sensor size. Both cameras are set on a tripod to avoid the effect of blurring.

Table 3. Comparison of the two cameras Nikon D800 and Fujifilm GFX 50S

	Unit	Nikon D800	Fujifilm GFX 50S
Image sensor	[mm]	35.9 x 24.0	43.8 x 32.9
Sensor type		CMOS	CMOS
Pixels		7360 x 4912	8256 x 6192
Image size	[MPixel]	36.8	51.4
Pixel pitch	[µm]	4.90	5.30
Sensitivity	[-]	ISO50-25600	ISO100-12800
Shutter speed	[min], [S]	30S to 1/8000	60 min to 1/16000 S
Weight without lens	[g]	1000	825
Used lens	[mm]	Sigma 50mm F1.4	Fujinon GF 63mm F2.8

11.4 Calibration of the camera

11.4.1 Calibration walls

Two calibration walls have been established at the University of Luxembourg (Figure 11.2). The first is located in a lecture room and the second in the new laboratory hall of the engineering group. The bar-coded targets on each calibration wall was surveyed by the total station Leica TS30 using angular intersection from two different positions. The coordinates of the targets were computed and adjusted in order to have a highly accurate reference. The precision of the angle measurement with total station is much higher as of the distance measurement. The small calibration wall has a dimension of approximately 7.0x3.0 m and 40 photogrammetric targets (Figure 11.2A). The targets are distributed fairly regularly over the entire wall whereas it is important for the calibration process to have targets at different distances from the camera, to form a three-dimensional set of targets [153] [154]. Therefore, the power strip, which has a

thickness of about 7 cm from the wall, serves as a second plane. The targets with coordinates, which are expected to be stable, serve as control points with an appropriate code number "123". This means that they have been mounted on immovable elements such as e.g. on massive walls as in this case. Since the power strip is assumed to be moveable, the targets, which are fixed on it, get a normal code number "0" in the software and are not used as control points. The distance between the targets varies between 0.60 m and 1.00 m.

The large calibration wall is established in the new laboratory hall of the University of Luxembourg (Figure 11.2B). This calibration wall with 163 targets and a dimension of about 14.0x6.0 m has two different planes. The first plane is the massive concrete wall in the background while the concrete columns serve as second plane. The difference between the two planes amounts to 65 cm. The photogrammetric targets were distributed relatively uniformly, whereby the target number in the central field is slightly higher. The distance between the targets varies between 0.50 m and 1.00 m.

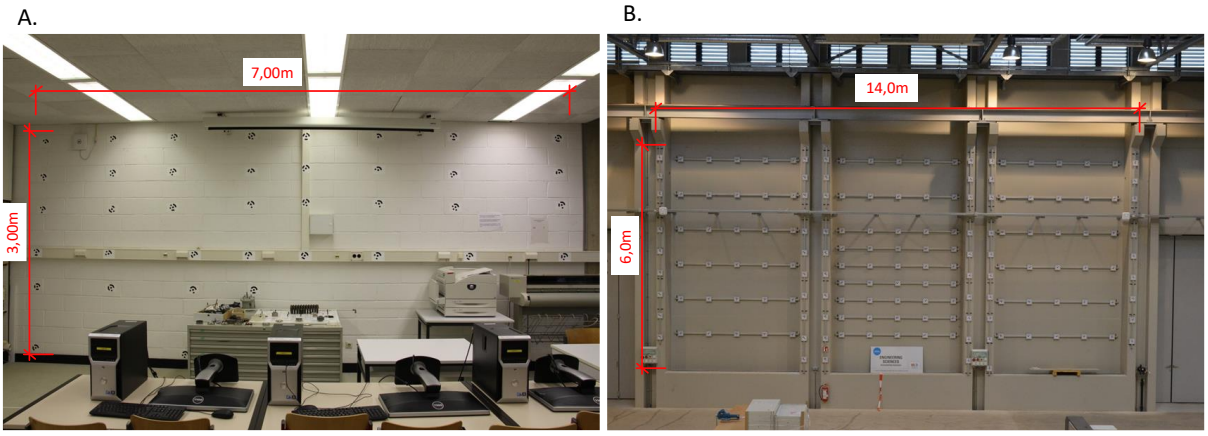

Figure 11.2. The two calibration walls of the University of Luxembourg A. 40 targets in a field of about 7.0x3.0 m; B. 163 targets in a field of about 14.0x6.0 m

11.4.2 Depth of field and focussing of the camera

Not only the calibration and the camera quality impact the precision achievable with the photogrammetric methods, but also the depth-of-field and the correct focussing of the camera [142]. Within the experiment, all image captures are done by using tripods. However, it should

be possible for practical reasons to be able to create the photos with low shutter speed without having to use a tripod. Therefore, the shutter speed should be kept as low as possible to avoid the effect of blurring. A rule of thumb applies for the shutter speed 1/focal length. This means by applying a 50 mm lens the shutter speed should not fall below 1/50. However, it can range depending on the requirement up to 1/125, 1/250 or even 1/2000. An optimally exposed picture depends on the depth of field, exposure conditions, shutter speed and the ISO-setting. The determination of the correct camera setup is done gradually as follows. Figure 11.3 and Figure 11.4 show the capture positions for the calibration processes for both calibration walls. The photos are taken at a distance of about 4.50-6.50 m from the calibration wall with 40 targets and about 5.0-11.2 m from the calibration wall with 163 targets. The captures are made in a semi-circular shape in relation to the wall to improve three-dimensionality. In case of the captures from one end of the field skewed to the calibration wall plane, the difference of the distance from the capturing position to the next target and to the last target is relatively large. Therefore, the depth of field should be as big as possible to have all targets sharply on the photo.

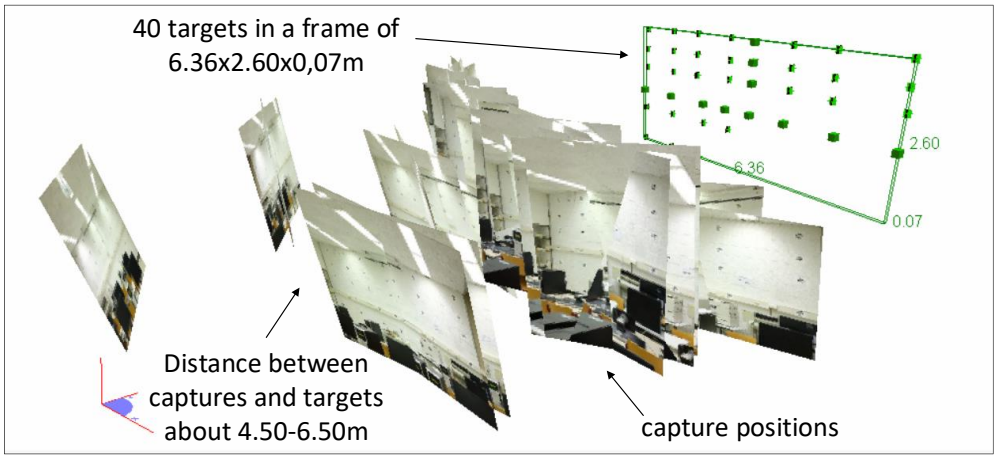

Figure 11.3. Capture positions and distances to the calibration wall with 40 targets

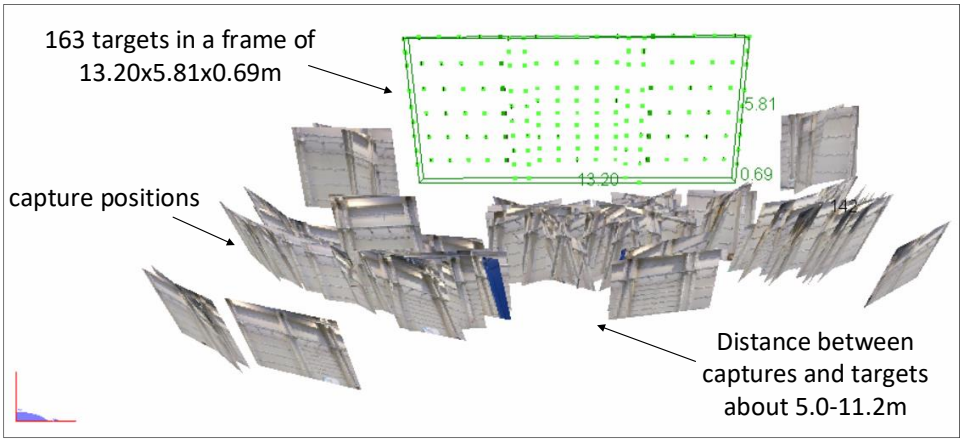

Figure 11.4. Capture positions and distances to the calibration wall with 163 targets

The images of the calibration walls are taken at different angles between 45° and 90° around the axis y according to Figure 11.5. The cameras were rotated around their own axis during the calibration process for the capture of the individual pictures, namely at 0°, +90°, +180°, +270° and at +360° around the axis z (Figure 11.5). Firstly, this improves the point distribution in the camera lens (Figure 6) and secondly, the control points in the upper wall area could be captured from the lateral or lower part of the lens and finally, to reduce the correlations between inner IOP and exterior orientation parameters EOP.

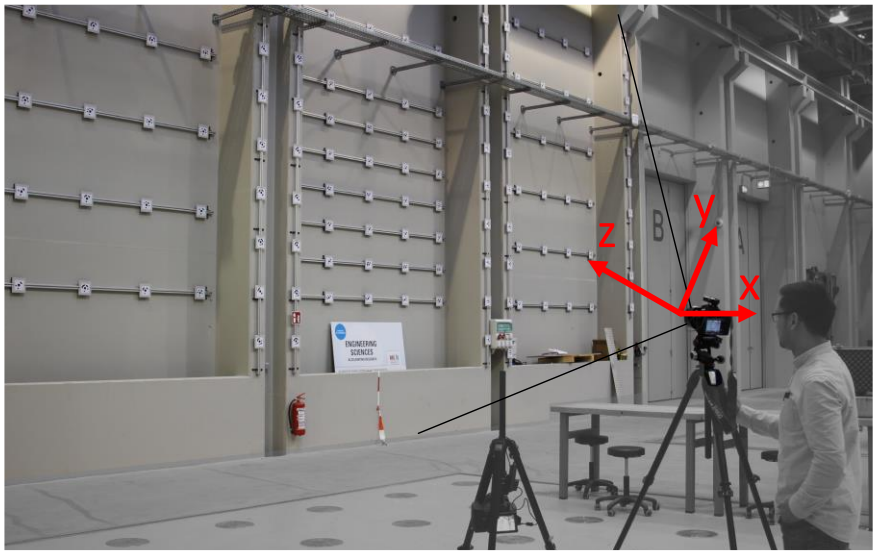

Figure 11.5. Definition of the referential axis for the rotation

The correct focussing of the camera from a certain distance to the object would allow the calculation of an optimal relationship between the shutter speed and the aperture [155]. The determination of the focussing distance to the object is calculated relating to [156]. The fixed focal lengths for the camera D800 amount to 50 mm and to 63 mm for GFX50S. The focussing of the camera is done at a distance to the object of about 7.0 m. The following setup is done for the Nikon D800: ISO-2000, f-stop f/11, shutter speed 1/80 sec., and for the Fujifilm GFX50S: ISO-2000, f-stop f/11, shutter speed 1/30 sec. The focus of D800 covers a depth of field of 3.28 m to 51.51 m and of GFX50S 4.11 m to 23.5 m [157]. Thus, the depth-of-field covers the complete test space, in order to be able to capture all targets sharply. After the focussing of the camera, every setting such as focussing, f-stop, image rotation and stabilizer are locked for the whole remaining captures and measurements. Figure 11.6 illustrates the distribution of the targets from the calibration process on the lenses of both cameras. The colour scale below Figure 11.6 illustrates the quality of the target distribution on the sensor for both cameras coming from the calibration process.

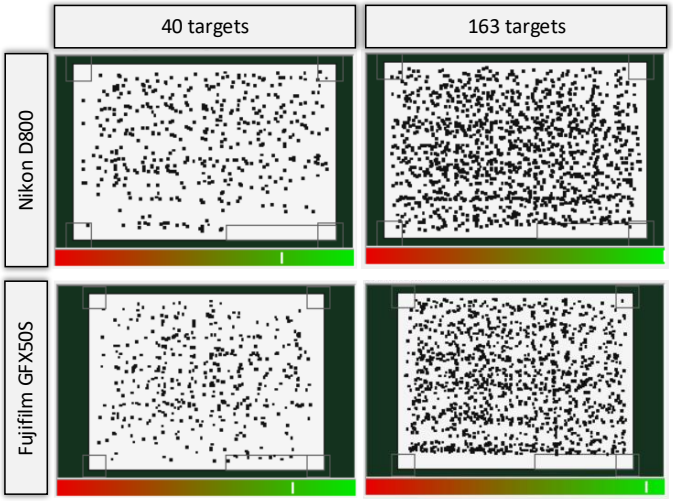

Figure 11.6. The distribution of the control points in the sensor of the cameras from the calibration process

11.4.3 Calibration runs

The investigation of the calibration quality takes place based on several experimental series. The flowchart in Figure 11.7 shows the runs. First, there are two different calibration walls, with 163 targets and with 40 targets. Then, there are different cameras namely the Nikon D800 and the Fujifilm GFX50S. Within the calibration process with each camera three different series have been done for each calibration wall. Each series from No.1 to No.3 includes independently captured images. This means that there are 6 series of images for each camera respectively for each calibration wall, so 12 series in total (part I in Figure 11.7).

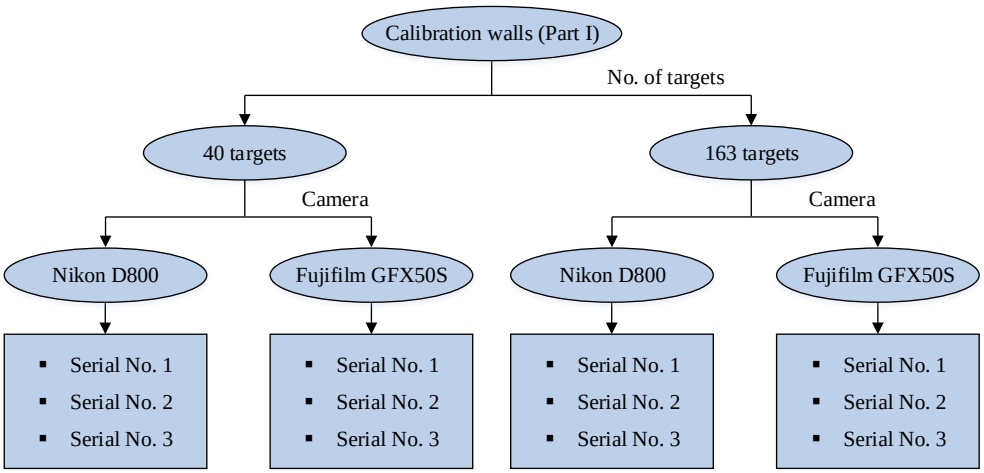

Figure 11.7. Presentation of the calibration runs

Subsequently, an additional calibration series was carried out especially for the mentioned load deflection experiment, by using both cameras and both calibration walls (part II in Figure 11.8). A more detailed description of the laboratory experiment is presented in section 11.6. The difference of part II (Figure 11.8) from part I is that the three different series from A to C (part II in Figure 11.8) are not created independently from each other, but the same photos are copied and used. In other words, the series A to C include the exact same images which are copied three times. This is done in order to investigate the repeatability of the software results, which gives an indication of the quality of the software. A similar investigation is carried out and presented in a paper of Napolitano et al., [142]. An additional evaluation of the deflection measurement is carried out for both cameras, but without any calibration of the camera (part III Figure 11.8).

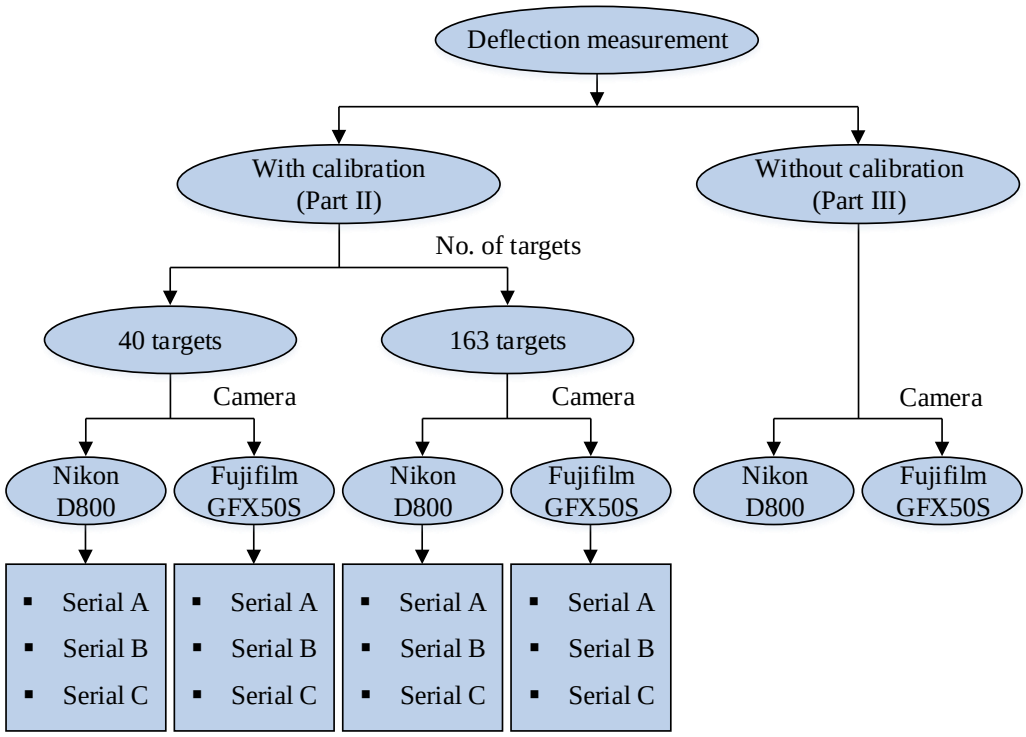

Figure 11.8. Calibration runs and deflection measurement of the experimental beam

11.5 Calibration results

A camera captures a spatial environment, which is figured on images with two dimensions. The spatial points of the environment are passed through a so-called perspective centre of the lens and recorded on the camera sensor. The spatial position of the perspective centre, principal distance and the location of the principal point are defined by the interior orientation IOP of the camera. The images show moreover usually radial lens distortion, decentring lens distortion and often also affinity errors [123]. Figure 11.9 shows the radial-symmetric lens distortion for both used cameras D800 and GFX50S. The scale of the distortion is given on the left side of each one. However, the calibration of the camera not only calculates the lens distortion, but also the mentioned principal distance and the coordinates of the principal point. Figure 11.10 illustrates the location of the principal points from the 12 series from part I and the 12 series from part II for both cameras and for both calibration walls. The numbers in the legend 40 respectively 163 indicate the calibration wall type based on the target number, while D800 and GFX50S indicate the camera type. However, the term CLE mentions the calibration for the

laboratory experiment from part II in Figure 11.8. The main difference between part I and part II is that the cameras are differently focused and the focus distances are locked. However, it can be seen that the position of the principal point for each camera varies repeatedly in the same range. The average xH value for D800 is -0.1045 mm and the yH is 0.0137 mm, while xH for GFX50S amounts -0.0592 mm and yH -0.0314 mm. In other words, the deviation of the principal point from the centre of the sensor is for about 36 % higher for the camera D800 than for the camera GFX50S. The deviation related to the sensor size is very small (up to 0.29 %), but important to be considered to enable a high-precision measurement.

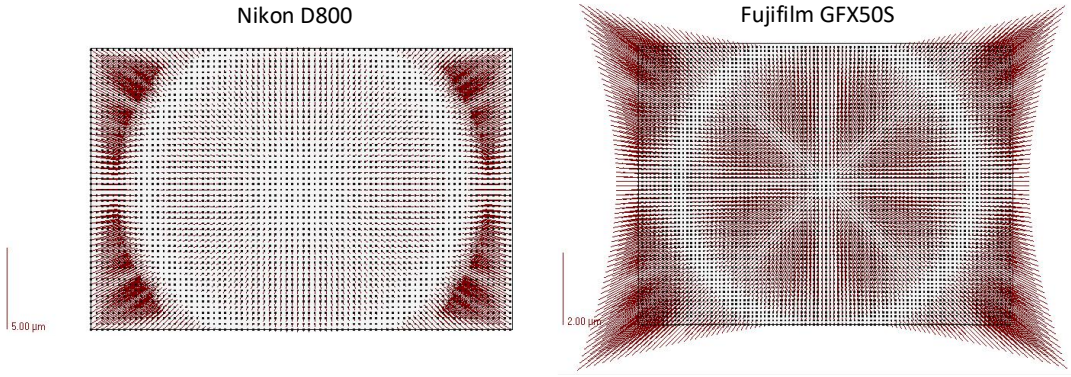

Figure 11.9. Radial-symmetric lens distortion, left: Nikon D800, right: Fujifilm GFX50S

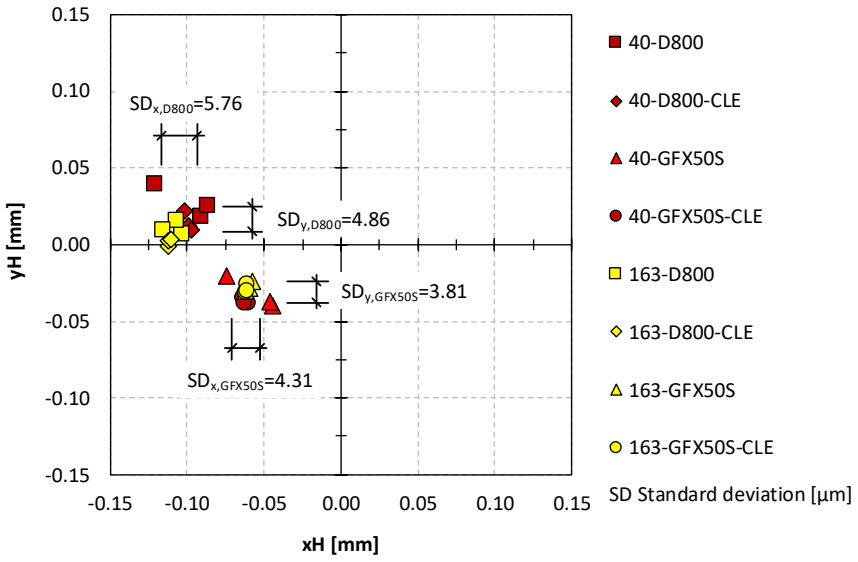

Figure 11.10. Location of the principal point corresponding to the cameras and calibration walls

The combination of the lens distortion (Figure 11.9) and the location of the principal point (Figure 11.10) leads to the Figure 11.11, namely to the radial-symmetric lens distortion respecting the principal-point location for both cameras. Within the calibration process, not only the lens distortion is determined (Figure 11.9) but also the location of the principal point. Thus, Figure 11.11 shows the radial-symmetric lens distortion respecting the principal point location. A further parameter of the calibration is the principal distance c. Figure 11.12 presents the deviation in principal distance for both cameras based on the used lenses. The camera D800 was equipped with a 50 mm lens and GFX50S with a 63 mm lens. The presented values in Figure 11.12 are the deviation from the focal length of the lens to the calculated principal distance from the calibration. The average values for the principal distance for the camera D800 amounts to 49.79 mm and for the camera GFX50S to 62.06 mm. These values are determined using the whole 12 series from part I and part II in Figure 11.7 and in Figure 11.8.

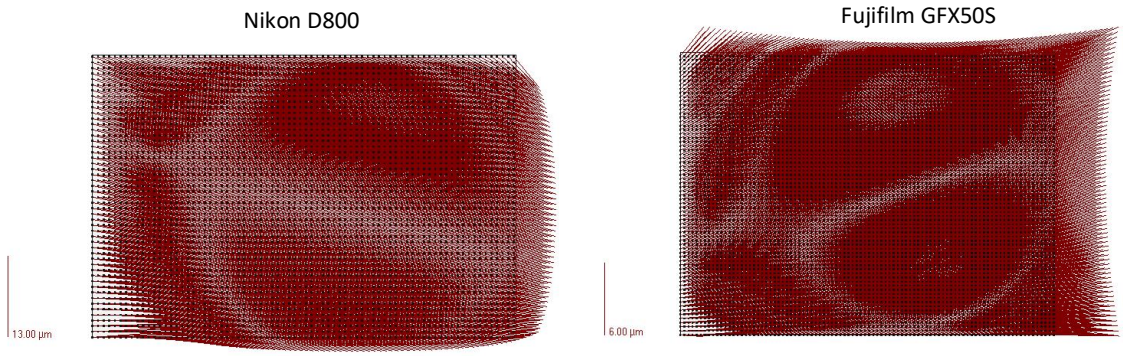

Figure 11.11. Radial-symmetric lens distortion respecting the principal-point location, left: Nikon D800, right: Fujifilm GFX50S

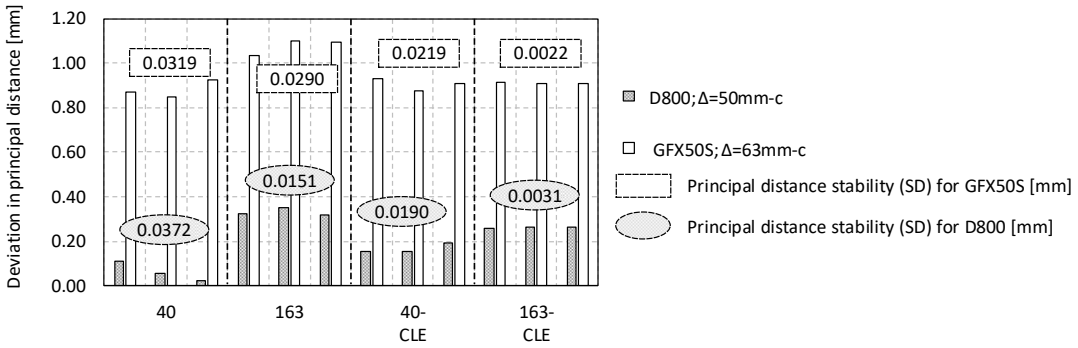

Figure 11.12. Deviation of the principal distance to the focal length

The applied photogrammetric software is the Elcovision 10. As already mentioned, all the targets (in the following also described as control points) for both calibration walls were surveyed using a Leica TS30 total station using angle intersection from two different positions. According to the technical data, the angle measurement precision of the total station amounts to 0.15 mgon (0.5") [158]. In the following steps, the further results from the calibration runs such as inner accuracy and external accuracy are examined. The inner accuracy is calculated based on the detected targets from the image measurements. This is the result of the bundle block adjustment, where only the image measurements are considered. The bundle block adjustment makes not only the photogrammetric evaluation of two overlapping images possible, but also the linking of multiple contiguous images. In the bundle block adjustment, the coordinates of the point cloud in 3D space, the position and orientation of the camera as well as its inner calibration parameters can be determined. Due to the calibration, the inner orientation IOP of the camera and lens combination is determined. For each different focussing of the camera, the position of the optical elements changes accordingly. The inner orientation IOP describes the position of the projection centre related to the image plane using three determinants, which are the location of the principal point (Figure 11.10), the camera constant (Figure 11.12) and the lens distortion (Figure 11.9). To determine the external accuracy the coordinates of the control points have to be considered in addition. Therefore, the control points exert a certain constraint on the image association into the direction of the given coordinates. The constraint can be manually defined in the settings and has been set to 1.0 cm within the study. In other words, a very poor accuracy is assumed, so that even bad control points do not bend the image association, because the expected accuracy of the total station is lower than the one of the photogrammetry. The expected accuracy of TS30 amounts to about 0.15 mm for the 40 targets with a measuring distance of about 8 m and to about 0.30 mm for the 163 targets with the measuring distance of 20 m. The accuracy values indicate the circle of probable error for the determination using angles intersection. If the accuracy level of the reference targets is expected to be the same as of the cameras, a much higher effort in the observations and analysis is required. They are not really needed though. Figure 11.13 and Figure 11.14 show the results from part I indicated in the flowchart in Figure 11.7. In the diagrams, the inner and external accuracy values are presented which are determined in relation to the focal length and given as angle values. Figure 11.13 shows the inner accuracy of the three calibration runs for both

cameras and both calibration walls. The shown values are the average, the standard deviation which are divided by the focal length of 50 mm for D800 and of 63 mm for GFX50S. Figure 11.14 shows the external accuracy of the three calibration runs. First, it becomes apparent that all different series deliver slightly different results. It is important to note, that the capturing process for the calibration series are realised one after the other in a row. They are not made from the exact identical position and not from the exact identical angle related to the calibration wall. Each series includes about 50 pictures for the calibration wall with 40 targets and about 90 pictures for the calibration wall with 163 targets. The precision for the calibration run using the 40 targets and Nikon D800 (Figure 11.13) ranges between 0.041 µm/mm and 0.053 µm/mm, while it ranges between 0.037 µm/mm and 0.045 µm/mm for the same camera but for the calibration with the 163 targets. The mean values are 0.046 µm/mm for the wall with 40 targets and 0.040 µm/mm for the wall with 163 targets (Figure 11.13). The same observations can be done for the camera Fujifilm GFX50S showing a mean value of means 0.027 µm/mm for the wall with 40 targets and 0.025 µm/mm for the wall with 163 targets. The trend based on the results in Figure 11.13 gives the impression that the inner accuracy increases if the middle format camera GFX50 is used instead of the full frame camera D800. Even the big format calibration wall with 163 targets deliver higher inner accuracy values for the calibration series. However, the values are in the range of micrometre and should be judged carefully. The final assessment about the accuracy and precision should be discussed by combination of the results from inner accuracy with the external accuracy. A reliable assessment about the influence of the camera and the calibration can be verified based on the deflection measurement data from the laboratory test.

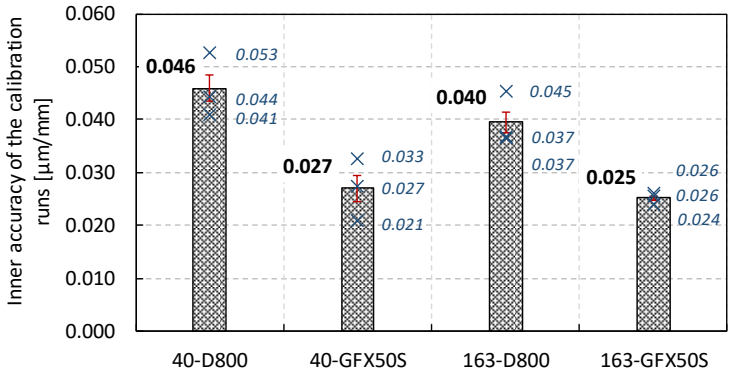

Figure 11.13. Inner accuracy of the calibration runs for the three series (part I)

Figure 11.14 presents the values for the external accuracy from the calibration runs. In the process of bundle block adjustment, a nonlinear inequality system is solved. The adjustment stops, when the maximal change from iterative calculation fall below a threshold value. In other words, if the increase in accuracy does not take place significantly in the iterative calculation process, the adjustment is considered as solved. Therefore, the accuracies are not only influenced by the different captures, but by the iterative calculation process and the accuracy of the control points. In addition, due to the automatic orientation process, the image pairs that initiate the process are randomly selected, from which slightly different a priori values for the adjustment are resulting. Therefore, to obtain the exact same results is not likely even with identical images. It is very difficult to compare the values of the inner orientation IOP, because they correlate with each other: e.g. a small change in the distortion parameters (radial-symmetric distortion parameters R1 and R2 in equation (48)) [159] also forces a small change in the camera constant, etc. Figure 11.14 clearly shows the difference between both cameras and both calibration walls. The results from the external accuracy are as follows (Figure 11.14): the improvement of the calibration wall delivers an accuracy increase of about 20.3 % for D800 and 9,50 % for GFX50S. The comparison of the cameras to each other shows also a significant difference, namely from 0.079 µm to 0.042 µm (46.8 %) respectively from 0.063 µm to 0.038 µm (39.7 %).

$$dr = R1 * (r^3 - r * R0^2) + R2 * (r^5 - r * R0^4) \quad (48)$$

with $r = \sqrt{x^2 + y^2}$ (49)

dr Distortion

r Radial distance from centre point (zero point)

R0 Second zero crossing of the distortion curve

R1, R2 Radial-symmetrical distortion parameter

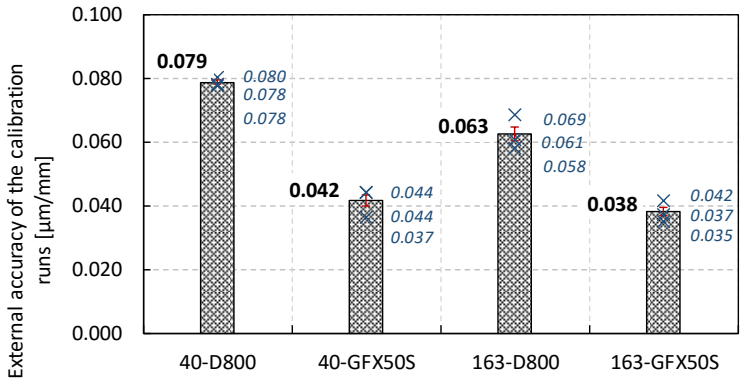

Figure 11.14. External accuracy of the calibration runs for the three series in part I

Figure 11.15 and Figure 11.16 show the results for part II, (see flowchart of Figure 11.8), which were carried out for the laboratory experiment in order to perform deflection measurements. The abbreviation "CLE" stands for calibration for the laboratory experiment (Figure 11.15). The special feature here is that the images from the calibration process were copied and calibrated three times for each camera. In other words, there are three calibration results for each camera, which are coming from exactly the same pictures. The capturing process for part II was the same as for part I, however the focus of the cameras was different between both parts. The main reason for this investigation is to verify the stability of the calibration process respectively the repeatability of the software results. As already mentioned, the accuracy of the calibration process is influenced by the random selection of the first image pair and the iterative evaluation process.

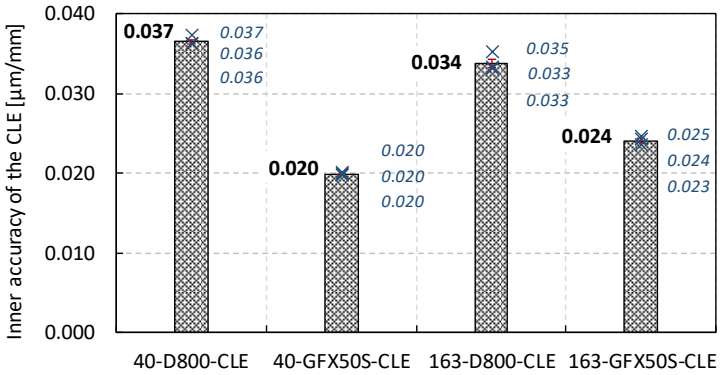

Figure 11.15. Inner accuracy of the calibration runs for the laboratory experiment in part II

Based on the results in Figure 11.15, the following conclusions can be drawn. The accuracy increases using the 163-target wall compared to the 40-target wall on average from 0.037 µm to 0.034 µm for the camera D800 (8,1 %). Between the cameras D800 and GFX50S, the accuracy increases from 0.037 µm to 0.020 µm (45.9 %) based on the 40-target wall and for the 163 targets wall from 0.034 µm to 0.024 µm (27.4 %). However, the average values for the GFX50S camera show a decrease in accuracy from 0.020 µm to 0.024 µm respectively from 40 target wall to 163 targets wall. As already mentioned, a final assessment over the accuracy based solely on calibration values in the range of micrometre is very vague. Therefore, a real deflection measurement and a noise analysis from the close-range photogrammetry measurement with all different calibration runs should deliver more reliable conclusion. The results from this investigation will be presented in the following sections.

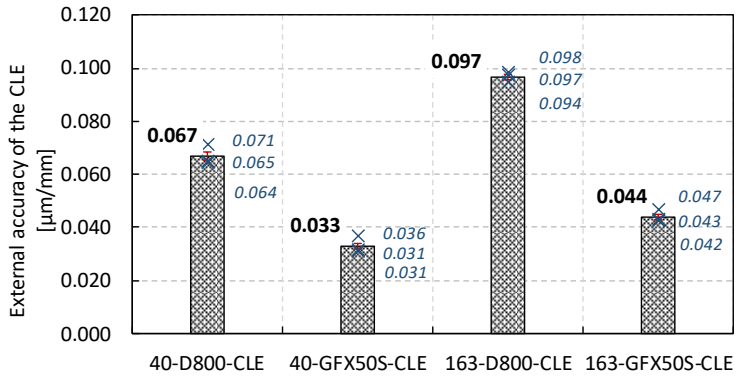

Figure 11.16. External accuracy of the calibration runs for the laboratory experiment in part II

Figure 11.17 and Figure 11.18 show the standard deviation values of the calibration parameters such as principal point distance and the location of the principal point. The both diagrams illustrate the similar tendency, namely higher standard deviation values for the calibration wall with 40 targets than the calibration wall with 163 targets. However, the differences between the cameras D800 and GFX50S remain small.

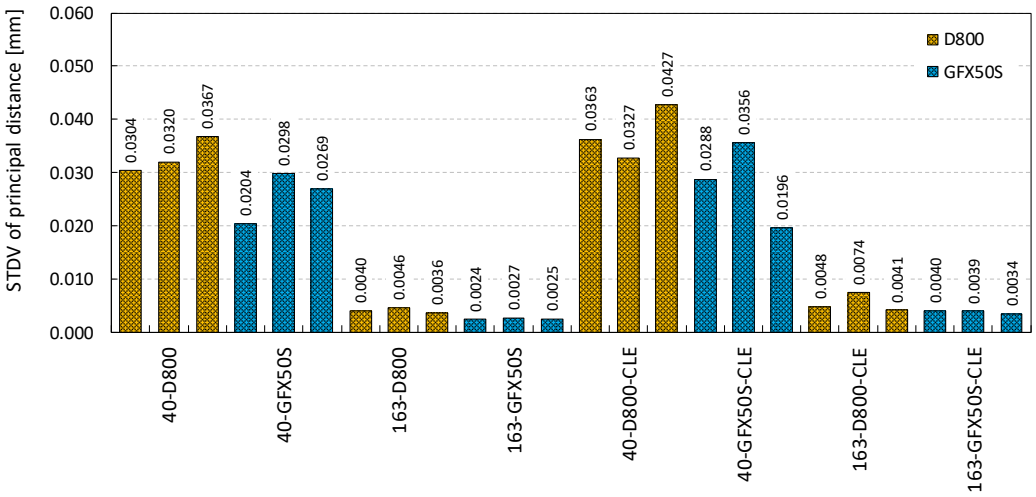

Figure 11.17. Standard deviation values for the principal distance

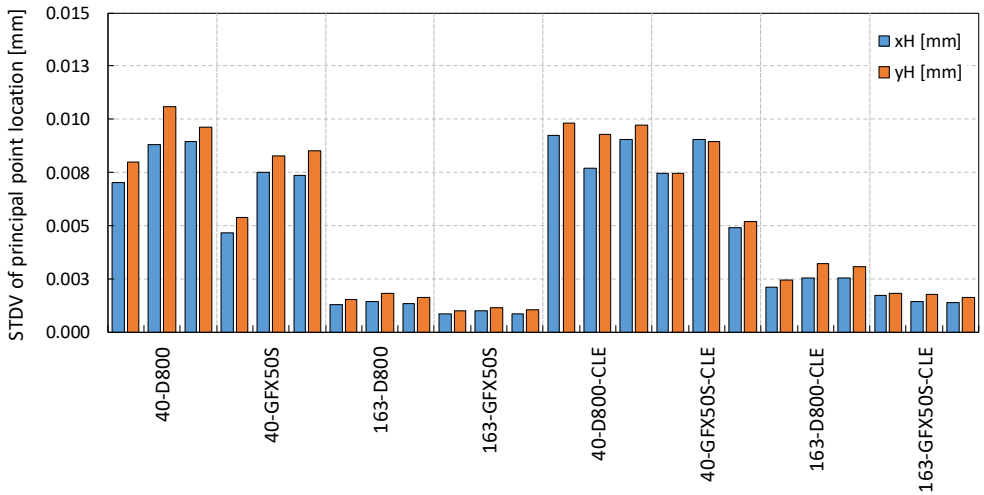

Figure 11.18. Standard deviation values for the principal point location

11.6 Close-range photogrammetric application for deflection measurement on a laboratory experiment

The laboratory experiment for the deflection measurement consists of a reinforced concrete beam, which is loaded stepwise (Figure 11.19). The dimensions of the beam are shown in Figure 11.20, namely the span of the beam amounts to 4.40 m and it is loaded at 1.80 m from the left

support. Due to different steps of the loading process, the reinforced concrete beam receives several stiffness reduction scenarios such as by cracking, by reaching the reinforcement yielding strength and by failure of the concrete in the compression zone. The discussion of the structural load bearing capacity will not be the subject of this study, but the discontinuities resulting from the different stiffness reductions influence the deflection measurements.

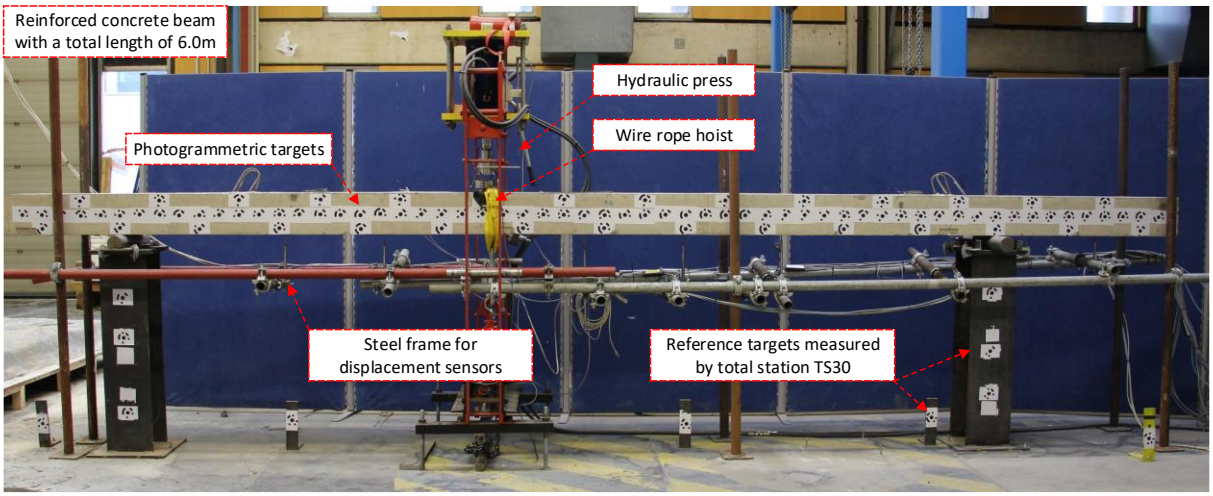

Figure 11.19. Experimental reinforced concrete beam

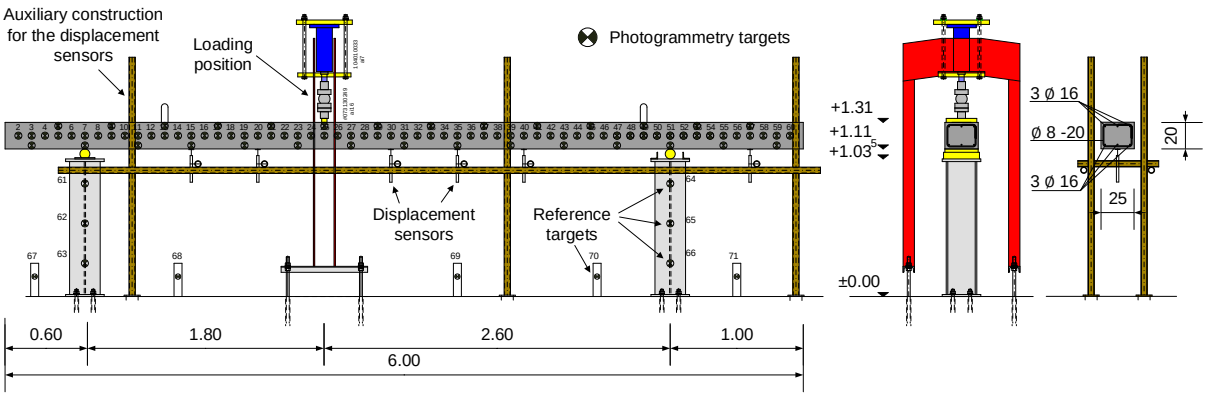

Figure 11.20. Dimensions of the experimental beam

The coded targets for the deflection measurement using the close-range photogrammetry were glued to the side of the beam at a regular distance of 10 cm. The coordinates of the reference targets on the support structures and on the floor along the beam were surveyed using a Leica TS30 total station. Displacement sensors, which are positioned under the beam on a scaffold, are installed to control the deflection of the beam during the experiment. The loading of the

beam was carried out using a path-controlled hydraulic press for higher load steps such as 20 kN, 30 kN and 40 kN. The lower load steps such as 2 kN, 5 kN and 10 kN are carried out using a wire rope hoist (Figure 11.19), to avoid the vibration from the hydraulic press and to negatively influence the measurement accuracy.

The targets in the middle of the beam are for the measurement of the deflection (Figure 11.21), however, there are also additional targets randomly distributed over the upper and lower half of the beam side (Figure 11.19). The additionally attached targets serve as auxiliary targets to stabilize the overlapping of the images (Figure 11.21). Without the auxiliary targets, the overlapping would only have stability along one axis (part A. in Figure 11.21), while the overlapping of the targets in a plane provide stability in two-dimensionality (part B. in Figure 11.21).

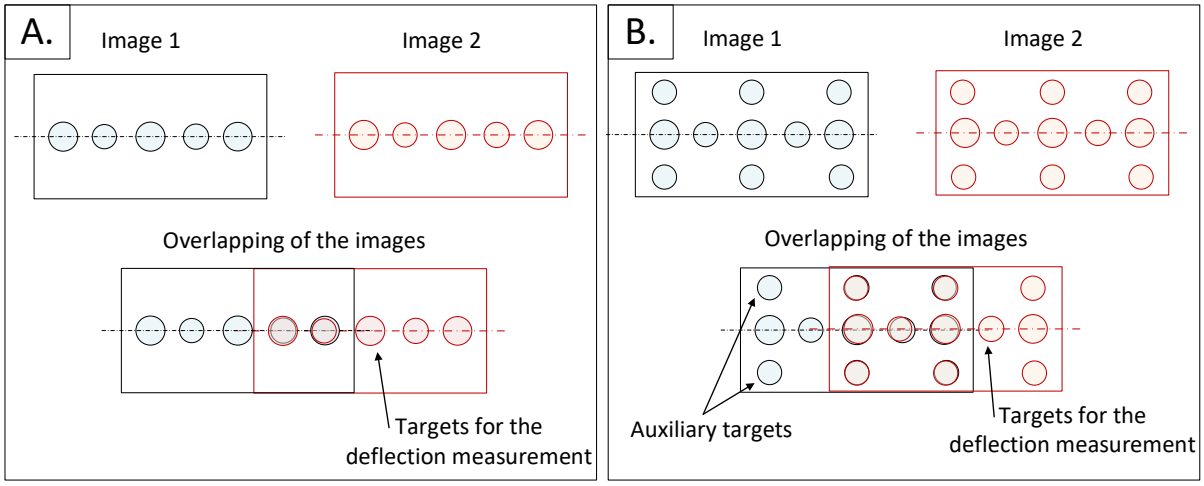

Figure 11.21. Overlapping of the targets for two variations A. without auxiliary targets; B. with auxiliary targets

Figure 11.22 shows in green dots the point cloud of the beam targets, the position and the directions of the image captures in red rectangles. The first row of the captures was taken in a distance of about 4.50 m to the beam and the second row at a distance of about 5.00 m. The additional three captures from larger distance are taken to have the total beam within a few pictures and to stabilise the adjustment process. These images help for the adjustment of all point clouds together, but they were captured with low resolution due to the high distance.

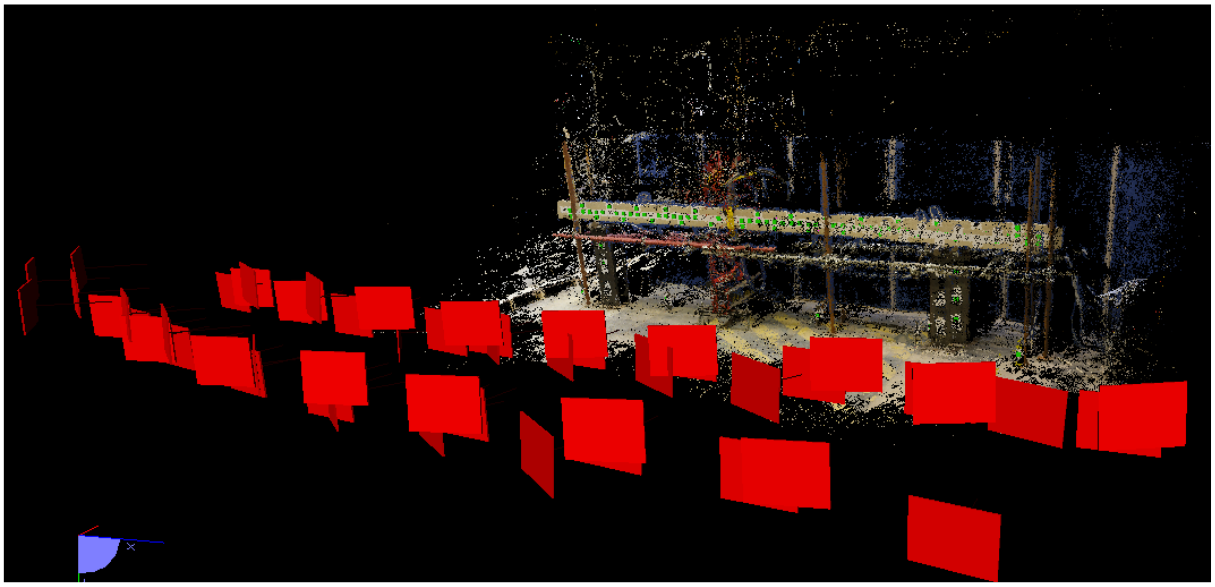

Figure 11.22. Point cloud, targets and capture positions for the beam laboratory experiment

Within the laboratory experiment, the deflection line of the beam is measured. The difficulty here is to judge the precision of the measurement only using the deformation values. The precision of a measurement is commonly evaluated by the measurement noise respectively by the standard deviation. The maximum deflection of the beam amounts to 1.25 mm for load step 2 kN, 3.52 mm for 5 kN, 8.87 mm for 10 kN, 20.9 mm for 20 kN, 30.3 mm for 30 kN and 38.5 mm and for 40 kN.

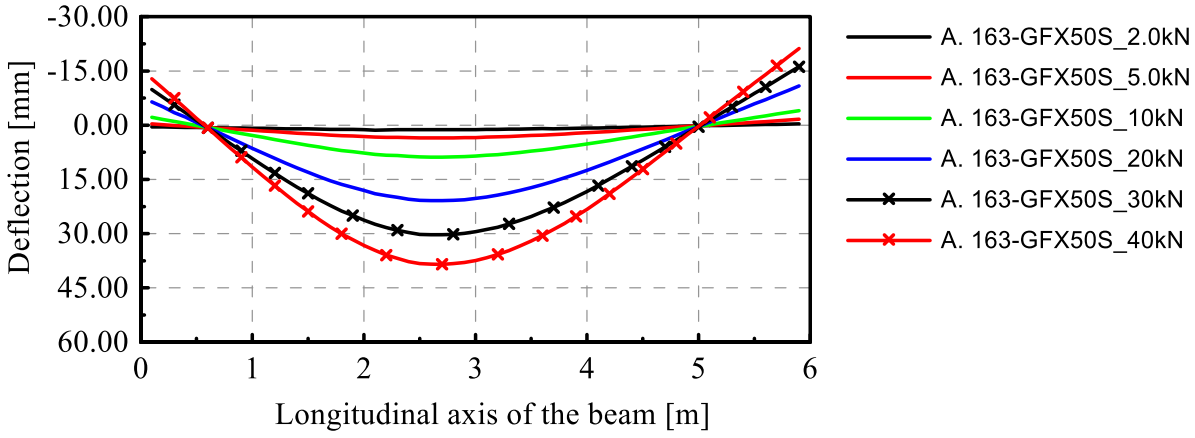

Figure 11.23. Measured deflection for the load cases 2 kN, 5 kN, 10 kN, 20 kN, 30 kN and 40 kN

The experimental beam is loaded due to its own weight and due to a point load as already mentioned. The deflection of the beam resulting from its own weight corresponds to a polynomial function of fourth-degree (equation(50)) while that of a point load to a polynomial function of third-degree (equation (51)). However, this theory only applies to the lower load steps before cracking of the concrete beam.

$$w(x) = \frac{q * l^4}{24 * EI_y(x)} \left[\frac{x}{l} - 2\left(\frac{x}{l}\right)^3 + \left(\frac{x}{l}\right)^4\right] \tag{50}$$

$$w(x) = \frac{F * l^3}{48 * EI_y(x)} \left[3\frac{x}{l} - 4\left(\frac{x}{l}\right)^3\right] \tag{51}$$

As mentioned above, the deflection line would be a continuous curve, but every measurement is influenced by a certain amount of noise. The continuous curve of the deflection can be calculated by using the polynomial regression based on the measured values. The standard deviation for the close-range photogrammetry is in the range of a few micrometre. Therefore, the noise resulting from the measurement precision would not become visible when considering only the deflection line (Figure 11.23). The measurement noise becomes only apparent, when only the continuous curve of the deflection line is deduced from the measured deflection line. Part A in Figure 11.24 shows exemplary the filtering of the deflection line in order to identify measurement noise. The black line with markers in part A of Figure 11.24 illustrates exemplary a deflection line with visible noise. The red-dashed line shows the polynomial regression of third degree calculated using the deflection values, which corresponds to the continuous deflection curve without any noise effect If the continuous polynomial regression is subtracted from the measured deflection values, the noise effect remains in visible dimension distributed over the vertical axis (Figure 11.24B). In the next step, the similar procedure is done to detect the noise effect on the measured deflection line in the experimental test presented here.

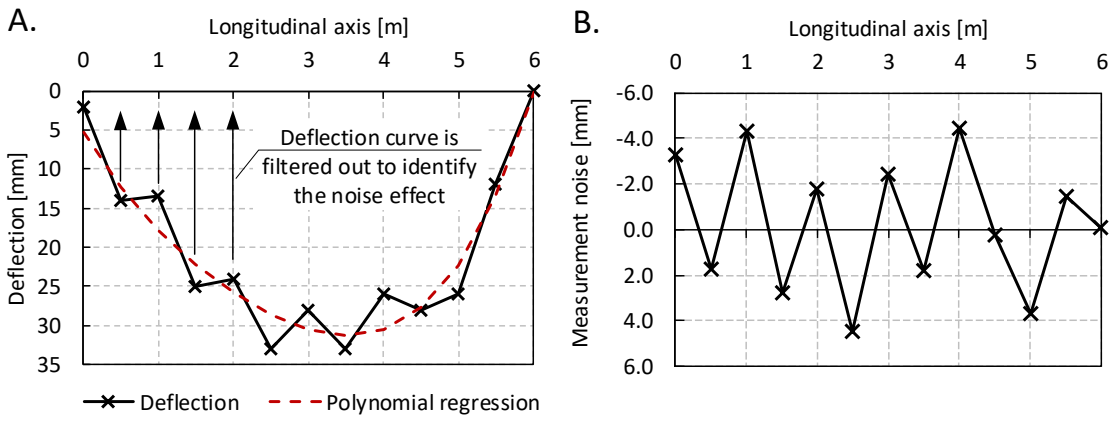

Figure 11.24. Investigation of the measurement noise, A. deflection of the beam before deducted by the polynomial regression; B. measurement noise along the deflection line

Within the laboratory experiment, as the reinforced concrete beam presents a non-linear load carrying behaviour with stiffness reductions, the deflection line is also non-linear. The deflection of a point-loaded beam is normally a cubic parable. However, due to the nonlinearity a higher degree of mathematical function is to be expected. In Figure 11.25, the difference between the deflection line and various polynomial regression of increasing degrees is presented.

The exemplary presentation of noise analysis depending on the degree of polynomial regression (Figure 11.25) is based on the deflection measurement by the camera GFX50S at load step 40 kN. Part A in Figure 11.25 shows the difference between the measured deflection line from the experiment and the polynomial regression of the first degree (linear course). Part. B shows the difference for the second degree, part C the third, and so on. Part I is the ninth degree of polynomial regression. It should be noted that the scale of the vertical axis for the respective diagrams varies depending on the max and min values. Figure 11.25 shows that the nonlinearity of the beam goes up to the sixth degree (part F) and that from a polynomial regression of the seventh degree on only the noise resulting from the measurement becomes apparent (part G-I).

Therefore, for lower load steps, the process of filtering out the noise effect using polynomial regression works better. For the higher load steps, an increase in the degree of the polynomial regression is required because of non-linearity of the stiffness in concrete structures.

Nevertheless, it should be mentioned that a too high degree for the polynomial regression could absorb some measurement noise resp. errors.

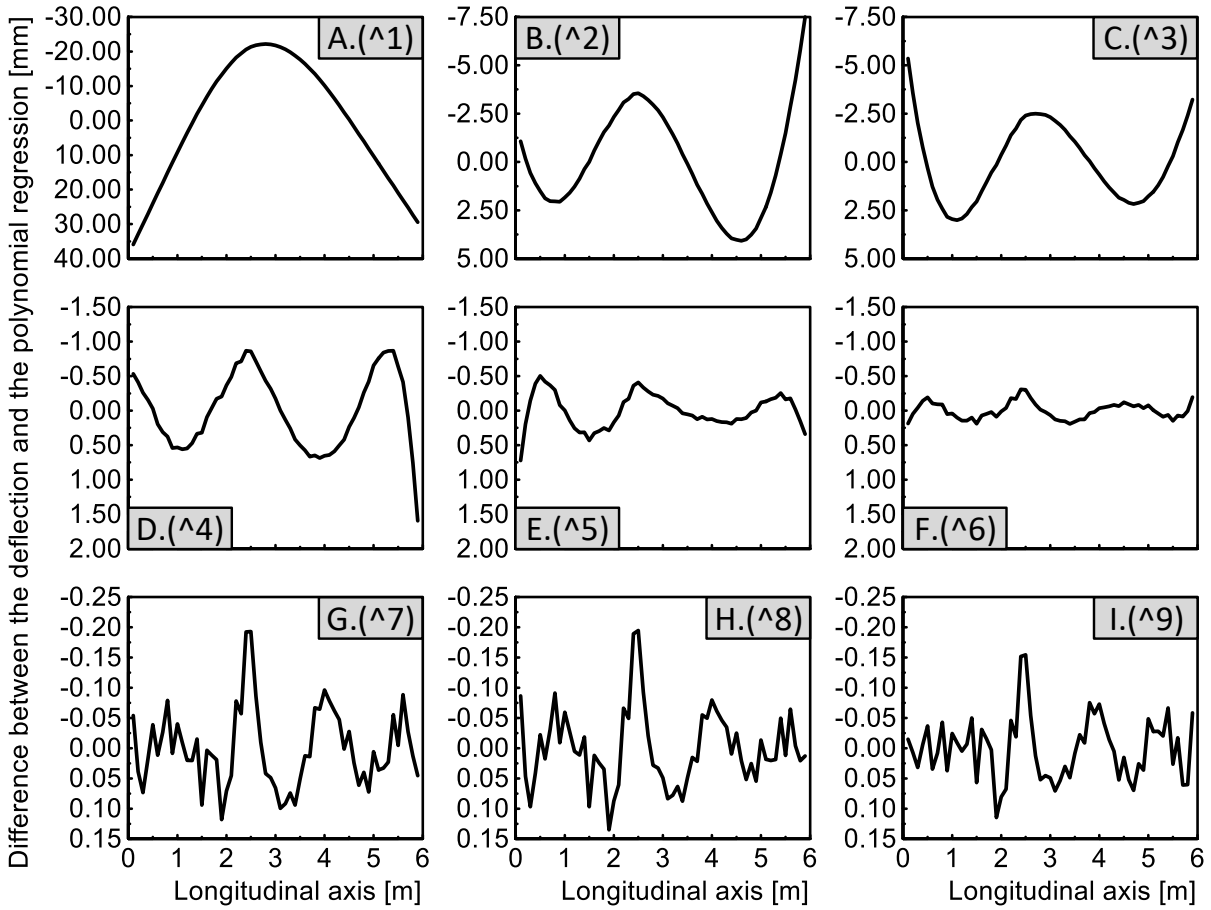

Figure 11.25. Difference between the deflection and the polynomial regression of several degrees

The duration of the photogrammetry measurement amounts about 10 min for each load step. The sability of the experimental beam is verified based on the displacement sensor measurement. Figure 11.26 shows the course of the displacement sensor measurements for the lower load steps from 2 kN to 5 kN. The load steps from 2 kN to 10 kN have been reached due to loading by a wire rope hoist (yellow strap at the position of loading in Figure 11.19). A hydraulic press is applied for higher load steps as from 20 kN to 40 kN. The wire rope hoist is able to very consistently keep the generated deflection in comparison to the hydraulic press which increases the effect of vibration. The constant amount of the deflection during the

photogrammetric measurement is visible in Figure 11.26. The duration of the photogrammetry measurement amounts about 10 minuts. The creep effect of the reinforced concrete beam is compensated by a decrease of the force applied to the beam, which is illustrated as black graph in Figure 11.26.

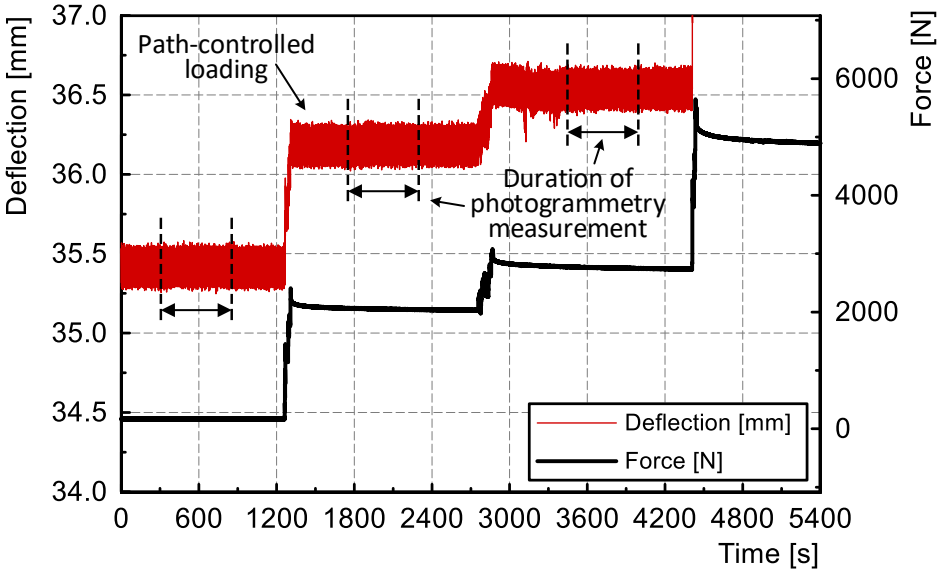

Figure 11.26. Loading process of the beam from 2 kN to 5 kN by wire rope hoist

Figure 11.28 illustrates the measurement noise calculated from the difference between the measured deflection and the polynomial regression of the ninth polynomial regression degree for the load steps 2 kN to 10 kN for the camera GFX50S and Figure 11.29 for the load steps 20 kN to 40 kN. The filtered measurement noise is affected by the non-linearity of the reinforced beam, especially for the higher load steps (Figure 11.29). At higher load steps, cracks develop in the concrete beam which causes discontinuity respectively leads to a reduction of the local stiffness. The presented DAD method in section 11.2 identifies the area with the reduced stiffness based on deflection measurement [96] [150]. An additional comparison of the standard deviation is presented in Figure 11.27. The vertical axis of the diagram illustrates the standard deviation in logarithmic scale. There are two horizontal axes, namely the red one (upper axis) for the degree of polynomial regression from 1 to 9 according to the Figure 11.25 and the black axis (bottom axis) illustrates the number of targets for deflection measurement in a distance of 10 cm to each other. These targets are positioned at the one side of the beam (Figure 11.19 and Figure 11.20). Some of the targets (target number 4, 15, 25, 26, 37, 38, 48,

60) were covered due to the steel scaffold and loading frame (Figure 11.19) and were detected only on few images. In order not to influence the results due to such boundary conditions of the experimental setup, they have been left out of this case. The standard deviation from load step 5 kN is shown depending on the variation of polynomial regression degree, which decreases relating to the increase of the regression degree. A point of intersection can be observed at the degree of 7th polynomial regression, which represents comparable tendency to the analysis based on Figure 11.25.

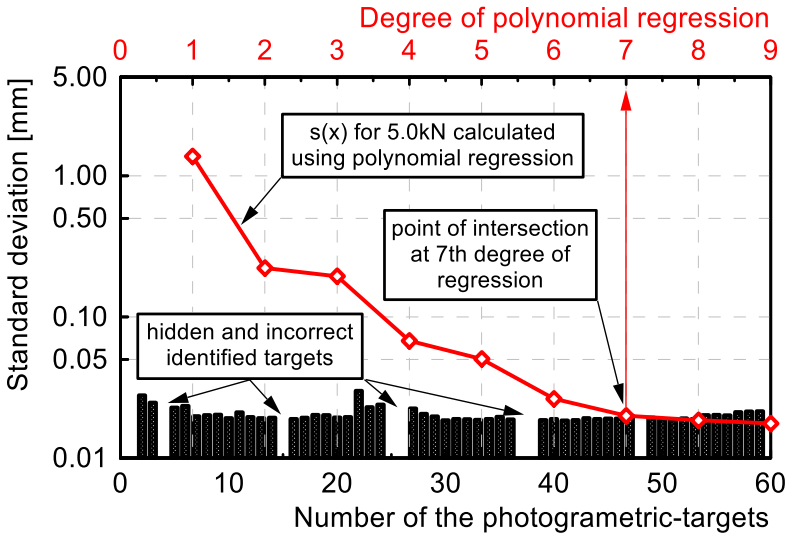

Figure 11.27. Comparison of standard deviation resulted from the inner orientation of the software for each target and from the noise analysis based on the degree of polynomial regression

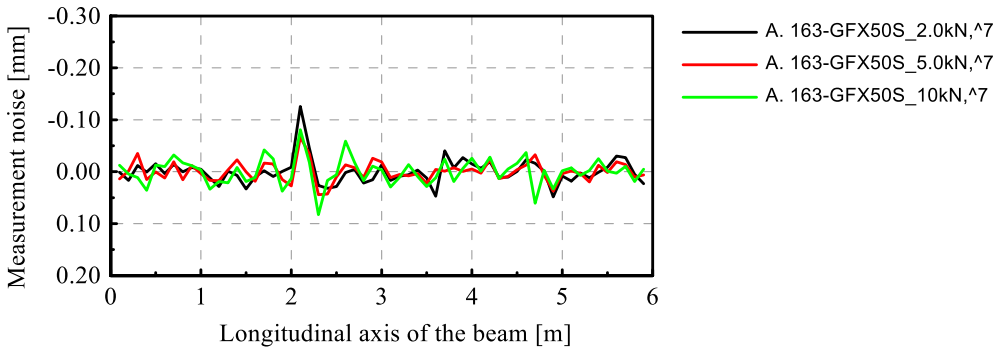

Figure 11.28. Noise effect resulting from the deflection measurements for 2 kN, 5 kN and 10 kN

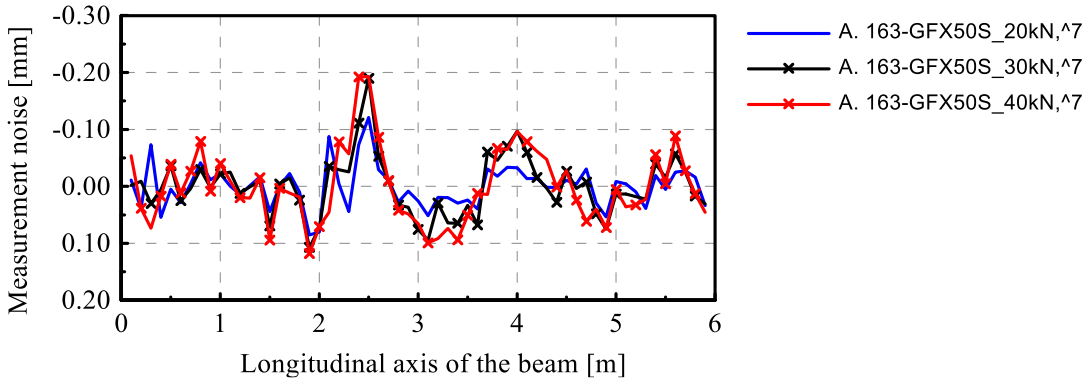

Figure 11.29. Noise effect resulting from the deflection measurements for 20 kN, 30 kN and 40 kN

A final and essential study of close-range photogrammetry measurement is presented in Table 4 to Table 6. The presented values of the standard deviation are resulting from the deflection measurement of the reinforced concrete beam in the laboratory experiment and they are calculated according to the noise analysis (Figure 11.25). The chosen degree of the polynomial regression amounts to seven (Figure 11.27) and the analysed load step is the load step of 5.0 kN (Figure 11.27). Table 4 includes the comparison of the close-range photogrammetric measurement without and with camera calibration based on the both cameras D800 and GFX50S. The column with the title “from” mentions the starting situation, namely without calibration with the corresponding standard deviation values on the right column. The column with title “to” illustrates the situation after camera calibration based on the smaller wall with 40 targets. The related standard deviation values are given in the next column. It is visible that the calibration of the cameras has a high influence on the measurement precision, 35.8 % for GFX50S and 44.6 % for D800. The average improvement of the precision amounts to 40.2 % if the camera is calibrated.

Table 4. Investigation of the precision difference between measurement without and with calibration of the camera

from [-]	Standard deviation [mm]		to [-]	Standard deviation [mm]	improvement [%]	average [%]
0-GFX50S	0.031350	->	40-GFX50S	0.020136	35.8	40.2
0-D800	0.052165	->	40-D800	0.028897	44.6	

Table 5 presents the results from the investigation of the influence of the camera quality improvement on the measurement precision. The investigation is done for three variations: 1. without calibration; 2. based on the calibration with 40 targets; 3. based on the calibration with 163 targets. The improvement in percentage varies in a quite similar range, so between 30.3 % and 39.9 %. The average improvement amounts to 34.0 % when the 51.4 MP GFX50S camera is used instead of the 36.8 MP D800 camera. For the determination of the bundle block adjustment, the overlapping of the images is of major importance. For the same capturing distance (in the range of 5.0 m to 6.0 m to the measuring object) and using the given lenses (50 mm for D800 and 63 mm for GFX50S), the overlapping of the images for GFX50S is about 8.7 % higher.

Table 5. Investigation of the influence of camera quality from full frame camera D800 with 36.8 MP to middle format camera GFX50S with 51.4 MP

from [-]	Standard deviation [mm]		to [-]	Standard deviation [mm]	improvement [%]	average [%]
0-D800	0.052165	->	0-GFX50S	0.031350	39.9	
40-D800	0.028897	->	40-GFX50S	0.020136	30.3	34.0
163-D800	0.028301	->	163-GFX50S	0.019345	31.6	

Table 6 presents the results from the investigation of calibration wall variation from 7.0x3.0 m with 40 targets to 14.0x6.0 m with 163 targets, which is also done for both cameras. As already

shown the calibration process improves the measurement precision considerably (40.2 %). However, the enlargement of the calibration wall does not lead to a large precision improvement. Thus, the improvement amounts only to 3.93 % for GFX50S and to 2.06 % for the D800, so in average to 2.99 %. A similar study is done for the investigation of the influence between 2D and 3D camera calibration with a consumer camera Nikon Coolpix L810. The authors reported about 50 % increase of precision when a 3D calibration is done instead of a 2D calibration [160]. Lin et al. [161] investigated the accuracy influence of different camera calibration distances. The achieved precision using the camera Canon EOS 5D ranged from 0.01 mm to 0.05 mm for self-calibration with and without tie line.

Table 6. Investigation of the influence of calibration wall size from 7.0x3.0 m to 14.0x6.0 m and target number from 40 to 163

from [-]	Standard deviation [mm]		to [-]	Standard deviation [mm]	improvement [%]	average [%]
40-GFX50S	0.020136	->	163-GFX50S	0.019345	3.93	2.99
40-D800	0.028897	->	163-D800	0.028301	2.06	

All values of Table 4 to Table 6 are illustrated in the following diagram (Figure 11.30). Within the study, the final achieved precision for the deflection measurement amounts to 0.019345 mm for GFX50S and to 0.028301 mm for D800. The total improvement of the precision amounts to 38.3 % for GFX50S and to 45.7 % for D800. Figure 11.30 shows that the calibration of the camera has the highest impact on precision. The calibration of the camera essentially increases the precision, particularly for the camera D800, respectively for both cameras in average by 40.2 %. The precision of the close-range camera increases, when the camera quality is increased from the 36.8 MPixel D800 camera to the 51.4 MPixel GFX50S camera. The improvement of the test field calibration situation from 40 targets to 163 targets amounts to about 2.99 % in average. Thus, the high potential of the high-precise measurement with close-range photogrammetry could be confirmed based on the minimal determined standard deviation values respectively on the extensive investigations.

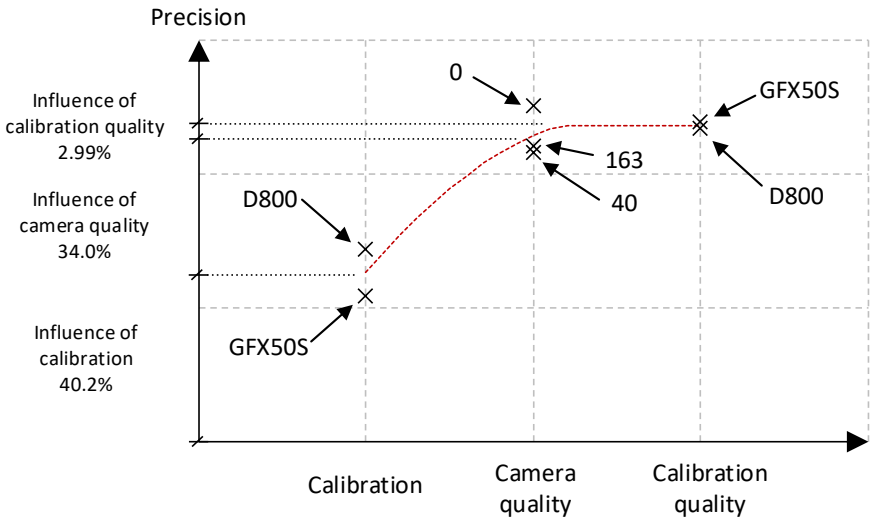

Figure 11.30. Summary of the investigation about the precision increase for all the variations

11.7 Conclusion and future works

The presented paper includes a discussion on the factors, which are influencing the accuracy of the measurement by the close-range photogrammetry. The question is to what extent the quality of the camera and the calibration of the camera influences the precision of the measurement. Within the study, both two different test-field calibration walls and two cameras were used. The first calibration wall has about 40 targets and a dimension of about 7.0x3.0 m, whereby the second wall has 163 targets and a dimension of about 14.0x6.0 m. The control points are measured by the total station Leica TS30 from two standpoints and the coordinates are calculated by angle intersections. The used camera is on the one hand the Nikon D800 with 36.8 megapixels and on the other hand the Fujifilm GFX50S with 51.4 megapixels. The applied software is the Elcovision 10, which is the state-of-the-art close-range photogrammetry tool for 3D measurements. In order to check the influence of the calibration runs, several series are done for both cameras and for both calibration walls, namely three series for each camera and three series for each calibration wall. Furthermore, a laboratory experiment for high-precise deflection measurement is carried out in order to determine the influence on real measurements. The laboratory experiment consists of a reinforced concrete beam with is stepwise loaded. There are six load steps with deflections, which vary between 1.25 mm and 38.5 mm. The

length of the experimental beam amounts to 6.00 m and the captures are done from a distance of about 4.50 m to 5.00 m. The results of the laboratory experiment were analysed based on the noise effect from the close-range photogrammetry measurement. The noise effect is determined from the difference between the measured deflection and the polynomial regression, which is calculated based on the measured values.

The process of the camera calibration bases on a nonlinear inequality system, which is iteratively analysed. The iterative calculation is solved by a stepwise increase of the reference value, whereby the adjustment breaks off from a limit value. Therefore, the same results are very rarely identical by using the same images, but only very similar. To compare the calibration results, the principal distance, the location of the principal point, the inner accuracy and the external accuracy from calibration process are considered. The accuracy defining values from the calibration process are in the range of micrometre, wherefore the values are very sensitive to the smallest influences such as e.g. already generated by repetition of the iterative calculation. However, the results from the additionally carried out laboratory experiment delivered values that enable the verification of the precision influencing factors. As already mentioned, the deflection of a beam structure is measured within the laboratory experiment. The noise effect resulting from the measurement precision is filtered out using the polynomial regression. However, the more detailed investigation showed the precision improvement of in average about 34.0 %. It also showed that the precision of the close-range photogrammetry increases by about 40.2 % in average when the camera is calibrated. Additionally, the improvement of the calibration wall from 7.0x3.0 m with 40 targets to 14.0x6.0 m with 163 targets amounts to about 2.99 %.

In summary, the measurement by close-range photogrammetry can reach very high precision if different parameters according to the camera calibration and quality are carefully observed. Many factors influence the precision of the survey. The influence of some factors is considerable and some are only interesting if very high precision is provided.

11.8 Acknowledgements

The authors would like to thank Mr Harald Krause, PMS Photo Mess Systeme AG for his professional advice and support with the regard to the correct application of the close-range photogrammetry.

12 Transition to the manuscript IV

12.1 Conclusion of the third manuscript

The study on the calibration and camera quality for close-range photogrammetry application was carried out for a various number of calibration series and structural deflection measurements. The highest impact factor on the measurement precision was achieved from the calibration of the camera. The precision of the deflection measurement increased by about 35.8 % for the camera GFX50S and about 44.6 % for the camera. The quality of the camera has the second highest influence on the precision of the measurements. It was found that, when the medium format camera GFX50S with 51.4 MPixel is used instead of the full-format camera D800 with 36.8 MPixel, the measurement precision increased by 34.0 %. Moreover, the quality of the calibration wall had a minor influence, that is about 3.0 %, if the cameras have been calibrated using the wall with 163 targets and with the dimension of 6.0x14.0 m than the wall with 40 targets and with the dimension of 3.0x7.0 m. The final achieved precisions for measurement of deflection were 0.019 mm for GFX50S and 0.028 mm for D800.

12.2 Introduction to the fourth manuscript

First of all, the fourth paper presents the first real bridge experiment and its results. The prestressed concrete experimental bridge has a span length of about 27 m. The bridge structure is loaded by six heavy trucks. The load did not exceed the serviceability limit state in order to enable a non-destructive test. Furthermore, it includes studies about the application limits for the DAD method, namely the detectable degree of damage, achievable measurement precision,

required structural deflection, number of measurement repetition, influence of damage location etc. Within the study, the measurement techniques such as levelling, total station, displacement sensors, laser scanner and photogrammetry are applied. The photogrammetry is carried out firstly on a tripod and secondly on a drone. In addition, the paper presents an analysis about the stability of drone flight, detection of damage using DAD method, theoretical cases with artificial noise effects etc.

13 Manuscript IV: Application of the DAD method for damage localisation on an existing bridge structure using close-range UAV photogrammetry

Abstract

A novel damage detection and localisation method, the so-called Deformation Area Difference method for localisation of damages in bridge structures is introduced. The method is based on static load-deflection experiments with the prerequisite of high precise deflection measurement. This study presents the first experiences of applying the DAD method on a real bridge structure. The investigated structure is a prestressed concrete slab bridge with a span of about 27 m, which was built in 2013. The loading on the bridge is applied using six heavy trucks, each weighing up to 32 t. A wide range of the modern measurement technologies were used to achieve high precision measurements of the bridge deflection along the longitudinal axis, namely the photogrammetry using a big size drone, laser scanner, total station, levelling and displacement sensors. The performed load-deflection test was non-destructive since the maximum deformation did not exceed the serviceability limit state. The exercise of the novel damage detection and localisation method on a real structure initiated further optimisation opportunities of the DAD method and the study of its limits. Several boundary conditions and methodical influence factors related to the applicability of the proposed method were analysed, such as impacts of measurement precision, damage degree, the position of damage, and the number of measurement repetitions.

13.1 Introduction

There exists an enormous amount of bridge structures worldwide guaranteeing a functional infrastructure as part of the public space. However, the constantly rising average age of bridges and the growing weight of heavy transporters further increase the applied stresses on the existing bridge structures [162]. The construction industry mostly uses natural resources. Therefore, the preservation of existing structures has a decisive influence on the ecological balance [163]. In general, the quality of the condition assessment depends on the experience of the bridge inspector and the applied state-of-the-art inspection methods. Although technological innovation has become much more prevalent in many areas, the construction industry is still lagging to implement new technologies in their processes [164] and, therefore, the bridge inspection according to the state-of-the-art is still mainly carried out by visual inspection [165].

Generally, the damages of bridge structures can be recognised on the structure surface by visual inspection. However, in case, the damage occurred inside the load-bearing structure, the damage detection becomes highly complex and the loss of stiffness cannot be detected in time. Some bridge inspection methods such as ultrasonic [166] or endoscopy are capable to examine the interior of the structure to a certain extent, but the location of the damage should be identified in advance. Recently, various research projects are dealing with the objective of damage assessment in bridge constructions based on different approaches. Oskoui et al. [167] developed a method for detection of cracks in bridges based on the structural influence line from moving load and the measurement of strains at multiple positions. The method was tested on a five-span 332-meter bridge and the analysis of the results led to the identification of five locations with anomalies. Visual inspection verified mini cracks at two locations and three misaligned sections. The method was mostly influenced by the big noise effect from the strain measurements. A comparative study based on strain gauges and influence line for damage detection in bridge structures was carried out by Wu et al. [168]. The focus of the study is on truck weight variations and vehicle speed to procedure the influence line. The authors report that the damage identification method is not affected by the truck speed but by the weight of the truck. An additional study for the damage extension is done based on a 1:10 scaled bridge model. The authors announced about higher damage identification accuracy for damages greater than 10 %. Further damage detection methods based on influence line are presented in

[169] [170] [171] [172]. Based on the theoretical principles, the detection of stiffness changes is feasible using the influence line, but the accuracy of the measurement related to the noise effect significantly affects the result of damage detection [173].

Besides to the examination of the moving load and the analysis of the resulting influence line, the investigation of the static load-deflection experiments on bridge structures provides information about the stiffness changes and the damages [174]. As bridge structures are built to bypass local obstacles, such as river, slope, road and valley etc., not all measurement techniques are applicable and it is often difficult to carry out deflection measurements along a bridge structure [175] [176].

Le et al. [177] present a method for damage localisation based on static load-deflection experiments. This study shows the results from finite element calculations for several steps of damage degrees. The theoretical results without noise effect show successful detection of damages at two positions for a one-span beam. Furthermore, a laboratory test was performed, where the cross-section of a U-profile is reduced at two different positions and the resulting deflection of a loading test is measured at seven locations with displacement transducers. Opposed to the finite element result, the experiment delivers deflection values affected by a measurement noise effect. The clear identification of damage is questioned and further examination with different noise level are examined [178] [179] [79].

Load-deflection tests on bridges have a long history and usually are carried out before the opening of the bridge or after the rehabilitation to demonstrate to the public about its load-bearing capacity. However, innovative measurement techniques open new possibilities to develop novel methods based on existing experiences and knowledge. Such a novel technique is the newly developed Deformation Area Difference (DAD) method for detection and localisation of damages in bridge structures, which is based on high precision deflection measurements of static load-deflection tests. The state-of-the-art methods for damage detection and the DAD method are presented based on theoretical examples and a laboratory experiment in [180]. The laboratory experiment consists of a reinforced concrete beam with the stepwise loading process. The study presented the successful identification of the cracked areas using the DAD method. Further development of the method tested on an additional laboratory

experiment is published in [150]. The main development of the method was to find out how to smooth the measurement noise to localise only the damages.

The current research investigates the boundary conditions and the needed measurement accuracy related to the detection of damages using the DAD method and presents the first application of the DAD method on a real prestressed concrete bridge with a span of about 27 m. All impact factors influencing the damage detection sensitivity, such as the measurement precision, the degree of the damage, damage position, required amount of experimental deflection, repetition of measurements etc., are investigated. The static load was applied using six heavy trucks, each of them weighing about 32 t (Figure 13.1). This study starts with the introduction of the theoretical background of the DAD method. Subsequently, the experimental setup of the experiment on the bridge is presented, followed by an investigation of the influencing factors for the DAD method. For the bridge experiment carried out in the current research, various modern measurement techniques were applied such as photogrammetry, laser scanner, total station, levelling and displacement sensors. Levelling delivered very high precision and was easy handling for application on a bridge structure. In particular, the application of photogrammetry installed on a big size drone showed very promising results and suitable application. Finally, an analysis is carried out to evaluate the detection of the degree of damage depending on the measurement precision, deflection size, damage position and measurement repetition.

Figure 13.1. Loading of the bridge by six trucks

13.2 Deformation Area Difference (DAD) method

The DAD method is developed to detect local damages in bridge structures. It considers the measured deflection of the structure $w_d(x)$ and the deflection from a reference system $w_t(x)$ (Figure 13.2). Beside an initial deflection measurement, also a simplified linear finite element model of the investigated bridge structure can be applied as a reference system. However, it is important that the reference system has a continuous deformation curve and it should consider the stiffness influencing structural parts like cross members, coves, coupling points of the prestressing cables etc. (Figure 13.2). The density of the values from the reference model should correspond to the density of the measurement points installed on the bridge structure. The DAD method is based on the fact that the measured deflection curve includes information about the local stiffness changes what will be further explained in the following section.

13.2.1 Relationship between deflection curve and stiffness of the structure

The study aims to develop a method to identify stiffness changes influenced by damages. Several research projects worked with the same goal based on dynamic [181] [182] [183] and static responses [184] [185] [186] of bridge structures. Both structural responses are influenced by stiffness changes e.g. due to damage. The localisation of the damage based on dynamic analysis presents more difficulties because the structural response on a dynamic excitation such as natural frequencies, mode shapes or damping are based on a global behaviour of a structure which renders the identification of local effects difficult. In contrast, the static structural responses deliver very promising results [187] [188].

The DAD method allows the localisation of stiffness reducing damages based on the deflection measurement of bridge structures. The stiffness of a structure under loading can be analytically calculated from the multiple derivatives of the deflection curve. The first derivative of the deflection corresponds to the inclination angle (equation (24)).

$$w'(x) = \frac{\delta w(x)}{\delta(x)} = \varphi(x) \tag{52}$$

In case of small deflections, the second derivative of the deflection curve, respectively, the first derivation of the inclination angle corresponds to the curvature of the structure (equation (53)). This condition is fulfilled when non-destructive load-deflection experiments are performed within the serviceability limit state. The determined curvature of the structure k(x) can be expressed as the ratio between the bending moment M(x) and the stiffness EI(x) (equation (54)). The known parameters of equation (54) are the curvature as the second derivative of the deflection curve and the bending moment resulting from the experimental load. Thus, each change of the stiffness EI(x) should be identifiable using the curvature and the bending moment. However, there are some issues related to the direct use the equation (54) for identification of damage.

$$w''^{(x)} = \varphi'(x) \cong k(x) \tag{53}$$

$$k(x) = \frac{M(x)}{EI(x)} \tag{54}$$

Opposed to the theoretical models, the real measurement of the deflection include measurement noise, which depends on the precision of the applied technique. Furthermore, the noise effect included in the deflection curve is increased by multiple derivations (equation (53)). The stiffness values expressed in equation (54) comprise the information about damage, planned stiffness changing areas (Figure 13.2) etc. Therefore, the challenge is to distinguish the discontinuities in the curvature curve between damage, measurement noise effect and stiffness changes inherent in the cross-section configuration. At this point, the DAD method becomes effective as it provides an alternative possibility to identify damages without using multiple derivations. It also considers the measurement noise effect and the stiffness changes resulting from the shape of the structure.

13.2.2 Background of the DAD-method

The DAD method investigates the difference in the area (green area in Figure 13.2) between the theoretical curves of the deflection line, the inclination angle and mainly the curvature with their corresponding curves from the experimental measurements. The deflection curve from the theoretical model of the bridge structure ($w_t(x)$ black curve in Figure 13.2) considers all planned stiffness influencing parameters of the structure such as cove, cross member etc. The principle of the DAD method is presented using a theoretical bridge girder with local damage of 60 %. The high amount of damage degree is chosen to clearly display the discontinuity resulting from the damage effect in the curvature curve. As long as the damage is not exactly at the point of a planned stiffness change, even the smallest degree of damage can be detected based on theoretical values. However, the real deflection measurement is affected by measurement noise which influences the detectable degree of the damage. Further investigation about the detectable degree of damage is presented in section 13.5.2.

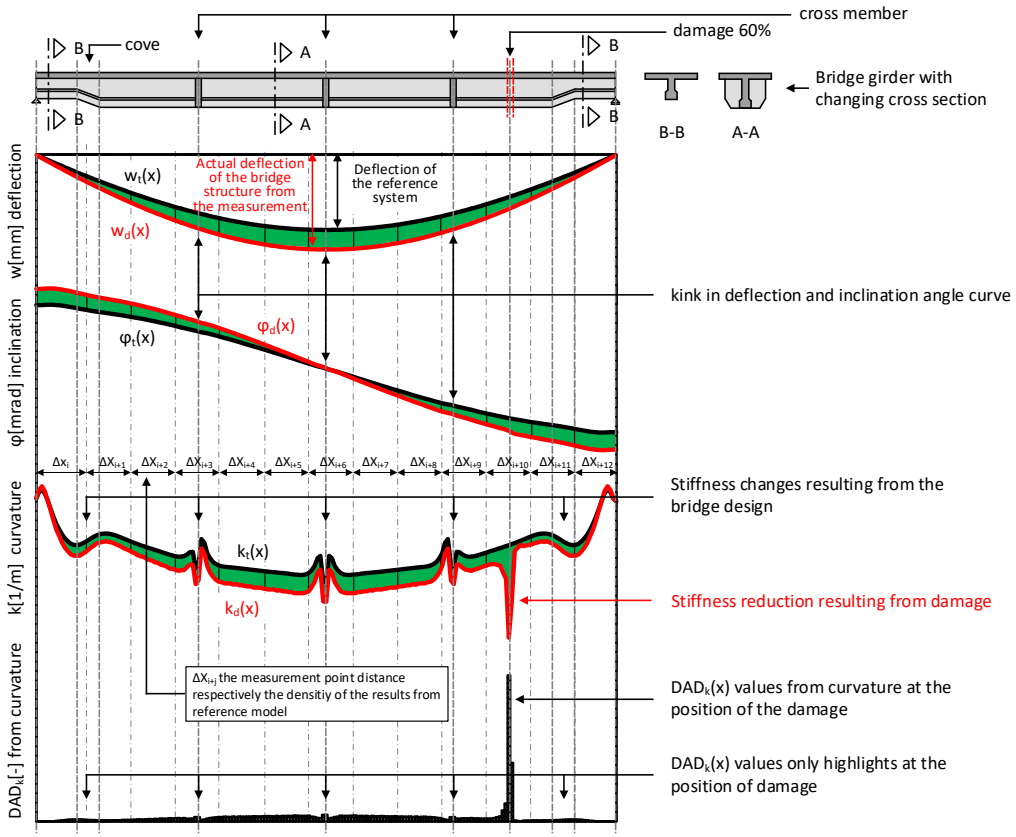

Figure 13.2. Principle of the Deformation Area Difference (DAD) method

$w_t(x)$ Deflection of the reference system (theoretical model)

$w_d(x)$ Actual deflection of the bridge structure from the measurement

$\phi_t(x)$ Theoretical inclination angle from the reference system

$\phi_d(x)$ Inclination angle from the first derivation of the measured deflection

$k_t(x)$ Reference curvature from the theoretical model

$k_d(x)$ Curvature from the second derivation of the measured deflection

Δx_i Distance between measurement points (mesh size of the model)

green area Area between the reference system and the measurement

$DAD_k(x)$ Deformation Area Difference (DAD) value from curvature

$A_{k,d,i}$ Area section under the damaged curvature curve

$A_{k,t,i}$ Area section under the reference respectively undamaged curvature curve

$\Delta A_{k,i}$ Area difference between damaged and undamaged curvature curve

Once the theoretical and experimental curvature curves are determined, the area under both curves from reference system and measurement is computed using the integral of the curvature functions (equations (55) and (56)), and the area difference is calculated according to the equation (57).

$$A_{\kappa,d,i} = \int_{i-1}^{i} \kappa_{d,i}(x)dx \tag{55}$$

$$A_{\kappa,t,i} = \int_{i-1}^{i} \kappa_{t,i}(x)dx \tag{56}$$

The disintegration of the function of curvature k(x) leads back to the function of the inclination angles φ(x) because the derivation of the inclination angle corresponds to the curvature (equation (53)). In other words, the DAD values for the curvature can be directly calculated using the first derivation of the deflection values respectively using the inclination angle values

(equation (57)). Using this method, the multiple derivations and the step of approximation according to equation (53) is avoided.

$$\Delta A_{k,i} = \int_{i-1}^{i} \kappa_{d,i}(x)dx - \int_{i-1}^{i} \kappa_{t,i}(x)dx = \\ = [\varphi_d(x)]_{i-1}^{i} - [\varphi_t(x)]_{i-1}^{i} = \varphi_d(x_i) - \varphi_d(x_{i-1}) - \varphi_t(x_i) \\ + \varphi_t(x_{i-1}) \tag{57}$$

The DAD method subdivides the area differences into several small sections Δx_i, as shown in Figure 13.2. The length of the section depends on the density of the measurement points and the mesh size of the finite element model used as a theoretical reference. Then, each difference area is separately squared and divided by the sum of the squared areas according to equation (46) to filter out of the known stiffness changing areas from the reference model and to represent the damaged section in a squared scale. Due to this normalisation, the effect of damage is strongly highlighted, which allows the increase of the sensitivity of the method on damage detection.

$$DAD_{\kappa,i} = \frac{\Delta A_{\kappa,i}^2}{\sum_{i=1}^{n} \Delta A_{\kappa,i}^2} = \frac{[\varphi_d(x_i) - \varphi_d(x_{i-1}) - \varphi_t(x_i) + \varphi_t(x_{i-1})]^2}{\sum_{i=1}^{n} [\varphi_d(x_i) - \varphi_d(x_{i-1}) - \varphi_t(x_i) + \varphi_t(x_{i-1})]^2} \tag{58}$$

13.2.3 Smoothing of the measurement noise

In case the measurement precision is known, the effect of noise can be filtered out from the measured deflection line. This procedure allows the reliable localisation of stiffness changes out of the range of the measurement noise. A detailed case study with a theoretical example and a laboratory test is presented in [150] and summarized in the following. The essential background of the noise smoothing process within the measurement standard deviation is applied based on equations (59) and (43). First of all, a polynomial regression $w_r(x)$ is determined based on the deflection curve $w_d(x)$, which is affected by noise (equation (59)). Then, the raw deflection curve $w_d(x)$ is filtered within the measurement standard deviation $s(x)$ and the smoothed deflection curve $w_{d,s}(x)$ can be obtained using equation (43).

$$\Rightarrow w_r(x) = \sum_{i=1}^{n} a_i x^i \tag{59}$$

$$\begin{cases} w_{d,s}(x) = w_d(x) - 0{,}50 \cdot s(x) \geq w_r(x)\,, & if \quad w_d(x) \geq w_r(x) \\ w_{d,s}(x) = w_d(x) + 0{,}50 \cdot s(x) \leq w_r(x)\,, & if \quad w_d(x) < w_r(x) \end{cases} \tag{60}$$

With:

$w_r(x)$ Polynomial regression

$w_d(x)$ Actual deflection of the bridge structure from the measurement

$w_{d,s}(x)$ The deflection function of the bridge structure from the measurement after smoothing

$s(x)$ Standard deviation resulting from the measurement technique

13.2.4 Identification of damages (outliers)

The DAD method is supposed to highlight the discontinuities resulting from a local damage. However, the evaluation is affected by the measurement noise and all stiffness influencing parts of the structure (Figure 13.2). After the application of the smoothing process, the outliers from the DAD values highlight the position of damages. However, it remains challenging to differentiate whether the highlighted discontinuities result from damage, from the measurement noise effects or from a stiffness change in the structure. Therefore, the widely used box plot method [189] [190] is applied to identify the real outliers of the DAD values (Figure 13.3).

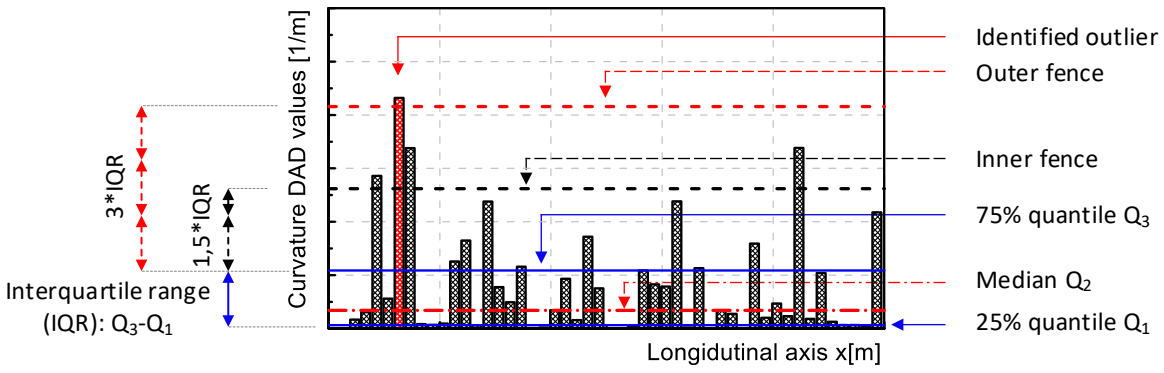

Figure 13.3. Identification of outliers based on the box plot method

The application of the box plot method defines an inner boundary value and an outer boundary value. The values from the investigated data which fall over the inner boundary value are considered as a minor outlier and those values over the upper boundary value are considered as major outliers. In a first step, the lower 25% quantile value (Q1 in Figure 3) and the upper 75% quantile value (Q3 in Figure 3) are computed to determine the interquartile range (IQR in Figure 3). Then, the inner boundary value is defined as the 75% quantile value plus 1.5 times the IQR, and the outer boundary value is defined as the 75% quantile value plus 3 times the IQR. The identified DAD values as a major outlier area are considered as locations where damage can be observed (Figure 13.3).

In the case of small damages in bridge structures, the discontinuity from the DAD values does not clearly highlight. Therefore, the identification of outliers enables the differentiation between the actual outlier and the discontinuity resulting from the noise effect. If outliers have been found, the DAD method was not able to identify any damages within the measurement precision. The impact of the damage position and the measurement precision on the detectable degree of damage is discussed in sections 13.5, 13.6 and 13.7.

13.3 Description of the bridge

The applicability of the DAD-method on a real bridge structure is investigated on a road bridge in Altrier, Luxembourg. The bridge was built in 2013 and serves as an overpass bridge crossing over a traffic road. The structural bridge superstructure is made of prestressed concrete with a span of about 27 m (Figure 13.4). The height of the bridge cross-section amounts to 93 cm. In total, the prestressing consists of thirty-six parabolic post-tensioned tendons with nineteen strands of class 1860 MPa. Concrete of compressive strength class C45/55 according to EC2 [191] was used. According to the official static design documents, the bridge is designed to accommodate trucks with a maximum weight limit of 60 tons. The cardinal direction of the bridge is oriented from the southwest (Luxembourg City) to northeast (Echternach), which allowed a uniform, natural illumination of the bridge side from morning until the afternoon. The favourable lighting of the structure was an optimal condition for the application of photogrammetry.

Figure 13.4. The experimental bridge in Altrier in Luxembourg

13.3.1 Applied techniques

The high precision measurement of the deflection line along the longitudinal axis of the bridge is an essential prerequisite for the successful application of the DAD method. On the one hand, the closer the distance between the measuring points, the higher the achievable precision on the localisation of the damage. However, on the other hand, a higher density of the measuring points leads to shorter height differences between the measuring points, which means that higher measuring accuracy is required to observe any differences. Therefore, it is important to find an optimum between these conditions. The different measurement techniques, which were applied for the experimental test, are as follows:

- Laser scanning: A laser scanner of type Leica P20 was used. This measuring unit can scan one million of measuring points per second to generate a point cloud with 0.8 mm density and has a range of up to 120 m [192].
- Total station: Two total stations of type Leica TS30 and Leica TS60 with very high accuracies, particularly in angle measurement (0,15 mgon) were applied [193]. Therefore, both total stations have been positioned at two different locations, and the targets have been measured using the angular intersection.
- Levelling: The levelling unit of type Leica DNA 03 with very high precision in height observations was used. The precision of the electronic measurement with the help of invar staff amounts to 0,30 mm [194]. The digital invar staff enables the faultless and precise recording of the measurement values.

- Photogrammetry: The technical equipment used for photogrammetry is a full-frame camera Nikon D800 set on a tripod and a medium-format camera Fujifilm GFX50S installed on a big size drone DJI Matrice 600 as shown in Figure 13.5. The calibration of both cameras was performed using the test-field calibration method. The captured images were processed using the software Elcovision 10 [195].
- Displacement sensors: Two displacement sensors from HBM [196] with the length of 50 mm have been applied among other things to enable the real-time monitoring

In addition, several temperature and humidity sensors were installed above and under the bridge to monitor the environmental conditions. Furthermore, an infrared camera of type InfraTec Variocam was used to observe the temperature distribution on the surface of the bridge. The photogrammetry with Nikon D800 is set using a tripod from a distance of about 10,0 m and 15,0 m from the bridge. The pictures are captured at every 2,00 m along the longitudinal axis of the bridge. The second measurement with photogrammetry is carried out using a Fujifilm GFX50S on a drone. The flight with the drone took place fully automatically, and the camera GFX50S took pictures every 2 seconds. The flights are done in two different heights, namely one at the same height as the bridge deck and one at about 2,5 m from the ground. The distance of the drone to the bridge amounts to about 12,0 m.

Figure 13.5. The drone DJI Matrice 600 and the camera Fujifilm GFX50S hold by a gimbal

13.3.2 Experimental setup

The experimental setup installed on the southeast side of the bridge is schematically shown in Figure 13.6. Fifty-one photogrammetry targets were mounted below the cross-section of the bridge structure at a distance of 50 cm to each other, and each ten reference targets were positioned at both bridge abutments. The measurement with levelling is carried out on the top of the bridge with 3,00 m distances. The measurement with the laser scanner is done from a single position orthogonal to the centre of the bridge at 15 m from the bridge.

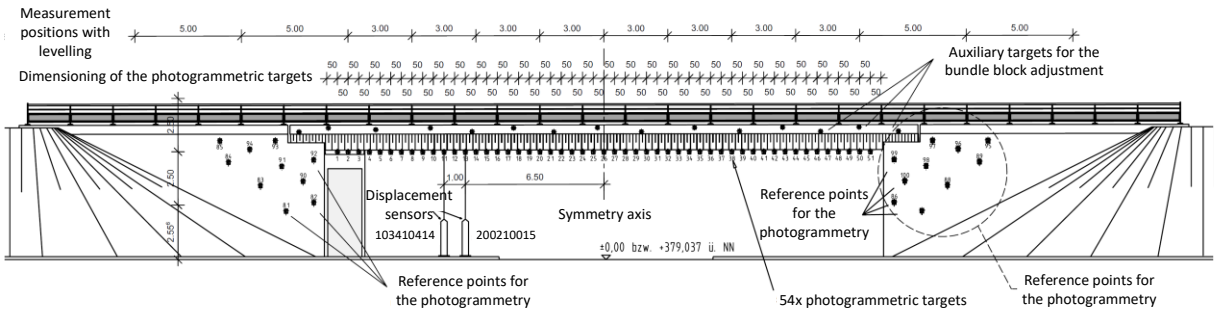

Figure 13.6. Side view of the experimental setup

Part A of Figure 13.7 shows the installation process of the photogrammetry targets and part B the dimensions of the setup. The used photogrammetric targets [195] have been printed out on dull adhesive films which are usually used for automobile foliation. The dull films have the advantage for the capturing process that it is not reflected by the sun. The adhesive films are resistant to ultraviolet light and rain or water.

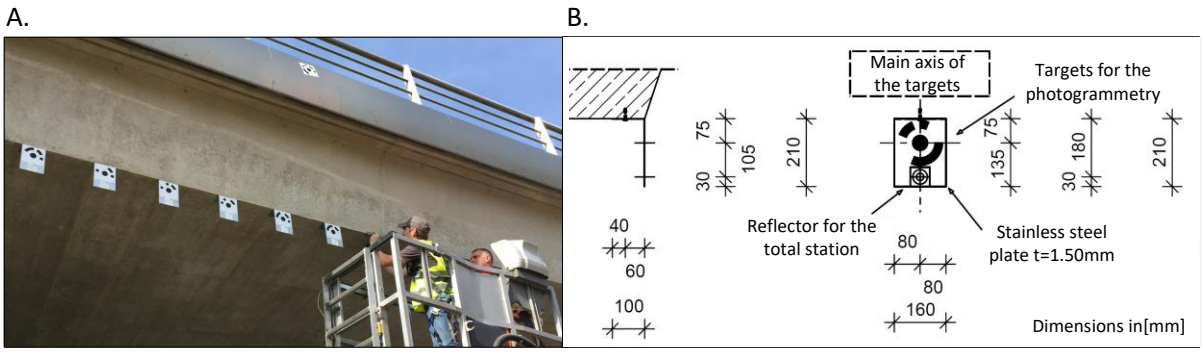

Figure 13.7. A installation of the targets; B. Dimensions of the setup for targets

For the measurement with the total station, the same targets as for photogrammetry were used. Both displacement sensors have been installed at 6.50 m respectively at 7.00 m from the centre of the bridge, as shown in Figure 13.6. In addition, the deflection of the bridge was measured with two displacement sensors. The height of the bridge cross-section amounts to 93 cm and at the mid to 1.075 m (Figure 13.8). Since a large number of measurement techniques were applied during the experiment, the whole traffic was closed from nine in the morning to four in the afternoon for totally seven hours.

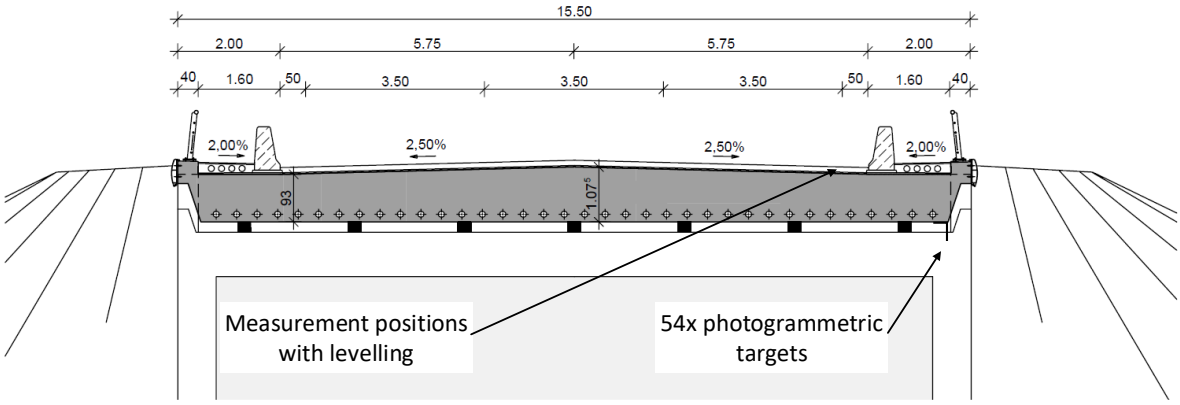

Figure 13.8. Cross-section of the bridge

13.3.3 Finite element model of the bridge

A finite element model of the bridge was designed using the software Sofistik (Figure 13.9). The FE-model functions as a reference system for the application of DAD-method. Furthermore, the dimension of the experimental load and the amount of the required trucks was defined based on the FE-calculation and the existing static documents of the bridge. The FE model is carried out based on linear calculation, which corresponds to the non-destructive load-deflection experiment on the bridge within the serviceability limit state. The realistic modelling of the bridge structure is usually a major challenge. The model updating is often required based on dynamic or static experimental results to enable the increase in the accuracy of the FE model. As already mentioned, the DAD method requires a theoretical reference system of the investigating bridge structure. However, the model does not have to respect a high requirement

regarding the accuracy of the FE model. In other words, the following conditions are important for the creation of the reference system:

- Static system respectively the span lengths
- Consideration of the changes in cross-section or changes in local stiffness changes
- Position of the experimental load

In return, the following points are not needed to be represented according to the real conditions of the studied structure, which makes the modelling of the reference system much easier:

- Amount of the structural deflection
- Amount of the load
- Global effects from both the dead load and the temperature
- Spring stiffness of the support structure
- Deflection due to shear force
- Effects from creep and shrinkage
- Linear material properties and linear calculation

The DAD method considers the area between the measured curvature curve and the reference curvature curve. The considered area is divided into several sections, which enables a relative comparison, respectively only identifies local changes in the deflection behaviour of the structure.

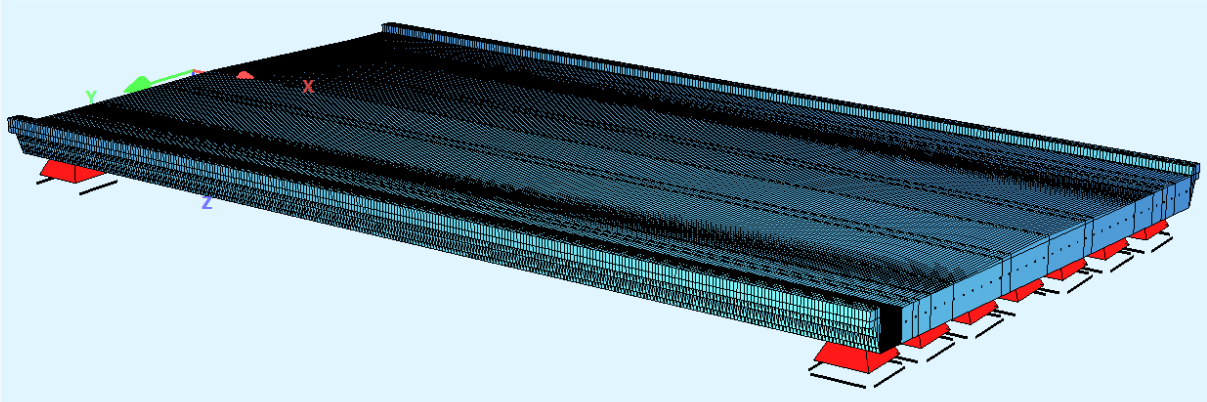

Figure 13.9. Finite element model of the experimental bridge using the software Sofistik

13.3.4 Loading of the bridge

The DAD method for localisation of damages bases on the measurement of the deflection curve of a bridge structure. The easiest way to apply loading on a bridge structure is to use heavy trucks. However, on the one hand, the load should not exceed the serviceability-limit-state, and on the other hand, the amount of deflection should be as big as possible to generate a measurable bridge deflection. The required amount of experimental deflection is investigated in section 13.5.3.

Within the presented bridge experiment, respecting the two constraints described in the previous paragraph, the determination of the loading led to six heavy trucks with a weight between 31 t and 33 t per truck (Figure 13.1 and Figure 13.10). During the experiment, the bridge structure is loaded step by step and the structural deflection is monitored in real-time using both displacement sensors (Figure 13.6).

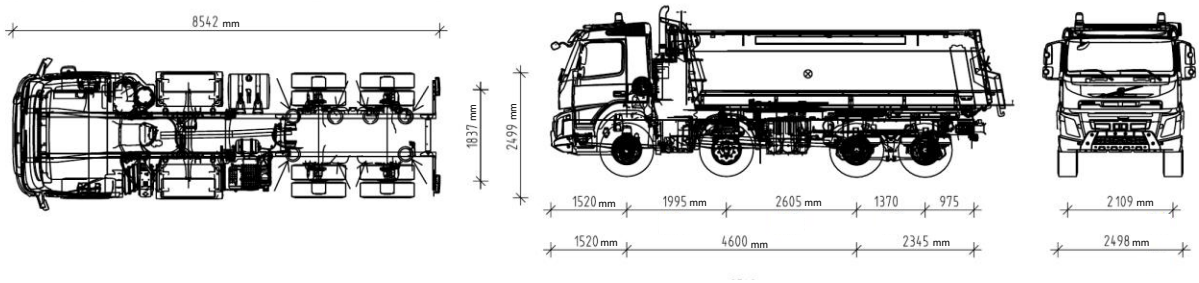

Figure 13.10. Dimensions and wheel distances of the trucks [197]

Figure 13.11 shows the expected and measured deflection as a function of time and related to the consecutive loading of the bridge by the six trucks. The presented deflection values (vertical axis) as a function of time (horizontal axis) were measured by both displacement sensors (Figure 13.6). The values in brackets represent the expected deflections resulting from the FE calculation. For trucks number 1, 3 and 5, small peaks can be observed at the beginning of the deflection curves due to the crossing of the bridge centre by the trucks before reaching their final position. The measured deflection values always lay below the expected values from FE calculation, which allowed to increase the number of trucks to all planned six trucks. The maximum deflection of the bridge at the midpoint amounted to about 11,0 mm, which corresponds to a span deflection ratio of about L/w = 27,0/0,011 ≈ 2500.

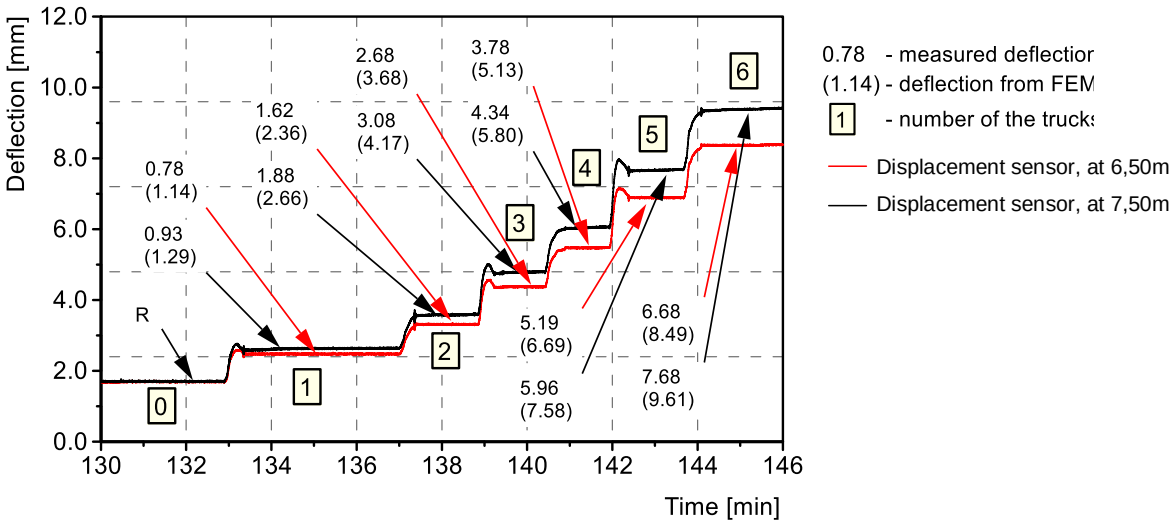

Figure 13.11. Loading of the bridge and measurement of the deflection by displacement sensors

13.3.5 Environmental conditions during the test

Figure 13.12 summarises the temperature and humidity measurements over time on top and under the bridge, as well as the deflections measured by the displacement sensors. The sensors are installed at about 8:40 am, which is visible in the diagram. After about 20 minutes, the sensors have been adapted to the surrounding conditions. The humidity and temperature sensors are battery operated and were switched on the day before the test and switched off the next day after the experiment. Therefore, Figure 13.12 includes recorded data about the humidity and temperature before and after the test day. These data show the environmental conditions of the transport vehicle and have no significance for the test conditions. The air humidity amounted to about 85% and decreased over time. The temperature slowly increased during the test day and amounted on average to about 16°C. The sky on the experimental day was cloudy, which represents an optimum condition for the use of the photogrammetry technique.

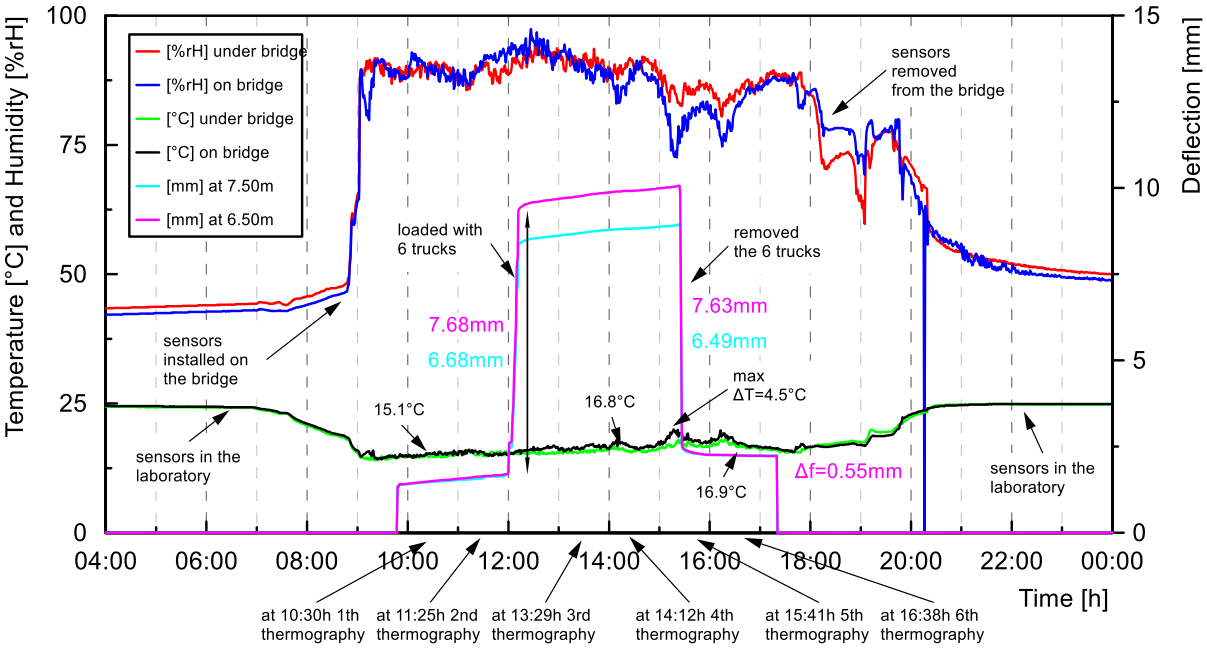

Figure 13.12. Determined humidity and temperature of the bridge Altrier, as well as its deflection measured by the displacement sensors on the test day

Figure 13.13 shows the six thermography images of the bridge, which were captured at an hourly basis from the start to the end of the experiment. Until 14:12h, uniform temperature distribution at the surface of the bridge can be observed, which were ideal conditions for the experiment and mainly resulted from the cloudy weather conditions. In contrast, the highest surface temperature difference was recorded at 15:41h, however, only a maximum temperature difference of 1.30°C was observed between the surface in the shadowed area and the areas exposed to the sunlight. Therefore, it can be assumed that the load-bearing structure had an uniform temperature distribution over the whole duration of the experiment. Nonetheless, it should be noted that the application of the DAD method is not affected by a uniform respectively a global temperature change [180]. The temperature change usually affects the whole structure, not at a local position. Since the DAD method carries a relative investigation comparing measured data to a reference data set for the detection of damage, the temperature effect has no influence (see section 13.3.3).

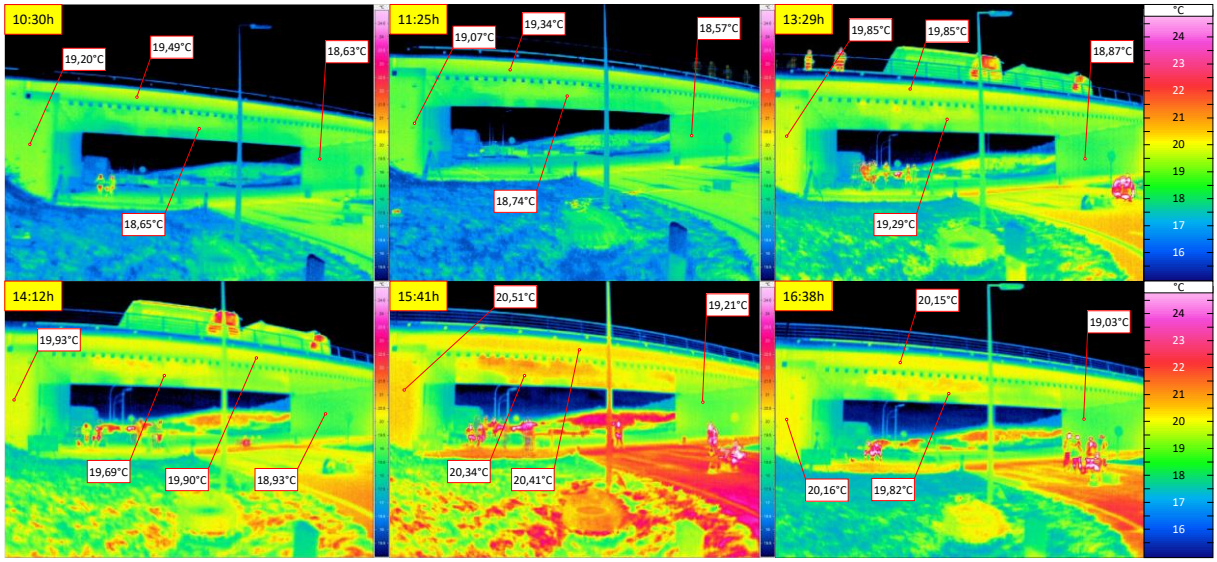

Figure 13.13. Thermography measurement of the bridge at different periods of the day

13.4 Results of the bridge experiment

In the past, the DAD method was applied for several case studies based on finite element calculations and on some laboratory experiments [180] [150] [99] [30] [198]. The current study shows the first time the application of the DAD method on a real bridge structure. The major aim for this study was to identify the measurement precision which is able to be achieved on a real-scale structure under outside environmental conditions and not the DAD values themselves as the newly constructed bridge was expected to be without any damage.

13.4.1 Measurement precisions

In this study, the deflection of the bridge is recorded by several most modern measurement techniques. Part A in Figure 13.14 shows the deflection of the bridge measured by photogrammetry. The maximum deflection by six heavy trucks amounts to about 11 mm. The targets were placed at a spacing of 50 cm along the longitudinal axis (Figure 13.14). Applying the photogrammetry, each measuring targets is captured several times from different angles and positions. The photogrammetry measurement was carried out based on the bundle block adjustment of all pictures and, the coordinates of the targets have been determined. The diagram

presented in Figure 13.14 shows the standard deviation of each target with an average value of about 0,07 mm (Part B. in Figure 13.14).

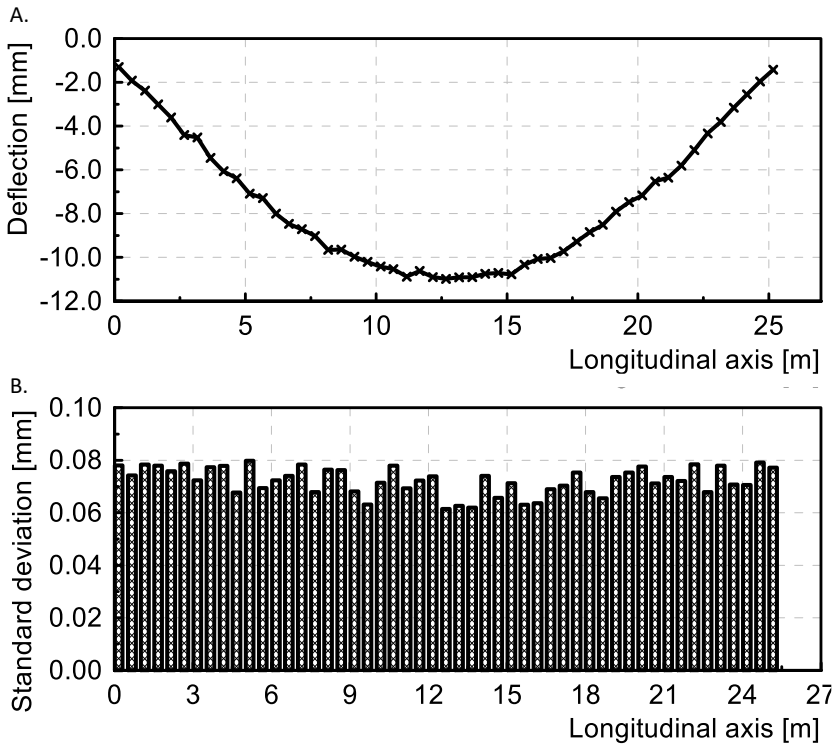

Figure 13.14. The deflection measurement by photogrammetry using the camera GFX50S and the drone (Part A.) as well as the standard deviation for each target (Part B.)

The precision of the measurement is determined based on the noise effect (Figure 13.15). The noise from the deflection effect is shown in black, and the measurement noise after the smoothing process according to section 13.2.3 is shown in red dashed line.

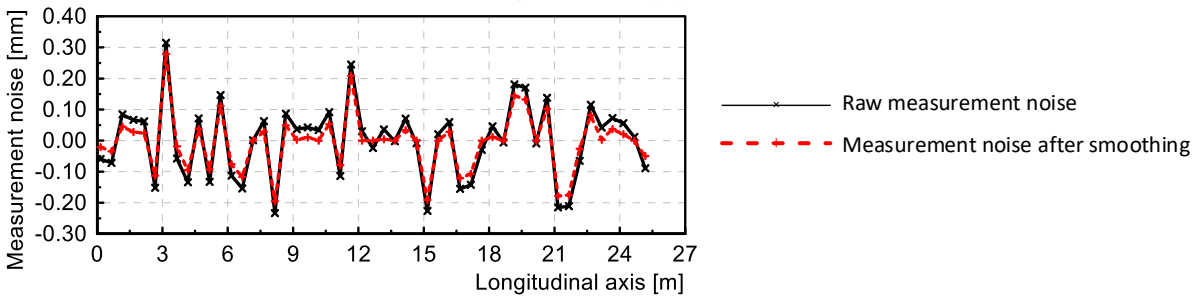

Figure 13.15. The filtered noise effect from raw measurement and after smoothing

In order to identify the accuracy of the measurement techniques, an exactly calibrated comparative measurement is normally carried out. Within the experiment, several most modern high–precision measurement techniques have been applied. However, every measurement technique delivers normally distributed measurement results. Therefore, in order to determine the standard normal distribution of the measurement results, the measurement noise effect has to be filtered out from the deflection line. Figure 13.16 shows the determination of the standard deviation of a measurement noise related to a straight line. However, in the case of a deflection measurement (Figure 13.17), the standard deviation cannot be determined directly, as shown in Figure 13.16. A polynomial regression is therefore created from the measurement data, which corresponds to the deflection curve of the experimental bridge structure and is subtracted from the measured deflection line. Then, only the noise of the measurement results would remain as shown in Figure 13.16. The advantage of this procedure is that the precision of the measuring techniques can be compared to each other (Figure 13.19). The disadvantage is that the polynomial regression does not correspond 100 % exactly to the deflection line and falsifies the result to a small extent. Based on this, the precision of all applied measuring techniques are finally compared by their standard deviations (Figure 13.19).

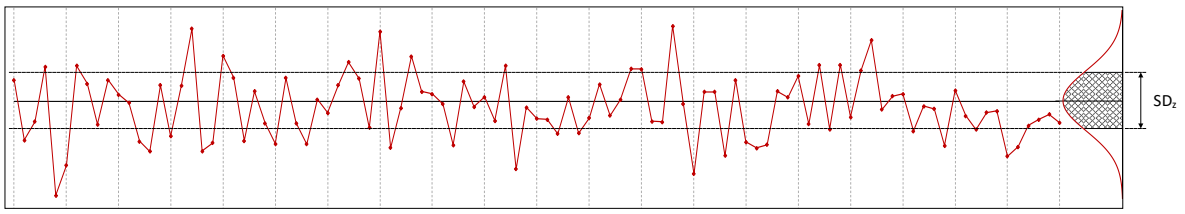

Figure 13.16. Measurement noise along a reference line and the standard deviation

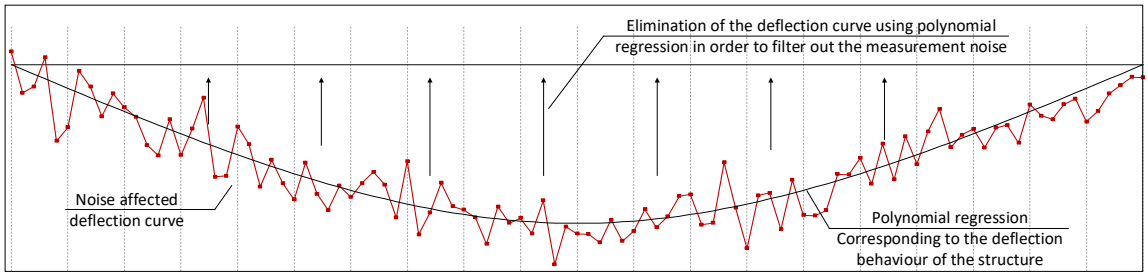

Figure 13.17. Exemplary, a noise affected deflection line and filtering out the measurement noise using polynomial function

The precision value of 3.0 mm for laser scanning is only an estimated value as the precision of the laser scanner depends on the roughness of the bridge surface, on atmospheric conditions, on internal safety mechanism and measuring configuration. Comparable studies [199] report the accuracies of about 0.50 mm to 5.00 mm for laser scanner Leica P20. Therefore, it is quite possible that the actual accuracy is much better than the estimated value of 3.00 mm. The displacement sensors deliver very high precise deflection values with a standard deviation of 0.0329 mm. However, the application of the DAD method using displacement sensors would not be practical, because of the high number of the required measurement points. The levelling is also a high precision measurement technique; however, the precision could be influenced by human handling. The measurement of a long bridge requires a big amount of measurement points, which extensively increases the involved measurement effort. Nonetheless, it could be used as control measurement with few measurement points at selected positions. The measurement with total station works automatically which decreased the measurement effort. The standard deviation of 0.2360 mm presented in Figure 13.19 was reached without using reflector targets as the use of reflector targets decrease the measurement precision [200]. In contrast, the close-range photogrammetry based on high-quality cameras which were calibrated in advance and by using one of them on a drone provided an optimal application for bridge deflection measurement. The achieved accuracy for the full-frame camera D800 amounts to 0.1451 mm and for the medium format camera installed on the drone amounts to 0.1186 mm. The precision of the photogrammetry was not influenced by the vibration from the drone flight (Figure 13.18 A.). The zoom of the photogrammetric target number 11 is shown in Figure 13.18 A., which is captured while the drone flight. The low shutter speed of 1/500 sec and the robust gimbal of the drone allowed the avoidance of the camera shake effect. A very stable gimbal DJI Ronin-MX and a very short shutter speed of the camera could avoid the blurring effect. In comparison, a capture done from the tripod using the remote release is shown in Figure 13.18 B. In both pictures, the sharp and not blurred pixels from white to black are clearly visible. The image stabiliser from the lens was not use, which would otherwise negatively affect the measurement precision.

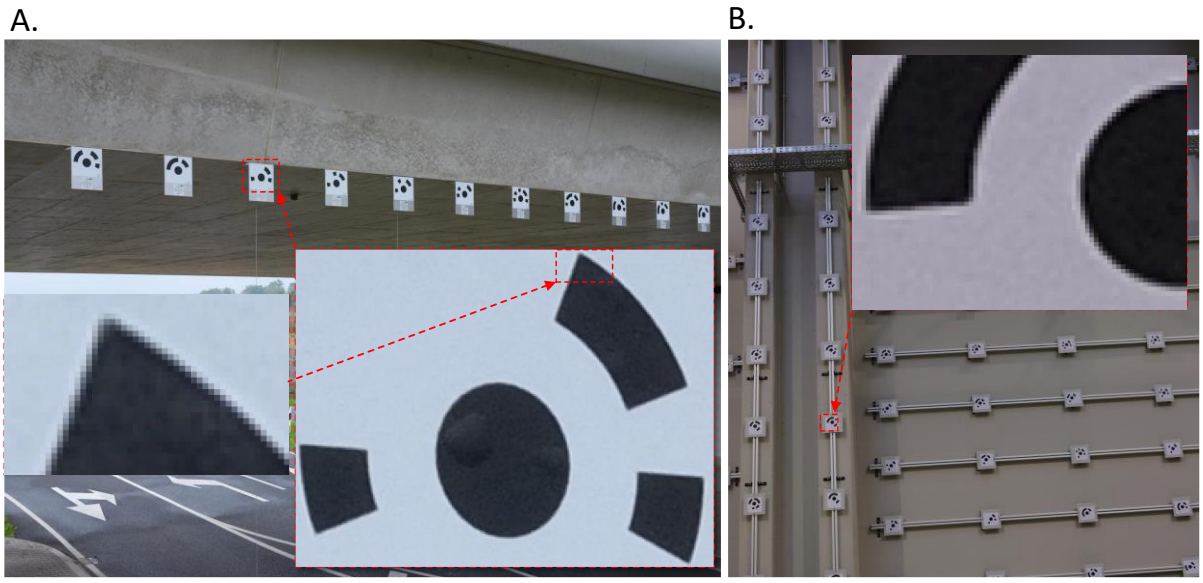

Figure 13.18. A. Capture while flying the drone without any blurring (shake) effect, B. capture done using tripod and remote release while calibration of the camera

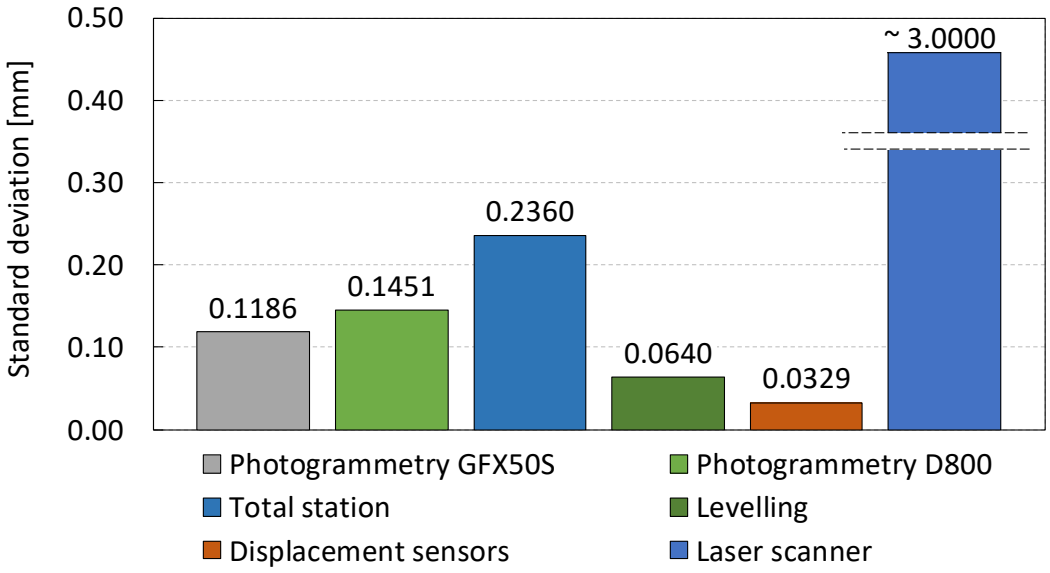

Figure 13.19. Reached accuracies for the applied measurement techniques for deflection measurement

13.4.2 The damage detection and the DAD values

The detection of damage on the investigated bridge using the DAD method is carried out based on deflection measurements performed by photogrammetry and by levelling. The DAD values from photogrammetry is done for two different measuring point distances. The analysis and the background of the horizontal measuring point distance are published in [150]. The horizontal distance between the measuring points has a significant influence on the precision of damage detection. A closer range between the measuring points allows a higher precision on the localisation of the damage. However, the closer the measuring points, the smaller is the inclination angle change resulting from damage. However, the smaller the measurable inclination change, the higher is the required precision of the deflection measurement. Figure 13.20 and Figure 13.21 show the impact of the considered measuring point distance, namely 50 cm respectively 100 cm, on the calculation of DAD values based on photogrammetry.

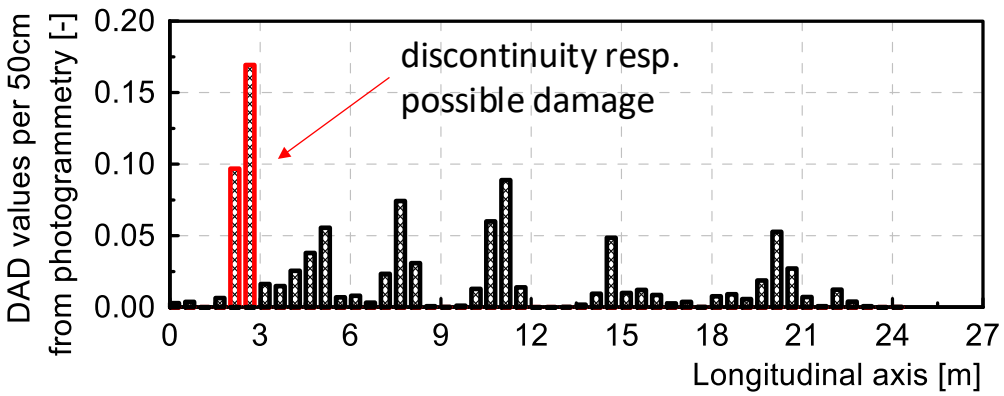

Figure 13.20. DAD values from curvature for measuring point distance of 50 cm and based on photogrammetry; red bars represent the outliers

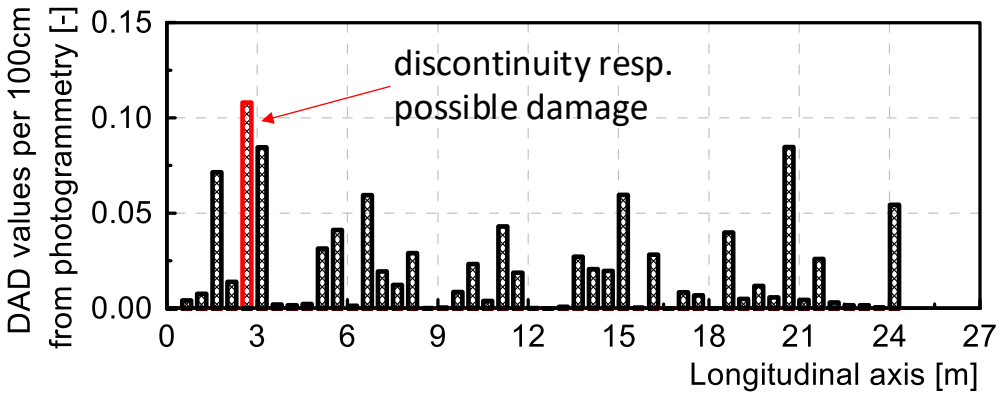

Figure 13.21. DAD values from curvature for measuring point distance of 100 cm and based on photogrammetry; red bars represent the outliers

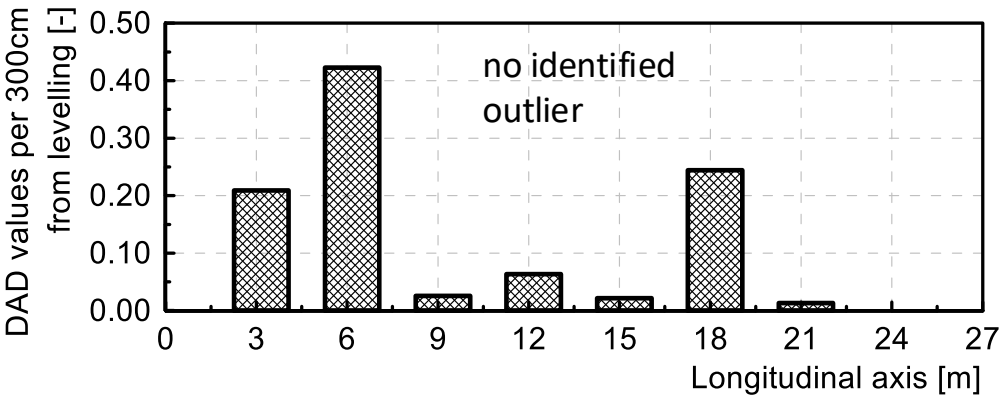

Figure 13.22. DAD values from curvature for measuring point distance of 300 cm and based on levelling

The outlier respectively the discontinuity of the DAD values was determined according to the method described in section 13.2.4. Figure 13.20 indicates some discontinuity at about 2,90 m. However, the discontinuity does not increase with increasing measurement point distance to 100 cm (Figure 13.21). As for smaller measuring point distances (Figure 13.20), the measurement noise has more influence on the DAD values than for bigger measuring point distances, the outlier in Figure 13.20 results from measurement noise and not from any damage. The DAD values for the measuring point distance of 100 cm present already a nearly uniform distribution so that it can be concluded that the structure is still undamaged. The results from

photogrammetry in Figure 13.21 is confirmed by the accurate measurement with levelling, which also does not have any outlier as shown in Figure 13.22.

In summary, no damage was identified using the DAD method in the investigated bridge structure. However, the following questions require further clarification:

- Identifiable damage degree for bridge structures;
- Required precision of the measurement technique for localisation of small damages;
- Influence of damage position;
- Required maximum deflection;
- Number of required measurement repetition.

Therefore, an additional investigation is carried out to answer the questions as mentioned above. These investigations are based on FE calculations using a model with artificial noise effects to get realistic deflection measurement values, whereas the artificial noise introduced into the deflection line of the numerical model corresponds to the noise from the real measurements by photogrammetry for the bridge test.

13.5 Measurement noise and its influence

Theoretical examples showed that the DAD method is able to identify already smallest stiffness variations down to 1 % [180]. However, the detectability of the damage using the DAD method depends on several parameters. The most important factor is the precision of the deflection measurement. The close-range photogrammetry represented promising accuracy and application-oriented handling. Furthermore, the reached accuracy under laboratory condition was between 0.01 and 0.03 mm [201] [99] and for real bridge experiment between 0.10 and 0.14 mm. In the following sections, the influence of the measurement precision, the damage degree, the damage position, the required deflection size and the required number of measurement repetitions are investigated. The investigations are carried out based on a finite element model of the bridge Altrier from the experimental test.

13.5.1 Artificial noise

The calculation results from the finite element method deliver exact mathematical results without any noise effect. However, real measurements are always affected by normal-distributed noise effect. Therefore, realistic test results are generated from the finite element model by incorporating an artificial noise which is produced based on the measured standard deviation range from photogrammetry. The normal distributed pseudo-random number is generated using the function NORM.INV() from Microsoft Excel [202] based on the Wichmann and Hill theory [203]. The NORM.INV() function consists of the variables such as probability, standard deviation and the mean value as arguments. The probability is associated with the standard normal distribution (equation (61)).

$$f(x,\mu,\sigma) = \frac{1}{\sqrt{2\pi\sigma}} e^{-\left(\frac{(x-\mu)^2}{2\sigma^2}\right)} \tag{61}$$

The left diagram of Figure 13.23 shows the normally distributed noise effect for the standard deviation of 0.10 mm and the right diagram of Figure 13.23 illustrates the real measurement noise from photogrammetry. Both are not identical, but they have the same value of standard deviation and are distributed normally.

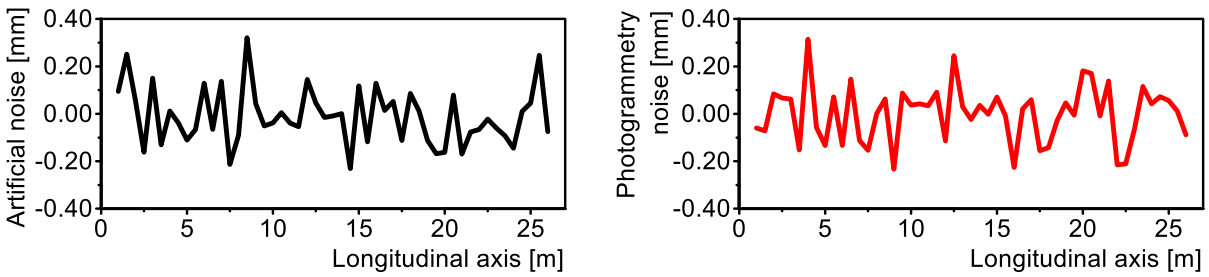

Figure 13.23. Left diagram: artificial noise, right diagram: real noise from photogrammetry measurement

13.5.2 Relation between the detectable degree of damage and the measurement precision for the use of DAD method

The detectable level of damage is investigated based on the measurement precision and the resulting DAD values. The study is done based on the theoretical model same to the static system of the experimental bridge. A local artificial damage is generated with several different levels by reducing the element stiffness. Figure 13.24 presents the DAD values from curvature at the damage position depending on the measurement precision and the damage level. The standard deviation varies from 0.01 mm to 0.10 mm. Each DAD value is determined from the average of 30 different calculations using artificial noise effects. A higher DAD value at a given damage position leads to more reliable damage identification. First, it can be considered that for smaller damage degrees, a higher precision of the deflection measurement is required. Furthermore, the trend lines of the relations between the precision of the measurement and the corresponding damage level follows an exponential curve.

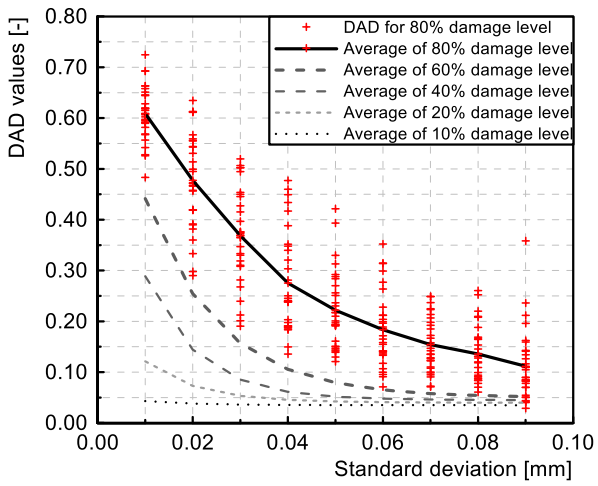

Figure 13.24. Relation between measurement precision and detectable degree of damage

13.5.3 Influence of the deflection size on the detectability of damage

Another significant factor influencing the damage detection using the DAD method is the size of the measured deflection. The maximum deflection of the bridge should not exceed a specific

allowed value of deflection size not to exceed the serviceability limit state and to allow a non-destructive condition assessment. In principle, there is no clear regulation regarding the deflection limitation in bridge design standards. Nonetheless, there are indications for structural deflection limitation depending on the type of construction. The allowed size of deflection varies from L/350 to L/2000 [204] [205]. Figure 13.25 shows the analysis of the range of damage detection using the DAD method. The diagram illustrates nine different curves, which represent the DAD values for different experimental deflection sizes starting from L/600 to L/2500. The horizontal axis of the diagram shows the level of a local stiffness reduction due to damage. The two dashed lines in red and black indicate the detectability of damage in function of the measurement accuracy. The red dashed curve represents the detectability limit for a measurement accuracy of 0,09 mm, which corresponds to the accuracy of the photogrammetry of the real bridge experiment. The black dashed line illustrates the detectability limit corresponding to the accuracy of measurement at laboratory condition of 0,01 mm. All DAD values above the dashed boundary line point out successful identification of damage. For example, based on an experiment with maximal deflection of L/600, the reliable identifiable damage degree starts at 60 % for a measurement accuracy of 0,09 mm. With the measurement accuracy of 0,01 mm, the identification of damages at 30 % would be possible.

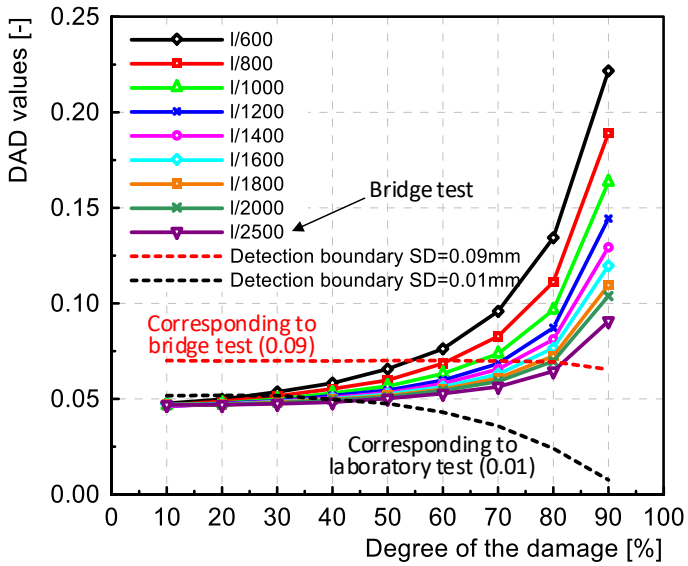

Figure 13.25. Damage identification based on deflection size and measurement precision

13.6 Influence of damage position on detection of damage

The position, at which damage has occurred, plays a role in the detection of damage using the DAD method. Figure 13.26 shows one-half of the studied FE-model. The influence of the damage position is examined on 30 measurements using random noise effects for each investigated position. The resulting DAD values are represented by an average line summarising the 30 measurements with the standard deviation of 0.03 mm indicated by single crosses in Figure 13.26 A. Figure 13.26 B. represents the resulting average trend lines from investigations with different standard deviations of 0,01 mm to 0,09 mm. A higher DAD value at the damage position corresponds to a more accurate damage localisation. The resulting DAD values clearly show that a better damage detection can be achieved closer to the maximum deflection area. In contrast, at a position with hardly any deflection, e.g. at the support structures, almost no damage can be detected.

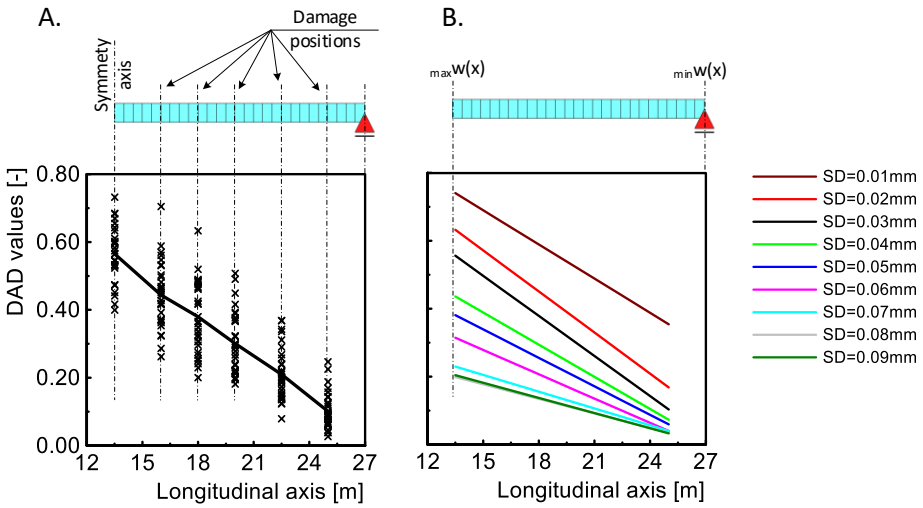

Figure 13.26. Influence of damage position on the detectability of damage

13.7 Influence of the repetition of measurements

The final investigation examines the influence of the repetition of the measurements on the variability of the resulting DAD values. This examination is carried out to understand how many deflection measurements are required to minimise the influence of measurement inaccuracy on the resulting DAD values. The problem is that the effect of normally distributed

measurement noise involves potentially outliers, which could be falsely detected as damage. However, the repetition of the measurement would not have the potential outlier from measurement inaccuracy at the same area again. Only the outlier resulting from the damage would always highlight at the same position. Equation (62) is used to calculate the arithmetic mean values of the DAD values for n measurements. Mostly, the discontinuity resulting from damage effect is highlighted at the position of damage. However, some outliers resulting from the measurement inaccuracy can occur randomly at various locations. The probability that an outlier resulting from noise effect occurs at the same location again is very low. Therefore, the repetition of the measurement helps to eliminate the effect of measurement noise and only to highlight discontinuities at the damage positions.

$$Average\ from\ n\ measurements = \frac{1}{n}\sum_{i=1}^{n} DAD_i(x) \tag{62}$$

Figure 13.27 shows the change of the DAD values at the damage position depending on the number of measurement repetitions. The presented DAD values cover the damage degrees from 10 % to 90 % and each value is based on average on ten artificially generated experimental values. The considered standard deviation amounts to 0,02 mm. The red curve illustrates the overall average from the nine different damage degrees. A stabilisation of the DAD values can be observed starting from the seventh repetition of the deflection measurements. In other words, the influence of the measurement noise effect can be optimally minimized starting from the seventh repetition of the measurements at a precision level of 0,02 mm. However, the number of required measurements varies depending on the measurement precision.

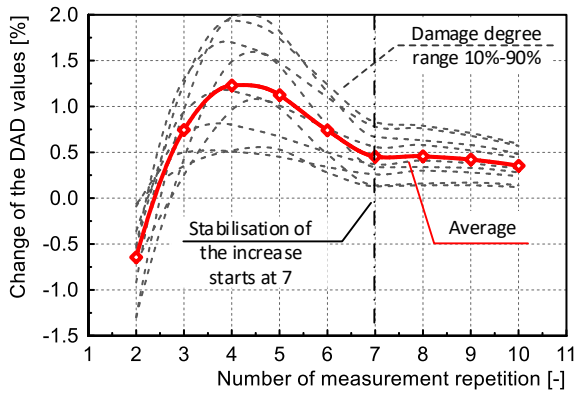

Figure 13.27. Influence of the measurement repetition on the precision of damage identification

13.8 Recommendation for practitioners

In principle, certain recommendations can be made for practitioners of the DAD method. With regard to the requirement for the measuring accuracy, it should be mentioned that the higher the span, the more precision is necessary. For multi-span bridges, it is advisable to position control points on every abutment. If the target can remain permanently on bridges, the exact location of the control points should be measured before each load-deflection experiment. The application of close-range photogrammetry with the help of a drone is highly recommended for larger, higher or even difficult accessible bridges. Nevertheless, displacement sensors or levelling should be used as a control measurement. Concerning the experimental load, it is advisable to approach the serviceability limit state in order to produce a measurable deflection. It is recommended to repeat the measurements for statistical reasons, i.e. more than 7 times.

The used camera should be focused as far as possible on infinity. The shutter speed should be kept as short as possible to avoid blurring effect. The automatic rotation function of the camera and the image stabilizer of the lens must be switched off. Underexposed images are better than overexposed ones.

The measurement of the environment temperature, humidity or thermography is not required. The investigation of the measurement noise is not necessary, but the sensitivity of the DAD method would increase, if the measured deflection line is smoothed within the range of the standard deviation. The density of the target can be chosen comparable to the presented study such as 50 cm, however depending on the length of the structure. The smaller the span the more density of the measuring targets are required.

13.9 Conclusion

The presented work summarises the experiences of the application of the so-called “Deformation Area Difference” (DAD) method on the detection of damage in existing real bridge structures. The applied method is based on the relationship between bending moment and curvature. The essential prerequisites of the method are a high precision measurement of the deflection line from a static load deflection test and a simplified linear finite element model

of the bridge structure. The presented real-scale experiment is carried out on a prestressed concrete bridge structure in Luxembourg with a span of 27 m. The applicability of the DAD method is investigated based on several modern measurement techniques, namely laser scanning, total station, levelling as well as displacement sensors and photogrammetry using two cameras mounted on a tripod and on a drone. The study deals with the precision of the measuring techniques and not with the accuracy. The accuracy gives an absolute value to a reference value, while the precision is a relative measurement value. The DAD method examines the measured deflection line relative to the reference curve. For the application of the DAD method a high precision measurement is sufficient.

From the findings of the different investigations, the following conclusions can be drawn:

- The reached precisions from the deflection measurements on the bridge structure amount to 0.1186 mm for photogrammetry, 0.236 mm for total station, 0.064 mm for levelling and 0.0329 mm for displacement sensors. As expected, no damage was detected on the newly constructed bridge structure using the DAD results from photogrammetry and levelling, which showed uniformly distributed values over the whole structure.
- Realistic experimental deflection measurement data was successfully generated based on theoretical models, which considered the artificial measurement noise effects.
- Theoretical models without measurement noise effect prove that the DAD method is able to detect smallest stiffness changes such as 1 % local damage.
- The influence of measurement precision is investigated based on finite element calculations with artificial measurement noise effect. The results showed that the effect of noise on lower measurement precision has an exponential influence on the damage detection.
- The size of the investigated structural deflection also has an essential impact, namely the higher the deflection, the lower is the damage level which can be detected.
- Damage close to higher deflections can be better localised than damage near to the support structures.

- The number of the measurement repetition is investigated to eliminate the falsely detected outliers resulting from measurement noise. The repetition number of more than seven delivered reliable interpretation about damage detection.

The applicability of the DAD method was already proven based on theoretical examples and laboratory tests [180] [150]. This study confirms the applicability of the DAD method on a real prestressed concrete bridge structure using most modern measurement techniques, especially with photogrammetry using a camera mounted on a big size drone delivered very promising results. Considering the discussed boundary conditions of the DAD method, this method offers a simple and reliable application for damage detection of bridge structures and contributes to the state-of-the-art of methods for condition assessment.

13.10 Acknowledgements

The authors would like to express their gratitude to the "Administration des Ponts et Chaussées" of Luxembourg for providing the opportunity to carry out experiments on a real bridge. Further gratitude is expressed to the team of Prof. Holger Voos of the University of Luxembourg for enabling the autonomous flight with the drone. Finally, special acknowledgements are expressed to the technical support team of the University of Luxembourg for their expertise and helpful contributions to the realisation of the large scale experiment.

14 Conclusion and outlook

14.1 Conclusion

The presented cumulative dissertation mainly consists of four papers in the field of engineering science. The further six conference papers have been introduced and referenced in the introduction. The focus of the work lies on the development of a method for localisation of damages in existing bridge structures. The successful application of the so-called “Deformation area Difference (DAD)” method was proven and presented using several theoretical examples, laboratory experiments as well as an in-situ experiment on a bridge structure.

The proposed DAD method bases on static-load deflection experiments and requires a high-precision deflection measurement along the longitudinal axis of the bridge structure. As a reference system, a simplified model of the bridge structure is used, which has a continuous course of deflection behaviour without any effect of possible damages. The comparison between the reference system and the measured values is carried out relatively. Therefore, the reference system does not require any model update, which makes the method more practical. The theoretical examples based on finite element calculations showed that the DAD method is able to detect the smallest local stiffness changes. However, every physical measurement has its limitation regarding the precision and the measured values are affected by normally distributed noise effect with corresponding standard deviation. Therefore, the localisation of damages based on the DAD method highly depends on the measurement precision, which has been extensively investigated within the study. The application of the DAD method for localisation of stiffness reducing damages is easy to use and requires no complex technical equipment and exceptional expertise.

The procedure of the DAD method is principally as follows:

- Creation of a theoretical reference system
- Definition of the experimental load within the serviceability limit state
- Implementation of the static load-deflection experiment (if applicable, repetition of the measurements)
- Definition of the required measurement precision based on the expected structural deflection and the requirement of the damage detection sensitivity
- High-precision measurement of the structural deflection along the bridge
- Smoothing of the measured deflection curve within the standard deviation
- Determination of the DAD values with evaluation of the data for different measurement point distances
- Identification of the outlier of the DAD values
- In case of measurement repetitions, comparison of the outliers

The very high demands on the measurement techniques led to the investigation of most modern measurement techniques such as levelling Leica DNA03, total station Leica TS30, laser scanner Leica P20, displacement sensors HBM and close-range photogrammetry using the software Elcovision 10. Depending on the bridge dimensions, environmental conditions and the requirement for the precision, the measurement techniques can be used individually. The findings from the laboratory experiments showed promising results of the close-range photogrammetry. Therefore, the close-range photogrammetry has been examined very closely, particularly with regard to the influence of camera and calibration quality. Within the first laboratory experiments, the close-range photogrammetry was applied using the camera Nikon D800 with 36.8 MP, which was calibrated using 40 targets on a wall with a dimension of 7.0x3.0 m. The improvement of the technical equipment was the camera Fujifilm GFX50S with 51.4 MP and the calibration wall with the dimension of 14.0x6.0 m and with 163 targets. The investigation was carried out based on several calibration series, deflection measurement with and without calibration using both cameras. The main outcomes are:

- The applied consumer cameras had very high quality concerning the lens and camera body. The position of the principal point hardly changed even after refocussing and remounting the lens.

- The greatest influence for the precision of deflection measurement is coming from the camera calibration. Namely, the calibration of the camera increases the measurement precision by 40.2 % in average.
- The experienced improvement of the camera, respectively the increase of the sensor format from 7360x4912 to 8256x6192 has an influence of about 34.0 %.
- A small increase of precision can be achieved by improving the calibration. The precision difference amounts to 3.0 % between the wall with 40 targets and 163 targets. However, the factor is important when very high precision is required.

Furthermore, the applicability of the close-range photogrammetry using a drone is investigated within the study. The load-bearing capacity of the applied drone DJI Matrice 600 amounts up to 6.0 kg and is able to carry the medium format camera GFX50S including the gimbal Ronin-MX. The duration of the flight is between 20-40 min depending on the equipment weight. Within the deflection measurement for the bridge test, the autonomous flight took place within less than 10 minutes. The study on the in-situ bridge test showed, that the camera GFX50S can capture very sharp images without any blurring effect. This was possible, because on the one hand the gimbal is able to compensate the flight vibration and on the other hand the high-quality camera and lens could make captures within the shutter speed of 1/500 sec.

The detection of damages was investigated based on three reinforced concrete beams and one steel beam. The reinforced concrete beams have been gradually loaded and had different stiffness reducing scenarios such as cracking, yielding of tensile reinforcement and failure of the concrete in the compression zone. The steel beam was loaded so that the maximum deflection does not exceed the serviceability limit state, namely l/250. The cross-section of the steel beam has been damaged due to slitting the bottom flange in several steps. The DAD method was able to detect damages as follows:

- The area with the reduced stiffness due to cracking of the concrete in the tensile zone. The reduction of the stiffness due to cracking amounts to about 60 % for the experimental beams.
- The yielding the reinforcement and failure of the concrete in the compression zone led to a stiffness reduction of about 80 %.

- The reached measurement precision amounted to 0.08 mm for the laboratory experiment with the steel beam. The local damages could be detected using the DAD method starting from 23.8 % of stiffness reduction. However, the reliable detection of the damage was possible for the degree of 49 % of stiffness reduction or more.

The study on the close-range photogrammetry and the optimisation of the laboratory tests could increase the achievable precision of the deflection measurement. However, the challenge was to achieve these accuracies and precision under real conditions. Therefore, the first in-situ bridge experiment has been planned and carried out in Altrier, Luxembourg. The non-destructive load-deflection experiment on the bridge made it possible to define the achievable measurement precision for real conditions. The precision for the close-range photogrammetry amounts 0.1186 mm, for total station 0.2360 mm, for levelling 0.0640 mm and for displacement sensors 0.0329 mm. The results of the DAD values applied on the bridge test were evenly distributed and could not identify any local damage. However, the question is what degree of damage can be detected using the DAD method if the measurement precision corresponds to the laboratory or real conditions. This investigation was carried out using the theoretical model of the bridge test and the artificial noise effect, which corresponds to the real measurement noise from photogrammetry. The creation of realistic experimental values and statistical analysis was possible based on the artificial noise effect and the finite element model of the bridge. The artificial noise effect delivers normal distributed random numbers and can vary for given standard deviations. Within this study, the following impacts of the DAD method could be identified:

- The influence of measurement precision is exponential in relation to the detectable degree of damage.
- The closer the damage is to the location of maximum deflection and the higher the amount of deflection size, the easier it can be detected.
- In order to improve the reliability of the damage detection, the measurement of the deflection should be repeated more than seven times.
- The detectable degree of damage amounts to 60 %-80 % depending on the amount of the experimental deflection with the reached precision of 0.09 mm. With the achieved precision value of 0.01 mm for laboratory condition, the damages with the degree of 30 % can be localised using the DAD method.

The presented DAD method is developed with the aim of damage detection in bridge structures. The application of DAD method would enable to detect damages, which influences the load-bearing capacity of the bridge structures. However, the method highly depends on the precision of the applied measurement techniques. The successful application of the DAD method contributes to the state-of-the-art for condition assessment of bridge structures. Thus, the stiffness reducing damages could be early detected, which could not be detected by visual inspections.

14.2 Outlook

Within the study, the damage detection DAD method is carefully investigated. The requirement, achievable technical recourses, the influencing factors of the method have been examined and presented. However, further investigations can still be carried out in order to open new possibilities, to develop the method ready for practice or to use alternative measurement techniques. The inspection of bridges takes periodically place according to the national standards. In case of the application of DAD method, the installation of the measuring targets on bridge structures should be optimised. Either measuring targets have to be resistant to UV-light, water etc. or they should be easily demountable. The investigation of the laser scanner has not been carried out in detail. The further investigation on it could open new advantages in view of three-dimensional deflection measurement and high-dense measuring points.

Within the study, the most precise measuring technique was the displacement sensor. However, the application of the displacement sensors for the measurement of structural deflection along the whole bridge structure requires disproportional effort. Therefore, the possibility to use the displacement sensor could be by measuring the structural deflection at single points and apply a moving load along the bridge structure. Figure 14.1 illustrates the static system, the damage position and the measurement of the deflection at a single point for the theoretical study. On the single span beam, a load is moved from the left side to the right side, which generates a structural deflection within the serviceability limit state. The structural deflection is measured at the position of the maximal deflection respectively at the mid of the span. A damage is generated due to the reduction of the bending stiffness at 4.00 m.

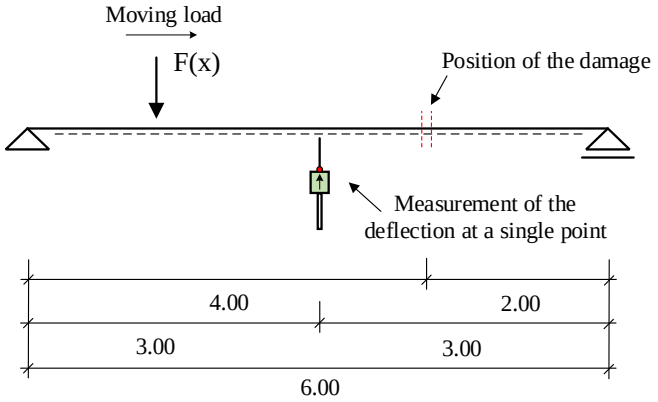

Figure 14.1. Principal illustration of the static system, damage position and deflection measurement for the damage detection method using a moving load

The measured deflection at a single point from the moving load includes the information about the position of damage. First, the position of the damage is not visible in the deflection curve. However, in case of a double derivation of the deflection curve, the position of damage is highlighted. The derivation of the deflection curve is carried out from each load position to the next load position. Figure 14.2 shows the double derivation of the deflection values for a moving load, which highlights at the position of the damage. However, in the future the measurement precision and the amount of the load required for such application of the DAD method will have to be analysed.

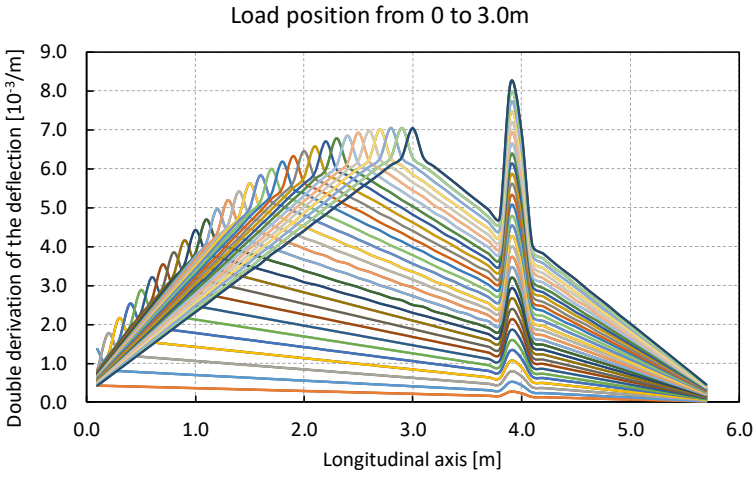

Figure 14.2. Detection of damage for deflection measurement at a single point and a moving load

First of all, a laboratory experiment with a moving load and deflection measurement at few points are recommended. The measurement of the deflection should take place at the position of the maximum deflection. In general, shorter displacement sensors are more precise than longer ones. However, the higher deflection which is created by a moving load, the clearer is the detection of damage. In the next step, a laboratory experiment with variable cross-section or a multi-span beam could be used.

Regarding the close-range photogrammetry, there is the possibility to improve the camera quality by either using a 100 MP camera or a metric camera. There is still some room for increasing the measurement precision of the close-range photogrammetry. Therefore, the application of the DAD method shows high potential to be used for localization of damages as standard application for the inspection of bridges.

15 List of figures

16 List of tables

A. Appendix

A.1 Reinforced concrete beams

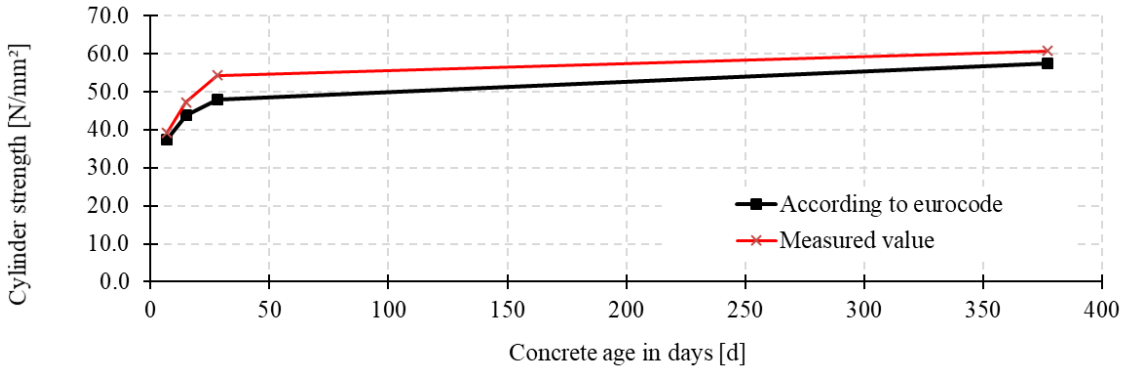

Figure A.1. Cylinder strength of the used concrete C40/50 for the experimental beams

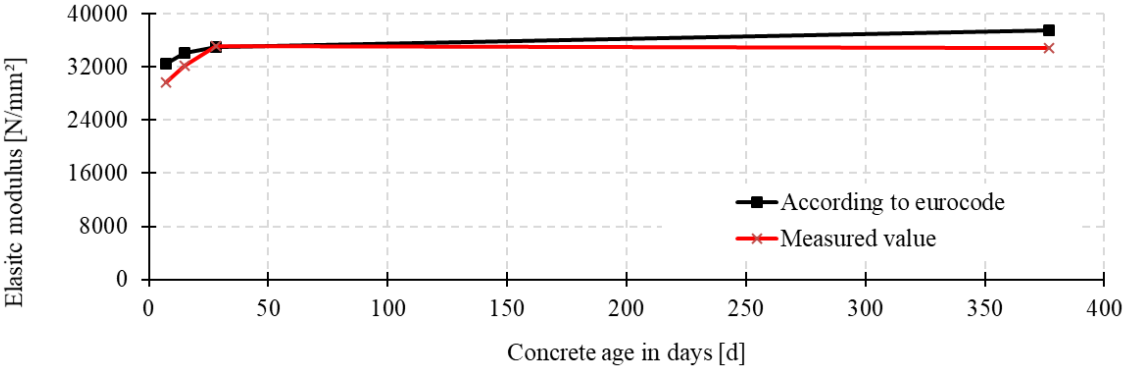

Figure A.2. Elastic modulus of the used concrete C40/50 for the experimental beams

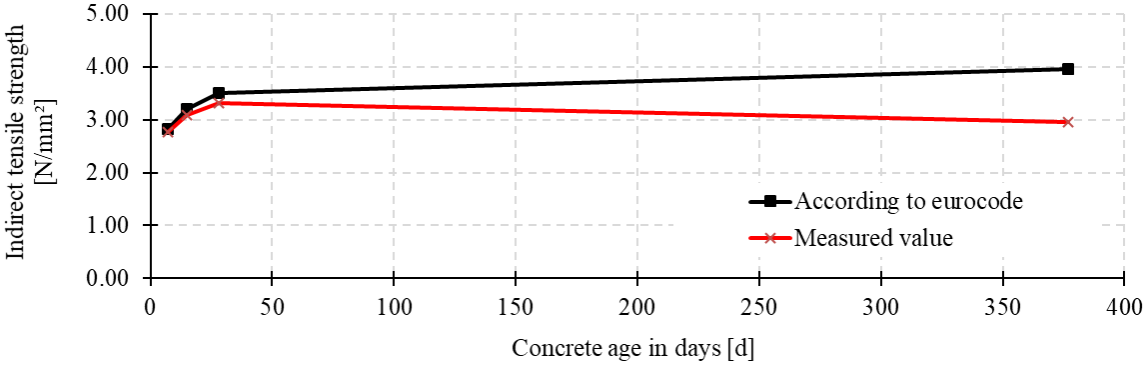

Figure A.3. Indirect tensile strength of the used concrete C40/50 for the experimental beams

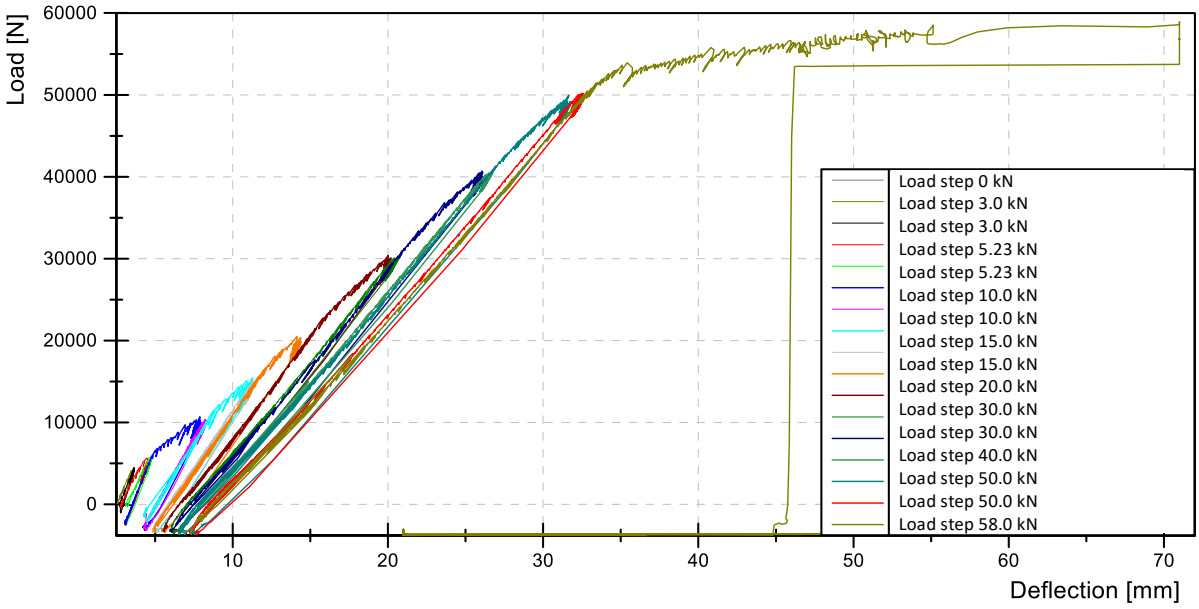

Figure A.4. Measured deflection by displacement sensor for the reinforced concrete beam (see section 7.3)

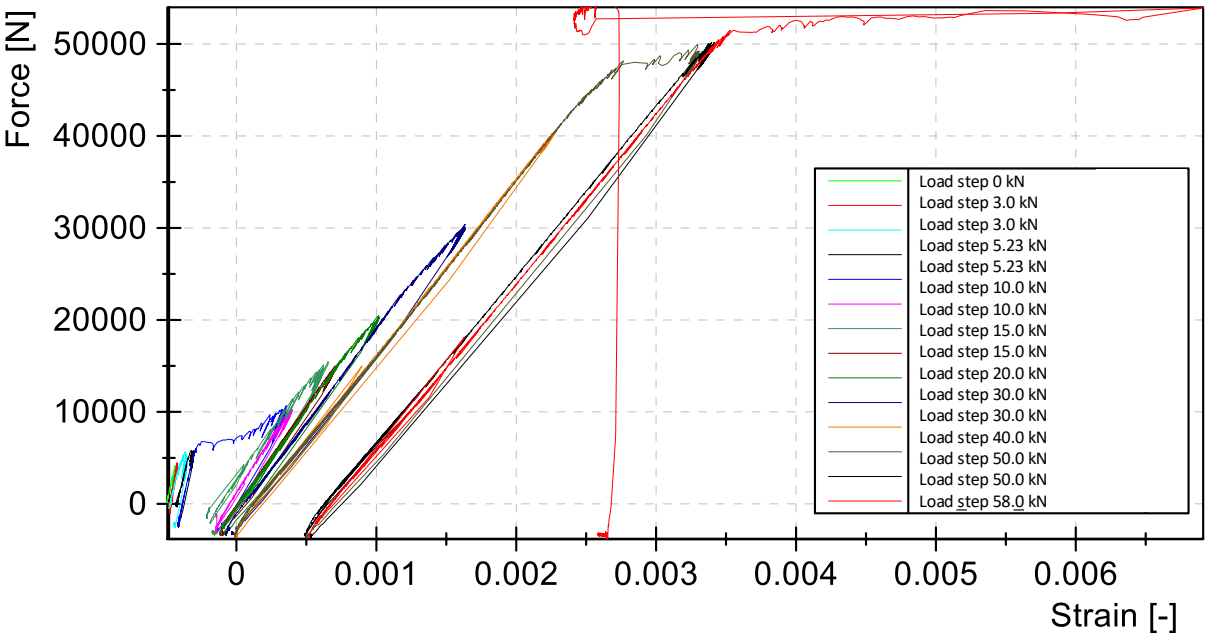

Figure A.5. Measured strain by strain gauges (see section 7.3)

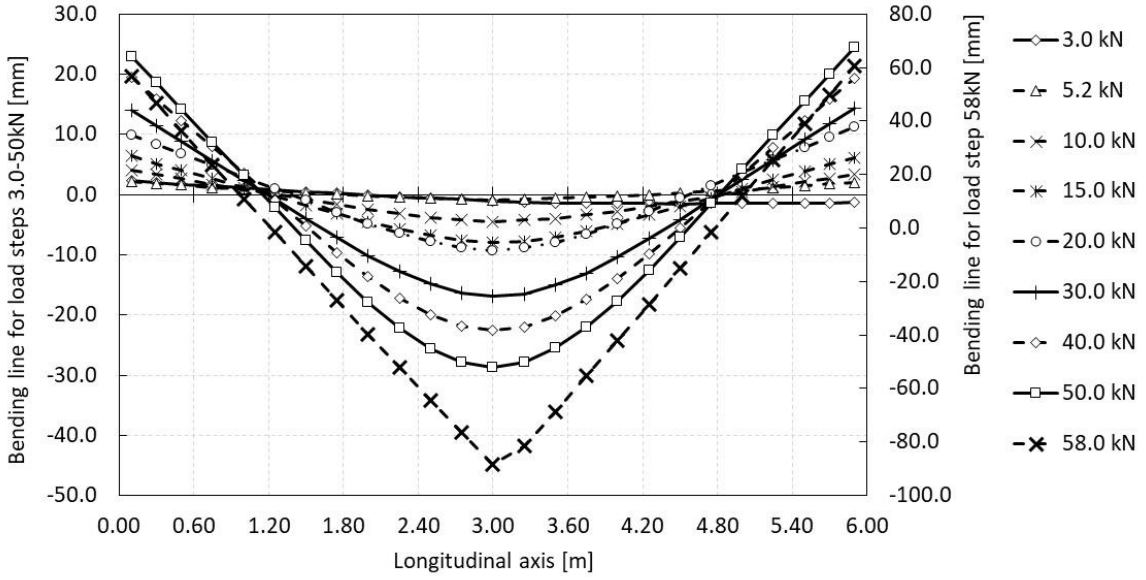

Figure A.6. Measured deflection of the reinforced concrete beam (see section 7.3)

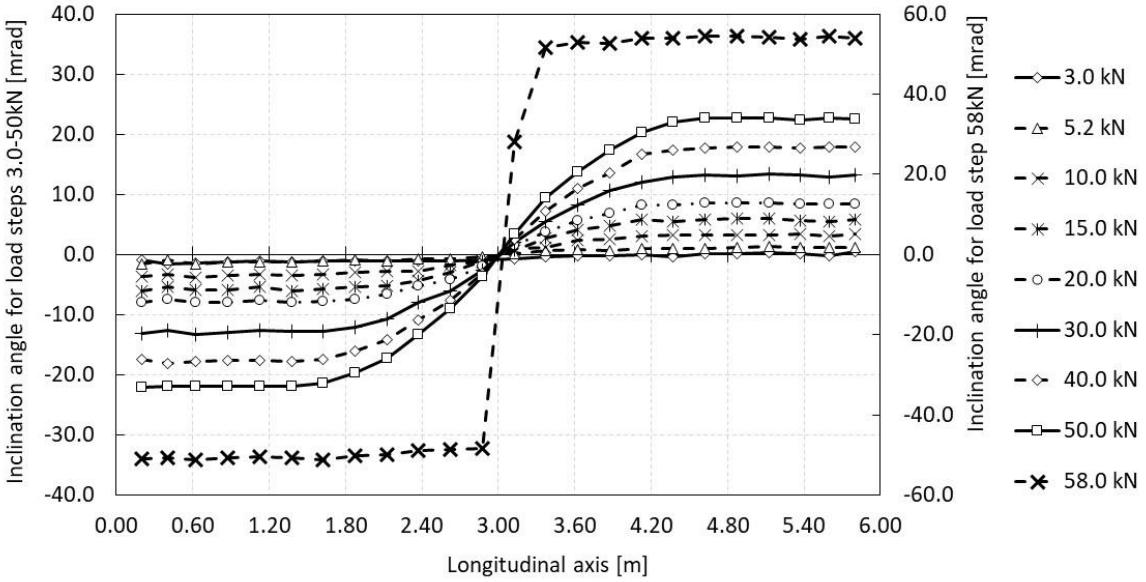

Figure A.7. Inclination angle of the reinforced concrete beam (see section 7.3)

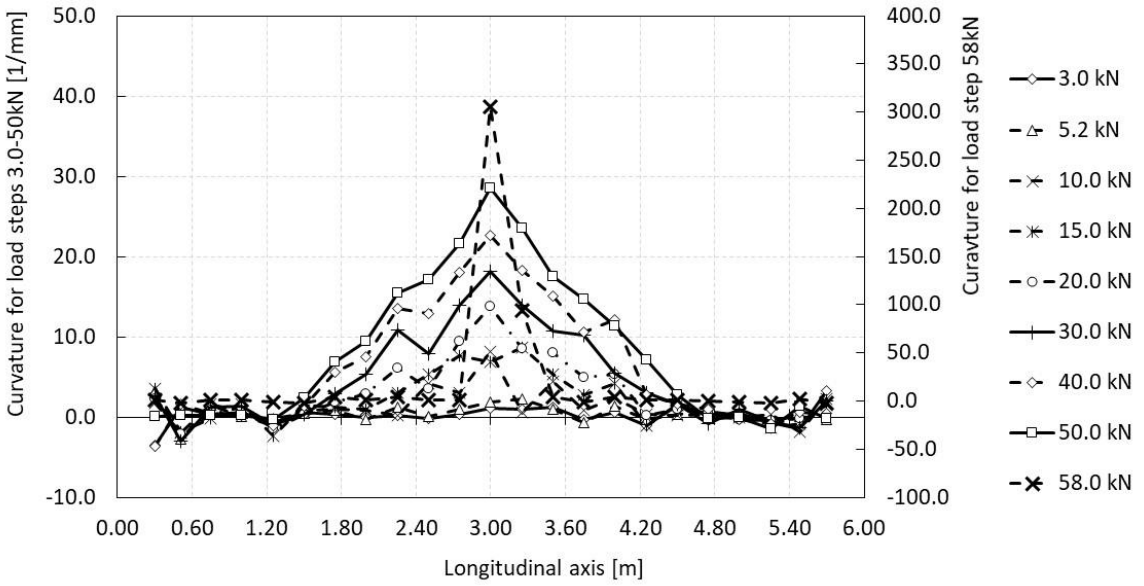

Figure A.8. Curvature of the reinforced concrete beam (see section 7.3)

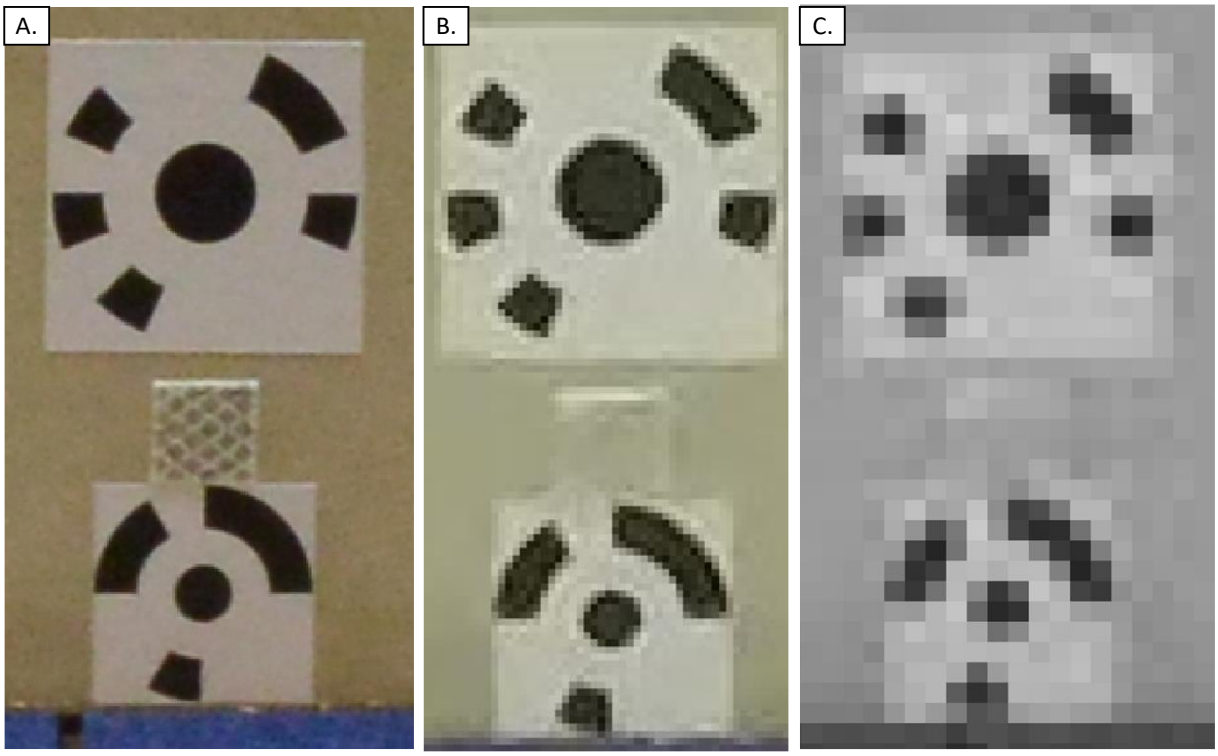

Figure A.9. Comparison of the target captures with different cameras within the laboratory experiments A. Nikon D800 with 7360x4912 pixels; B. DJI Zenmuse X3 4k camera with 3840x2160 pixels; C. DJI Zenmuse X3 1k camera 1280x720 pixels

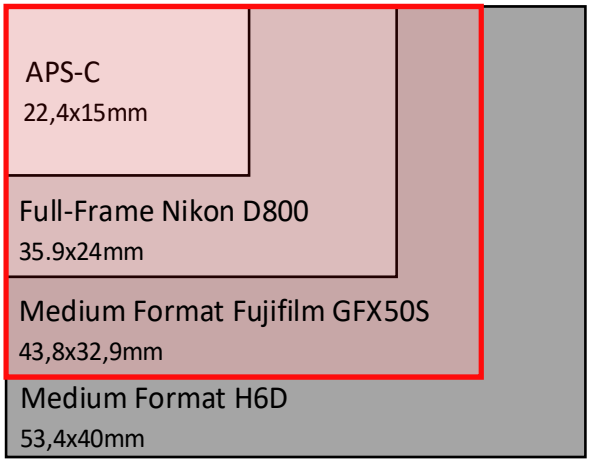

Figure A.10. Comparison of different sensor sizes of cameras

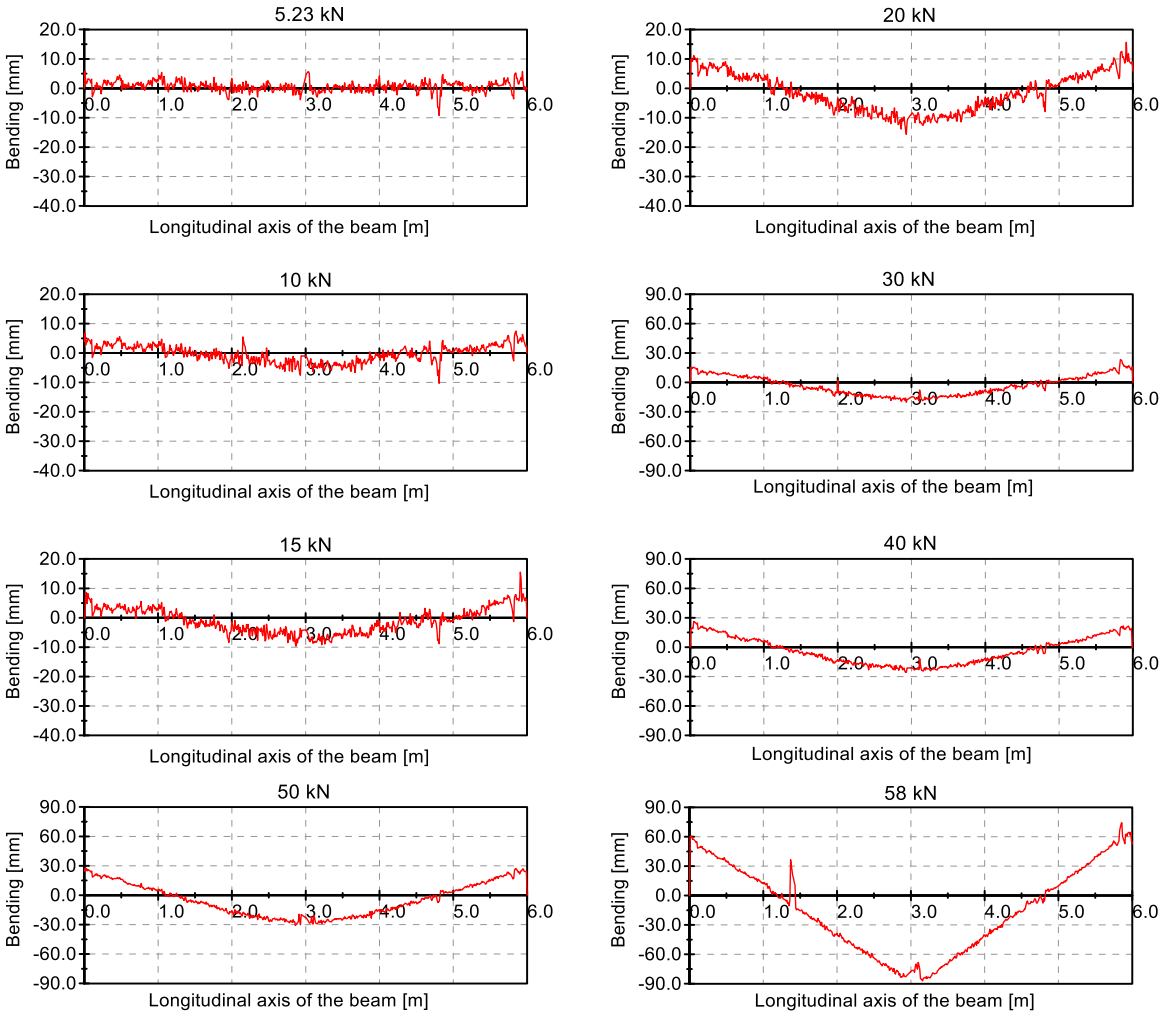

Figure A.11. Measured deflection with laser scanner P20 Leica (see section 7.3)

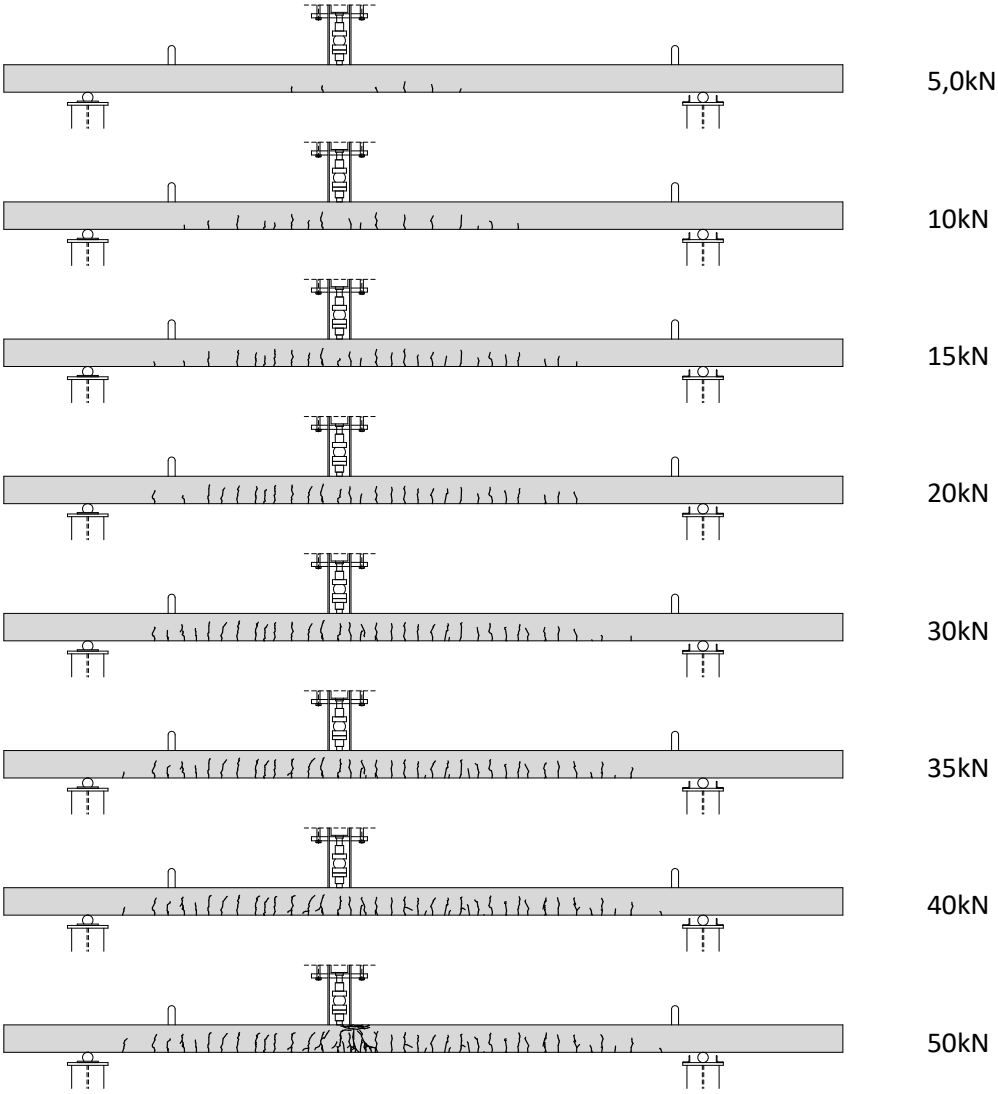

Figure A.12. Crack pattern of the experimental beam (see section 11.6)

A.2 Bridge experiment

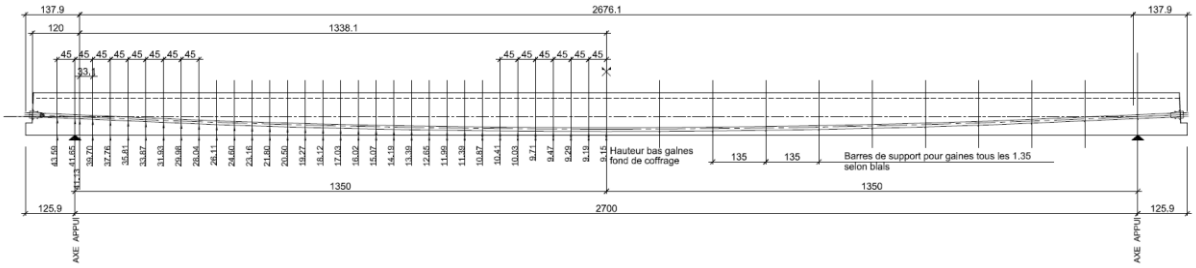

Figure A.13. Course of the prestressing cables (see section 13.3)

Properties of the materials and dimension of the experimental bridge in Altrier

- Concrete — C45/55
- E-modulus — 36000 N/mm²
- Tendon type — 17 T 15s TBR
  Steel Class: 1860 N/mm²
  Maximum tension: 0,80x1860=1488 N/mm²
  Steel section: 19x150=2850 mm²
  E-modulus: 190.000 N/mm²
- Dead load of the used materials — Asphalt: g_{rev}=2,20 kN/m²
  Sidewalk: g_{trd}=4,80 kN/m²
  Fixed guard: n_{br}=1,85 kN/m²
  Guardrail and metallic cornice n_{bord}=1,80 kN/m²
  Waterproofing protection membrane g_{et}=0,72 kN/m²

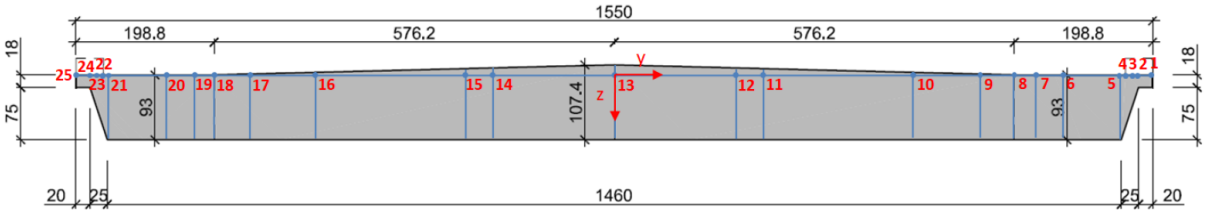

Figure A.14. Description of the nodes in Sofistik (see section 13.3.3) [157]

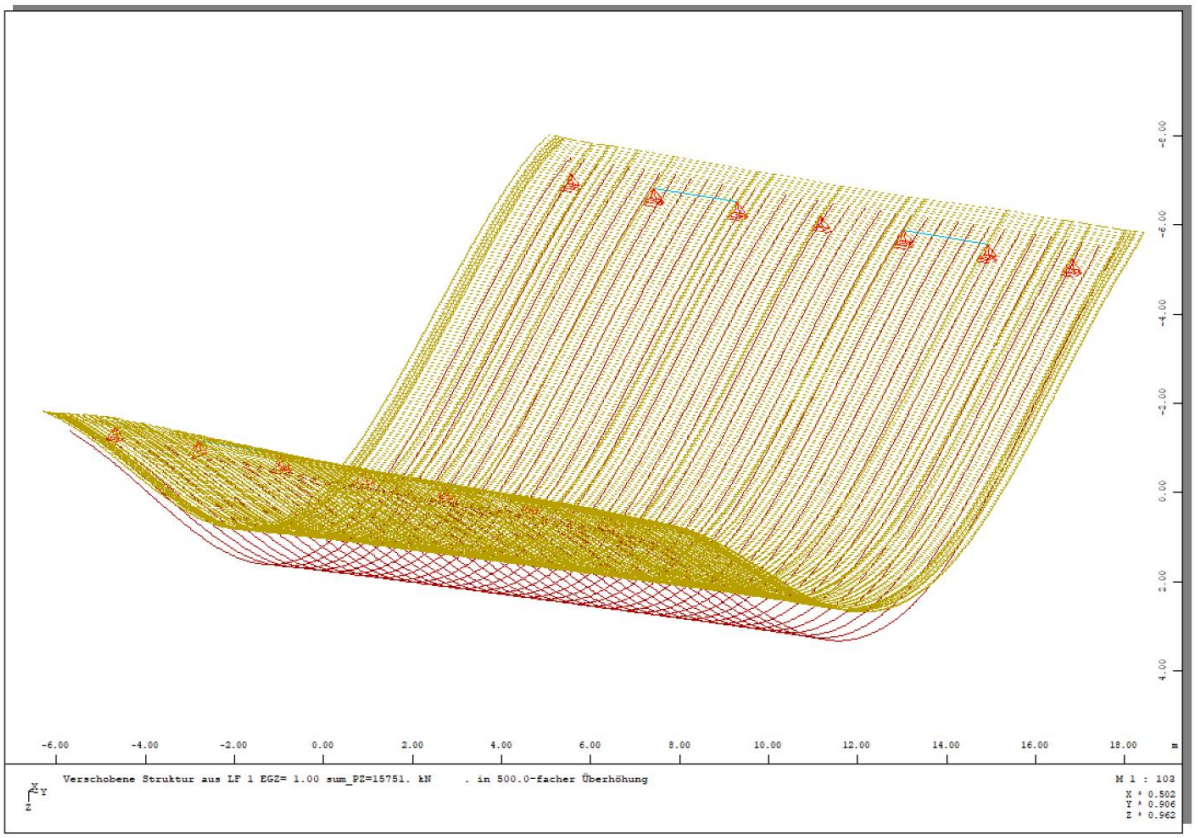

Figure A.15. Illustration of the deformation by 6 SLW60 (see section 13.3.3) [157]

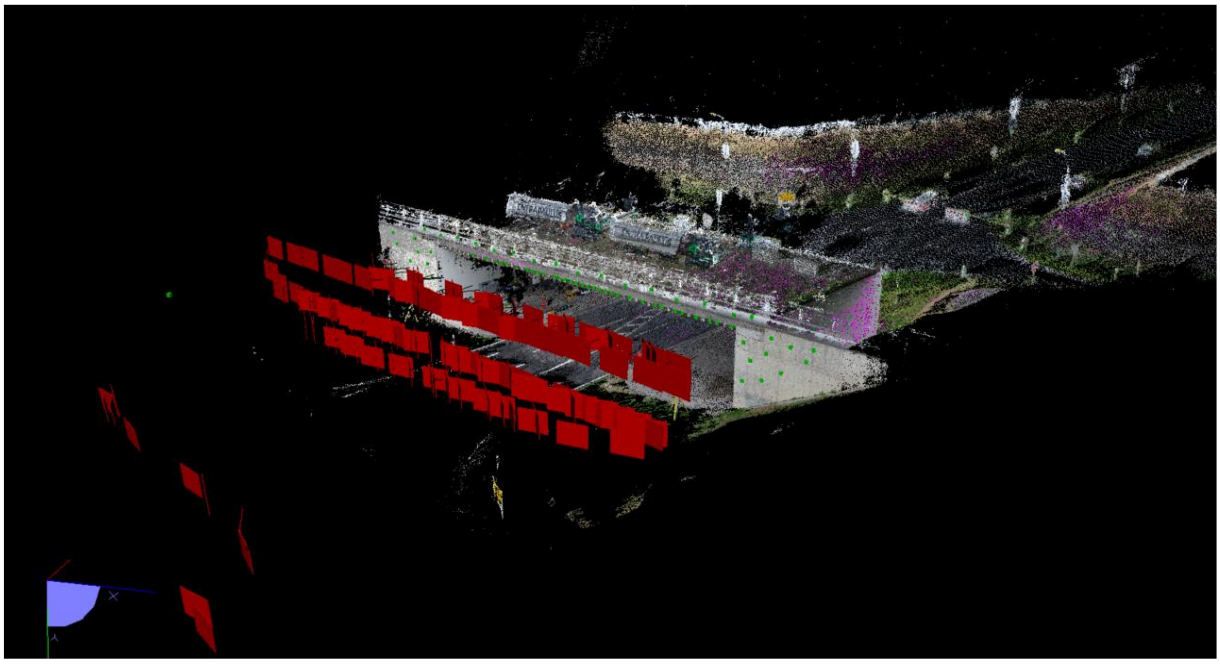

Figure A.16. Point cloud and capturing positions from close-range photogrammetry applying on the drone

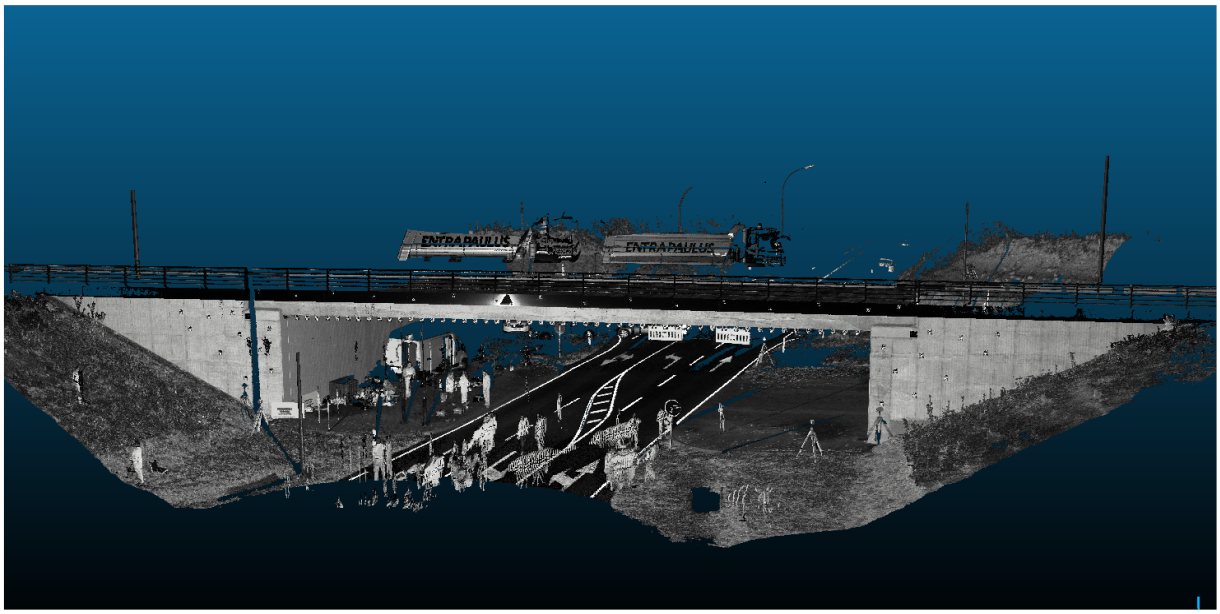

Figure A.17. Point cloud from the measurement by laser scanner

17 References

[1] M. o. T. o. China, "Number of bridges in China from 2010 to 2018," 23 September 2019. [Online]. Available: https://www-statista-com.proxy.bnl.lu/statistics/258358/number-of-road-bridges-in-china/.

[2] M. Shirato and T. Tamakoshi, "Bridge inspection standards in Japan and US," in *29th US-Japan Bridge Engineering Workshop*, Tsukuba Japan, 2013.

[3] U. D. o. Transportation, "Statista," [Online]. Available: https://www-statista-com.proxy.bnl.lu/statistics/190386/number-of-road-bridges-in-the-united-states/. [Accessed 23 September 2019].

[4] B. f. Straßenwesen, "www.bast.de," [Online]. Available: https://www.bast.de/BASt_2017/DE/Statistik/statistik-node.html. [Accessed 23 September 2019].

[5] L. Hsien-Ke, M. Jallow, Y. Nie-Jia, J. Ming-Yi, H. Jyun-Hao, S. Cheng-Wei and C. Po-Yuan, "Comparison of Bridge Inspection Methodologies and Evaluation Criteria in Taiwan and Foreign Practices," in *ISARC*, Taipei, 2017.

[6] "SJR, Scimago Journal & Country Rank," Scimago Lab, [Online]. Available: www.scimagojr.com. [Accessed 24 09 2019].

[7] G. König, R. Maurer and T. Zichner, Spannbeton: Bewährung im Brückenbau, Berlin: Springer-Verlag, 1986.

[8] J. Scheer, Failed Bridges: Case Studies, Causes and Consequences, Hannover: Wilhelm Ernst & Sohn, 2010.

[9] M. Niggemann, Angewandter Straßenbau, Hameln: Springer Vieweg, 2012.

[10] F. Federal Highway Administration, "National Bridge Inspection Standards," AASHTO The American Association of State Highway and Transportation, 2009.

[11] DIN 1076, *Deutsches Institut für Normung: Ingenieurbauwerke im Zuge von Straßen und Wegen - Überwachung und Prüfung*, Berlin: Beuth Verlag GmbH, 1999.

[12] K. Bergmeister, F. Fingerloos and J.-D. Wörner, Beton Kalender, Berlin: Ernst&Sohn, 2013.

[13] AASHTO, "AASHTO Bridge Element Inspection Guide Manual," American Association of State Highway and Transportation Officials, USA, 2010.

[14] M. Waltering, "Damage assessment of civil engineering structures and bridges using non-linear dynamic characteristics," University of Luxembourg, 2009.

[15] V. Bungard, "Condition assessment of concrete structures and bridges using vibration monitoring in comparison to changes in their static properties," Shaker Verlag, Aachen, 2010.

[16] J. Mahowald, "Evaluation of dynamic damage indicators on real-life civil engineering structures: Measurement uncertainty and environmental influences considered," Shaker Verlag, Aachen, 2014.

[17] F. Scherbaum, "Zustandsbewertung von Brücken unter Berücksichtigung der temperaturabhängigen Steifigkeit des Fahrbahnbelages," Shaker Verlag, Aachen, 2018.

[18] K. Zilch and G. Zehetmaier, Bemessung im konstruktiven Betonbau, Berlin: Springer, 2010.

[19] E. Tennstedt, Beitrag zur rechnerischen Ermittlung von Zwangsschnittgrößen unter Berücksichtigung des wirklichen Verformungsverhalten des Stahlbetons, Braunschweig: Heft 26, 1974.

[20] "DIN EN 13670: Ausführung von Tragwerken aus Beton DIN 1045-3: Überwachen von Beton auf Baustellen," Beuth, 2011.

[21] T. Luhmann, S. Robson, S. Kyle and I. Harley, Close Range Photogrammetry, Dunbeath: Whittles Publishing, 2011.

[22] K. Kraus, Photogrammetry, Fundamentals and Standard Processes, Köln: Verlag H. Stam GmbH, 2000.

[23] Goris and Schmitz, Bemessungstafeln nach Eurocode 2, Köln: Bundesanzeiger, 2014.

[24] A. Rytter, “Vibration Based Inspection of Civil Engineering Structures,” Dept. of Building Technology and Structural Engineering, Aalborg, 1993.

[25] Q. Yang, J. Liu, B. Sun and C. Lang, “Damage localization for beam structure by moving load,” *Advances in Mechanical Engineering,* vol. 9, no. 3, 2017.

[26] S. Jang, S. Sim and B. Spencer, “Structural damage detection using static strain data,” in *Proceedings of the World Forum on Smart Materials and Smart Structures Technology*, China, 2007.

[27] E.-T. Lee and H.-C. Eun, “Disassembling-Based Structural Damage Detection Using Static Measurement Data,” *Shok and Vibration,* no. Hindawi, 2019.

[28] F. Huseynov, C. Kim, E. Obrien, J. Brownjohn, D. Hester and K. Chang, “Bridge damage detection using rotation measurements - Experimental validation,” *Mechanical Systems and Signal Processing,* vol. 135, 2020.

[29] W.T. Yeung and J.W. Smith, “Damage detection in bridges using neural networks for pattern recognition of vibration signatures,” *Engineering Structures,* pp. 685-698, 2005.

[30] D. Erdenebat, D. Waldmann and F. N. Teferle, “Numerical investigation of bridges with the aim of condition assessment in applying the Deformation Area Difference method (DAD-method) and selecting appropriate measurement techniques,” in *IALCCE2016,* Delft, 2016.

[31] Srinivasan, Murthy, Wiggenhauser, Nagesh R Iyer and Ravisankar, “Identification of Reinforcements in Reinforced Concrete Structures using Ground Penetrating Radar,” December 2009.

[32] P. Cotic, D. Kolaric, V. B. Bosiljkov, V. Bosiljkov and Z. Jaglicic, “Determination of the applicability and limits of void and delamination detection in concrete structures using infrared thermography,” *NDT&E International,* vol. 74, pp. 87-93, 2015.

[33] H. Azari, S. Nazarian and D. Yuan, “Assessing sensivity of impact echo and ultrasonic surface waves methods for nondestructive evaluation of concrete structures,” *Construction and Building Materials,* pp. 384-391, September 2014.

[34] Y. Y. Kim, J. M. Kim, J.-W. Bang and S.-J. Kwon, “Effect of cover depth, w/c ratio, and crack width on half cell potential in cracked concrete exposed to salt sprayed condition,” *Construction and Building Materials,* vol. 54, pp. 636-645, 2014.

[35] S. K. U. Rehman, Z. Ibrahim, S. A. Memon and M. Jameel, “Nondestrictive test methods for concrete bridges: A review,” *Construction and Building Materials,* pp. 58-86, 06 01 2016.

[36] Strategic Highway Research Program SHRP 2, "Nondestructive Testing to Identify Concrete Bridge Deck Deterioration," Washington, D.C., 2013.

[37] N. Gucunski, A. Imani, F. Romero, S. Nazarian, D. Yuan, H. Wiggenhauser, P. Shokouhi, A. Taffe and D. Kutrubes, "Nonndestructive Testing to Identify Concrete Bridge Deck Deterioration," Strategic highway research program, Washington, 2013.

[38] H.-G. Knieß, *Verfahren zur Untesuchung von Spanngliedern - Methods to investigate prestressing reinforcement,* 1986.

[39] A. Brencich, G. Cassini, D. Pera and G. Riotto, "Calibration and Reliability of the Rebound (Schmidt) Hammer Test," *Civil Engineering and Architecture,* pp. 66-78, 2013.

[40] M. P. Limongelli, D. Siegert, É. Merliot, J. Waeytens, F. Bourquin, R. Vidal, L. V. Corvec, I. Gueguen and L. M. Cottineau, "Damage detection in a post tensioned concrete beam – Experimental investigation," *Engineering Structures,* pp. 15-25, 01 12 2016.

[41] W. Zhang and L. M. Sun, "Damage identification through finite element model updating using wavelet damage function," in *IALCCE,* Delft, 2016.

[42] K. Helmi, T. Taylor, A. Zarafshan and F. Ansari, "Reference free method for real time monitoring of bridge deflections," *Engineering Structures,* pp. 116-124, 2015.

[43] W. Zhang, C. Cai and F. Pan, "Nonlinear fatigue damage assessment of existing bridges considering progressively deteriorated road conditions," *Engineering Structures,* pp. 1922-1932, 14 09 2013.

[44] N. Boumechra, "Damage detection on bridge structures based on static deflection measurements of a single point," *Civil and Environmental Research,* 2013.

[45] S. Stöhr, M. Link, R. Rohrmann and W. Rücker, "Damage detection based on static measurements on bridge structures," in *IMAC-XXIV,* USA, 2006.

[46] L. Li, "Damage and material identification using inverse analysis," Electronic Theses and Dissertations, 2012.

[47] Z. Sheena, A. Zalmanovitch and A. Unger, "Theoretical stiffness matrix correction by static test results," in *24th Israel Annual Conference of Aviation and Astronautics,* 1982.

[48] J.-H. Chou and J. Ghaboussi, "Genetic algorithm in structural damage detection," *Computers & Structures,* vol. 79, pp. 1335-1353, 2001.

[49] W.-Y. He, W.-X. Ren and S. Zhu, "Damage detection of beam structures using quasi-static moving load induced displacement responce," *Engineering Structures,* vol. 145, pp. 70-82, May 2017.

[50] W.-Y. He, "Baseline-free damage localization method for statically determinate beam structures using dual-type response induced by quasi-static moving load," *Journal of Sound and Vibration,* vol. 400, pp. 58-70, April 2017.

[51] W. Zhang, J. Li, H. Hao and H. Ma, "Damage detection in bridge structures under moving loads with phase trajectory change of multi-type vibration measurements," vol. 87, pp. 410-425, 15 March 2017.

[52] F. Cavadas, I. F. Smith and J. Figueiras, "Damage detection using data-driven methods applied to moving-load responses," *Mechanical Systems and Signal Processing,* vol. 39, no. 1-2, pp. 409-425, September 2013.

[53] K. V. Nguyen, "Comparison studies of open and breathing crack detections of a beam-like bridge subjected to a moving vehicle," *Engineering Structures,* vol. 51, pp. 306-314, March 2013.

[54] Z. Sun, T. Nagayama and Y. Fujino, "Minimizing noise effect in curvature-based damage detection," *Journal of Civil Structural Health Monitoring,* vol. 6, pp. 255-264, April 2016.

[55] H. C. Gomez, P. J. Fanning, M. Q. Feng and S. Lee, "Testing and long-term monitoring of a curved concrete box girder bridge," *Engineering Structures,* pp. 2861-2869, 07 07 2011.

[56] D. Waldmann, D. Erdenebat, F. Scherbaum and S. Maas, "Investigation of temperature-dependent stiffness variation of a layer of asphalt and their possible effect on the deformation behaviour of concrete structures," in *EVACES*, Dübendorf, 2015.

[57] A. J. Reiff, M. Sanayei and R. M. Vogel, "Statistical bridge damage detection using girder distibution factors," *Engineering Structures,* pp. 139-151, 18 12 2015.

[58] Y.-C. Sung, T.-K. Lin, Y.-T. Chiu, K.-C. Chang and K.-L. Chen, "A bridge safety monitoring system for prestressed composite box-girder bridges with corrugated steel webs based on in-situ loading experiments and a long-term monitoring database," *Engineering Structures,* vol. 126, pp. 571-585, 2016.

[59] J. J. Lee and C. B. Yun, "Damage diagnosis of steel girder bridges using ambient vibration data," *Engineering Structures,* pp. 912-925, 20 12 2005.

[60] D. Erdenebat and D. Waldmann, "Condition assessment and damage loaclisation for bridges by use of the Deformation Area Difference Method (DAD-Method)," in *fib Symposium*, Cape Town, 2016.

[61] M. Fastabend, “Zur ingenieurmäßigen Bestimmung des Steifigkeitsabfalls von Stahlbeton im Zustand II,” Ernst & Sohn, Berlin, 2002.

[62] G. König and N. Viet Tue, Grundlagen des Stahlbetonbaus, Einführung in die Bemessung nach DIN 1045-1, vol. 2. Auflage, Wiesbaden: Teubner, 2003.

[63] J. Valença, E. Júlio and H. Araújo, “Application of Photogrammetry to Bridge Monitoring,” in *Structural Faults & Repair, 12th International Conference*, 2008.

[64] H.-G. Maas and U. Hampel, “Photogrammetric Techniques in Civil Engineering Material Testing and Structure Monitoring,” in *American Society for Photogrammetry and Remote Sensing*, 2006.

[65] J. Albert, H.-G. Maas, A. Schade and W. Schwarz, “Pilot studies on photogrammetric bridge deformation,” in *2nd International Symposium on Geodesy for Geotechnical and Structural Engineering*, Berlin, 2002.

[66] M. Fuchs, “Beschränkung der Durchbiegung von Straßenbrücken im Grenzzustand der Gebrauchstauglichkeit unter besonderer Berücksichtigung der Biegeschlankheti von Stahlbetonbrücken aus Normalbeton,” in *Massivbau in ganzer Breite*, Berlin, Springer, 2005, pp. 95-100.

[67] M. Barker, J. Staebler and K. Barth, “Serviceability limits and economical steel bridge design,” Federal Highway Administration, Washington, 2011.

[68] P. Ferrari, “The effect of the competition between cars and trucks on the evolution of the motorway transport system,” *Transportation Research Part C,* vol. 17, pp. 558-570, May 2009.

[69] E. Commission, “The EU explained: Transport,” Publications Office of the European Union, Luxembourg, 2014.

[70] P. Croney and D. Croney, The Design and Performance of Road Pavements, 1994.

[71] B. f. S. (bast), “http://www.bast.de,” [Online]. Available: http://www.bast.de/DE/Statistik/statistik-node.html. [Accessed 11 10 2017].

[72] S. L. Davis and D. Goldberg, “The Fix We're In For: The State of Our Nation's Bridges 2013,” Transportation for America, 2013.

[73] G. Brunell and Y. J. Kim, “Effect of local damage on the bevavior of a laboratory-scale stees truss bridge,” *Engineering Structures,* vol. 48, pp. 281-291, 2013.

[74] M. Döhler, F. Hille, L. Mevel and W. Rücker, "Structural health monitoring with statical methods during progressive damage test of S101 bridge," *Engineering Structures,* vol. 69, pp. 183-193, 2014.

[75] G. Bolle, G. Schacht and S. Marx, "Loading tests of existing concrete structures - historical development and present practise," in *fib Symposium PRAGUE,* Czech Republic, 2011.

[76] C.-C. Comisu, N. Taranu, G. Boaca and M.-C. Scutaru, "Structural health monitoring system of bridges," *Procedia Engineering,* vol. 199, pp. 2054-2059, 2017.

[77] V. Kaplan and P. Dvorak, "Reflection on the Possibilities for Monitoring the Aging Bridge Structures," *Procedia Engineering,* vol. 187, pp. 649-655, 2017.

[78] P. Kotes, M. Brodnan, M. Ivaskova and K. Dubala, "Influence of reinforcement corrosion on shear resistance of RC bridge girder subjected to shear," *Procedia Engineering,* vol. 111, pp. 444-449, 2015.

[79] E. O. Lantsoght, C. v. d. Veen, A. d. Boer and D. A. Hordijk, "State-of-the-art on load testing of concrete bridges," *Engineering Structures,* vol. 150, pp. 231-241, 2017.

[80] S. Stöhr, M. Link, R. Rohrmann and W. Rücker, "Damage detection based on static measurements on bridge structures," in *IMAC-XXIV,* USA, 2006.

[81] W. Zhang, L. M. Sun and S. W. Sun, "Bridge-Deflection Estimation through Inclinometer Data Considering Structural Damages," *Journal of Bridge Engineering,* vol. 22, no. 2, February 2017.

[82] Y. Koleková, M. Kovác and I. Baláz, "Influence Lines of bridges with Box-Girder Cross-Section under Torsion and Distorsion," *Procedia Engineering,* vol. 190, pp. 603-610, 2017.

[83] W.-Y. He, W.-X. Ren and S. Zhu, "Baseline-free damage localization method for statically determinate beam structures using dual-type response induced by quasi-static moving load," *Journal of Sound and Vibration,* vol. 400, pp. 58-70, April 2017.

[84] W. Zhang, J. Li, H. Hao and H. Ma, "Damage detection in bridge structures under moving loads with phase trajectory change of multi-type vibration measurements," *Mechanical Systems and Signal Processing,* vol. 87, pp. 410-425, 2017.

[85] J. Li and H. Hao, "Damage detection of shear connectors under moving loads with relative displacement measurements," *Mechanical Systems and Signal Processing,* Vols. 60-61, pp. 124-150, August 2015.

[86] A. J. Carr, D. V. Jáuregui, B. Reveiro, P. Arias and J. Armesto, "Structural evaluation of historic masonry arch bridges based on first hinge formation," *Cunstruction and Building Materials,* vol. 47, pp. 569-578, 2013.

[87] J. Baqersad, P. Poozesh, C. Niezrecki and P. Avitabile, "Photogrammetry and optical methods in structural dynamics - A review," *Mechanical Systems and Signal Processing,* vol. 86, pp. 17-34, February 2017.

[88] H. Lee and H. Rhee, "3-D measurement of structural vibration using digital close-range photogrammetry," *Sensors and Actuators A: Physical,* vol. 196, pp. 63-69, March 2013.

[89] P. Arias, J. Armesto, D. Di-Capua, R. González-Drigo, H. Lorenzo and V. Pérez-Gracia, "Digital photogrammetry, GPR and computational analysis of structural damages in a mediaeval bridge," *Engineering Failure Analysis,* vol. 14, pp. 1444-1457, 2007.

[90] R. Jiang, D. V. Jáuregui and K. R. White, "Close-range photogrammetry applications in bridge measurement: Literature review," *Measurement,* vol. 41, pp. 823-834, 2008.

[91] R. Jiang and D. V. Jauregui, "Development of a digital close-range photogrammetric bridge deflection measurement system," *Measurement,* vol. 43, pp. 1431-1438, 2010.

[92] S. Nishiyama, N. Minakata, T. Kikuchi and T. Yano, "Improved digital photogrammetry technique for crack monitoring," *Advanced Engineering Informatics,* vol. 29, pp. 851-858, 2015.

[93] B. Riveiro, H. González-Jorge, M. Varela and D. V. Jáuregui, "Validation of terrestrial laser scanning and photogrammetry techniques for the measurement of vertical underclearance and beam geometry in structural inspection of bridges," *Measurement,* vol. 46, no. 1, pp. 784-794, 2013.

[94] P. Capéran, M. Poljansek, E. Gutiérrez, S. Primi and C. Paulotto, "Optical 3-dimensional measurements on a FRP beam tested at serviceability limit," *Composite Structures,* vol. 94, pp. 3465-3477, 2012.

[95] D. Erdenebat, D. Wadmann, F. Scherbaum and F. N. Teferle, "The Deformation Area Difference (DAD) method for condition assessment of reinforced structures," *Engineering Structures,* vol. 155, pp. 315-329, 2018.

[96] D. Erdenebat and D. Waldmann, "Condition assessment and damage localisation for bridges by use of the Deformation Area Difference Method (DAD-Method)," in *fib Symposium*, Cape Town, 2016.

[97] D. Erdenebat, D. Waldmann and F. N. Teferle, "Laboratory experiment for damage assessment using the DAD-method," in *Fourth Conference on Smart Monitoring, Assessment and Rehabilitation of Civil Structures*, Zürich, 2017.

[98] B. N. Patel, D. P. Sivakumar and M. Srinivasan, “A simplified moment-curvature based approach for large deflection analysis of micro-beams using the consistent couple stress theory,” *European Journal of Mechanics A/Solids,* vol. 66, pp. 45-54, 2017.

[99] D. Erdenebat, D. Waldmann and F. N. Teferle, “Static load deflection experiment on a beam for damage detection using the Deformation Area Difference Method,” in *IALCCE2018*, Ghent, 2018.

[100] H. Hanan, D. Suwardhi, T. Nurhasanah and E. S. Bukit, “Batak Toba Cultural Heritage and Close-range Photogrammetry,” *Procedia - Social and Behavioral Sciences,* vol. 184, pp. 187-195, 2015.

[101] J. Balsa-Barreiro and D. Fritsch, “Generation of visually aesthetic and detailed 3D models of historical cities by using laser scanning and digital photogrammetry,” *Digital Applications in Archaeology and Cultural Heritage,* vol. 8, pp. 57-64, 2018.

[102] T. Luhmann, “Close range photogrammetry for industrial applications,” *ISPRS Journal of Photogrammetry and Romete Sensing,* vol. 65, pp. 558-569, 2010.

[103] Z. Ding-bang, Z. Yi, C. Tao, M. Yuan, F. Kun, G. Ankit and G. Akhil, “Measurement of displacement for open pit to underground mining transition using digital photogrammetry,” *Measurement,* vol. 109, pp. 187-199, 2017.

[104] A. Stumpf, J. P. Malet, P. Allemand, M. Pierrot-Deseilligny and S. Grzegorz, “Ground-based multi-view photogrammetry for the monitoring of landslide deformation and erosion,” *Geomorphology,* vol. 231, pp. 130-145, 2015.

[105] F. Esmaeili, M. Varshosaz and M. Saadatheresht, “Displacement Measurement of Soil Nail Walls using Close Range Photogrammetry,” *Procedia Engineering,* vol. 54, pp. 516-524, 2013.

[106] K. G. Nikolakopoulos, K. Soura, I. Koukouvelas and N. G. Argyropoulos, “UAV vs classical aerial photogrammetry for archaeological studies,” *Journal of Archaeological Science,* vol. 14, pp. 758-773, 2017.

[107] B. Ruzgiene, T. Berteska, S. Gecyte, E. Jakubauskiene and V. C. Aksamitauskas, “The surface modelling based on UAV Photogrammetry and qualitative estimation,” *Measurement,* vol. 73, pp. 619-627, 2015.

[108] J. O'Driscol, “Landscape applications of photogrammetry using unmanned aerial vehicles,” *Journal of Archaeological Science: Reports,* vol. 22, pp. 32-44, 2018.

[109] R. Michienzi, S. Meier, L. C. Ebert, R. M. Martinez and T. Siebrth, “Comparison of forensic photo-documentation to a photogrammetric solution using the multi-camera system "Botscan",” *Forensic Science International,* vol. 288, pp. 46-52, 2018.

[110] K. Sheppard, J. Cassella and S. Fieldhouse, “A comparative study of photogrammetric methods using panoramic photgraphy in a forensic context,” *Forensic Science International,* vol. 273, pp. 29-38, 2017.

[111] C. Villa, M. J. Flies and C. Jacobsen, “Forensic 3D documentation of bodies: Simple and fast procedure for combining CT scanning with external photogrammetry data,” *Journal of Forensic Radiology and Imaging,* vol. 12, pp. e2-e7, 2018.

[112] E. Verolme and A. Mieremet, “Application of forensic image analysis in accident investigations,” *Forensic Science International,* vol. 278, pp. 137-147, 2017.

[113] J. S. Leal, R. M. C. Aroeira, V. Gressler, M. Greco, A. E. Pertence and J. A. Lamounier, “Accuracy of photogrammetry for detecting adolescent idiopathic scoliosis progression,” *The spine journal,* pp. 1-9, 2018.

[114] D. T. Connor, P. G. Martin, N. T. Smith, L. Payne, C. Hutton, O. D. Payton, Y. A. Yamashiki and T. B. Scott, “Application of airborne photogrammetry for the visualisation and assessment of contamination migration arising from a Fukushima waste storage facility,” *Environmental Pollution,* vol. 234, pp. 610-619, 2018.

[115] Y. Shigeta, R. Hirabayashi, T. Ikawa, T. Kihara, E. Ando, S. Hirai, S. Fukushima and T. Ogawa, “Application of photogrammetry for analysis of occlusal contacts,” *Journal Prosthodontic Research,* vol. 57, no. 2, pp. 122-128, 2013.

[116] S. I. Granshaw, “Photogrammetric terminology: Third Edition,” *The Photogrammetric Record,* vol. 154, no. 31, pp. 210-251, 2016.

[117] P. Kohut, K. Holak, T. Uhl, L. Ortyl, T. Owerko, P. Kuras and R. Kocierz, “Monitoring of a civil structure's state based on noncontact measurements,” *Streuctural Health Monitoring,* pp. 411-429, 2013.

[118] T. Luhmann, C. Fraser and H.-G. Maas, “Sensor modelling and camera calibration for close-range photogrammetry,” *ISPRS Journal of Photogrammetry and Remote Sensing,* vol. 115, pp. 37-46, 2016.

[119] U. Ethrog, “Goniometer-like laboratory method for determining a digital camera's interior orientation, as well as relative orientation in multiple-lens systems,” in *ISPRS,* 2008.

[120] E. Rosten and R. Loveland, “Camera distortion self-calibration using the plumb-line constraint andminimal Hough entropy,” *Machine Vision and Applications,* vol. 22, no. 1, pp. 77-85, 2009.

[121] M. Mohan, S. Ramulu and S. Solanki, “On-the-job Calibration of a Digital Camera for Industrial Photogrammetry,” 2002.

[122] R. I. Hartley, “Self-calibration from multiple views with rotating camera,” in *European Conference on Computer Vision ECCV'94*, 2005.

[123] T. Luhmann, S. Robson, S. Kyle and J. Boehm, Close-Range Photogrammetry and 3D Imaging, 2nd edition ed., Göttingen: Hubert & Co. GmbH, 2014.

[124] T. Luhmann, “Erweiterte Verfahren zur geometrischen Kamerakalibrierung in der Nahbereichsphotogrammetrie,” C.H. Beck, München, 2010.

[125] H. Bingwei, W. Gongjian, Z. Xing and L. Deren, “Accurate geometric camera calibration technique using multi-views of a non-metric planar grid,” *Optics and Lasers in Engineering,* vol. 51, pp. 432-439, 2013.

[126] D. C. Brown, “Close-Range Camera Calibration,” *Photogramm Eng,* vol. 37, pp. 855-866, 2002.

[127] J. Peipe and W. Tecklenburg, “Photogrammetric camera calibration software - comparison,” in *ISPRS Commission V Symposium "image Engineering and Vision Metrology,* 2006.

[128] C. S. Fraser, “Digital camera self-calibration,” *Photogrammetry & Remote Sensing,* vol. 52, pp. 149-159, 1997.

[129] H. Babapour, M. Mokhtarzade and M. J. Valadan Zoej, “Self-calibration of digital aerial camera using combined orthogonal models,” *ISPRS Journal of Photogrammetry and Remote Sensing,* vol. 117, pp. 29-39, 2016.

[130] O. D. Faugeras, Q. T. Luong and S. J. Maybank, “Camera self-calibration: Theory and experiments,” in *ECCV European Conference on Computer Vision*, 1992.

[131] J. F. Kenefick, M. S. Gyer and B. F. Harp, “Analytical Self-Calibration,” *Photogrammetric Engineering,* vol. 38, pp. 1117-26, 1972.

[132] X. Chen and Y. Zhao, “The projected circle centres and polar line for camera self-calibration,” *Optik,* vol. 126, pp. 2565-2570, 2015.

[133] D. Liu, X. Liu and M. Wang, “Camera Self-Calibration with Lens Distortion from a Single Image,” *Photogrammetric Engineering & Remote Sensing,* vol. 82, pp. 325-334, 2016.

[134] J. Liu, T. Wark, R. Lakemond and S. Sridharan, “Self-calibration of wireless cameras with restricted degrees of freedom,” *Computer Vision and Image Understanding,* vol. 116, no. 10, pp. 1033-1046, 2012.

[135] K. Kraus, Photogrammetrie; Band 2, Bonn: Ferd. Dümmlers Verlag, 1996, p. 467.

[136] Q. Sun, X. Wang, J. Xu, L. Wang, H. Zhang, J. Yu, T. Su and X. Zhang, "Camera self-calibration with lens distortion," *Optik,* vol. 127, pp. 4506-4513, 2016.

[137] D. Moe, A. Sampath, J. Chrisopherson and M. Benson, "Self calibration of small and medium format digital cameras," in *ISPRS TC VII Symposium,* Vienna, 2010.

[138] "http://www.accurexmeasure.com," Aicon DPA Pro, [Online]. Available: http://www.accurexmeasure.com/dpa-pro.htm. [Accessed 17 04 2019].

[139] "http://www.k2-photogrammetry.de/," K² Photogrammetry. [Online]. [Accessed 17 04 2017].

[140] "www.photometrix.com," Photometrix, [Online]. Available: https://www.photometrix.com.au/australis/. [Accessed 17 04 2019].

[141] E. Honkavaara, E. Ahokas, J. Hyyppä, J. Jaakkola, H. Kaartinen, R. Kuittinen, L. Markelin and K. Nurminen, "Geometric test field calibration of digital photogrammetric sensors," *ISPRS Photogrammetry and Remote Sensing,* vol. 60, pp. 387-399, 2006.

[142] R. K. Napolitano and B. Glisic, "Minimizing the adverse effects of bias and low repeatability precision in photogrammetry software through statical analysis," *Jounral of Cultural Heritage,* vol. 31, pp. 46-52, 2018.

[143] Agisoft, "https://www.agisoft.com/," 01 03 2019. [Online]. Available: https://www.agisoft.com/.

[144] M. Smith and E. Cope, "The effects of temperature variation on single-lens-reflex digital camera calibration parameters," in *ISPRS,* Newcastle upon Tyne, 2010.

[145] A. Pullivelli, "Low-Cost Digital Cameras: Calibration, Stability Analysis, and Applications," University of Calgary, Calgary, 2005.

[146] A. F. Habib, M. Morgan and Y.-R. Lee, "Bundle Adjustment with Self-Calibration using Straight Lines," *Photogrammetric Record,* vol. 17, pp. 635-650, 2002.

[147] A. Habib and M. Morgan, "Stability Analysis and Geometric Calibration of Off-the-Shelf Digital Cameras," *Photogrammetric Engineering & Remote Sensing,* vol. 71, pp. 733-741, 2005.

[148] "www.elcovision.com," PMS Photo Mess Systeme AG, [Online]. Available: https://www.elcovision.com/index.html. [Accessed 17 04 2019].

[149] K. B. Atkinson, Close range photogrammetry and machine vision, Whittles, 1996.

[150] D. Erdenebat, D. Waldmann and N. Teferle, “Curvature based DAD-method for damage localisation under consideration of measurement noise minimisation,” *Engineering Structures,* vol. 181, pp. 293-309, 2019.

[151] J. Albert, H.-G. Maas, A. Schade and W. Schwarz, “Pilot studies on photogrammetric bridge deformation measurement,” in *IV Symposium on Geodesy for Geotechnical and Structural Engineering*, 2002.

[152] M. E. Stravroulaki, B. Riveiro, G. Drosopoulos, M. Solla, P. Koutsiantis and G. . Stravroulakis, “Modelling and strength evaluation of masonry bridges using terrestrial photogrammetry and finite elements,” *Advances in Engineering Software,* vol. 101, pp. 136-148, 2016.

[153] D. C. Merchant, Analytical Photogrammetry: Theory and Practice, Ohio: The Ohio State University, 1980.

[154] A. E. Kenarsari, S. J. Vitton and J. E. Beard, “Creating 3D models of tractor tire footprints using close-range digital photogrammetry,” *Journal of Terramechanics,* vol. 74, pp. 1-11, 2017.

[155] Y. Piao, M. Zhang, X. Wang and P. Li, “Extended depth of field intergral imaging using multi-focus fusion,” *Optics communications,* vol. 411, pp. 8-14, 2018.

[156] A. Douglas and P. E. Kerr, “Depth of Field in Film and Digital Cameras,” *70th birthday series,* no. 10, 2006.

[157] M. Kajevic, “Application of the DAD-method on a laboratory experiment with a reinforced concrete beam and on a real bridge model,” Luxembourg, 2018.

[158] H.-M. Zogg, W. Lienhart and D. Nindl, “Leica TS30 - White Paper,” Leica Geosystems AG, Heerbrugg, 2009.

[159] P. PHOTO-MESS-SYSTEME, “Elcovision 10,” PMS PHOTO-MESS-SYSTEME AG, Margrethen, 2017.

[160] A.-M. Loghin and E. Oniga, The influence of camera calibration parameters on 3D building models creation, University "1 Decembrie 1918" of Alba Iulia, 2014.

[161] J.-Y. Lin and S.-H. Chio, “The accuracy influence of different camera calibration conditions to bundle adjustment of closerange images,” in *The 33rd asian conference on remote sensing*, Pattaya, 2012.

[162] M. Pregnolato, “Bridge safety is not for granted - A novel approach to bridge management,” *Engineering Structures,* vol. 196, pp. 109-193, 2019.

[163] Z. Kala, "Global sensitivity analysis of reliability of structural bridge system," *Engineering structures,* vol. 194, pp. 36-45, 2019.

[164] Y. Bao, Z. Chen, S. Wei, Y. Xu, Z. Tang and H. Li, "The State of the Art of Data Science and Engineering in Structural Health Monitoring," *Engineering,* vol. 5, pp. 234-242, 2019.

[165] S.-H. Huang, Y.-H. Huan, C. A. Blazquez and G. Paredes-Belmar, "Application of the an colony optimization in the resolution of the bridge inspection routing problem," *Applied Soft Computing,* vol. 65, pp. 443-461, 2018.

[166] W. Megid, M.-A. Chainey, P. Lebrun and R. Hay, "Monitoring fatigue cracks on eyebars of steel bridges using acoustic emission: A case study," *Engineering Fracture Mechanics,* vol. 211, pp. 198-208, 2019.

[167] E. A. Oskoui, T. Taylor and F. Ansari, "Method and monitoring approach for distributed detection of damage inmulti-span continuous bridges," *Engineering Structures,* vol. 189, pp. 385-395, 2019.

[168] B. Wu, G. Wu and C. Yang, "Parametric study of a rapid bridge assessment method usingdistributed macro-strain influence envelope line," *Mechanical Systems and Signal Processing,* vol. 120, pp. 642-663, 2019.

[169] M. M. Alamdari, K. Kildashti, B. Samali and H. V. Goudarzi, "Damage diagnosis in bridge structures using rotation influence line:Validation on a cable-stayed bridge," *Engineering Structures,* vol. 185, pp. 1-14, 2019.

[170] S.-Z. Chen, G. Wu and D.-C. Feng, "Damage detection of highway bridges based on long-gaugestrain response under stochastic traffic flow," *Mechanical Systems and Signal Processing,* vol. 127, pp. 551-572, 2019.

[171] J. Zhang, S. Guo, Z. Wu and Q. Zhang, "Structural identification and damage detection through long-gaugestrain measurements," *Engineering Structures,* vol. 99, pp. 173-183, 2015.

[172] B. Wu, G. Wu, C. Yang and Y. . He, "Damage identification method for continuous girder bridgesbased on spatially-distributed long-gauge strain sensing undermoving loads," *Mechanical Systems and Signal Processing,* vol. 104, pp. 415-435, 2018.

[173] N.-B. Wang, L.-X. He, W.-X. Ren and T.-L. Huang, "Extraction of influence line through a fitting method from bridgedynamic response induced by a passing vehicle," *Engineering Structures,* vol. 151, pp. 648-664, 2017.

[174] W.-J. Cao, C. G. Koh and I. Smith, "Contents lists available atScienceDirectEngineering Structuresjournal homepage:www.elsevier.com/locate/engstructEnhancing static-load-

test identification of bridges using dynamic data," *Engineering Structures,* vol. 186, pp. 410-420, 2019.

[175] R. Jiang and D. V. Jauregui, "Development of a digital close-range photogrammetric bridge deflection measurement system," *Measurement,* vol. 43, pp. 1431-1438, 2010.

[176] P. J. Sousa, F. Barros, P. J. Tavares and P. M. Moreira, "Experimental measurement of bridge deflection using Digital Image Correlation," *Procedia Structural Integrity,* vol. 17, pp. 806-811, 2019.

[177] N. Le, D. Thambiratnam, A. Nguyen and T. Chan, "A new method for locating and quantifying damage in beams from staticdeflection changes," *Engineering Structures,* vol. 180, pp. 779-792, 2019.

[178] M. Gatti, "Structural health monitoring of an operational bridge: A case study," *Engineering Structures,* vol. 195, pp. 200-209, 2019.

[179] O. Mirza, S. K. Shill and J. Johnston, "Performance of Precast Prestressed Steel-Concrete Composite Panels Under Static Loadings to Replace the Timber Transoms for Railway Bridge," *Structures,* vol. 19, pp. 30-40, 2019.

[180] D. Erdenebat, D. Waldmann, F. Scherbaum and F. N. Teferle, "The Deformation Area Difference (DAD) method for condition assessment of reinforced structures," *Engineering Structures,* vol. 155, pp. 315-329, 2018.

[181] X. Min and L. O. Santos, "Dynamic Assessment of the Sao Joao Bridge Structural Integrity," *Procedia Structural Integrity,* vol. 5, pp. 325-331, 2017.

[182] S. Ataei and A. Miri, "Investigating dynamic amplification factor of railway masonry arch bridges through dynamic load tests," *Construction and Building Materials,* vol. 183, pp. 693-705, 2018.

[183] H. Wang, J.-X. Mao and B. Spencer Jr, "A monitoring-based approach for evaluating dynamic responses of riding vehicle on long-span bridge unter strong winds," *Engineering Structures,* vol. 189, pp. 35-47, 2019.

[184] M. d. Pristo, M. Scola and G. Zani, "On site assessment of Azzone Visconti bridge in Lecco: Limits and reliability of current techniques," *Construction and Building Materials,* vol. 209, pp. 269-282, 2019.

[185] A. Bayraktar, T. Türker, J. Tadla, A. Kursun and A. Erdis, "Static and dynamic field load testing of the long span Nissibi cable-stayed bridge," *Soil Dynamics and Earthquake Engineering,* vol. 94, pp. 136-157, 2017.

[186] N. Kovacs, B. Kövesdi, L. Dunai and B. Takacs, "Loading test of the Rákóczi bridge in Budapest," *Procedia Engineering,* vol. 156, pp. 191-198, 2016.

[187] S. Maas, A. Zürbes, D. Waldmann, M. Waltering, V. Bungard and D. G. Roeck, "Damage assessment of concrete structures through dynamic testing methods. Part 2: Bridge tests," *Engineering Structures*, vol. 34, pp. 483-494, 2012.

[188] V. H. Nguyen, S. Schommer, S. Maas and A. Zürbes, "Static load testing with temperature compensation for structural health monitoring of bridges," *Engineering Structures*, vol. 127, pp. 700-718, 2016.

[189] A. Bakker, R. Biehler and C. Konold, "Should Young Students Learn about Box Plots?," in *Curricular Development in Statistics Education*, Schweden, 2004.

[190] S. Lem, P. Onghena, L. Verschaffel and W. V. Dooren, "The heuristic interpretation of box plots," *Learning and Instuction*, vol. 26, pp. 22-35, 2013.

[191] E. Standard, "EN 206-1," CEN, Brussels, 2000.

[192] L. Geosystems, "Leica ScanStation P20," Heerbrugg, Switzerland, 2013.

[193] L. Geosystems, "Leica TS30," Heerbrugg, Switzerland, 2009.

[194] L. Geosystems, "Leica DNA Digitalnivelliere," Heerbrug, Switzerland, 2006.

[195] "www.elcovision.com," PMS Photo Mess Systeme AG, [Online]. Available: https://www.elcovision.com/d_pmsag_kontakt.html. [Accessed 26 08 2019].

[196] "www.hbm.com," Höttinger Baldwin Messtechnik GmbH. [Online]. [Accessed 26 08 2019].

[197] "http://vbi.truck.volvo.com/index.php," 23 August 2019. [Online]. Available: http://vbi.truck.volvo.com/index.php.

[198] D. Erdenebat and D. Waldmann, "Condition assessmend and damage localisation for bridges by use of Deformation Area Difference Method (DAD-Method)," in *fib Symposium*, Cape Town, 2016.

[199] G. f. G. G. u. L. DVW, "Terrestrisches Laserscanning 2018," Wißner-Verlag, Augsburg, 2018.

[200] "Berntsen," 05 11 2013. [Online]. Available: https://berntseninternational.com/Home/News-Events/ArtMID/1869/ArticleID/16/Understanding-the-Differences-Between-Reflective-Targets-and-Prism-Survey-Systems. [Accessed 10 10 2019].

[201] D. Erdenebat, D. Waldmann and F. N. Teferle, "Laboratory experiment for damage assessment using the DAD-method," in *SMAR*, Zurich, 2017.

[202] E. Jeschke, H. Reinke, S. Unverhau, E. Pfeifer, B. Fienitz and J. Bock, Excel 2010 Formulas & Functions Inside Out, Washington: Microsoft Press, 2012.

[203] B. Wichmann and I. Hill, "Generating good pseudo-random numbers," *Computational Statistics & Data Analysis,* vol. 51, pp. 1614-1622, 2006.

[204] N. N. M. Kyaw, K. L. Htat and S. Y. Khaing, "Investigation on the Behaviours of Long-Span Suspension Bridge with Self Anchorage System," *International Journal of Science, Engineering and Technology Research,* vol. 3, no. 6, pp. 1697-1700, 2014.

[205] F. Samim and S. Nakamura, "Study on Serviceability of Cable-Stayed Bridges," *Proceedings of the School of Engineering of Tokai University,* vol. 40, pp. 21-28, 2015.

[206] G. Marciukaitis and L. Juknevicius, "Deviation in deflections of eccentrically prestressed reinforced concrete structures," *Procedia Engineering,* vol. 172, pp. 706-710, 2017.